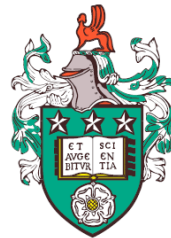


Modelling and Characterization of Soft Materials for Bio-inspired Series-elastic Actuators



Rodrigo Daniel Solis Ortega

University of Leeds

Institute of Design, Robotics and Optimization

School of Mechanical Engineering

Submitted in accordance with the requirements for the degree of

Doctor of Philosophy

August, 2020

Intellectual Property Statement

The candidate confirms that the work submitted is his own, except where work which has formed part of jointly authored publications has been included. The contribution of the candidate and the other authors to this work has been explicitly indicated below. The candidate confirms that appropriate credit has been given within the thesis where reference has been made to the work of others.

Chapter 3 of this thesis is based on a jointly-authored conference paper: *Solis-Ortega, R.D., Dehghani-Sanij, A.A. and Martinez-Hernandez, U., 2017, July. Characterization of kinetic and kinematic parameters for wearable robotics. In Annual Conference Towards Autonomous Robotic Systems (pp. 548-556). Springer, Cham..*

Chapter 5 of this thesis is based on a jointly-authored conference paper: *Solis-Ortega, R.D., Dehghani-Sanij, A.A. and Martinez-Hernandez, U., 2018, August. The assessment of viscoelastic models for non-linear soft materials. In 2018 7th IEEE International Conference on Biomedical Robotics and Biomechatronics (Biorob) (pp. 1274-1279). IEEE..*

The contributions of the candidate to these papers include the literature review, data collection, design and execution of simulation, statistical analysis, and writing. The contributions of the other authors to these papers include guidance, supervision, and revision.

This copy has been supplied on the understanding that it is copyright material and that no quotation from the thesis may be published without proper acknowledgement.

The right of Rodrigo Daniel Solis Ortega to be identified as Author of this work has been asserted by him in accordance with the Copyright, Designs and Patents Act 1988.

© 2020 The University of Leeds and Rodrigo Daniel Solis Ortega.

Acknowledgements

I would like to express my most sincere gratitude to my supervisor Professor Abbas Dehghani-Sanij, and to Dr Uriel Martinez Hernandez for guiding me through the development of this project. I would also like to thank my family for supporting me during the most difficult times, despite of the enormous distance between us. I am very grateful to my wife, who accompanied me during the most challenging stages of this life experience, and for encouraging me when I needed it the most. I would also like to thank all my friends and the many people who directly or indirectly were involved in this personal goal. Lastly, I would like to thank my financial sponsor, the Consejo de Nacional de Ciencia Y Tecnologia (CONACYT).

Abstract

In the field of Soft Robotics, viscoelasticity has been proved beneficial for human assistance applications. The human skeletal muscle system, as well as many soft materials commonly used in soft robotic applications, have viscoelastic properties. Viscoelasticity can be modelled using a set of equations known as the Linear Viscoelastic Models (LVMs). This modelling approach has two main limitations: high mathematical complexity and high computational cost. Here, these limitations are addressed in two ways. Firstly, the Piecewise Linearisation method is used to reduce the mathematical complexity of LVMs. Secondly, a modelling approach based on feedforward artificial neural networks (ANNs) is used to reduce the computational cost. The aim of both modelling approaches is to describe the non-linear, strain-dependent, and time-dependent stress response of seven thermoplastic elastomers.

On the one hand, the implementation of the Piecewise Linearisation method yielded the PL-SLS model and the PL-Wiechert model. Both models were successful in predicting the viscoelastic behaviour of the materials, outperforming similar modelling tools documented in the literature. On the other hand, four different architectures of ANN models are developed, categorized in rate-dependent and rate-independent. Results highlight the rate-dependent architecture as the most suitable. The ANN models achieved a similar prediction performance as the PL models.

The ANN model for the natural rubber material is further validated in a real-time simulation environment, in Simulink. This soft material is found to be the best candidate to imitate the mechanical properties of the human tendon. On the one hand, the performance prediction of the ANN models is adequate for a sine wave strain input, when the strain rate is constant. On the other hand, the response of the ANN model is unstable under variable strain rates. This highlights an important limitation of the training set used for developing the ANN models, which only contains data for three different strain rates. Finally, the three modelling tools developed in this research are a direct improvement to current modelling approaches. Nonetheless, a richer training set is required to improve the ANN models real-time response.

CONTENTS

1	Introduction	1
1.1	Background	2
1.2	Motivation	4
1.3	Aims and Objectives	5
1.3.1	Aims	5
1.3.2	Objectives	5
1.4	Research Scope	6
1.5	Research Contributions	6
1.6	Thesis Outline	7
2	Literature Review	10
2.1	Introduction	11
2.2	The Field of Soft Robotics	11
2.3	Human Assistance Applications	14
2.3.1	Soft Actuation Technologies	15
2.3.1.1	Pneumatic Artificial Muscles	15
2.3.1.2	Cable-driven Actuators	22
2.3.1.3	Shape Memory Materials	23
2.3.2	Soft Perception Technologies	28
2.3.3	Control Technologies	32
2.4	Biomechanics of the Human Lower Limb	34
2.5	The Muscle-tendon Component	38
2.6	Modelling Tools for Soft Materials	42
2.7	Summary	45
3	Design Guidelines for Assistive Devices	49
3.1	Introduction	50

CONTENTS

3.2	Characterization of Kinematic and Kinetic Parameters for Activities of Daily Living	50
3.2.1	Gait Analysis Data	51
3.2.2	Extracting Design Guidelines	53
3.3	Summary	57
4	Characterization of the Mechanical Properties of Soft Materials	59
4.1	Introduction	60
4.2	Mechanical Properties of Soft Materials	60
4.2.1	Elasticity	62
4.2.2	Viscoelasticity	63
4.3	Characterization Process	65
4.3.1	Tensile Strength Test	66
4.3.1.1	Data Processing	67
4.3.1.2	Elastic Properties of the Material	70
4.3.2	Stress Relaxation Test	82
4.3.2.1	Stress Relaxation Properties	85
4.4	Summary	88
5	Soft Materials Modelling: Linear Viscoelastic Models	90
5.1	Introduction	91
5.2	The Linear Viscoelastic Models	92
5.3	The Piecewise linearisation Method	94
5.4	Model fitting	96
5.5	Findings	101
5.5.1	Analysis of the Optimal Number of Strain Segments	102
5.5.2	Analysis of the Model Fit Accuracy	109
5.5.3	Analysis of the Velocity-dependent Stress Response	114
5.6	Summary	121
6	Soft Materials Modelling: Artificial Neural Networks	124
6.1	Introduction	125
6.2	Artificial Neural Networks	126
6.3	Soft Materials Modelling	129
6.4	Model Development	135
6.4.1	Analysis of the Model Inputs Selection	137

6.4.2	Analysis on the Optimal Number of Neurons	141
6.5	Summary	147
7	Modelling a bio-inspired series-viscoelastic actuator	149
7.1	Introduction	150
7.2	Matching the Human Tendon Properties	151
7.3	Validation in Simulated Real-time	153
7.4	Series-viscoelastic Actuator: Design Concept	159
7.5	Summary	161
8	Summary, Conclusions, and Future Work	163
8.1	Summary	164
8.2	Conclusions	168
8.3	Future Work	169
A	Appendices	170
A	Characterization of the Human Body Lower Limb	172
A.1	Stacked Clustered Bar Charts	173
R	References	179

CONTENTS

LIST OF FIGURES

2.1 Bio-inspired active soft orthosis concept for the treatment of ankle-foot pathologies. From top to bottom: artificial muscles attached to the soft wearable garment, a strain sensor for ankle angle measurements, the tendon-ligament system and pressure sensor for gait cycle detection.	17
2.2 Soft orthosis components, (a) pneumatic artificial muscle in its relaxed and contracted state, (b) complete tendon-ligament system without ligaments and with ligaments.	17
2.3 Soft sleeve prototype. (a) Original shape. (b) All muscles activated, contracting the whole body and amplified image of one muscle. (c) Partial contraction, only the 1st and 2nd top rows are activated. Both (d) and (e) illustrate bending movements, only two adjacent columns are activated.	18
2.4 Virtual anchor concept. The three key anchors (red square) located at the foot, hip and shoulder are interconnected with the soft actuators (orange) and auxiliary connectors (black) in specific points called virtual anchors (red circle) to stabilize the forces created by the actuators.	19
2.5 (a) Flat elastomer pneumatic actuator in (1) pressurized and (2) relaxed states. (b) Implementation of the flat actuator in medical leg model assistance, along with the achieved (1) extension, and (2) flexion motion.	20

LIST OF FIGURES

2.6 (a) IPAM developed in its relaxed and pressurized state, the small radial expansion and large axial expansion is appreciated. (b) Cross-sectional view of the jamming effect ongoing inside the actuator, and (c) bending effect caused by heavy load, and correction of the bending using the jamming effect.	21
2.7 (a) Developed Bowden cable-based soft exosuit prototype. (b) Initial design concept highlighting the main parts of the soft exosuit.	22
2.8 Multi-joint actuated soft exosuit. There are two anchor points, one at the pelvis (1) and one at the shank (5). The suit is actuated by a bowden cable (2) and positioned at the front of the knee. The contractile element is connected connected to the two anchors by webbing elements (4). Knee module to increase the lever arm (3). Red arrows: reaction forces, and orange arrows: actuation force.	24
2.9 Shape memory alloys made of Nitinol. The contraction effect under the increase in temperature is illustrated.	25
2.10 Ankle joint soft orthosis. The developed SMA artificial muscle along the main parts are highlighted.	26
2.11 Flexible wrist exoskeleton prototype.	27
2.12 Schematic illustrating McKibben with embedded SMP functionality. T_g : transition temperature, P_H : high pressure, P_L : low pressure.	28
2.13 Soft strain sensor. The microchannel filled with liquid metal can be appreciated in: (a) concept design and (b) the prototype.	29
2.14 Soft sensor sleeve: (a) design concept, (b) developed prototype, (c) magnified view of the embedded sensor-actuator concept. (d) Soft strain sensor change in resistance during stretch and relax.	30
2.15 Implementation of soft strain sensors into a Soft sensing suit, (a) hip sensor, (b) knee sensor and (c) ankle sensor position.	30
2.16 Hybrid soft strain sensor, the interface between the liquid metal and the ionic solution can be clearly seen in dark areas.	31
2.17 ‘Smart Braid’ concept. The variation in the actuator length cause a change in the electric circuit inductance.	32
2.18 Control system architecture implemented for the ankle soft orthosis. .	33
2.19 Dimensional spaces used to understand human motions: (a) Sagittal plane, (b)Horizontal plane and (c)Frontal plane.	35

LIST OF FIGURES

2.20 Lower limb motions for (a) sagittal plane, (b) horizontal plane and (c) frontal plane.	37
2.21 Hill's model of the skeletal muscle. The contractile element (CE), the parallel element (PE) and the series element (SE) are shown.	38
2.22 Tendon stress-strain curve.	40
2.23 Tendon curves for the experiments of: (a) stress relaxation and (b) creep. The experiments were executed several times under the same conditions, the curve labelled <i>n</i> illustrates the tendon reaching a steady state where repeatability between experiments is achieved. . .	41
2.24 Hysteresis of the human tendon. (a) Deformation chart shows both loading and unloading paths for few cycles and (b) displacement chart shows 200 loading-unloading cycles. The preconditioned state of the tendon is reached for cycles above 50.	41
2.25 Series-viscoelastic actuator proposed by Parietti et al. The end- effector is rigidly mounted on the revolving lever (i), which also sup- ports the laser sensor. A Nylon line (ii) connects the end-effector handle to the high-precision piezoelectric force sensor (iii), which is fixed to a rigid support.	43
2.26 Developed soft rotary spring: (a)photo and (b)cross-section.	44
2.27 Benchtop setup for rubber characterization and observer testing. The load side of the rubber is fixed. Load cells in-line with the rubber give rubber force measurements for testing. The choice of electric motors and transmission is illustrated.	45
3.1 Clustered-stacked bar charts of reviewed gait analyses.	54
3.2 Torque range values during several activities. The values for the max- imum and minimum torque are mean values from the data of all the different gait analysis experiments enclosed in one main activity. . .	55
3.3 Comparison between subjects' age and the knee range of motion dur- ing walking over ground. The areas surrounded by solid lines and dotted lines represent the intersection between three and two areas, respectively. The overlapping squares highlight the great similarity among the range of motion despite subjects' age. The data used to create this chart is presented in Table 3.1	57

LIST OF FIGURES

4.1	Typical stress-strain curve of elastomers. There are three main regions: the toe region ($1.0 < \lambda < 1.5$), the elastic region ($1.5 < \lambda < 3.5$), and the yield/failure region ($\lambda > 3.5$)	62
4.2	Hysteresis in stress-strain curve.	65
4.3	Specimen Type C Dumbbell Layout from the ASTM D412. In this example, the specimen thickness is 3mm, the width is 6mm, and the initial length, l_o , is 33mm.	66
4.4	Undesired data on the tensile strength results. On the top left, the take-up slack phenomenon at the beginning of the experiment is observed. On the right, the different failure points of each specimen from the same material are highlighted.	68
4.5	Abrupt changes observed at the last portion of the stress-strain curve, caused by the different failure points for each specimen. This phenomenon is observed after unifying the data from all individual specimens of a specific strain rate, into a single stress-strain curve.	69
4.6	Stress-strain curves, during different strain rates, for the (a) EPR and (b) FR materials. On the bottom right, the initial section of the curve is presented.	72
4.7	Stress-strain curves, during different strain rates, for the (a) NatPolR and (b) NR materials. On the bottom right, the initial section of the curve is presented.	73
4.8	Stress-strain curves, during different strain rates, for the (a) PR and (b) SR materials. On the bottom right, the initial section of the curve is presented.	74
4.9	Stress-strain curve, during different strain rates, for the NatR. On the bottom right, the initial section of the curve is presented.	75
4.10	Offset Yield Strength for the FR material	76
4.11	Offset Yield Strength for the NatPolR material	77
4.12	Offset Yield Strength for the NR material	78
4.13	Offset Yield Strength for the PR material	79
4.14	Offset Yield Strength for the NatR material	80
4.15	Offset Yield Strength for the SR and EPR (50mm/min) material.	81
4.16	Offset Yield Strength for the EPR (500mm/min) material	82

4.17 Stress Relaxation curves for (a) 180 minutes and (b) 15 minutes, of the EPR, FR, NatPolR, NR and SR materials. Different values of ε_o are investigated.	86
4.18 Stress Relaxation curves for (a) 180 minutes and (b) 15 minutes, of the PR, and NatR materials. Different values of ε_o are investigated. . .	87
 5.1 Hooke's Law and linear viscoelastic models: (a) Hooke's Law (b) Kelvin-Voigt, (c) Maxwell, (d) Standard Linear Solid, and (e) Burger. The parameters k and η represent the spring stiffness and the dashpot viscous constant, respectively.	93
5.2 Wiechert Model. The components k_1 , η_1 , and the equilibrium spring k_e , together represents the SLS model. The components k_j , and η_j represents the Maxwell Branch. The Wiechert model can contain as many branches as required, this is symbolised by the subscript j . . .	95
5.3 (a) Standard Linearized Solid model with Strain-Dependent Stiffness. (b) Piecewise linearisation method applied to the slope of the material load-displacement curve. This is analogous to many parallel springs which contribute to the material response depending on the material strain.	96
5.4 SLS model fitted to a typical stress relaxation curve of a viscoelastic material. The parameters k_e , k_1 and η can be obtained by analysing three points in the curve: $t = 0$, $t = \tau$, and $t = \infty$. The variable τ is the time constant of the exponential decaying curve.	97
5.5 Obtained fit from the Standard Linear Solid (SLS) and Wiechert model of the stress relaxation curve of the Silicone Rubber material. The obtained optimal number of branches of the Wiechert model fit is $j = 8$	99
5.6 Description of the implemented Piecewise linearisation method.	102
5.7 Algorithm for obtaining the right number of strain segments to be fitted based on the variation of the stress-strain curve slope.	103
5.8 Impact of the proposed tolerance criteria on the relationship between the number of strain segments and the achievable accuracy of the PL method. (a) EPR material (b) FR material.	105
5.9 Impact of the proposed tolerance criteria on the relationship between the number of strain segments and the achievable accuracy of the PL method. (a) NR material (b) NatPolR material.	106

LIST OF FIGURES

5.10 Impact of the proposed tolerance criteria on the relationship between the number of strain segments and the achievable accuracy of the PL method. (a) PR material (b) SR material.	107
5.11 Impact of the proposed tolerance criteria on the relationship between the number of strain segments and the achievable accuracy of the PL method. NatR material	108
5.12 Best fit for the PL-SLS and PL-Wiechert models on the stress-strain curve of (a) EPR material (b) FR material. The parameters required for this fit can be found in Table 5.1.	111
5.13 Best fit for the PL-SLS and PL-Wiechert models on the stress-strain curve of (a) NR material (b) NatPolR material. The parameters required for this fit can be found in Table 5.1.	112
5.14 Best fit for the PL-SLS and PL-Wiechert models on the stress-strain curve of (a) PR material (b) SR material. The parameters required for this fit can be found in Table 5.1.	113
5.15 Best fit for the PL-SLS and PL-Wiechert models on the stress-strain curve of NatR material. The parameters required for this fit can be found in Table 5.1.	114
5.16 Prediction of the PL-SLS (circles) and the PL-Wiechert (squares) model under different strain rates for the (a) EPR material (b) FR material. Strain rates are in millimetres per minute. Filled markers indicate the strain rate used to extract the strain dependent stiffness k^*	116
5.17 Prediction of the PL-SLS (circles) and the PL-Wiechert (squares) model under different strain rates for the (a) NR material (b) NatPolR material. Strain rates are in millimetres per minute. Filled markers indicate the strain rate used to extract the strain dependent stiffness k^*	117
5.18 Prediction of the PL-SLS (circles) and the PL-Wiechert (squares) model under different strain rates for the (a) PR material (b) SR material. Strain rates are in millimetres per minute. Filled markers indicate the strain rate used to extract the strain dependent stiffness k^*	118

LIST OF FIGURES

5.19 Prediction of the PL-SLS (circles) and the PL-Wiechert (squares) model under different strain rates for the NatR material. Strain rates are in millimetres per minute. Filled markers indicate the strain rate used to extract the strain dependent stiffness k^* .	119
6.1 (a) Feedforward artificial neural network (b) Internal structure of an artificial neuron.	127
6.2 Generalization error, based on a 10-fold cross-validation, for the (a) EPR, (b) FR, (c) NatPolR, (d) NR, (e) PR, and (f) SR materials. The best input combination is the one with the smallest generalization error, which in most cases is the FFRD4 configuration.	140
6.3 Generalization error, based on a 10-fold cross-validation, for the NatR material. The best input combination is the one with the smallest generalization error, i.e. the FFRD4 configuration.	141
6.4 Impact of the number of neurons on the R^2 value (a), (c), (e), and the Generalization error (b), (d), (f), for the EPR, FR, and NatPolR materials. A total of 200 ANN models are trained per soft material. The best R^2 value is circled in (a), (c), (e). The optimal number of neurons is circled in (b), (d), (f).	143
6.5 Impact of the number of neurons on the R^2 value (a), (c), (e), and the Generalization error (b), (d), (f), for the NR, PR, and SR materials. A total of 200 ANN models are trained per soft material. The best R^2 value is circled in (a), (c), (e). The optimal number of neurons is circled in (b), (d), (f).	144
6.6 Impact of the number of neurons on the R^2 value (a) and the Generalization error (b), for the NatR material. A total of 200 ANN models are trained per soft material. The best R^2 value is circled in (a). The optimal number of neurons is circled in (b).	145
7.1 Simulink implementation of the ANN model. The ANN model takes the strain and strain rate as inputs, and delivers the stress response of the material in MPa as output. The gain blocks ensure that the units are consistent.	155

LIST OF FIGURES

7.2 ANN model stress response to a sine wave strain input. The solid and dotted blue line are the strain and strain rate, respectively. (a) and (b) positive and unknown strain rate values, (c) negative values of the strain and strain rate, (d) strain rate saturated to avoid negative values.	156
7.3 ANN model stress response to a sine wave strain input and a constant strain rate. The solid and dotted blue line are the strain and strain rate, respectively. (a-b) positive and unknown strain values, (c) negative values of the strain.	158
7.4 CAD Design of the detachable clamping device (a) Bottom part, (b) Final assembly, the soft material is coloured in black, and the T-shape attachment in blue. Units are in millimetres.	161
A.1 Knee joint characteristics for walking over ground activities. The weight next to the name of some activities dictates the load carried by the subjects during the experiment.	173
A.2 Ankle joint characteristics for walking over ground activities. The weight next to the name of some activities dictates the load carried by the subjects during the experiment.	174
A.3 Hip joint characteristics for step ascending/descending experiments. .	174
A.4 Ankle joint characteristics for step ascending/descending experiments.	175
A.5 Hip joint characteristics for ramp ascending/descending experiments. Inclination in brackets.	175
A.6 Knee joint characteristics for ramp ascending/descending experiments. Inclination in brackets.	176
A.7 Ankle joint characteristics for ramp ascending/descending experiments. Inclination in brackets.	176
A.8 Hip joint characteristics for sit to stand/stand to sit experiments. In brackets (h) healthy subjects, and (p) subjects with Parkinson's. . .	177
A.9 Knee joint characteristics for sit to stand/stand to sit experiments. In brackets (h) healthy subjects, and (p) subjects with Parkinson's. .	177
A.10 Ankle joint characteristics for sit to stand/stand to sit experiments. In brackets (h) healthy subjects, and (p) subjects with Parkinson's. .	178

LIST OF TABLES

2.1	Main features of pneumatic artificial muscles.	16
3.1	Colour code used in Figure 3.3 for each combination of age range and knee range of motion.	56
4.1	Number of specimens per type of test.	67
4.2	Elastic properties of the selection of soft materials. The materials are: Polyethylene Rubber (PR), Ethylene Polypropylene Rubber (EPR), Natural Rubber with Polyester (NatPolR), Natural Rubber (NatR), Silicone Rubber (SR), Fluorocarbon Rubber (FR), and Nitrile Rubber (NR).	83
4.3	Stress relaxation tests parameters and total collected datasets. . . .	84
4.4	Stress relaxation parameters for the selection of soft materials. . . .	85
5.1	Best accuracy of the PL-SLS model (1), the PL-Wiechert model (2), and the degree of improvement achieved by the PL-Wiechert model. .	110
5.2	Best generalization error of the PL-SLS (1) and the PL-Wiechert (2) models.	120
6.1	Summary of proposed and optimized hyper-parameters.	136
6.2	Total number of training samples per soft material for the number of neurons optimization. In here, the total number of training samples represents the 100% of the whole dataset.	136
6.3	Proposed ANN architectures. The architectures FFRI1, FFRI2 and FFRI3 are rate-independent, whereas the architecture FFRD4 is rate-dependent.	138
6.4	Proposed parameters for the selection of best inputs	139
6.5	Proposed hyper-parameters for the number of neurons optimization .	142

LIST OF TABLES

6.6 Comparison between the performance of the best case ANN model, the PL-SLS model, and the PL-Wiechert model. The generalization error, Gen. Error (6.7), is based on the mean NRMSE value from all training sessions, whereas the GE (5.13), is based on the mean NRMSE among all available strain rates as described in Chapter 5. . .	146
7.1 Viscoelastic properties of the patellar tendon and the quadriceps ligament, compared against the viscoelastic properties of the studied soft materials (Tables 4.2 and 4.4).	151
7.2 Matching factors required for the soft materials to achieve the human tendon E_{small} value. The width proposed for the material strips is 66 mm.	153
7.3 Simulation parameters	160

Abbreviations

ADL	Activities of Daily Living	NatPolR	Natural Rubber with Polyester
ANN	Artificial Neural Network	NMAD	Normalized Mean Absolute Difference
ASTM	American Society for Testing and Materials	NR	Nitrile Rubber
BR	Bayesian Regularization	NRMSE	Normalized Root Mean Square Error
CE	Contractile Element	PAM	Pneumatic Artificial Muscle
CAM	Computer Assisted Manufacturing	PE	Passive Element
EPR	Ethylene Polypropylene Rubber	PL	Piecewise Linearization
FEA	Finite Element Analysis	PHRI	Physical Human-robot Interaction
FFNN	Feedforward Artificial Neural Network	PR	Polyethylene Rubber
FFRD	Feedforward Rate-dependent	RMSE	Root Mean Square Error
FR	Fluorocarbon Rubber	SE	Series Element
FFRI	Feedforward Rate-independent	SDS	Strain-dependent Stiffness
HMS	Human Musculoskeletal System	SEA	Series-elastic Actuator
IMU	Inertial Measurement Unit	SLS	Standard Linear Solid
IPAM	Inverse Pneumatic Artificial Muscle	SMA	Shape Memory Alloy
KKP	Kinetic and Kinematic Parameters	SMP	Shape Memory Polymer
LDA	Large Deformation Actuators	SSE	Sum of Square Errors
LM	Levenberg-Marquardt	SR	Silicon Rubber
LVM	Linear Viscoelastic Model	SVA	Series-viscoelastic Actuator
MAD	Mean Absolute Difference	TSSE	Total Sum of Square Errors
MSE	Mean Square Error	TPE	Thermoplastic Elastomer
NLS	Non-linear Spring	TPU	Thermoplastic Polyurethane
NatR	Natural Rubber		

Common Symbols

A_o	Cross-sectional Area
ΔL	Elongation
ΔL_o	Initial Elongation
E	Elastic Modulus
E_{large}	Elastic Modulus at Large Strains
E_{small}	Elastic Modulus at Small Strains
ε	Strain
ε_o	Initial Strain
ε_{offset}	Strain Offset
ε_u	Ultimate Strain
ε_{ue}	Engineering Ultimate Strain
ε_y	Yield Strain
η	Damper Constant
F	Force
k	Spring constant
k_e	Equilibrium Spring constant
k^*	Strain-dependent Spring
l_o	Initial Length
λ	Extension Ratio
<i>S.R.</i>	Stress Relaxation
σ	Stress
σ_{end}	Final Stress
σ_o	Initial Stress
σ_u	Ultimate Stress
σ_{ue}	Engineering Ultimate Stress
σ_y	Yield Stress
R^2	Coefficient of Determination

CHAPTER 1

Introduction

1. INTRODUCTION

1.1 Background

The field of Soft Robotics deals with the implementation of soft and deformable materials in traditional robotic applications. The interest in this field has increased in the past decade. The latter is due to the outstanding progress in manufacturing of soft and smart materials which can be actuated by heat, light, and magnetism. Early applications in Soft Robotics were inspired in nature, by observing that most biological organisms are not rigid [1]. This inspiration gave birth to several soft bio-inspired robots.

The design and development of soft robots is full of challenges, such as: actuation of soft materials, development and implementation of soft sensors into soft robots, control systems capable of dealing with the nonlinear behaviour of soft materials, and modelling tools able to accurately predict the mechanical behaviour of soft materials in real-time [2, 3]. Nonetheless, the potential benefits are many, such as: soft robots have the potential of being very dexterous due to the ability of modifying their shape depending on the environment; soft robots can manipulate objects of different shapes, sizes; and most importantly soft robots are safe to interact with humans in the event of an unplanned collision [4]. These benefits highlight the potential of soft robotic applications for physical human-robot interaction (PHRI) such as, orthoses, surgical tools, and wearable devices. This research aims to contribute to the technological advance of Soft Robotics for human assistance applications.

For a long time, humans have pursued the idea of increasing their strength, stamina and speed through different means. Nowadays, this is a reality due to the technological advances on wearable robotic devices, commonly known as robotic exoskeletons. This wearable device was motivated by military applications where a soldier is required to carry a heavy load in its back for a long period of time, ultimately causing him injuries or early fatigue. The robotic exoskeleton is able to carry a payload and transmit the payload weight to the ground, ideally relieving the wearer from feeling the payload, which allows the wearer to walk greater distances without premature fatigue. The rigid nature of these devices and the big actuators implemented to achieve forces able to enhance humans, impose many limitations, such as, restriction of body movements, interference on subject natural biomechanics and high inertia which impedes the device to follow the subject intentions smoothly, creating a drag feeling [5].

In the field of Soft Robotics, a soft version of the robotic exoskeleton, formally called soft exosuit, is being developed. Soft exosuits are wearable robotic systems

meant to be worn in the same way as clothes. In this context, both the actuation and perception systems are attached to a soft structure made of textiles which is strapped to the human body. Despite the many benefits of this technology, available prototypes cannot deliver enough mechanical power to be called an enhancement device. Therefore, these devices are mainly for human assistance applications. This limitation is caused by the challenge of having a soft structure to transmit the forces generated by the actuators that are distal to the assisted joint. Moreover, these forces can create discomfort to the user. Nonetheless, there are areas of the human body which naturally sustain high amounts of forces which are commonly used in the design of soft exosuits [6]. Another alternative to address the latter limitation is to deploy the actuators proximal to the assisted joint, closer to the human skeletal muscle system functionality [7, 8].

In most soft exosuits, the lack of a robust modelling tool for the prediction of the mechanical behaviour of soft materials, makes it difficult to implement a control system. There are two modelling approaches commonly used for this task. One is based on the Linear Viscoelastic Models (LVMs), the other is based on machine learning models. On the one hand, the LVMs describe the mechanical behaviour of a soft material using two basic mechanical components, a spring and a dashpot. Inside this family of models, there are two models that can be expanded as required. In theory, they are capable of describing the most complex soft material. In practice, expanding a mathematical model is translated into solving more differential equations which at the same time translates into higher computational cost. Therefore, modeling tools based on the LVMs have an important trade-off between achievable accuracy and required complexity. In some cases, deploying these models to hardware, i.e. control systems, is prohibitive.

On the other hand, the modelling approach using machine learning tools is commonly based on Artificial Neural Networks (ANNs). ANNs excel at identifying complex relationship in large datasets. Their development, specially their training process, is time consuming. However, the time required for an ANN to make a prediction is very small once trained. This is the main advantage of ANNs in comparison to model-driven approaches, which have to perform intensive calculations every time new data is presented as input. Plenty of research can be done on both modelling approaches with the aim of developing a robust modelling tool to accurately describe the complex mechanical behaviour of soft materials. The latter has the potential of increasing the adoption of soft materials in robotic applications, as

1. INTRODUCTION

well as creating more efficient wearable systems.

1.2 Motivation

The global percentage of elderly population is constantly rising. The World Health Organization has estimated that the global percentage of people aged 65 or older will triple by 2050, with respect to 2010 [9]. Moreover, the amount of elderly people living alone is also increasing. Solely in the United Kingdom, there are 1 million people aged over 65 living on their own [10]. Although, the social triggers of the mentioned phenomena are out of the scope of this research, they represent a strong motivation to push forward the research on soft robotic applications for human assistance. Currently, there are viable concepts of assistive exosuits targeted to increase the quality of life of elderly people during activities of daily living, such as walking over ground, ascending stairs, and using a chair. However, the concept of an assistive exosuit is relatively new, the first documented prototype is dated from 2013 [6]. The idea behind an exosuit is to translate the proven concept of a robotic exoskeleton, which is a heavy and bulky wearable device aimed to enhance the strength of humans, into a soft, light weight and compliance version aimed to provide assistance to the elderly or disabled people.

One of the main challenges in this field of research is the modelling of the mechanical behaviour of soft materials. The accuracy of current modelling approaches is proportional to the required computational power. Due to this, the most accurate modelling tools are difficult to be deployed in control systems where the hardware computational power is limited. The necessity for commercial-grade exosuits for human assistance is pushing the development of robust modelling tools capable of predicting the viscoelastic behaviour of soft materials. Therefore, the main motivation of this research is to contribute to the technological development of robust modelling tools. This can translate into more efficient soft actuators, hence soft exosuits, which will improve the quality of life of the elderly and disabled population in the near future.

1.3 Aims and Objectives

1.3.1 Aims

The aims of this research are:

- To investigate the concept of implementing viscoelasticity, a property found in the human skeletal muscle system, in soft robotic applications for the assistance of the human lower limb.
- To develop a reliable modelling tool to be implemented in a bio-inspired soft actuator model for the prediction of the stress response of soft materials in real-time.

1.3.2 Objectives

In accordance to the research aims, the following objectives are identified:

- Survey the literature to identify: the terminology related to the biomechanics of the human lower limb, and the current soft robotic developments on the field of human assistance.
- Investigate the biomechanics of the human lower limb during activities of daily living.
- Characterize the viscoelastic properties of suitable soft materials.
- Identify the soft materials with the most similar mechanical properties to the human tendon.
- Address current limitations on modelling tools for the prediction of the viscoelastic behaviour of soft materials.
- Investigate the performance of current modelling tools under simulated real-time conditions.
- Design a bio-inspired soft actuator for human-assistance applications.

1. INTRODUCTION

1.4 Research Scope

This research is focused on developing a reliable modelling tool, able to be implemented in a control system, for the prediction of the mechanical behaviour of soft materials. Therefore, the following is included in the scope of the research.

The biomechanics from the lower limb of the human body during several activities of daily living are characterized. The potential benefits of using a viscoelastic material instead of the traditional metallic spring in series-elastic actuators, is investigated. For this reason, the following soft materials are studied: ethylene polypropylene rubber (EPR [11]), fluorocarbon rubber (FR [12]), nitrile rubber (NR [13]), natural rubber with polyester (NatPolR [14]), polyethylene rubber (PR [15]), silicone rubber (SR [16]), and natural rubber (NatR [17]). A recent and accurate modelling approach, based on a piecewise linearisation of the Linear Viscoelastic Models (LVMs), is studied. Furthermore, a systematic analysis on the performance of a popular machine learning tool, Artificial Neural Networks (ANNs), is executed. The analysis includes the effect of the number of neurons, output activation function, training algorithm, and combination of inputs/outputs presented to the ANN. Moreover, the performance of the developed ANN models under simulated real-time conditions, is assessed. Finally, the most suitable modelling approach for this application is identified.

1.5 Research Contributions

This research contributes to the field of Soft Robotics for human assistance by investigating the performance of Artificial Neural Networks, as an alternative to the Linear Viscoelastic Models, for the modelling of viscoelasticity in soft materials. Some parts of this thesis are published in peer-reviewed conference papers. The contributions are summarized as follows:

- Three modelling tools for the prediction of the non-linear, strain-dependent, and time-dependent stress response of soft materials. The models are: the PL-SLS model, the PL-Wiechert model, and the ANN model.
- Identification of design guidelines for the selection of actuator technologies, based on the kinetic and kinematic parameters of the human body, when developing assistive devices.

- Incremental improvement of the piecewise linearisation method by proposing a tolerance criteria to define the required complexity of the method depending on the desired prediction accuracy.
- Concept design of a modular clamp mechanism aim to hold a bundle of strings of soft materials in a bio-inspired series-elastic actuator.

1.6 Thesis Outline

This thesis is divided and organized in eight chapters, as follows:

- **Chapter 1:** This chapter presents the research background, motivation of the researcher, aims and objectives. Moreover, the specific contributions of this research to the respective field of knowledge, and the scope of the thesis are also presented in here.
- **Chapter 2:** The second chapter presents an overview on the field of Soft Robotics. The applications related to human assistance are described in terms of the actuation, perception and control system technologies. The recent trend about implementing the functionality of the human skeletal muscle system in soft robotic application is discussed. Due to this, the terminology related to the human biomechanics is included. In addition to this, the challenges of modelling the mechanical behaviour as well as the modelling tools currently used are introduced in this chapter. Finally, the gaps in the body of knowledge are identified and presented.
- **Chapter 3:** In this chapter, the process of extracting design guidelines for robotic assistive devices from clinical studies focused on the human gait analysis is presented. Moreover, the characterization of the kinetic and kinematic parameters of the human lower limb during activities of daily living (ADLs), is performed. A total of four main ADLs are investigated from clinical trials: ground level walking, going up/down steps, going up/down a ramp and sitting down/standing up from a chair. The compiled data is processed to obtain a graphical representation and facilitate the comparison and analysis of the parameters variations from subject to subject and activity to activity. The work done in this chapter was substantial enough to produce a conference paper [18].

1. INTRODUCTION

- **Chapter 4:** In this chapter, the characterization of a selection of seven thermoplastic elastomers is presented. The mechanical tests of tensile strength and stress relaxation are performed to characterize the viscoelastic properties of the materials. The processing of the data and extraction of the materials parameters are described in detail.
- **Chapter 5:** This chapter describes the development process of two modelling tools based on the Linear Viscoelastic Models (LVMs). The work in here is inspired by the Piecewise linearisation method, which has been successful in improving the performance of the LVMs. Two modelling tools are developed, PL-Wiechert and the PL-SLS models. The performance of these models is assessed for the description of the non-linear, strain-dependent, and time-dependent stress response of viscoelastic materials. The work done in this chapter was substantial enough to produce a conference paper [19].
- **Chapter 6:** In this chapter, the development of a modelling tool based on artificial neural networks (ANNs), is presented. The research about implementing ANNs in the field of composite materials is very scarce. Nonetheless, ANNs have been proven useful for many function approximation applications. Two hyper-parameters of the developed ANN models are optimized: the number of neurons in the hidden layers, and the selection of inputs. The performance of the developed ANN models is compared against the developed PL models.
- **Chapter 7:** This chapter presents the design concept of a bio-inspired series-elastic actuator. The work on this chapter is focused on design due to time limitations. Nonetheless, the proposed design takes the bio-inspiration from the concept of mimicking the human skeletal muscle functionality. Therefore, a comparison analysis between the mechanical properties of the human tendon and the studied soft materials is performed. Also, the prediction capabilities of the ANN models are evaluated in simulated real-time conditions when being deployed as part of a control system. In here, the design of a clamping mechanism is presented, which is aimed to be the interface between the actuator and a load in a series-viscoelastic actuator.
- **Chapter 8:** The final chapter is reserved for the summary, conclusions, and future work.

CHAPTER 2

Literature Review

2.1 Introduction

This chapter presents the literature review about soft robotic applications implemented in human assistance in the following order. Firstly, the field of Soft Robotics is introduced. Secondly, an overview of many soft robotic applications for human assistance is provided. Thirdly, the terminology around the biomechanics of the human lower limb is introduced. Fourthly, the mechanical properties of the human muscle-tendon component are described. Fifthly, the modelling tools currently being implemented for the prediction of the mechanical properties of soft materials is investigated. Lastly, resulting from the extensive literature review, the gaps on the body of knowledge are identified and described in the summary section of this chapter.

2.2 The Field of Soft Robotics

The field of Soft Robotics deals with the implementation of soft and deformable materials in traditional robotic applications. The interest in this field has increased in the past decade. The latter is due to the outstanding progress in manufacturing of soft and smart materials which can be actuated by heat, light, and magnetism.

The coordination action called RoboSoft, supported by the IEEE Robotics and Automation Society (RAS) and the European Commission, has played a very important role in spreading the awareness of the wide number of soft robotic applications. The RoboSoft committee formally defines the field of Soft Robotics as “Soft robot/devices that can actively interact with the environment and can undergo ‘large’ deformations relying on inherent or structural compliance” [2]. The categorization of when a robotic application fall into the field of Soft Robotics depends on the material’s Young Modulus, a mechanical property which relates the material’s deformation with the amount of stress applied to it; which must be between the range of 10^2 – 10^6 Pascals (Pa). The Young’s modulus is usually a measure of a solid material stiffness; a high value refers to a stiff material in the same way as a low value refers to an elastic or soft material. In the context of Soft Robotics, the term compliance is commonly used instead of stiffness since it refers to the adaptability of the material under certain circumstances.

Early applications in Soft Robotics were inspired in nature, by observing that most biological organisms are not rigid, e.g. the human skeleton only contributes with 11% of an adult’s weight, on contrast, the skeletal muscle in our body only

2. LITERATURE REVIEW

contributes with 42% of the weight [1]. This inspiration gave birth to several soft bio-inspired robots, as well as the interest in studying the embodied intelligence of biological organisms. The latter refers to the ability of biological organisms to adapt to different situations by exploring their body morphology and properties. This is one of the main differences between soft and rigid robots. The embodied intelligence of soft robots releases the controller from the task of accurately controlling the position of the robot and of constantly monitoring the working environment; allowing the controller to focus on the execution of commands. This is only possible with the implementation of soft and deformable materials able to automatically adapt to perturbations from the environment, such as uneven terrains and obstacles. Bio-inspired soft robots are now being developed for a broad range of applications, such as locomotion, manipulation, and even replicating biological processes such as digestion. The research done in the field of Soft Robotics has an interesting multidisciplinary potential. For example, the locomotion of caterpillars and snakes could be studied by building a soft robot which replicates this motion. The knowledge extracted from this could be useful for the development of actuated bendable soft cylinders which ultimately could replace the current rigid tools being used in laparoscopic surgery [20].

The mechanical behaviour of soft materials is very difficult to model using traditional mathematical models due to their non-linear, time-dependent and strain-rate-dependent stress response. This great challenge motivated the research in Soft Robotics to develop bio-inspired soft bodies, arms and legs able to perform the task at hand using minimal control. This caused a shift in the traditional design approach for rigid robots from “rigidity by design, safety by sensors and control” to the design approach used in soft robots, “safety by design, performance by control”. The added feature of safety, inherent in most soft robots, allowed the development of physical human-robot interaction (PHRI) applications [21]. Many other challenges faced by this emerging field are: actuation of soft materials, development and implementation of soft sensors into soft robots, control systems capable to deal with the nonlinear behaviour of soft materials, and modelling tools capable to accurately predict the mechanical behaviour of soft materials in real-time [2, 3]. Most of these limitations come from the simple fact that soft robots cannot be considered as a chain of rigid links able to rotate or slide as common robots are, but soft robots are deformable and continuous which means that all the foundation in which Robotics is based on, is not easily transferable to the Soft Robotics field.

The design and development of soft robots is very challenging, but the potential benefits are many such as: soft robots have the potential of being very dexterous due to the ability of modifying their shape depending on the environment; soft robots can manipulate objects of different shapes, sizes; and most importantly soft robots are safe to interact with humans in the event of an unplanned collision [4]. These benefits highlight the potential of soft robotic applications for PHRI such as, orthoses, surgical tools, and wearable devices. This research aims to contribute to the technological advance of Soft Robotics for human assistance applications.

For a long time, humans have pursued the idea of increasing their strength, stamina and speed through different means. Nowadays, this is a reality due to the technological advances on wearable robotic devices, commonly known as robotic exoskeletons. This wearable device was motivated by military applications where a soldier is required to carry a heavy load in its back for a long period of time, ultimately causing him injuries or early fatigue. The robotic exoskeleton is capable to carry a payload and transmit the payload weight to the ground, ideally relieving the wearer from feeling the payload, which allows the wearer to walk greater distances without premature fatigue. The rigid nature of these devices and the big actuators implemented to achieve forces able to enhance humans, impose many limitations, such as, restriction of body movements, interference on subject natural biomechanics and high inertia which impedes the device to follow the subject intentions smoothly, creating a drag feeling [5].

In the field of Soft Robotics, research is being done to develop a soft version of a robotic exoskeleton, formally called soft exosuit, in an attempt to solve the previously mentioned limitations. Soft exosuits are wearable robotic systems meant to be worn in the same way as clothes, by attaching both the actuation and perception systems into a wearable structure, made of textiles, strapped to the human body which will ultimately assist the wearer's motions. Despite the many benefits of this technology, in comparison to the robotic exoskeleton, current developments of soft exosuits are not capable to deliver enough mechanical power to be called an enhancement device. Currently, soft exosuits are categorized as assistive devices. This limitation is inherent from the idea of having a soft wearable device. The accurate delivery of assistive forces generated by the actuators attached to a wearable textile, or directly to the user's body, is very challenging. In a rigid exoskeleton the reaction forces produced by the actuators are sustained by the exoskeleton mechanical frame, but this is not the case in soft exosuits, where the reaction forces must be

2. LITERATURE REVIEW

dissipated through the worn textile attached to the human body, which generates uncomfortable frictions between the user skin and the textile. Nevertheless, the human body naturally possesses regions capable of sustaining high amounts of forces. These regions are used in soft exosuit designs to prevent discomfort, skin injury, and to increase the efficiency of transmitted forces. The latter principle is implemented in [6] where a lower limb soft exosuit using pneumatic muscles is developed. The other, most common approach is to fix a wearable soft material to the skin, as in [7, 8] where pneumatic artificial muscles (PAM) were attached to a soft cloth and disposed in such a way that they can mimic the biological musculoskeletal behaviour of a human foot. Among the available soft exosuit developments, few of them implements a closed loop control system, due to the high complexity of dealing with the non-linearity of soft materials. These technologies are described in detail in the following section.

2.3 Human Assistance Applications

The adoption of soft robotics in human assistance applications started with the replacement of rigid and bulky actuators, commonly used in traditional robotic exoskeletons, with soft and flexible actuators such as Pneumatic Artificial Muscles (PAMs) and cable-driven actuators. The latter gave birth to hybrid systems as found in [22], where a combination of both the previously mentioned technologies were implemented to overcome the limitation of having high inertia in robotic exoskeletons. The latter work also describes the first attempt of imitating the functionality of the human musculoskeletal system by using cable-driven actuators to transmit the forces created by the PAMs. The latter resembles the functionality of human muscle-tendon component.

During the following years of this adoption process, many rigid devices were implementing soft actuators motivated by the same principle as mentioned earlier. However, in the early stages of soft robotics there was a lack of available soft materials to be implemented as actuators which encouraged researchers to focus mainly on pneumatic actuators [23]. As soft robotics gained popularity, researchers in the field of material sciences started to develop new soft materials capable of functioning as actuators. Nonetheless, more research is required to make these new materials safe to be used in soft robotic applications for human assistance. Due to this, current developments in soft exosuits and soft orthoses are built around two well established

technologies: pneumatic artificial muscles (PAMs) and cable-driven actuators, commonly based on electric motors, using Bowden cables as the pulling element. In a lesser quantity, technologies such as shape memory alloys (SMAs) and shape memory polymers (SMPs) have been implemented in soft orthoses with unsuccessful results mainly due to their large recovery time which make them unsuitable for human assistance applications. The extent of how these technologies have been implemented in soft robotic applications is presented in the next subsection.

2.3.1 Soft Actuation Technologies

2.3.1.1 Pneumatic Artificial Muscles

The usage of compressed air or gases into engineering applications is called Pneumatics, if an incompressible fluid is used, it is called Hydraulics. In Soft Robotics, the latter principles are translated to expand or contract a soft material to generate forces. Nonetheless, this can also be used to produce different types of locomotion in particular soft robots. As previously mentioned, soft pneumatic actuators were extensively researched in different applications for Soft Robotics. In fact, the usage of soft polymers, such as silicone and elastomers, in combination with PAMs enabled different applications such as legged locomotion [24], pneumatic fingers for grasping objects with sensing capabilities [25], soft skin with embedded sensors [26, 27] and even implantable cardiac stimulators [28]. In the field of human assistance, soft pneumatic actuators can be categorized in four main groups: textile muscles, braided fluid muscles (McKibben type), large deformation actuators (LDA) bellows and LDA worms. Only the former three are suitable for some kind of human assistance. However, according to Belforte et al. [23], the most suitable for a biomedical application in rehabilitation are the McKibben muscles due to the advantages described in Table 2.1.

Early works on the assistance of the human lower limbs include the development of a soft orthosis for the foot to treat gait pathologies such as drop-foot [8, 29]. One important aspect of this device is its design, inspired in the musculoskeletal human system. The actuation system was designed to mimic the natural functionality of the muscle-tendon-ligament (Figure 2.1). The soft orthosis is powered by Mckibben-type pneumatic actuators. They are attached to a soft support structure consisting of an adapted neoprene knee sleeve and a five toed leather shoe. A total of three off-the-shelf pneumatic muscles assisted the dorsiflexion, eversion and in-

2. LITERATURE REVIEW

Table 2.1: Main features of pneumatic artificial muscles. Modified from [23].

Muscles Type	Advantages	Limits	Applications
Textile muscles	Easily connected to textiles: they can be used with flat end fittings	Operating pressure range: 1 bar; not negligible hysteresis; contractions of 10%–15%	Biomedical applications in rehabilitation
Braided fluid muscles (McKibben type)	Operating pressure range: up to 4 bar; Higher strength; Negligible hysteresis; Behavior independent of the applied load; Contractions of 25%; Easily connected to textiles: they can be used with flat end fittings		Biomedical applications in rehabilitation
Large deformation actuators: Bellows	Lightweight; Compact; Easy to handle; Large elongations	Possible misalignments in elongation phase	Movement of upper limbs
Large deformation actuators: Worm	Lightweight; Compact; Easy to handle; Large elongations	Low forces	Mini robot

version movements of the ankle joint by generating and transmitting tension forces through artificial tendons made of a flexible but non-extensible metal cables (Figure 2.2(a)). The tendons were located inside a low-friction material tube to minimize losses during transmission; two of these tendons were anchored to a single point in the foot brace while the other one was anchored in four different points in order to distribute the pulling force, again, mimicking the human body behaviour. The artificial ligaments delivered the same functionality as the biological ones, which is to restrict the movement of the tendons in all the directions other than the one of actuation (Figure 2.2(b)). The pneumatic actuators were strategically anchored in two points, at the bottom of the knee sleeve providing nonrestrictive motion of the knee, and at the foot brace.

Another soft orthosis using pneumatic actuation is presented in [30] which extends the concept of embedded sensor and create an embedded sensor-actuator module, which is referred to as a muscle-sensor unit. In order to obtain some degree of compliance with the human lower limb, the device has a cylindrical shape and

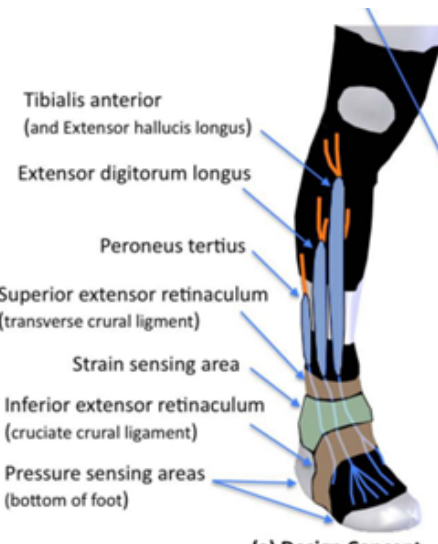


Figure 2.1: Bio-inspired active soft orthosis concept for the treatment of ankle-foot pathologies. From top to bottom: artificial muscles attached to the soft wearable garment, a strain sensor for ankle angle measurements, the tendon-ligament system and pressure sensor for gait cycle detection [8].

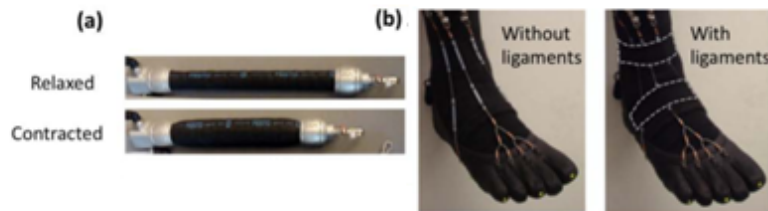


Figure 2.2: Soft orthosis components, (a) pneumatic artificial muscle in its relaxed and contracted state, (b) complete tendon-ligament system without ligaments and with ligaments [8].

it is made of a flexible silicone elastomer (EcoFlex 0300). The muscle-sensor units are embedded into the latter shape to form a distributed array of four columns and four rows (16 actuators), allowing the device to have a wide range of motions and assistive torques depending on the number of active actuators (Figure 2.3). During the casting process, each column of actuators is tied to each other with Kevlar fibres so they can pull each other when contracting. The fibres are anchored to both caps of the cylinder to create the desired movement. When the pneumatic muscle is activated, its radius increases and its length decreases, creating a compression force. This design provides some degree of modularity due to the large number

2. LITERATURE REVIEW

individually-controlled actuators used. Nevertheless, it has little compliance with the human lower limb which ultimately complicates the conversion of generated forces into assistive torques.

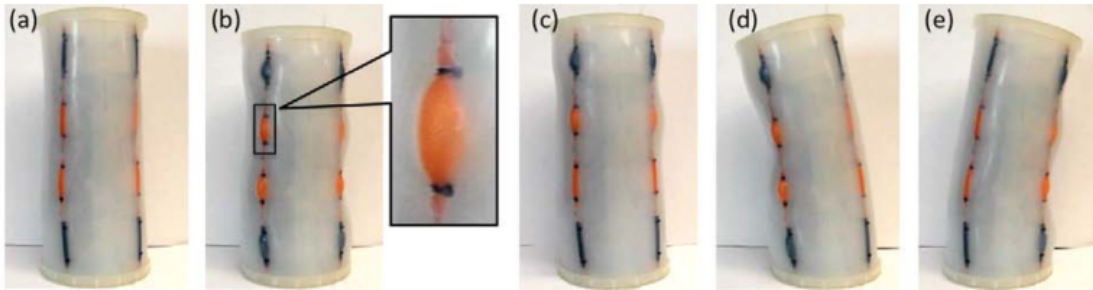


Figure 2.3: Soft sleeve prototype. (a) Original shape. (b) All muscles activated, contracting the whole body and amplified image of one muscle. (c) Partial contraction, only the 1st and 2nd top rows are activated. Both (d) and (e) illustrate bending movements, only two adjacent columns are activated [30].

In recent works, the virtual anchor technique, a very novel concept which uses pneumatic artificial muscles is described [6]. This concept, attempts to address the challenges on force transmission using soft materials attached or strapped to the skin, such as discomfort and slippage. The key anchor points of the human body are defined as the ones exhibiting large bony landmarks. These regions are capable of withstanding high forces and of minimizing the slippage or chaffing of soft materials positioning on them. The virtual anchor technique is also motivated by the changes in length of some parts of the skin surface during joint motion, where some parts exhibit more changes than others. The soft exosuit was developed by interconnecting PAMs and nylon straps, replicating the extensible and non-extensible paths of the skin, respectively, in the specific points where the changes in the skin length take place. These places are called virtual anchor points which in combination with the key anchor points allow a good transmission of forces without causing discomfort to the user. The concept is illustrated in Figure 2.4, where the orange lines represent the pneumatic actuators interconnected with the key anchors and the virtual anchors. These interconnections constrain the actuator movements other than the desired, as well as redirect the actuator reaction forces to the areas of the body capable of withstanding these forces. Finally, this design was able to reduce the metabolic cost caused by wearing the complete device (10 kg), by almost 100%. Considering that no control system, other than a timed activation sequence, and no perception

system was implemented, this technique opens the door for further improvements to achieve a better degree of assistance.

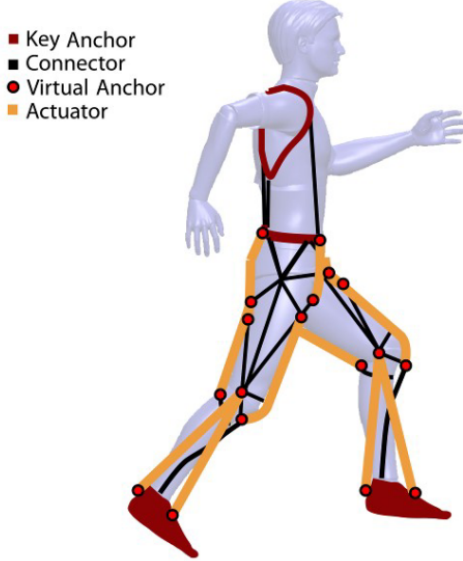


Figure 2.4: Virtual anchor concept. The three key anchors (red square) located at the foot, hip and shoulder are interconnected with the soft actuators (orange) and auxiliary connectors (black) in specific points called virtual anchors (red circle) to stabilize the forces created by the actuators [6].

Putting aside the McKibben-type actuators as the most common choice for pneumatic muscles, elastomers such as high-flexible silicone can be used to build PAMs as shown in [31]. This PAM consists of interconnected flat chambers made of silicone rubber which inflate when pressurized air is injected (Figure 2.5), the innovative concept in this work is the zero-volume air chamber which provides a higher degree of compliance and compactness (traditional PAMs retain air inside them even when they are not actuated). Kevlar fibres are embedded inside this soft actuator to constrain the expansion direction, creating a contraction movement when pressurized. The flatness of these actuators simplifies the casting process. Furthermore, the chamber-based design makes it possible to join each chamber together not only in series, which increases the contraction length, but in parallel as well to increase the contraction force. In order to test the actuator performance, a soft exosuit similar to the previously described was developed using nylon straps and hooks to connect the soft actuator to the points of interest. The developed soft orthosis, intended for infant-toddler rehabilitation, was capable of delivering a 38 N contraction force and 18 mm contraction length by implementing a muscle with an array of four elastomer

2. LITERATURE REVIEW

actuators inter-connected in series. In addition, a total excursion for the knee joint of 132° was achieved, considering both flexion and extension motions (Figure 2.5). Moreover, in a most recent development by [32], it can be found the implementation of elastomers for ankle assistance, in this case the pulling force of the PAM is generated when the actuator deflates and a pushing force is generated when it inflates, an inverted behaviour in comparison to previously mentioned applications. This soft orthosis consists of a regular sock which is attached to both ends of the PAM, that is enclosed into textile to restrict its longitudinal and radial expansion mainly. Despite the simplicity and assistance capabilities of the device, it cannot be worn with shoes, restricting the assistance to indoor activities

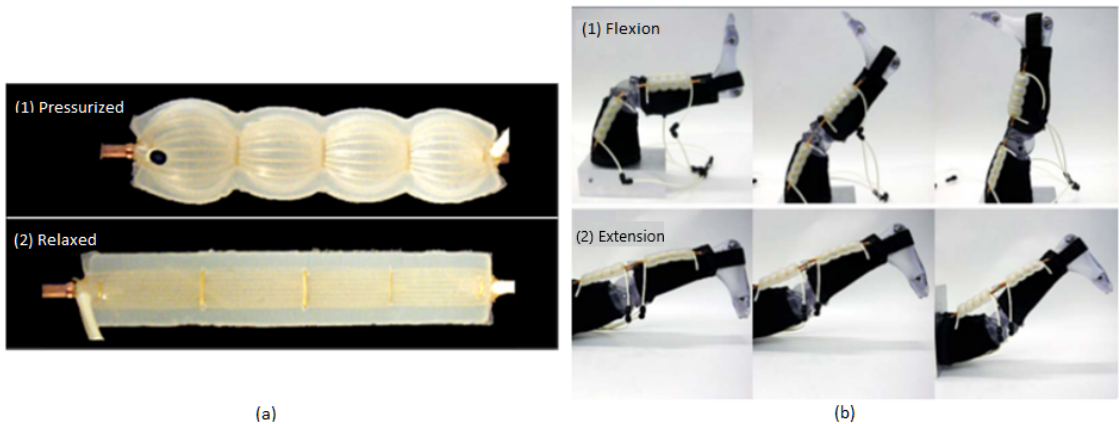


Figure 2.5: (a) Flat elastomer pneumatic actuator in (1) pressurized and (2) relaxed states. (b) Implementation of the flat actuator in medical leg model assistance, along with the achieved (1) extension, and (2) flexion motion [31].

This concept, of expanding instead of contracting the PAM when pressurizing, is called Inverse PAM (IPAM). This soft actuator is called ‘Hydro Muscle’, and is directly compared with McKibben muscles since it overcomes the main limitations of the latter. The main difference between this actuator and the previously mentioned is the shift from pneumatic technology to hydraulics, in fact, it is reported that the pressure found in homes tap water is enough to actuate it [33]. Therefore, the cylindrical shape ‘Hydro Muscle’ is capable of elongating axially, increasing its stiffness radially, when pressurized; and of the exact opposite behaviour when depressurized (Figure 2.6). The actuator functionality is due to two structural layers of different materials. The inner layer is a tube made of an elastic material (latex showed better performance than the commonly used silicon) and the outer layer is made of a soft but inelastic material, such as polyester, which restricts the inner

layer radial expansion and allows its axial expansion. Despite the simplicity of the design, this new concept of actuator is free of energy losses in radial expansion. Also, the energy losses inherent when using compressed air as the power source are not present in this design (in comparison to PAMs).

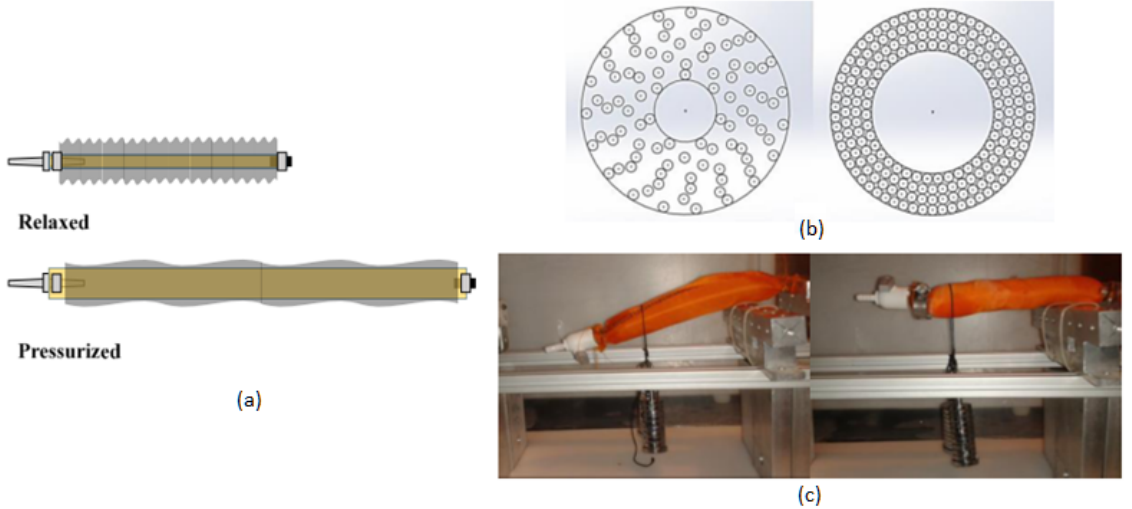


Figure 2.6: (a) IPAM developed in its relaxed and pressurized state, the small radial expansion and large axial expansion is appreciated. (b) Cross-sectional view of the jamming effect ongoing inside the actuator, and (c) bending effect caused by heavy load, and correction of the bending using the jamming effect [33].

The experiments performed in this work showed that this innovative soft actuator is 33% more efficient in comparison to a McKibben muscle using hydraulics. Furthermore, this actuator can be easily manufactured with off-the-shelf components. Nonetheless, the convenience of using both pneumatic and hydraulic muscles for performing pulling instead of pushing tasks, is to prevent the bending effect caused when the actuator is fixed in one of its ends and has a heavy load attached to the other end. The latter effect is amplified for pushing tasks being one of the main drawbacks of the proposed actuator concept. The solution to this is to use the principle of jamming by filling the gap between the inner and outer layer with granular media which will jam when the actuator is pressurized (Figure 2.6). Another IPAM which implements a very similar concept as the one illustrated in (Figure 2.6) can be found in [34]. This IPAM managed to achieve a strain of 300% of its length, which is three times more the achieved strain of the IPAM illustrated in (Figure 2.6). This improvement is achieved due to the complete restriction on the stretchable material in the inner layer to only expand along its axis and not radially. The main benefits

2. LITERATURE REVIEW

of recent IPAMs in comparison with traditional PAMs are: high strain and nearly linear control (since no radial deformation is present). Finally, the ability to achieve high strains make IPAMs suitable for joints like the elbow.

2.3.1.2 Cable-driven Actuators

Another actuation technology implemented in soft orthoses is cable-driven actuators, based on electric motors, in combination with Bowden cables. Following the same principle as pneumatic muscles, this technology relies on generating tensions along a cable which, with a right positioning along the human lower limb, can transmit torques to the human body. The work in [35] presents the design and implementation of a battery operated soft exosuit built with Bowden cables (Figure 2.7).

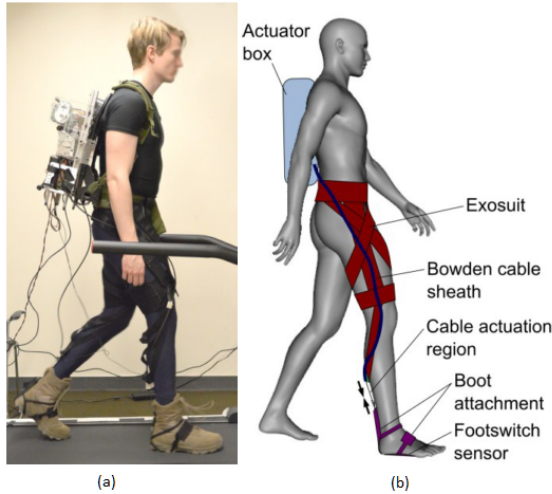


Figure 2.7: (a) Developed Bowden cable-based soft exosuit prototype. (b) Initial design concept highlighting the main parts of the soft exosuit [35].

The exosuit is based on the leg's muscles functionality during normal walking, with the objective of assisting the forward propulsion stage of the gait. The soft exosuit structure made of fabrics is attached to the waist and above the knee, from the former the Bowden cable follows a path of webbing straps into the lower limb, ending at the ankle. In order to minimize the chaffing and displacement on the webbing strap structure caused by the tension on the cables while actuated, the strap along the waist of the user terminates at the hip which is a natural bony part of the human body. In other words, there is almost no muscle and fat tissue between the skin and the bone, which improves the transmission of forces without causing discomfort to the user. This soft exosuit delivers 18% and 30% of the

torques required for normal walking on the knee and hip, respectively. However, despite the innovative design, the main limitation of this exosuit structure is the large displacement experienced on its structure, of 13 cm, when the cables are under tension. This displacement caused the cable-driven actuators to have a very low efficiency since almost 45% of the generated mechanical power is lost in the form of friction forces in the soft exosuit structure. Nonetheless, the proposed multi-joint concept allows the actuation of two joints using a single actuator.

Following the multi-joint actuation concept, another soft exosuit is designed in [36] with the objective of not only providing assistance but also to enable impaired users. This concept, illustrated in (Figure 2.8), exploits the benefits of using a single cable-driven actuator to control more than one joint, i.e. multi-joint actuation. The difference in this case is the deep analysis performed regarding the compatibility of the joints, taking into account synergy of torque and equal polarity of torque. In order to assist the desired movements of sit-to-stand, walking and stairs ascend, the knee and the hip joints were selected as the most suitable combination. Despite the limited scope of this work, being focused only on the concept design, the authors expect the selected joint combination to support the movements of sit-to-stand and stairs ascend.

The next follow up on the concept of multi-joint actuation is documented in [37] where a testing platform for soft exosuits was developed. The aim of this platform is to study the performance of the multi-joint actuation concept when being implemented in different soft exosuits. The off-board platform integrates several cable-driven actuators and the sensors required to evaluate their performance. In addition, this platform can deploy sensors to be attached to the exosuit and compare relevant metrics such as mechanical power efficiency. This platform, which can be reconfigured to meet different applications, has been used to evaluate the advantages of implementing single joint and multi-joint actuation, highlighting the benefits of the latter [38]. Furthermore, the study performed with the aid of this platform provided designing parameters for the development of an exosuit, in other words, the multi-joint platform assists the designing phase, ultimately reducing designing times.

2.3.1.3 Shape Memory Materials

The two main groups of shape memory materials implemented in soft robotics are: shape memory alloys (SMAs) and shape memory polymers (SMPs). Both technolo-

2. LITERATURE REVIEW

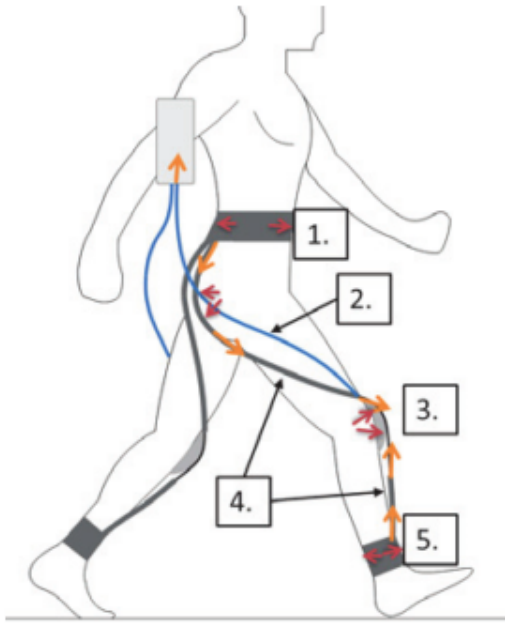


Figure 2.8: Multi-joint actuated soft exosuit. There are two anchor points, one at the pelvis (1) and one at the shank (5). The suit is actuated by a bowden cable (2) and positioned at the front of the knee. The contractile element is connected to the two anchors by webbing elements (4). Knee module to increase the lever arm (3). Red arrows: reaction forces, and orange arrows: actuation force [36].

gies function under the same principle: they can switch to a different shape when a stimulus such as heat is in contact with them. Nevertheless, there are some differences to be mentioned. The SMAs have two main phases, one for high temperature (austenite) and one for low temperature (martensite), when they suffer deformation while being in the martensite phase they can recover from the deformation by exposing them to heat, therefore SMAs convert the energy from heat into mechanical energy to return to their original shape [39]. This property is usually exploited to cause contraction changes in the material (Figure 2.9). Therefore, SMAs are commonly used in combination with cable-driven actuators.

The implementation of SMAs into robotic applications have three main challenges to be addressed: response speed, high power consumption and low operational bandwidth. The functionality of SMAs is based on the property found in metals in which heat is generated when an electric current flows through it, this is also known as the Joule effect. Depending on the metals used in the alloy, the amount of heat

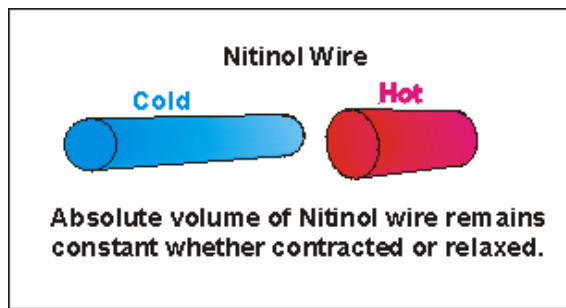


Figure 2.9: Shape memory alloys made of Nitinol. The contraction effect under the increase in temperature is illustrated [39].

required for the SMA to recover from deformation is high enough to melt plastics, this excess of energy is what makes SMAs inefficient [40, 41]. Furthermore, SMAs have a very low response time due to the large amount of time required to cool them down, limiting their operation frequency. This limitation is only present when air convection is used as the cooling process. Due to this, SMAs have been found to be unsuitable for most orthoses in which an operating frequency of roughly 6 Hz is required. However, plenty of authors have successfully developed the latter devices, in both rigid [42] and soft variations [43], capable of assisting human motions. This proves the feasibility of using SMAs for applications such as clinical rehabilitation where slow and repetitive cycles are required [44, 45]. An example of these applications are: re-positioning, muscle toning, functional exercise and assistive robotics [46, 47]. Currently, extensive research is being done to address the main limitation of SMAs, as documented in [47].

J. Zhang proposed a novel SMA-based artificial muscle [48]. This configuration facilitates the addition of a cooling system, due to the cylindrical hollow shape of the artificial muscle. Therefore, a mini pump is used to create a flow of air inside the artificial muscle, effectively reducing the cooling time by 10 times. The performance of this artificial muscle is further improved by considering the hysteresis behaviour typically found in SMAs when shifting between the low and high temperature phases. Furthermore, there is again evidence of trying to replicate the muscle-tendon functionality, in this case by adding a spring in series with the artificial muscle which aids the SMA recovery phase. The latter simulate a more realistic behaviour, similar to the human muscles behaviour. Moreover, this is the first documented work that deals with the modelling of the actuator behaviour, allowing the implementation of a robust control system which can be also used in other scenarios involving SMAs. Finally, this artificial muscle is deployed as part of an active foot orthosis capable of

2. LITERATURE REVIEW

large contractile forces by using in parallel more than one SMA wire to form each of the pulling tendons (Figure 2.10). Low efficiency and low operational bandwidth were identified as the main drawbacks of this design.

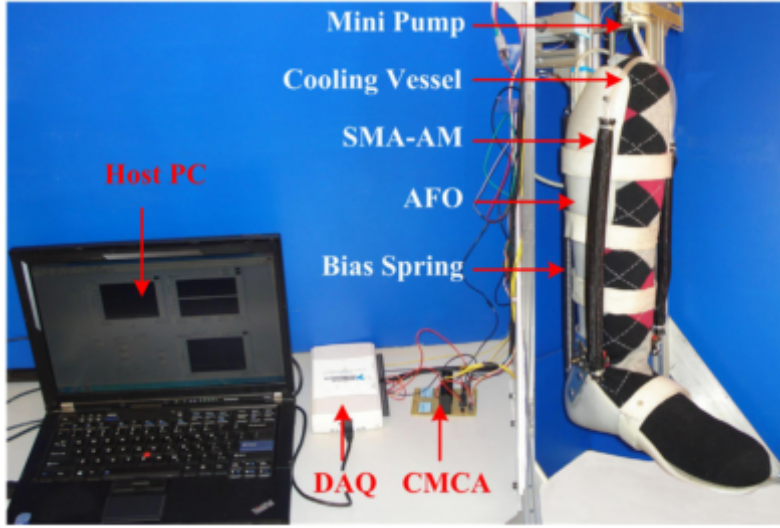


Figure 2.10: Ankle joint soft orthosis. The developed SMA artificial muscle along the main parts are highlighted. [48].

Current SMAs are also limited by the amount of contraction they can achieve, i.e. operational bandwidth, which is commonly 3% of its original length. Recent solutions to this, are based on deploying the SMAs in several loops, exploiting the same concept of using pulleys with cables, essentially increasing the usable length of the SMA wire without increasing the size of the final actuator. However, relying on pulleys in a soft actuator greatly reduces compliance, increases the actuator weight, and may cause twisting between the individual turns of the SMA wire. Therefore, a new approach described in [49], make use of the outer sheath of Bowden cables to contain the SMA wires inside. This concept allows the SMA to be directed in many ways to the point of interest, allowing the actuator to have different shapes that can be compliant with the user's body, e.g. the SMA can be wrapped around the user's arm in a solenoid-like shape which also increases the SMAs wire length (Figure 2.11). Furthermore, pulleys are also implemented to allow the SMAs to have a maximum number of three turns contained inside the Bowden sheath. Two main drawbacks were discovered during an experimental testing: SMAs wires were twisting between each other which caused high friction losses and prevented the SMA to completely recover its initial length; the other drawback was the Bowden sheath material which was found to have low force transmission efficiency. In order

to solve the latter, the Bowden cable sheath made of nylon was replaced by flexible tubes of Polytetrafluoroethylene (PTFE) and every SMA wire turn was individually encased in a narrow-gauge sheath. The final experiments showed that the developed actuator is capable to contract 9% of its length which is three times the theoretical contraction length of an SMA wire.



Figure 2.11: Flexible wrist exoskeleton prototype. [49].

Shape memory polymers (SMPs) are a little bit more complex than SMAs. They have two main phases: a glassy state (high stiffness) and a rubbery state (low stiffness). Furthermore, when they are in their rubbery state, they can be deformed by applying small forces and preserve the deformation by cooling the SMP. In this state, the SMP can be considered rigid and it has to be heated to the point of the transition temperature to return to its original shape, hence having shape memory. This property of preserving a deformation is analysed by K. Takashima et al. in an attempt to boost the McKibben artificial muscle performance [50]. McKibben actuators are unable to maintain their contraction shape unless precise and continuous control is implemented which cause premature wear on controlling elements as well as higher energy consumption. Therefore, a SMP is embedded into the McKibben braid which, by controlling the SMP temperature, allows the artificial muscle to hold its contracted position as illustrated in Figure 2.12. It is worth mentioning that SMPs can be stimulating in different ways to obtain the change of shape, such as infrared light, electric field, magnetic field and even manipulating the material water content. In the previous work, the SMP was stimulated by heat and cooled down using a compressor, which drastically limits the actuator portability.

The benefits of SMPs, in comparison to SMAs, can be summarized as: lightweight, low cost, rigidity in low temperature and flexibility in high temperature,

2. LITERATURE REVIEW

higher strains (around 400% in comparison with 7% for SMAs), and they can be easily moulded into 3D shapes. Furthermore, the main positive aspects of the improved McKibben artificial muscles are: allows rigidity fixing, the parameter to control stiffness can be used to control actuation, and controllability of the actuator surface by individually stimulating certain segments of the SMP.

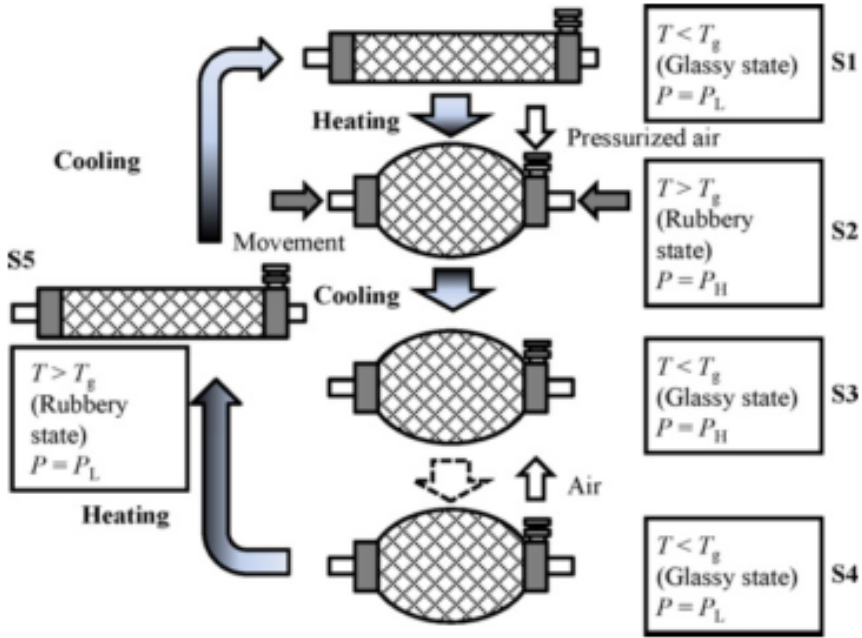


Figure 2.12: Schematic illustrating McKibben with embedded SMP functionality. T_g : transition temperature, P_H : high pressure, P_L : low pressure [50].

2.3.2 Soft Perception Technologies

Currently, the most common soft perception technologies are based on liquid metal alloys embedded into soft materials such as elastomers. These strain soft sensors are widely used in soft orthoses, such as the one in [8]. The materials used in this case were Eutectic Gallium Indium (eGaIn), as the liquid metal alloy, and silicon rubber as the flexible layer, which creates a highly deformable sensor (Figure 2.13). The sensor was implemented to measure changes in the ankle joint proportional to the skin strain which it was attached to, by measuring the changes in resistance caused by the variations in the path length and cross-sectional area of the channel containing the liquid metal. Nevertheless, the developed soft orthoses implemented two other non-soft sensors: an inertial measurement unit (IMU) as an angle position

detection and a pressure sensor attached to the shoe insole to detect foot strikes, hence the gait cycle. The developed strain sensor delivered good performance and contributed in the development of a feedback controller for this soft orthosis.

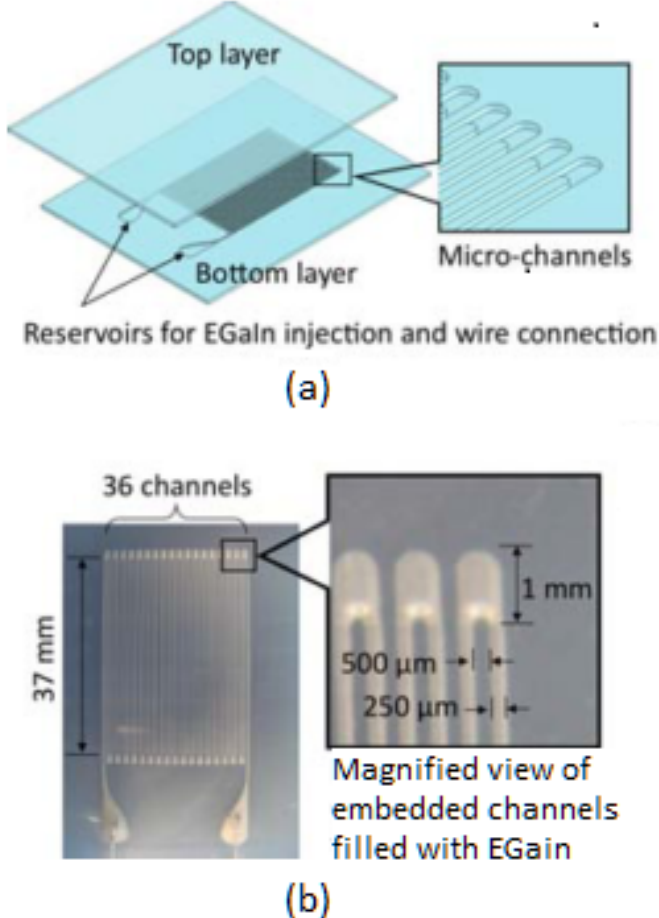


Figure 2.13: Soft strain sensor. The microchannel filled with liquid metal can be appreciated in: (a) concept design and (b) the prototype [8].

Liquid metal alloys are also implemented in [30], as previously described, in the form of embedded muscle-sensor units (Figure 2.14). The soft strain sensor was capable of estimating the contraction length of a pneumatic muscle by measuring its radial expansion. In order to preserve softness, thin flexible copper wires were embedded into the cylindrical soft orthosis to obtain the sensor readings.

Taking the application of soft strain sensors with eGaIn a step further, a wearable soft suit capable of sensing the joint angles of the hip, knee and ankle joints, is presented in [51]. With the sensors properly positioned along the lower limb, by measuring the strain caused by the joint rotation, the joint angle can be known. The sensors tracked the user motions with a mean absolute error of 8°, being the

2. LITERATURE REVIEW

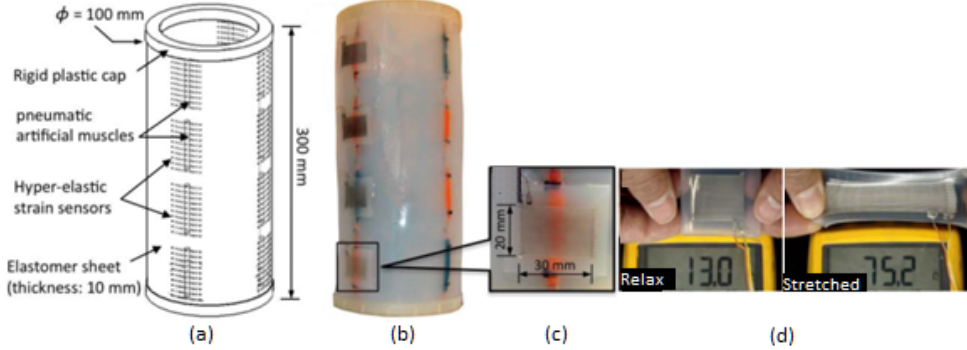


Figure 2.14: Soft sensor sleeve: (a) design concept, (b) developed prototype, (c) magnified view of the embedded sensor-actuator concept. (d) Soft strain sensor change in resistance during stretch and relax [30].

most precise tracking achieved on the hip joint and the less precise on the ankle joint. In the mentioned work, only sagittal plane motions were measured, however, due to the great success and linearity of the sensors, they are planned to be implemented to measure motions in the frontal plane as well. The complete suit characterization can be found in [52], and is illustrated in Figure 2.15.

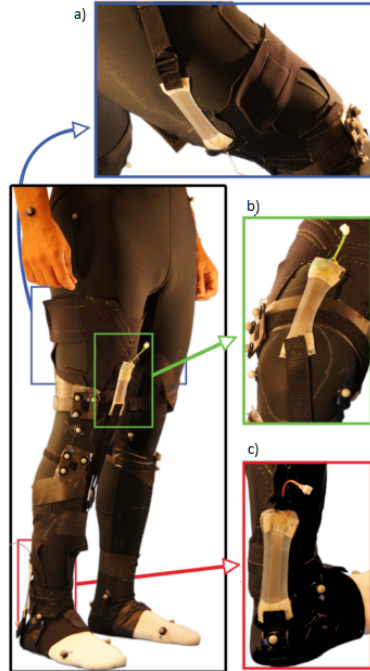


Figure 2.15: Implementation of soft strain sensors into a Soft sensing suit, (a) hip sensor, (b) knee sensor and (c) ankle sensor position [51].

A potentially improved version of these soft strain sensors is presented in [53]

where the highly stretchable elastomer is filled with two different conductive liquids, a traditional liquid metal and an ionic solution, instead of one. Interconnecting the strain soft sensor with the external application has been a big challenge, since the strain caused by the connection, usually soft wires, affects the sensor accuracy by increasing the total electrical resistance and by generating additional strain. Nevertheless, the ionic solution is intended to decouple the signal routing part from the sensing part to solve the latter challenge, creating a noise-free interface with the external application (Figure 2.16).

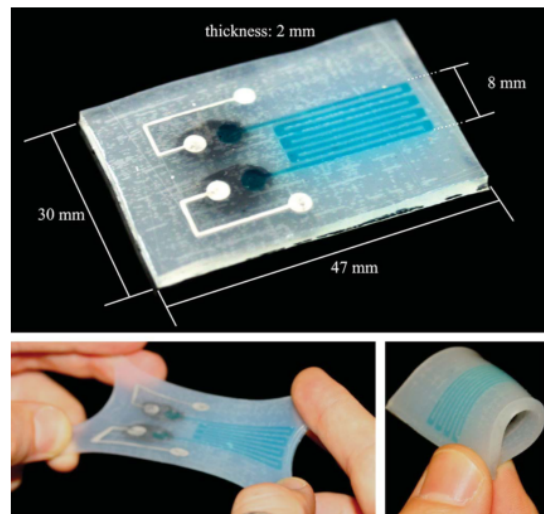


Figure 2.16: Hybrid soft strain sensor, the interface between the liquid metal and the ionic solution can be clearly seen in dark areas [53].

One direct implementation of the embedded microchannel with conductive fluid sensors, can be seen in a recent improvement to the McKibben type PAM (Figure 2.17). McKibben actuators were widely adopted in soft robotics applications and there is plenty of information in the literature about their implementations. However, accurately sensing the deformation and force of these actuators still remains challenging. This has been addressed in many ways such as: cylindrical dielectric elastomers with carbon grease disposed on their surface to function as electrodes [54]; and also by attaching soft elastomer sheaths to the actuator, which are capable of sensing deformation due to their microchannels filled with conductive fluid [55]. The implementation of carbon grease electrodes and conductive microchannels allows the measuring of the actuator deformation. The conductive elements, mentioned before, change their electrical resistance when they are deformed. Furthermore, the concept of attaching these sensors to the actuator was refined in

2. LITERATURE REVIEW

[56, 57], where the sensing elements surrounding the actuator are now disposed in a helical shape. From the electric circuit created, it is possible to measure both the output force and length deformation of the actuator by correlating them with the circuit resistance and inductance respectively. This work proposed the implementation of conductive wires to build the reinforced braid of a McKibben actuator allowing the actuator to ‘sense’, from there the given name of ‘Smart Braid’, creating a solenoid-like circuit from which the inductance can be measured using a couple of mathematical approximations such as: the Neumann approximation and the long solenoid approximation, being the former one the most accurate and general; but at the same time the most expensive in terms of computation. The author exerts that this new sensing concept can be applied to multitude of scenarios in soft robotics, which includes soft orthosis.

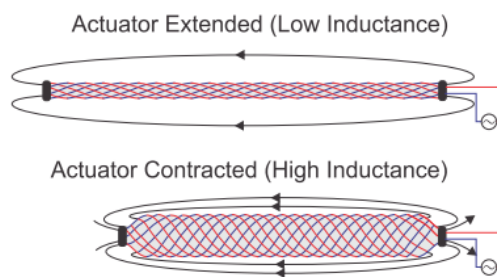


Figure 2.17: ‘Smart Braid’ concept. The variation in the actuator length cause a change in the electric circuit inductance [57].

2.3.3 Control Technologies

One of the successfully implemented control systems is documented in [8], which forms part of the previously mentioned concept illustrated in Figure 2.13. The control system is composed of several micro-controllers for parallel processing, and is divided in four main stages: sensing, signal processing, control and actuation (Figure 2.18). The soft orthosis makes use of three different sensor technologies which requires different sampling and signal processing algorithms for each one, the IMU being the most complex one. Thereafter, another micro-controller with access to all the sensors, decides when to activate the solenoid valves that control the pneumatic muscles by generating pulse width modulated (PWM) signals. The latter describes a basic proportional control system. No mathematical model was deduced to describe the non-linear behaviour of the pneumatic muscles, instead, simpler

controller approaches as feed-forward and feedback controller were implemented, with the latter being able to achieve a response time of 500 ms when a perturbation was present on the system, such as letting a weight hang from the device toe. The feedback controller made use of a soft strain sensor (Figure 2.13) to correct the ankle angle. Finally, although the controller performance is good it is still not enough to provide active gait assistance nor to predict user intentions. Another drawback is that the system requires calibration every time a new user wears it. Nevertheless, the developed soft orthosis is suitable for rehabilitation because it can achieve a dorsiflexion of 12° and 20° when foot was at resting position, and when foot was forced to a plantar flexion position, respectively. Moreover, the perception system could provide the clinician with meaningful data about the patient progress. The previous work was continued in [7] where a new controller was designed by considering the interaction between the soft exosuit and the human body as a black box, i.e. instead of trying to model the non-linear behaviour of the whole system some experiments were performed to obtain a system input/output relationship. Following this, classic control techniques were implemented to model a linear time-invariant controller. The results were promising since the original complex system performed adequately using simple techniques. Finally, the implementation of electromyography sensors was discussed to add the involuntary muscle contractions of the user into the system as a disturbance and improve the accuracy during different scenarios.

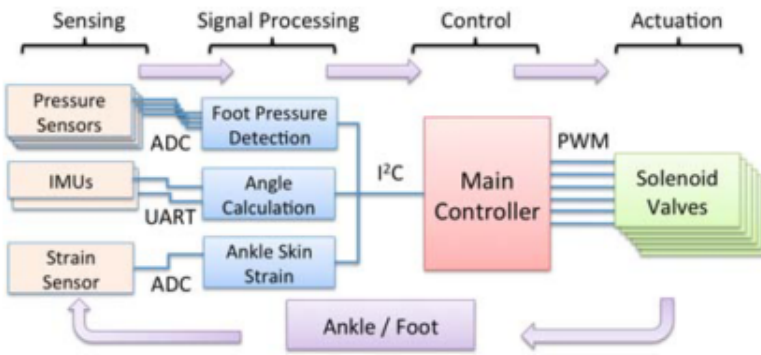


Figure 2.18: Control system architecture implemented for the ankle soft orthosis [8].

In some cases, the design and development complexity of a control system for soft robotic applications limits the research to focus only on the implementation and study of the soft actuation and perception systems. This is the case for the work documented in [30], the cylindrical soft sleeve with embedded muscle-sensor units. In the latter work, the developed controller is well designed but does not

2. LITERATURE REVIEW

implemented a close-loop architecture nor complex mathematical models to predict the soft material behaviour. The control system consists of several micro-controller units, each of these communicating with their surrounding neighbours (Figure 2.14). Each of the 16 nodes embedded into the cylindrical soft sleeve has a microcontroller unit with independent functionalities, such as collecting and distributing the data. On top of this, there is a scheduling routine embedded in each unit which allows synchronization between them. Every unit has four tasks to execute at a given time and a given order: sensing, communicate, process data and actuate. The actuation parameters are generated using a mathematical approximation of the soft material behaviour which assumes no other deformation around the soft sleeve is caused by the compression of the pneumatic actuators. This assumption neglects the fact that when one side of the cylinder is under compression, the opposite side is under tension, i.e. the length on this side does not remain constant. The authors highlighted the necessity for a better approximation method when analysing the experimental results. For a desired bending angle of 15° , an actual bending angle of 11.5° was achieved. In simulation, feeding the soft sensors data into the mathematical approximation, a bending of 13° was estimated, which translates into an accuracy of 76%.

The fact that few soft exosuit developments fully implement a control system does not imply that no research is being performed in the field. The implementation of current soft actuators into functional devices, as well as the proof of concept of emerging soft actuators are usually followed by an extensive study about modelling their behaviour to translate that information into a control system. On the field of PAMs, many interesting new approaches are being researched, such as implementing fuzzy logic techniques to improve their performance [58–61]. The next step in the research cycle of all soft actuation technologies is to implement the tested models into functional devices, which then will allow new concepts to be developed, hence new modelling research to be performed.

2.4 Biomechanics of the Human Lower Limb

The biomechanics of the human lower limb are self-contained between three planes of action, which are the sagittal plane, the frontal plane and the transverse (horizontal) plane [62]. In combination with these planes there are three axes used to identify specific motions: frontal horizontal axis, vertical axis and sagittal horizontal axis.

The positioning of each of them is illustrated in Figure 2.19. The sagittal plane divides the body vertically into left and right parts, the frontal plane divides the body vertically into front (posterior) and back (anterior) parts and the transverse plane divides the body horizontally into upper (superior) and lower (inferior) parts. This coordinate system allows the many motions of each joint in the human body to be clearly identified.

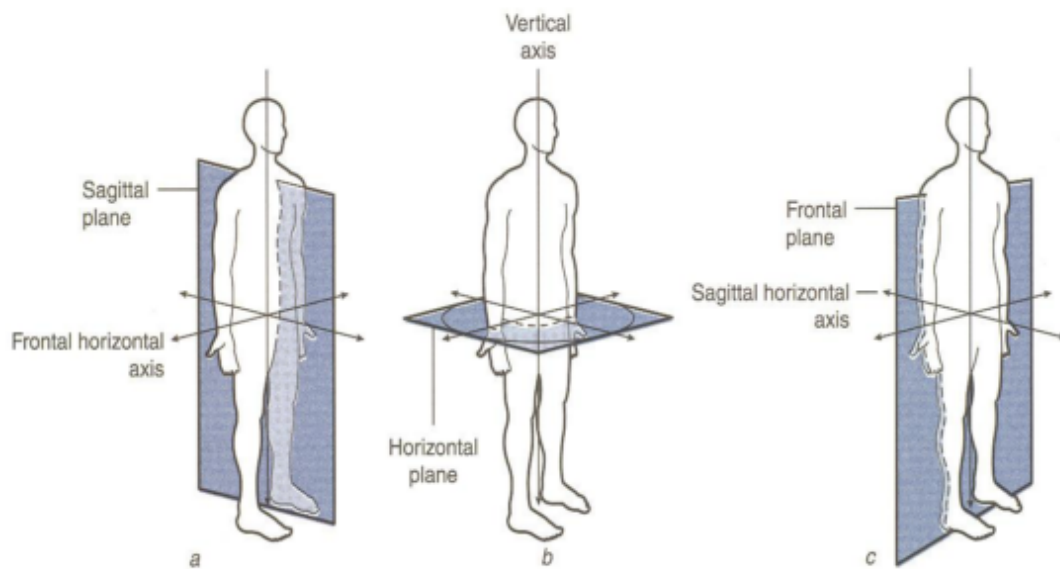


Figure 2.19: Dimensional spaces used to understand human motions: (a) Sagittal plane, (b) Horizontal plane and (c) Frontal plane [62].

2. LITERATURE REVIEW

The motions of each joint are named with respect to the plane and axis where they happen. This allows the easy recognition of the human body motions (Figure 2.20). The biomechanics of the lower limb are categorized in five groups, each containing two individual motions, as follows:

- Flexion and extension describe the bending motion which decreases, or increases the angle between two parts of the body, respectively.
- Abduction and adduction describe the motion away from, or towards the body midline, respectively.
- Eversion and inversion of the foot describe the motion away from, or towards the body midline, respectively.
- External rotation and internal rotation describe the motion away from, or towards the body midline, respectively.
- Horizontal abduction and adduction describe the motion away from, or towards the body midline, respectively.

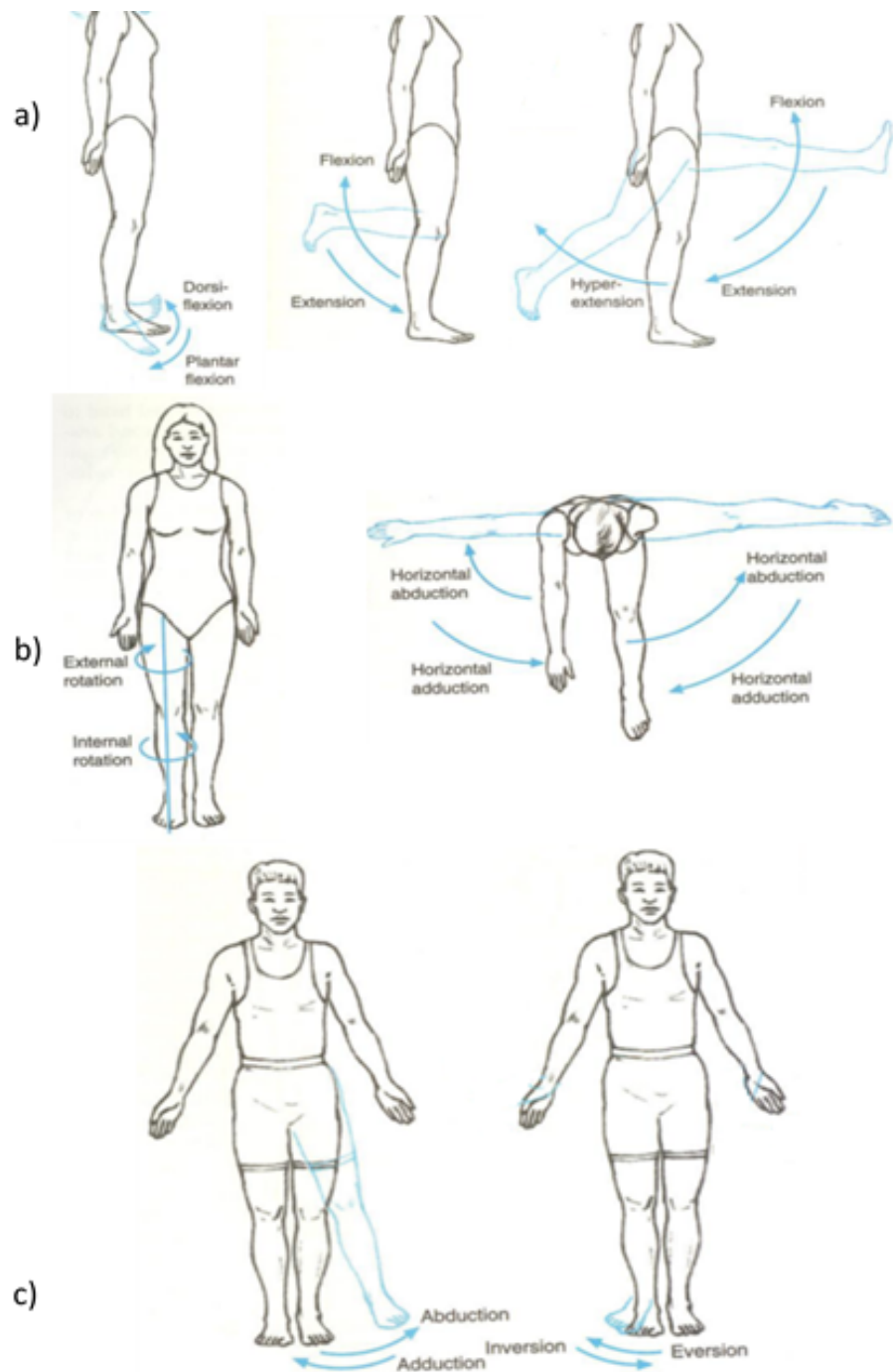


Figure 2.20: Lower limb motions for (a) sagittal plane, (b) horizontal plane and (c) frontal plane. Image adapted from [62].

2. LITERATURE REVIEW

2.5 The Muscle-tendon Component

Having defined the terminology involved in the biomechanics of the human skeletal muscle system, this section focuses on describing the muscle-tendon component from a mechanical point of view. In the literature, the mechanical model commonly used to describe the mechanical behaviour of the muscle-tendon component is the Hill's model [63]. This model is considered the most representative of all the available models [64]. Hill's model describes the skeletal muscle as a three elements system, which contains a contractile element, a passive element, and a series element. The contractile element (CE) represents the muscle fibres in charge of generating the contractile forces, the parallel (passive) element (PE) is formed by the tissue surrounding the muscle which prevents it from over stretching, and the series element (SE) represents the human tendon, as illustrated in Figure 2.21.

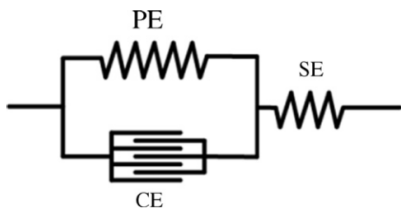


Figure 2.21: Hill's model of the skeletal muscle. The contractile element (CE), the parallel element (PE) and the series element (SE) are shown [63].

Hill's model makes the important assumption of considering the SE to be purely elastic, i.e. the deformation of the element is entirely dependent on the force applied to it. Nevertheless, the non-linear viscoelastic properties of the human tendon are acknowledged in his work. The latter simplification is a common practice among studies of the skeletal muscle system because the muscle and tendon are studied as a whole (muscle-tendon component) [65]. Evidence of the actual benefits of this simplification is found in the literature for the field of robotics exoskeletons. The complex muscle-tendon model developed in [66], considered the viscoelastic properties of the human tendon to estimate forces and joint torques in real time. The model achieved high accuracy at the cost of high computational load. In an attempt to reduce the computational load, the assumption of an infinitely stiff tendon was made which proved to be reliable as well [67].

In a similar way, developments in the field of soft robotics which are inspired in the skeletal muscle system functionality are also based in Hill's model, as highlighted in Section 2.3.1. Commonly, springs [8] or Bowden cables [48] are implemented as

the SE of the muscle-tendon model. Nevertheless, the fact is that the human tendon has viscoelastic properties [68]. Most of the documented literature is mainly focused on developing and testing soft materials to be used as the contractile element in soft artificial muscles. The latter, previously identified as a research opportunity, indicates that the viscoelastic properties of soft materials have not been studied with the aim of developing a soft artificial tendon, which in combination with current soft artificial muscles could deliver better performance in soft robotic applications for human assistance.

Tendons are connective tissues that link muscles with bones. They have a non-linear viscoelastic behaviour, i.e. the proportional relationship between the reaction force experienced by the tendon and the applied deformation is not constant throughout the whole range of possible deformations. This reaction force is also dependent on the history of previous deformations. At rest, the collagen fibres (core components of tendons) are in a relaxed wavy state. When the tendon experiences a tensile force, the collagen fibres are easily stretched and realigned, opposing little resistance to deformation. However, when the collagen fibres are completely stretched they begin to offer more resistance to deformation which is proportional to the applied force. Finally, fibres can be stretched to their limit and failure of the tendon will occur [69]. This non-linear response to the applied deformation is better explained using Figure 2.22 where the characteristic S-shape curve for a tendon stress-strain curve is appreciated.

The stress-strain curve in Figure 2.22 illustrates the mechanical properties of a human tendon. The stress is described as the tensile force per cross-sectional unit area experienced by the tendon. This stress causes the tendon to elongate. In the chart, the elongation is represented as the strain, which is the tendon deformation in relation to its original length. Along with the stress-strain curve, the force-elongation curve is also used to visualize the mechanical properties of tendons. These experiments are performed in a static state, i.e. the strain rate is the same throughout the whole experiment. Therefore, they do not provide any information about the viscoelastic properties of the tendon.

Viscoelastic materials exhibit both elastic and viscous characteristics. Viscosity describes a fluid's resistance to flow, the more viscous a fluid is, the more slowly it will flow and vice versa. The latter suggests a time-dependent behaviour. In the case of viscoelastic materials, this time-dependent behaviour is shown when subjecting the material to different rates of strain or deformation. For example, the stress-strain

2. LITERATURE REVIEW

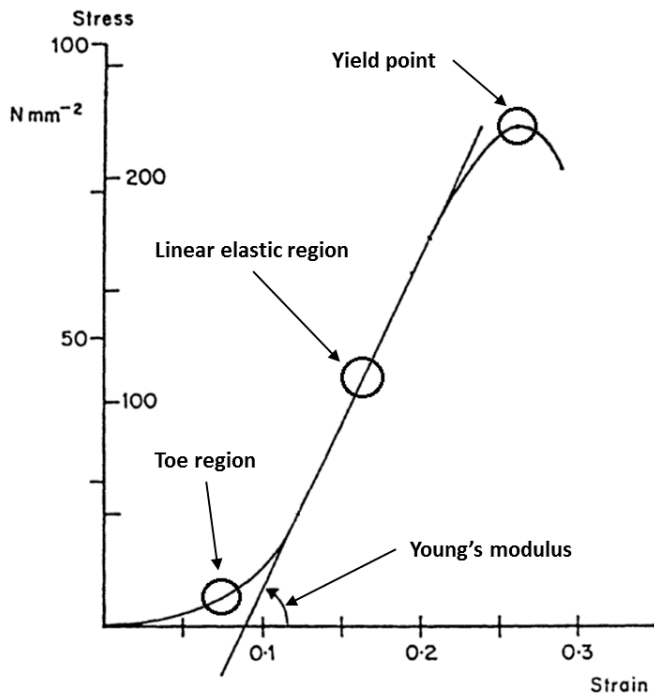


Figure 2.22: Tendon stress-strain curve. Image adapted from [68].

curve of the human tendon, illustrated in Figure 2.22, would have a greater slope in the elastic region if a greater strain rate is applied. The viscoelastic behaviour of the human tendon can be analysed with the following mechanical tests: stress relaxation, creep (deformation over time) and hysteresis [69].

During the stress relaxation experiment, the tendon is subjected to a constant deformation (length remains the same throughout the whole experiment). To avoid plastic deformations, i.e. incorrect measurements, the parameter of deformation for this experiment must not exceed the linear region of the material. The initial force/stress triggered as a response of the applied deformation will decrease over time (relax) until reaching equilibrium. From this experiment a chart of force against time is generated (Figure 2.23). In a similar way, in the creep experiment a constant force is applied to the material. The material will creep as time passes, in other words, the deformation caused by the applied force will increase over time until reaching equilibrium. A chart of deformation against time is generated (Figure 2.23). Finally, during the hysteresis experiment the tendon is subjected to cyclic tests where a load is applied up to a certain stress level and then released (unloading). The tendon behaviour shows two different paths, one for loading and one for unloading. Due to the time-dependent behaviour of viscoelastic materials, each cycle will generate

different load-unload paths since the time interval for each cycle to be executed are intentionally defined to prevent the material from reaching equilibrium (Figure 2.24).

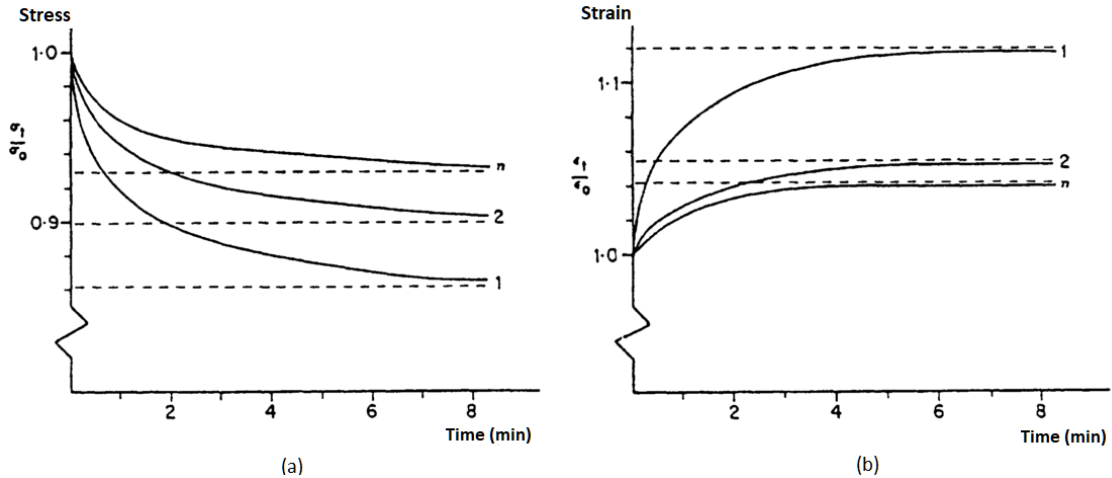


Figure 2.23: Tendon curves for the experiments of: (a) stress relaxation and (b) creep. The experiments were executed several times under the same conditions, the curve labelled n illustrates the tendon reaching a steady state where repeatability between experiments is achieved. Image reproduced from [68]

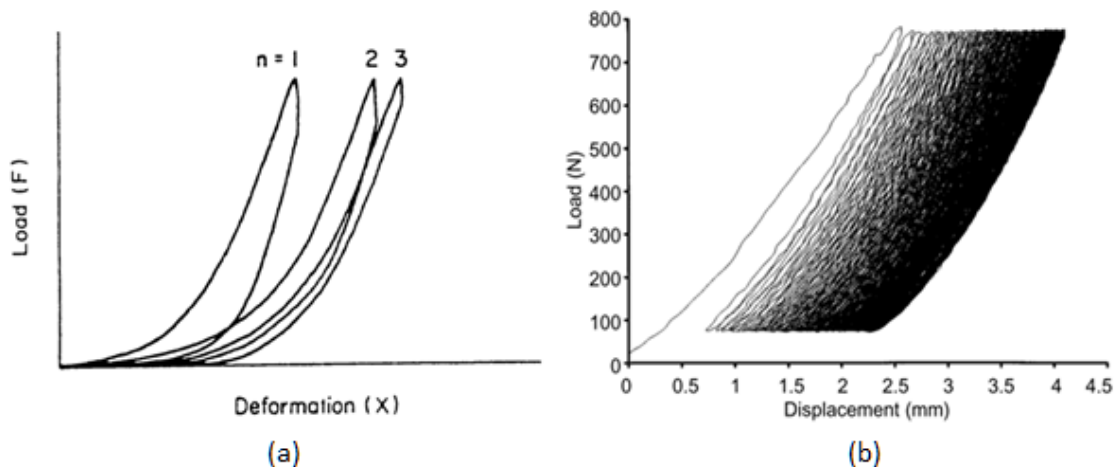


Figure 2.24: Hysteresis of the human tendon. (a) Deformation chart shows both loading and unloading paths for few cycles and (b) displacement chart shows 200 loading-unloading cycles. The preconditioned state of the tendon is reached for cycles above 50. Images taken from [68, 70] respectively.

When performing mechanical experiments to find the tendon properties at failure, the obtained results are different between a preconditioned and an unconditioned tendon, as proved in [70]. This effect is illustrated in Figure 2.23 as well, for

2. LITERATURE REVIEW

both experiments, the tendon relaxation and creep are smaller for each new testing cycle until reaching an equilibrium state, i.e. the preconditioning state. The previous set of experiments is useful to characterize the non-linear viscoelastic properties of tendons and soft materials.

2.6 Modelling Tools for Soft Materials

The majority of the soft robotic applications implement soft materials from the family of thermoplastic elastomers (TPE). These type of materials are known to have a non-linear stress response, low stiffness, high deformation lengths, time-dependent and temperature-dependent stress response [71]. These mechanical properties are similar to the ones found in biological skin or muscle tissue. Due to this, soft materials are being implemented in soft robotic applications. However, it is imperative to have a reliable modelling technique to fully take advantage of the viscoelastic properties of soft materials.

The stress response of soft materials, such as TPE is non-linear and viscoelastic. The majority of the documented modelling approaches to predict the viscoelastic behaviour of soft material is based on the development of a mathematical constitutive model. The Linear Viscoelastic Models (LVMs) are commonly used for this task [72–75]. This is also the case when for the modelling of biological tissues [76]. The LVMs are a set of mathematical models that use two basic components, a spring and a dashpot, in different configurations and quantities to describe the viscoelastic mechanical behaviour of materials [77]. Inside this family of mathematical models, there are a couple of them which, in theory, can describe the viscoelastic behaviour of any material, as long as the required number of parameters is met. This immediately imposes the restriction of having enough computational power to deal with the model complexity when high accuracy is required.

The implementation of soft materials in soft robotic applications for human assistance has recently gained more attention. Most of the efforts are focused on improving the traditional series-elastic actuator (SEA) by replacing its elastic element, commonly a metallic spring, with a viscoelastic material, such as rubber. SEAs are from the family of cable-driven actuators and are commonly paired with electric motors. The main feature of these actuators is that they have an elastic element between the actuator and the load. SEAs have greatly impacted the field of robotics, specifically in legged robotics and powered orthoses, due to many benefits such as:

greater shock tolerance, low output impedance, passive energy storage, and better force feedback accuracy [78–80]. SEAs are now a mature actuation technology, and as such, they have a well-defined trade-off, caused by the fixed stiffness provided by linear springs traditionally used. More often than not, variable stiffness is more suitable for legged robots and powered orthoses. The latter limitation have been addressed by developing variable stiffness actuators [81], using non-linear metallic springs [82], and very recently by using viscoelastic materials, such as polymers and rubber [83–85]. However, most of these works, still face the challenge of accurately modelling the mechanical behaviour of soft materials.

In [84], where the concept of a series-viscoelastic actuator (SVA) is first mentioned, the modelling of the soft material is based on the Burger Model, one of the most complete LVMs, in combination with a controlling technique known as the state space observer. The accuracy of the system was found to be proportional to the complexity of the mathematical model used. The studied material in this work was a rigid-acrylic based photopolymer (FullCure720). The reported control system contained the viscoelastic model, the state space observer, and a cascaded force-velocity scheme, in other words, a very complex and well thought control system for a linear viscoelastic polymer. The developed SVA is illustrated in Figure 2.25.

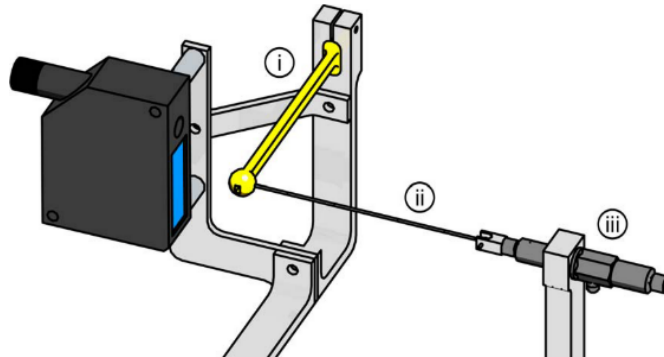


Figure 2.25: Series-viscoelastic actuator proposed by Parietti et al. The end-effector is rigidly mounted on the revolving lever (i), which also supports the laser sensor. A Nylon line (ii) connects the end-effector handle to the high-precision piezoelectric force sensor (iii), which is fixed to a rigid support [84].

Following this line of research, Rollinson et al. attempted to add viscoelasticity to a SEA, this time a soft material is used, natural rubber, instead of a rigid polymer [83]. The developed SEA has a rotary spring. Two different types of rubber, and a type of neoprene, were studied. In here, the stress response of the materials is

2. LITERATURE REVIEW

considered linear and instead, the hysteresis of the material is modelled. Again, the modelling of the soft material is based on one of the LVMs, the Standard Linear Solid (SLS) model, which is slightly less complex than the Burger model. Thanks to the proposed mechanical design for the rotary SEA, the reported stress response of the studied rubbers was surprisingly linear under a specific range of deformations. The authors concluded that more work is required to create better modelling techniques for the hysteresis and non-linear behaviour of soft materials like elastomers. The developed rotary spring is illustrated in Figure 2.26.

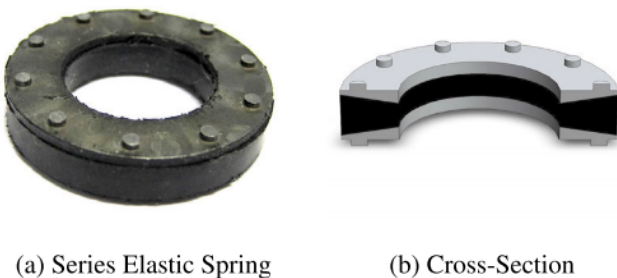


Figure 2.26: Developed soft rotary spring: a)photo and b)cross-section [83].

Following a more traditional approach, Schepelmann et al. incorporated viscoelasticity in cable-driven SEA by using a rubber material as the elastic element, instead of the traditional metallic spring [85]. In here, no LVMs are used, instead the non-linear stress response of the rubber is simplified by fitting a second order exponential curve to the stress-strain curve of the material. The main motivation of this work is to tackle the limitations of SEA with non-linear springs (NLS), where computer-aided manufactured (CAM) structures are used to define a known deflection trajectory of the spring, thus defining a torque trajectory. Essentially, CAM structures can relate the spring deformation with the generated torque, allowing the implementation of control systems. This work successfully validated the suitability of rubber to be incorporated as part of a SEA (Figure 2.27). However, under the limited range of testing parameters, the authors were not able to observe any velocity-dependency on the stress response of the rubber. In the conclusions, a state space observer is recommended to improve the accuracy of the reported forces transmitted by the soft material, i.e. to allow the controller to compensate the hysteresis and non-linear stress response of the material.

In an attempt to relieve the controller for such load, the latter work was continued by Austin et al. in [86], this time the focus was on developing a modelling

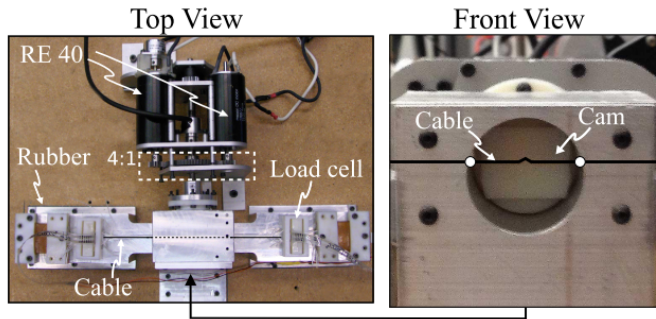


Figure 2.27: Benchtop setup for rubber characterization and observer testing. The load side of the rubber is fixed. Load cells in-line with the rubber give rubber force measurements for testing. The choice of electric motors and transmission is illustrated [85].

tool to better describe the complex behaviour of rubber. In here, the complexity of modelling the non-linear and strain-dependent stress response of soft materials is addressed, for the first time, by upgrading the SLS model without greatly increasing its complexity. A piecewise linearisation is implemented, to transform the equilibrium spring in the SLS model into several springs in parallel which sequentially engages in proportion to the strain applied to the material. The developed mathematical model is called the Standard Linear Solid model with Strain-Dependent Stiffness. (Std. Lin. SDS). Although, the SLS is not the most complete model among the LVMs, the reported accuracy of the developed model is impressive. The control system implemented a state space observer, as well, which was capable of estimating the torque generated by the rubber spring. However, despite the large improvement in accuracy obtained by the developed Std. Lin. SDS, the hysteretic properties of the rubber lead to instability at higher frequencies, suggesting that there is still work to be done in this field.

2.7 Summary

The available literature suggests a growing interest in the research and development of soft actuation technologies, soft perception systems, and control systems to pair with the latter two. Also, and following the bio-inspiration driving the field of Soft Robotics, many works are attempting to imitate the capabilities of the human musculoskeletal system by developing soft actuators capable of behaving like the human muscle-tendon component. This is more evident when looking at the avail-

2. LITERATURE REVIEW

able works on Pneumatic Artificial Muscles (PAMs) where the actuator is used as the contractile force generator element (muscle), and a flexible interface (tendon) is used to transmit that force to the desired location. Similarly, established technologies such as electric motors, which can deliver forces in both directions of rotation, are being used in combination with Bowden cables to create pulling forces. This type of setup is known as a redundant system because more than one actuator is required to control both directions of rotation of a joint. Moreover, the research and development of new soft materials, such as the SMA and SMP, are also focused on creating materials that can contract when stimulated. There is still plenty of work to be done in this matter, which is why this is identified as one gap in the body of knowledge.

The majority of the literature is focused on testing a new soft actuation concept in an open-loop environment, i.e. with no control system implemented. This is caused by the fact that modelling the mechanical behaviour of a soft material is very complex. Even the control system of the most documented work in the literature, the ankle-foot orthosis, does not implement a modelling technique to monitor the behaviour of the PAMs, instead it is focused on extracting as many information as possible from the environment and to use this to decide when and how to activate the PAM [8]. The literature dealing with the control systems of soft robotic applications is limited. Recently, attempts of adding viscoelasticity to well-established actuation technologies have been done. Specifically, viscoelasticity has the potential to address many of the limitations found in series-elastic actuators. The available literature on the subject is scarce but very well documented. In general, the reviewed works face a common challenge, the modelling of the viscoelastic properties of the materials used to accurately estimate their reaction force or torque. Rubber is the most common choice in these applications. Almost all of the documented modelling approaches are based on the Linear Viscoelastic Models, for the prediction of the material behaviour. However, the work performed by Austin et al. in [86], is the first attempt to upgrade the potential of the LVMs using a Piecewise linearisation method. The authors succeeded in developing a mathematical model, called the Standard Linear Solid model with Strain-Dependent Stiffness. (Std. Lin. SDS) which achieved higher accuracy than traditional models. However, even with the aid of controlling techniques such as the state space observer, the implemented control system is still incapable of accounting for properties of the material, such as hysteresis and the velocity-dependency in their stress response. Nevertheless, the

developed mathematical model has the potential to be upgraded further by using the same Piecewise linearisation method but on a more complex LVM. The latter clearly indicates a growing interest in this field of research, its importance and a current gap in the body of knowledge.

Therefore, two main gaps are considered in the body of knowledge which are addressed by this research. On the one hand, more research is required to understand the functionality of the human musculoskeletal system, and to develop a soft actuation technology which mimics the functionality of the muscle-tendon component. On the other hand, there is a lack of reliable modelling tools to predict the complex mechanical behaviour of soft materials being used in soft actuation technologies.

CHAPTER 3

Design Guidelines for Assistive Devices

3. DESIGN GUIDELINES FOR ASSISTIVE DEVICES

3.1 Introduction

The development of wearable robotic assistive devices requires a deep understanding of human biomechanics. Specifically, the kinematic and kinetic parameters are fundamental for the design stage and the assessment stage of an assistive device. The kinematic parameters describe the human body motion in terms of the angle, velocity, and acceleration of a joint. The kinetic parameters describe the forces involved in the motion of a joint in terms of torque and mechanical power. The characterization process of these parameters involves reviewing several clinical studies focused on gait analysis. Commonly, the scope of the latter process is limited to the end-application of the assistive device, e.g. assisting healthy adults to walk at the ground level. Therefore, the characterization of the kinematic and kinetic parameters dictates the applicability of the assistive device, in terms of the end-user characteristics. This important step in the design stage of an assistive device is often overlooked. The limitations of the resulting device are then solved by over-sizing it.

This chapter introduces several techniques to facilitate the extraction of design guidelines for the development of assistive devices through visual representation of the kinematic and kinetic parameters taken from clinical studies on gait analysis. The chapter is organized as follows.

The kinematic and kinetic parameters of the human lower limb during activities of daily living (ADLs) are introduced. These parameters are extracted from clinical studies focused on gait analysis. The underlying difficulties of extracting these parameters from the available literature are discussed. Subsequently, the extracted parameters are categorized and visually represented using different chart designs. Lastly, the benefits of each chart design, in the context of extracting design guidelines for the development of assistive devices, is discussed.

3.2 Characterization of Kinematic and Kinetic Parameters for Activities of Daily Living

The kinetic and kinematic parameters of each joint are an important part of the biomechanics of the human body. The kinematic parameters describe the human body motion in terms of the joint angle, velocity, and acceleration. The kinetic parameters describe the forces causing this motion, e.g. joint torque and power. Motion capture is the most commonly used method to extract these parameters. However, other

3.2 Characterization of Kinematic and Kinetic Parameters for Activities of Daily Living

technologies such as soft strain sensors [52], electrogoniometers [87], and inertial measurement units (IMU) have also been used. The process of characterizing these parameters is very important for the development of any wearable robotic device. This allows the intended device to be tailored for a specific application, it being assisting an elder adult or enabling a disabled subject to move. Alternatively, the kinetic and kinematic parameters can be also used to measure the effectiveness and compatibility of an already available assistive device. Measuring the effectiveness of an assistive device in this way is more convenient than calculating the metabolic cost reduction, which involves specialized equipment [88].

The kinetic and kinematic parameters can be obtained from gait studies. These studies differ between one another in many aspects, in addition to the technology of choice, such as subjects' gender, age, weight, etc., as well as the setup of the experiments. Therefore, the following subsection describes the process of extracting and processing the kinetic and kinematic parameters from gait studies. As previously mentioned, these parameters are useful design guidelines for wearable robotic devices. The gait studies compiled in the following section cover the main activities of daily living (ADLs), which are: walking, ascending/descending stairs, ascending/descending ramps and chair sitting down/standing up. In the context of studying the human lower limb, the joints of interest are the hip, knee and ankle joints.

3.2.1 Gait Analysis Data

In clinical studies focused on analysing the human gait, parameters regarding the subjects involved and the experiment performed are commonly provided. Regarding the subjects characteristics, information about their age, subject age, weight, height, gender and health condition are included. Similarly, contextual information about the experiment performed such as: loading conditions, plane geometry, and activity of choice is provided. Subjects characteristics are always presented as mean values. In a similar way, measured and calculated data, such as torque and power, are presented in normalized values. The gait cycle is usually normalized using the subjects height, whereas the joint torques are normalized using the subjects weight. The latter is clearly expressed in the units of the reported values, being Nm/kg for the joint torque, and W/kg for the joint mechanical power. Nonetheless, some studies do not follow the same guidelines when reporting the obtained results, or when normalizing the calculated values, preventing the reported information to be

3. DESIGN GUIDELINES FOR ASSISTIVE DEVICES

compared against other clinical studies [89].

The diversity on the subjects characteristics difficult the comparison process against similar clinical studies. Due to this, some clinical studies focus on studying a common characteristic among all participants, such as age or health condition. This is the case for the study in [90], where the study group is segmented in two age groups. One group included subjects from 22 to 72 years old, meanwhile, the subjects from the other group have ages ranged from 6 to 17 years old. With this segmentation approach, the clinical study can present the results with respect to age range. In some cases where the difference between age groups is very small, the clinical study condense the reported data into a single dataset [89].

The technology of choice to extract the kinematic parameters of the human gait, such as the joint angle, is motion capture. Similarly, the human body kinetics parameters are extracted by measuring the ground reaction forces using force plates. The latter is required to calculate the joint torque and joint power. Therefore, the three most common parameters found in gait analysis studies are the angle, torque, and power of the joint of interest. The gait cycle of the studied activity is usually presented in a chart accompanied with tables to clearly indicates the maximum, minimum and mean values of the gait cycle. The difference between the maximum and minimum values of the kinematic and kinetic parameters of a gait cycle are very important for the characterization process. Commonly, these values are provided in the studies in the form of tables and charts [91, 92], in other cases the complete experiment dataset is included [93]. The extraction of the parameter of interest is straightforward when the data is presented in a form of a table. Alternatively, when data is provided in the form of charts, the process of extracting it must be done by visual inspection, which inherently add some degree of error to the extracted data [94–98]. Likewise, it can be the case for some studies to focus on specific features of the gait cycle, such as maximum and minimum values of each parameter; or to not provide one or more of the parameters of interest (angle, torque or power). Due to all these different scenarios, the process of curating and compiling the data found in clinical studies is very lengthily. The latter motivated the process described in the following section in which the data of several clinical studies is compiled and visually presented to serve as design guidelines for the development of soft robotic applications for human assistance.

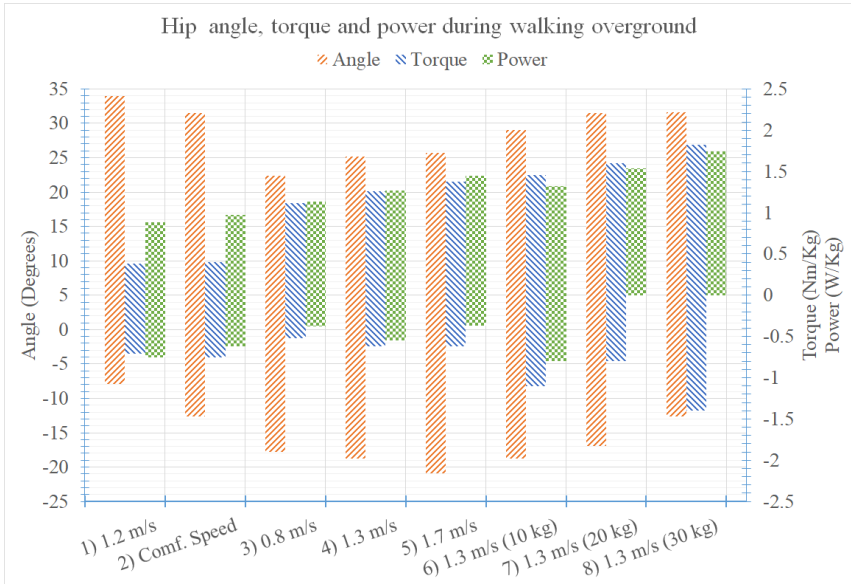
3.2.2 Extracting Design Guidelines

The variations of the data from one experiment to another can be reduced by focusing on the range obtained from the difference between the maximum and minimum values of each parameter. This is illustrated in Figure 3.1a, despite the variations between the maximum and minimum values from one experiment to another, the actual range of each parameter is similar among all the experiments. The mean range of motion for the hip joint angle throughout different walking over-ground experiments was found to be 44.63° (Figure 3.1a). Also, the greatest variation between the mean range value and the range value of each experiment is 18% of the mean value. The previous calculation can be used to decide design parameters of wearable robotic devices, such as which range of motion should be covered by the device depending on which sector of the population is intended to be assisted. Alternatively, the device can be tailored to cover as much of the population as possible by choosing the maximum and minimum values of the range of motion, out of all the experiments.

Different design guidelines can be extracted when visually analysing other parameters together. For example, in Figure 3.1b , the parameters of the knee joint are now compared against many experiments of stairs ascending/descending. Now, the main feature is not the range of motion of the knee, but the characteristics of the torque values. They appeared mirrored, in other words, the torque values required for descending stairs are of similar magnitudes but opposite in direction. Also, the amount required for ascending stairs is generally twice as much as the amount required for descending stairs. The latter illustrates an optimization opportunity. When designing a wearable robotic device for human assistance, the actuator is chosen to satisfy a certain torque range of a particular activity. Without the characterization of the parameters performed, the actuator is most likely to be oversized to comply with the most demanding part of the activity. However, a different approach could be proposed: agonist-antagonist actuators; a technique implemented in several wearable robotic devices which at the same time complies with the actual functionality of the human skeletal muscle system.

Another useful way of extracting design guidelines from the gait analyses is to plot the range of a specific parameter against different ADLs. To the best of the author's knowledge, this approach has only been documented once in [100], where the range of motion of the knee joint is compiled into a chart for 11 different ADLs. This concept, illustrated in Figure 3.2, can provide insight of two important design

3. DESIGN GUIDELINES FOR ASSISTIVE DEVICES



(a) Hip joint characteristics for walking over ground activities. The weight next to the name of some activities dictates the load carried by the subjects during the experiment [18]. Data collected from: (1) [90], (2) [89], (3-8) [91].



(b) Knee joint characteristics for several stairs ascending/descending experiments. The number enclosed in brackets represents the stairs slope. Data collected from: (1) [95], (2-4) [99].

Figure 3.1: Clustered-stacked bar charts of reviewed gait analyses [18].

3.2 Characterization of Kinematic and Kinetic Parameters for Activities of Daily Living

parameters. On the one hand, the actuators meant for this application must be capable of delivering torques in both directions of rotation, i.e. clockwise and anti-clockwise. On the other hand, the selected actuation technology must meet the torque requirements of the activity of interest. Figure 3.2 was constructed using the mean range of the hip joint torque during different activities [89–91, 94–98].

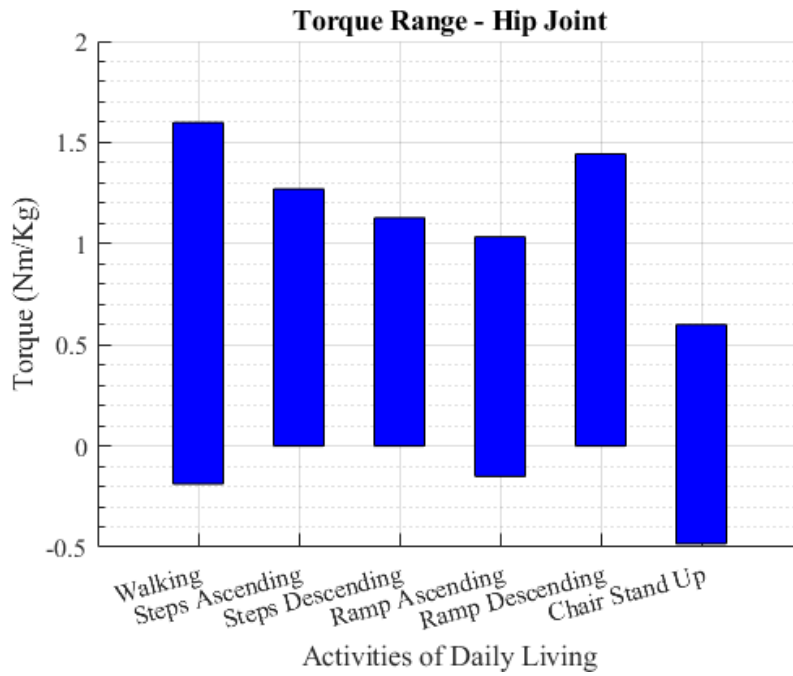


Figure 3.2: Torque range values during several activities. The values for the maximum and minimum torque are mean values from the data of all the different gait analysis experiments enclosed in one main activity. [18, 89–91, 94–98]

Another alternative of visual representation of the data can be done by grouping the range of a specific parameter and comparing it with any of the subjects' physical characteristics, e.g. the age range. This is illustrated in Figure 3.3, where the dependency of the subjects' age with the knee range of motion is evidenced. The colour code used in Figure 3.3, the age ranges and knee ranges of motion are presented in Table 3.1. The chart shown in Figure 3.3 concentrates the data from three different gait analyses, in which six age groups are contained. The approach used in Figure 3.3 is to overlap areas of different colours, each area represents the range of motion of the knee for a specific age range. The area in which several areas intersect can be appreciated due to the enabled transparency property. Nevertheless, the areas where three and two areas are intersected are manually highlighted by a surrounding solid line and dotted line respectively, to improve their visualization.

3. DESIGN GUIDELINES FOR ASSISTIVE DEVICES

This simple intersection of areas can provide information regarding the required range of motion to be delivered by the wearable robotic device with respect to the aimed population sector. For example, if a wearable robotic device is aimed to assist the population sector aged from 50 to 70 years old, then a range of motion of the knee joint from 5° to 63° would suffice to meet the requirements. The range of motion is taken from the triple intersection of areas illustrated in Figure 3.3, which can provide a certain degree of confidence since three different clinical studies are compared. This approach can be used to compare other characteristics, e.g. subject's weight against torque. Summarizing, the overlapping areas approach can provide guidelines to avoid over sizing of wearable robotic devices by analysing the intersection of different areas which ultimately provides a degree of confidence when deciding design parameters.

Table 3.1: Colour code used in Figure 3.3 for each combination of age range and knee range of motion [18].

Colour Code	Knee Range of Motion ($^\circ$)	Age Range (Years)	Clinical Study
Red	2.2 - 67.4	49 - 90	[100]
Green	5 - 66.5	6 - 17	[90]
Blue	4.5 - 63.5	22 - 72	[90]
Yellow	0 - 69	18 - 30	[89]
Magenta	0 - 69	50 - 70	[89]
Cyan	8 - 63.6	23 - 27	[91]

In this section the process of characterizing the human lower limb kinematics and kinetics parameters during some ADLs is described. The relevant information provided in gait analysis experiments, and the challenges faced when extracting it from the clinical trials, are also explained. Data compiled for the activities of walking, ascending/descending stairs, ascending/descending ramps and chair standing up are presented in the form of clustered stacked bar charts. This type of chart allowed quick and easy detection of similarities between several clinical trials of the same activity. In contrast, the spotted differences, as the ones for the knee torque values during ascending/descending stairs, are indicators for optimization opportunities where instead of using a single actuator to satisfy the torque range, an agonist-antagonist system is more suitable.

The reliability of the data can also be observed using the type chart of overlapping areas with subjects' ranges of age against the knee ranges of motion. In other words,

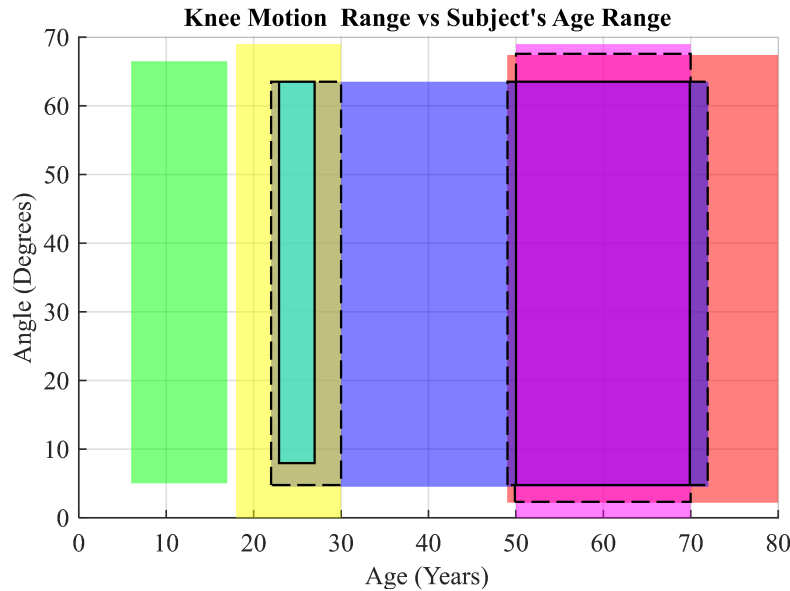


Figure 3.3: Comparison between subjects' age and the knee range of motion during walking over ground. The areas surrounded by solid lines and dotted lines represent the intersection between three and two areas, respectively. The overlapping squares highlight the great similarity among the range of motion despite subjects' age. The data used to create this chart is presented in Table 3.1 [18].

the specific ranges in which the data from different experiments overlaps, gives a measure of consistency which can be used to tailor the developed wearable device coverage.

The chart style with ranges of motion versus activities, facilitates the choice of the actuator type and dimension (depending on the activities of interest). The styles used to represent the charts are kept as simple as possible while providing useful information about the KKP. However, more complex plotting methods can be used. Finally, a total of 12 charts are produced in Excel® using the compiled data from the gait analyses. In favour of keeping the length of this section adequate, only two out of the 12 charts are included. The remaining charts are in the Appendix A.

3.3 Summary

The characterization of the kinetic and kinematic parameters of the hip, knee and ankle joints is performed by reviewing many clinical trials about gait analysis of the lower limb. The collected data can be used as design guidelines when developing robotic devices targeted for human assistance. Therefore, many visualization

3. DESIGN GUIDELINES FOR ASSISTIVE DEVICES

techniques are proposed and analysed in this context. The latter work resulted in a published conference paper (Section 3.2). In summary, the main findings of this chapter are as follows:

The visual approach presented in Figure 3.1 makes use of clustered-stacked bars. Visualizing the parameters of angle, torque, and power, against different variations of a specific activity in this way allows the extraction of design guidelines in terms of the intended coverage of the assistive device. In other words, decisions to prioritize specific walking speed, to mention one factor, can be made depending on the application of the assistive device. The visual approach presented in Figure 3.2 makes use of stacked bars to illustrate the full range of each parameter. This is useful when deciding the capacity of the actuator to be implemented, specially when implementing the antagonist-agonist functionality of a muscle group. In contrast, the information in these charts can also be used to tailor half of the full range of motion of the joint to reduce costs associated with actuators working in pairs. Lastly, the visual approach presented in Figure 3.3 makes use of overlapping square shapes. These shapes represent ranges of two variables of two variables of interest. In the example provided in this chapter, the range of motion of the knee is compared against the subjects age. The information in this chart allows the comparison of physiological aspects of the subject against the joint range of motion. This allows the intended assistive device to be fine tune to a specific target group. In other words, this allows the properly selection of the actuator to be implemented in the assistive device.

CHAPTER 4

Characterization of the Mechanical
Properties of Soft Materials

4. CHARACTERIZATION OF THE MECHANICAL PROPERTIES OF SOFT MATERIALS

4.1 Introduction

In Chapter 2, the trend in soft robotic applications for human assistance of mimicking the human skeletal muscle system is identified. This trend is mainly focused on the contractile element (CE) of the muscle-tendon component. Recently, research has been done on implementing soft materials as the elastic element of series-elastic actuators (SEAs). This is motivated by the fact that viscoelasticity, found in biological tissue and many soft materials, has the potential to overcome current limitations on SEAs. This is inline with the literature, which states that polymers, such as polyethylene, have similar mechanical properties as the human tendon. The literature available on the concept of series-viscoelastic actuators (SVAs) is very scarce and is currently facing the challenge of accurately estimating the force/torque transmitted by soft materials, such as rubber. One of the aims of this research is to develop a reliable modelling tool to address the latter. Therefore, this chapter covers the following points.

Firstly, a selection of different off-the-shelf soft materials is made from the family of composite materials, specifically thermoplastic elastomers (TPEs). The selection is based on the literature, which suggest that this type of materials have similar viscoelastic properties as the human tendon. The materials are as follows: Polyethylene Rubber (PR), Ethylene Polypropylene Rubber (EPR), Natural Rubber with Polyester (NatPolR), Natural Rubber (NatR), Silicone Rubber (SR), Fluorocarbon Rubber (FR), and Nitrile Rubber (NR). All the materials are acquired from RS Components UK®, with the exception of the Natural Rubber, which is acquired from CoreZone Sports® in the form of resistance bands of different thickness.

Secondly, the mechanical property of viscoelasticity of this type of materials is discussed. Thirdly, the characterization of the mechanical properties of these materials is presented. In here, the mechanical tests of tensile strength and stress relaxation are performed to extract both the elastic and viscoelastic properties of the materials. As previously mentioned, the study of the creep and hysteresis effect is out of the scope of this research. Finally, the collected data is processed in Matlab® prior to creating the visual representation of the studied properties.

4.2 Mechanical Properties of Soft Materials

The selection of soft materials to be studied in this research is based on the literature about tendon reconstruction applications. A comprehensive review about the usage

of synthetic materials in tendon reconstruction is made by Andullah in [101], where the most common materials used as artificial tendons and for tendon reconstruction are reported as: carbon, polyester, polytetrafluoroethylene, among others. The latter suggest that polymers are highly compatible with the human skeletal system and have similar mechanical properties as the human tendon. This assumption is further verified in the study performed by Duenwald et al. in [102], which is about the viscoelastic relaxation and recovery of the human tendon. In the previous work, a high density polyethylene material is tested to find great similarities between this material and the mechanical properties of the human tendon. In fact, the viscoelastic properties of the human tendon during loading and unloading are similar to the ones found in polyethylene. However, high density polyethylene cannot sustain high strains without suffering plastic deformations nor it has a very fast elastic response.

Among the current developments in soft orthoses, silicone rubber is a common choice, due to its high compliance, high elasticity and softness. Silicone rubber is usually implemented to create inflatable elements, but it is also known to have non-linear elastic properties, as reported in [103]. These findings suggest that the limitations of polymers, in terms of their elasticity, could be circumvented when combined with elastomers, such as rubber. A material with the latter characteristics, is known as a composite material. Many composite materials are created by injecting polymer particles, such as the previously mentioned polyethylene, into a rubber mixture. Thanks to the advances in manufacturing of composite materials, there is a wide variety of commercially available materials that fit with the requirements of this research. Due to the latter information, the selection of the soft materials to be studied in this work are from the family of composite materials, as follows: Polyethylene Rubber, Ethylene Polypropylene, Natural Rubber with Polyester, Natural Rubber, Silicone Rubber, Fluorocarbon Rubber, and Nitrile Rubber. All the materials are acquired from RS Components UK®, with the exception of the Natural Rubber, which is acquired from CoreZone Sports® in the form of resistance bands of different thickness.

The soft materials studied in this work belong to the family of thermoplastic elastomers or TPE. These materials are created by mixing a thermoplastic material, such as natural or synthetic rubber, with other materials, such as carbon and sulfur. This process is called vulcanization which creates cross-linked structures inside the material. Since elastomers are based on rubber, the terms elastomer and rubber are often used interchangeably. Elastomers are known to have nonlinear stress response,

4. CHARACTERIZATION OF THE MECHANICAL PROPERTIES OF SOFT MATERIALS

low stiffness and to achieve high deformation lengths. Some elastomers can fully recover their shape after stretched many times their length. They are also known to exhibit both elastic and viscoelastic properties. The latter means the stress response of elastomers is also time-dependent [71]. The main mechanical properties of elastomers are described in following paragraphs.

4.2.1 Elasticity

Elasticity, or elastic behaviour, refers to the ability of a material to be deformed up to a certain length and completely recover its shape and dimensions when the load deforming it is removed. Elasticity also refers to ability of a material to comply with the law of constant proportionality between the stress and the strain, described by Hooke's Law. However, elastomers are not purely elastic materials and tend to have a nonlinear stress-strain response, i.e. they do not obey Hooke's Law over the whole range of strains in the sense that the proportionality between the stress and the strain does not remain constant. This typical nonlinear behaviour in the stress-strain curve of elastomers is illustrated in Figure 4.1.

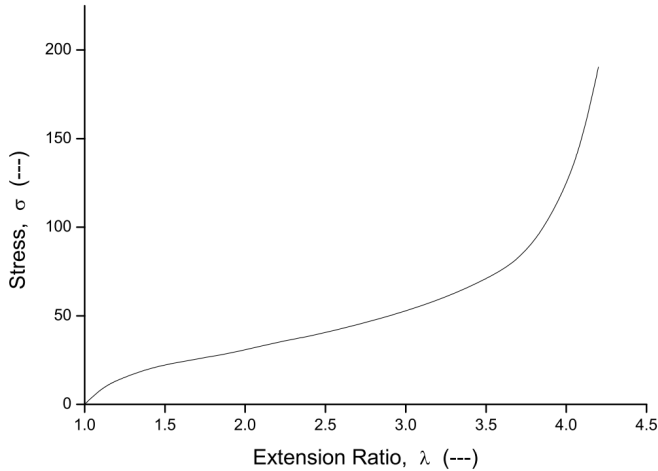


Figure 4.1: Typical stress-strain curve of elastomers. There are three main regions: the toe region ($1.0 < \lambda < 1.5$), the elastic region ($1.5 < \lambda < 3.5$), and the yield/failure region ($\lambda > 3.5$) [71].

The stress-strain curve of elastomers has three main regions: the toe region ($1.0 < \lambda < 1.5$), the elastic region ($1.5 < \lambda < 3.5$), and the yield/failure region ($\lambda > 3.5$) (Figure 4.1). In the toe region, the internal molecular chains of the material are misaligned, experiencing greater friction forces which greatly oppose to initial deformations. In contrast, when the molecular chains are aligned the friction

forces decrease and the material deforms as a whole. The latter conditions dictates the beginning of the elastic region, in which the slope of the curve (stiffness) is slightly smaller than in the toe-region. The elastic region of many materials exhibit a proportional or linear relationship between the stress and the strain. This is not the case for elastomers, where most of them exhibit a nonlinear relationship. When the internal molecular chains have been elongated to its maximum length they demand higher forces to fail, this is observed as a peak in the stress-strain curve which also highlights the beginning of the yield/failure region [71].

Elastomers exhibit elastic behaviour over a certain range of deformations, i.e. the elastic region or elastic limit. Beyond this limit the material is likely to undergo plastic or permanent deformation, this means the material will not recover its original shape completely. In some cases, the elastic limit is not easily visible on the stress-strain curve of a material, and instead the proportional limit is used to approximate the location of the elastic limit. The proportional limit is defined as the point in the stress-strain curve where the nonlinear response (change in the curve's slope) is first observed. Another way to approximate the elastic limit of a material is based on using the yield strength, which is defined as the largest stress value on the curve, or the first point in which an increase in strain occurs without an increase in the stress [104]. These are some of the parameters that can be extracted from the tensile strength test and are useful to delimit the operating conditions of the materials. For this reason, particular care is put into accurately defining the elastic region, hence the safe operating conditions, of the studied soft materials. This is better described in Section 4.3.1.2.

4.2.2 Viscoelasticity

Viscoelasticity, is a property of some materials which are not purely elastic, i.e. do not fully obey Hooke's Law, nor purely viscous, i.e. do not fully obey Newton's Law in the sense that stress is not proportional to the rate of change of the strain with time. In other words, the stress experienced by viscoelastic materials depends on both the strain and the strain rate applied. An example of a purely elastic material is a spring; whereas an example of a purely viscous material is a dashpot. The mechanical model of a viscoelastic material contains both elements, which can be arranged in different configurations. The set of mathematical models created out of these different configurations are known as the Linear Viscoelastic Models (LVMs). The time dependency or viscosity, of viscoelastic materials is appreciated

4. CHARACTERIZATION OF THE MECHANICAL PROPERTIES OF SOFT MATERIALS

in phenomena such as creep, stress relaxation, hysteresis, the Mullin's Effect and in the Van der Waals forces.

Stress relaxation and creep are both time-dependent phenomena observed in elastomers. On the one hand, stress relaxation refers to the decrease over time of the stress experienced by a material when subjected to a constant strain (or deformation). On the other hand, creep refers to the increment over time of the material strain when subjected to a constant stress (or load). The latter phenomena is observed in elastomers because they are composed of an internal network of molecular chains. Inside this network, entanglements form naturally. According to J. Bauman in [71], stress relaxation is mainly caused by the slipping of these entanglements ultimately causing a loosening of force applied by the network of molecular chains. Stress relaxation and creep occur in both constant and cyclic deformations. There are two mechanical tests designed to study these behaviours, from where the relaxation modulus and creep modulus of a material can be extracted [105].

Hysteresis in a material is defined as the mechanical energy dissipated as heat when the material is undergoing deformations. This phenomenon is observed in a loading-unloading cycle, where the stress trajectory of the material while loading (extension) is different than the trajectory during unloading (retraction), as illustrated in Figure 4.2. Hysteresis is mainly caused by internal friction of the molecular chain, also known as Van der Waals forces, in both elongation and contraction. Van der Waals forces are caused by the momentary bonding experienced between molecular chains that are close together. This constant making and breaking of bonds caused by deforming a material produces heat which ultimately becomes a mechanism to dissipate mechanical energy. This energy is represented as the enclosed area in Figure 4.2. Stress relaxation and creep play a role in the amount of hysteresis experienced by a material in each consecutive loading-unloading cycle. The effect of hysteresis alone can be isolated by subjecting the elastomer to a conditioning process (preconditioning) in which it undergoes several loading-unloading cycles until the stress response stops changing with every new cycle.

The Mullin's effect is another important phenomenon in the mechanical behaviour of elastomers. This effect refers to the breakage of tense molecular chains resulted from the manufacturing process of the material. Therefore, the very first time the material is subjected to deformations it exhibits a larger stress response in comparison to consecutive deformations. The latter is also referred to as a weakening of the material. This effect is more dramatic than the stress relaxation but can

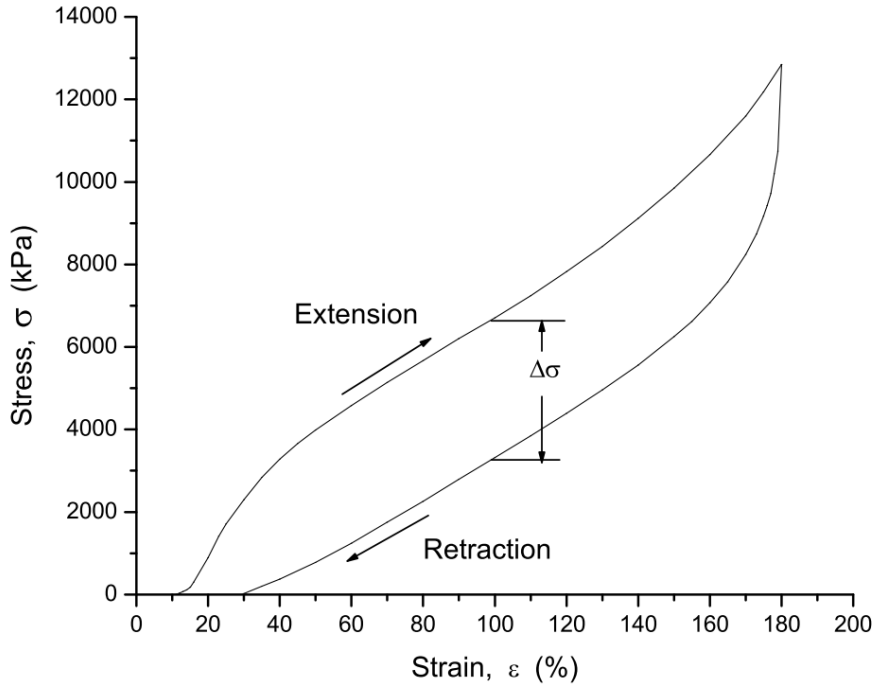


Figure 4.2: Hysteresis in stress-strain curve. [71].

be easily avoided when preconditioning the material. Having defined the expected mechanical properties of elastomers, the mechanical tests of tensile strength and stress relaxation are described in the following section.

4.3 Characterization Process

In this section, the mechanical tests of tensile strength and stress relaxation, performed as part of the characterization process, are described. The tests are performed in an Instron 3369 Dual Column Testing System equipped with a 50 kN load cell, at room temperature (25°C). The experimental data is expected to contain some noise due to the accuracy limitations of the available load cell. The algorithm implemented to filter this noise is described in the next section. As previously mentioned, the elastomers selected for this research are: Polyethylene Rubber (PR), Ethylene Polypropylene (EPR), Natural Rubber with Polyester (NatPolR), Natural Rubber (NatR), Silicone Rubber (SR), Fluorocarbon Rubber (FR), and Nitrile Rubber (NR). The Natural Rubber material is acquired from CoreZone Sports® and comes in the form of resistance bands of different thickness. The other materials are acquired from RS Components UK®, and come in the form of a rectangular sheets. Laser cutting was used to extract individual specimens from each material

4. CHARACTERIZATION OF THE MECHANICAL PROPERTIES OF SOFT MATERIALS

sheet with the layout illustrated in Figure 4.3, as recommended in the Standard Test Method for Vulcanized Rubbers - Tension (ASTM D412) [106]. Finally, all the specimens were preconditioned prior to testing by applying a small deformation to them.

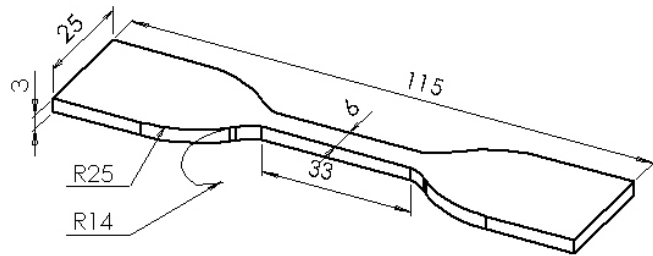


Figure 4.3: Specimen Type C Dumbbell Layout from the ASTM D412 [106]. In this example, the specimen thickness is 3mm, the width is 6mm, and the initial length, l_o , is 33mm.

4.3.1 Tensile Strength Test

In a tensile strength test the material is loaded to failure at a certain deformation (strain) rate. The main purpose of this test is to extract the stress-strain curve of the material. From the stress-strain curve, the elastic properties of the material, such as stiffness, elastic modulus, ultimate strain, ultimate stress, elastic limit and yield strength, can be extracted.

The tensile strength test performed in this work is in accordance with the Standard Test Method for Vulcanized Rubbers - Tension (ASTM D412) [106]. Also, the Standard Test Method for Tensile Properties of Plastics (ASTM D638), was consulted on how to interpret the obtained stress-strain curves [107]. In here, it is recommended to elongate the material specimen until failure using a deformation rate of 500 mm/min, whenever possible. However, under certain circumstances where the previous deformation rate is not suitable, the test can be performed using the deformation rate of 250 mm/min. The latter was required for the silicon rubber, natural rubber and some resistance bands, where the gripper of the testing machine was not able to hold the material during the entirety of the test. In addition to the previous two deformation rates, a third one of 50 mm/min is used whenever possible. In summary, most of the materials are tested using at least two out of the three deformation rates of 50, 250 and 500 mm/min. The decision of characterizing

the mechanical behaviour of the materials under different strain rates is motivated by the known velocity-dependency of the stress-response of this type of materials. This will be useful during the modelling stage. The exact number of tests performed to each material is summarized in Table 4.1.

Table 4.1: Number of specimens per type of test.

Type of Rubber	Thickness mm	50	250	500
		mm/min	mm/min	mm/min
Ethylene Polypropylene	1.5	16	—	5
Fluorocarbon	1.5	8	8	5
Natural with Polyester	1.5	11	5	1
Nitrile	1.5	8	7	6
Silicone	1.5	15	7	—
Polyethylene	6	13	7	1
Natural (Resistance Bands)	0.33 – 1.49	1	33	11

The testing machine used for these experiments output the following parameters: reaction force, elongation, and time. In this work, the conventional parameters of stress, σ , and strain, ε , are used instead of the reaction force, F , and elongation, ΔL . The latter is calculated using the initial length $l_o = 33\text{mm}$, and cross-sectional area A_o , of the specimen, illustrated in Figure 4.3 and Table 4.1, respectively. Then it follows that $\sigma = F/A_o$, and $\varepsilon = \Delta L/l_o$.

4.3.1.1 Data Processing

The main objective of the data processing stage is to get rid of any noise added to the experimental data, normally due to sensor limitations, and also to filter out any undesired data. Removing noise from the data, i.e. filtering or smoothing, is avoided whenever possible because meaningful data can be lost in the process. Unfortunately, some of the collected datasets showed signs of high frequency noise which make it vary rapidly. A smoothing algorithm was applied to these datasets. In addition to noise, there are two sections of the collected stress-strain curve which are not desired. The first one is the section of the curve beyond the failure point of the material, when the stress value precipitates to zero. The working conditions of the soft material are desired to be limited to its elastic region, therefore, the final section of the stress-strain curve is not critical for the modelling of the materials

4. CHARACTERIZATION OF THE MECHANICAL PROPERTIES OF SOFT MATERIALS

behaviour. The second undesired section of the stress-strain curve is located at the very beginning. According to the literature, the very first portion of the stress-strain curve can be contaminated with phenomena such as: take-up of slack, and seating of the specimen. This effect was observed for most of the studied materials in here. The process of how to get rid of this phenomenon is called toe compensation (for a detailed description, refer to [107]). The mentioned sections are illustrated in Figure 4.4.

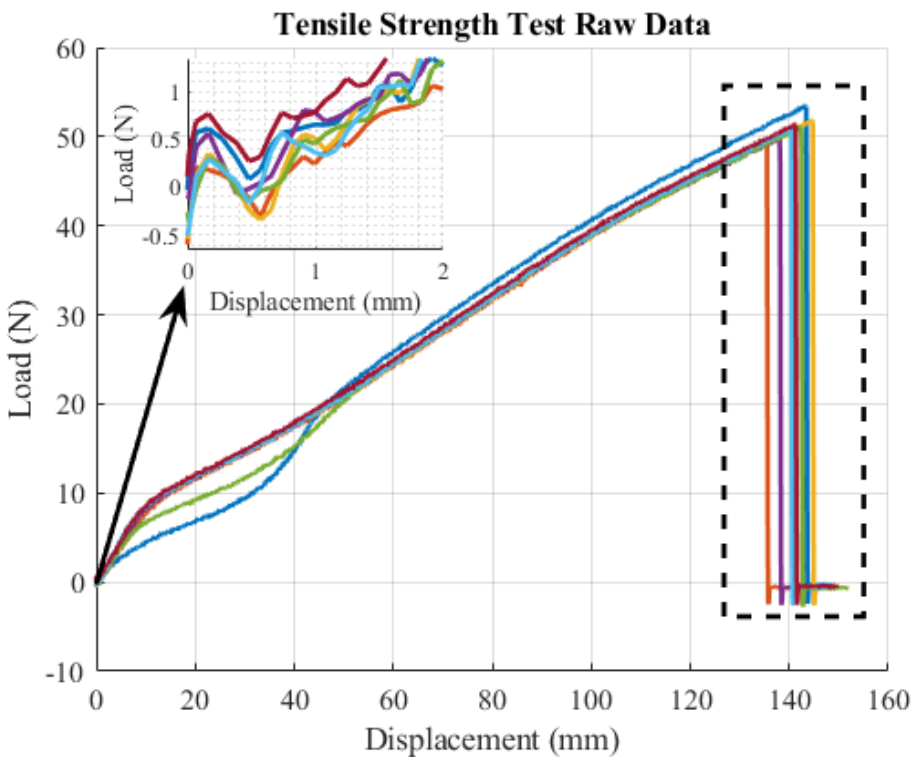


Figure 4.4: Undesired data on the tensile strength results. On the top left, the take-up slack phenomenon at the beginning of the experiment is observed. On the right, the different failure points of each specimen from the same material are highlighted.

The stress-strain curve from different specimens of the same material is expected to be slightly different, as illustrated in Figure 4.4. This variability is caused by many reasons such as the manufacturing process, temperature, and micro-fissures inside the material due to handling. For this reason, and as recommended in [106, 107], the engineering ultimate values of stress σ_{ue} and strain ε_{ue} are reported as the median value, per strain rate, from all the tests for a single type of material. Similarly, the previously mentioned variability is removed by calculating the mean value along the available stress-strain curves. The latter generates a single stress-strain curve from

all the specimens involved in a test. This is required for the modelling process.

The impact of the abrupt changes around the end section of the stress-strain curves, caused by the different failing points of each specimen (Figure 4.4) are illustrated in Figure 4.5. The presence of this variation is not critical for the modelling stage because the soft material is unlikely to be elongated to such lengths in a real wearable robotic application. However, the decision of discarding this section of the curve in favour of calculating the mean ultimate values of stress σ_u and strain ε_u , is made. This section of the curve is also not included when generating the final stress-strain curves of the materials.

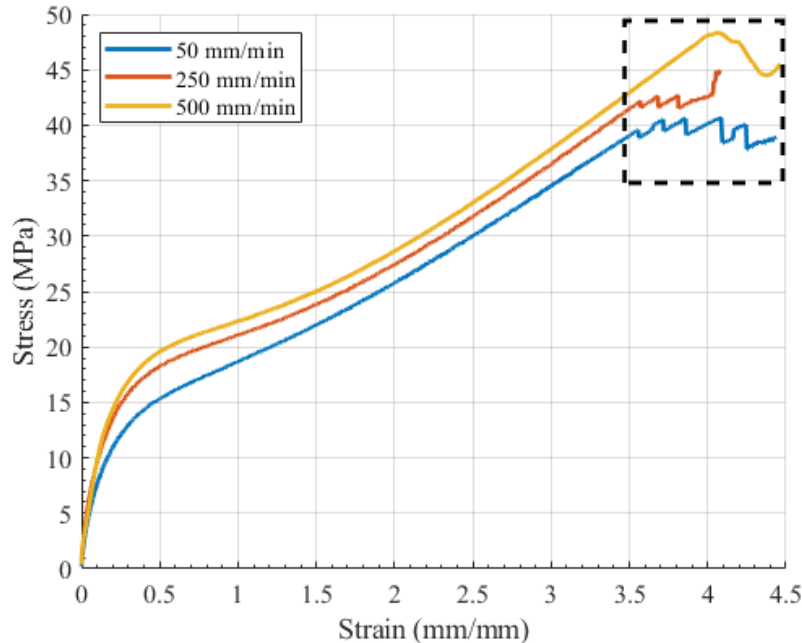


Figure 4.5: Abrupt changes observed at the last portion of the stress-strain curve, caused by the different failure points for each specimen. This phenomenon is observed after unifying the data from all individual specimens of a specific strain rate, into a single stress-strain curve.

The processing algorithm, developed in Matlab ®, is applied to the datasets with large amount of noise. These datasets were identified by looking at positive and negative peaks, specifically by looking at the mean absolute difference (MAD). Any dataset with peaks having a MAD greater than zero is considered noisy and subsequently filtered out. The filtering of the noise is done using the `smoothdata` function with the Savitsky-Golay algorithm. This function requires a window parameter to which the smoothing algorithm is applied, the larger the window, the

4. CHARACTERIZATION OF THE MECHANICAL PROPERTIES OF SOFT MATERIALS

greater the smoothing. However, a large window size also introduces a bias or offset to the extreme points of the data. This trade-off is described in [108]. Due to this, the chosen window size is based on the amount of data contained in one second. In this way the window size depends on both the strain rate and the sampling frequency for each case. The implemented data processing is summarized as follows:

1. Load raw data from tensile strength tests which contains the test timestamp, applied elongation and measured reaction force (load).
2. Discard portion of the stress-strain curve beyond the failure point.
3. Extract engineering ultimate load and ultimate displacement, latter converted to stress and strain.
4. Discard take-up slack phenomenon.
5. Unify processed data from all specimens into a single dataset by calculating the mean value.
6. Smooth datasets which have a peak-to-peak MAD greater than zero in the initial portion of the curve.
7. Discard negative offset induced by processing and smoothing.
8. Calculate $\sigma = F/A_o$, and $\varepsilon = \Delta L/l_o$.

4.3.1.2 Elastic Properties of the Material

One of the main parameters to extract from the stress-strain curves is the elastic limit of each material. As previously mentioned in Section 4.2, this parameter dictates the maximum amount of deformation a material can sustain without losing the ability to fully recover its original shape. Commonly, the proportional limit is used to approximate the location of the elastic limit, and by extension, the elastic region. The proportional limit is the point in the curve where the proportionality between stress and strain becomes nonlinear. It can be safely assumed that the elastic region of the material is located below this point. However, most elastomers do not have a clear elastic region due to their nonlinear stress-strain curve, hence the proportional limit cannot be obtained. Under this circumstance, the elastic region of the material can be approximated using the yield strength of the material. The latter is defined as the first point in the curve where an increment in strain happens without an increment in the stress, in other words when the slope becomes zero or even negative [107]. The yield strength is inside the region of plastic deformations of the material, hence this parameter by itself is not a safe way to approximate the elastic region.

A better alternative to approximate the elastic region is the offset yield strength. This parameter requires an offset strain value, and the elastic modulus E (slope of the curve) at a specific strain, to be calculated. In the literature, an offset strain of $\varepsilon_{offset} = 0.02$, or 2%, is recommended for plastics and elastomers [109]. This recommendation is mainly to allow comparisons between different laboratories data and does not indicate a goodness of fit when approximating the elastic region or the yield point of a material. In here, a strain offset $\varepsilon_{offset} = 0.2$, or 20%, is chosen due to the large values of elongation achieved by most of the materials. The main recommendation to calculate E is to choose a strain range inside the initial part of the stress-strain curve in which a linear behaviour can be observed. The elastic modulus is then approximated using a function fitting method such as linear regression.

The stress-strain curves of all the materials studied under different strain rates are presented in Figures 4.6 to 4.9. The optimal strain range for E is extracted by visual inspection of the stress-strain curves illustrated in Figures 4.6 to 4.9. The process to obtain the stress-strain curve of the Natural Rubber material is longer than for the other materials, due to the different available thicknesses. This material comes in the form of resistance bands commonly used in rehabilitation. A total of two different batches are acquired. Each batch contained one band for each strength level, a total of six levels. The weakest band is the tiniest, whereas the strongest band is the thickest. The measured reaction force of one band from the same strength level varied from one batch to the other. The measured thickness, per type of resistance band, is not consistent from batch to the other. This is directly related to manufacturing practices and is reported in the literature [110]. For this reason, the individual thickness of each type of rubber band, from each batch is used to convert the raw data to the final stress-strain curve. With this, the impact from the latter differences is decreased and the material behaviour is better captured.

4. CHARACTERIZATION OF THE MECHANICAL PROPERTIES OF SOFT MATERIALS

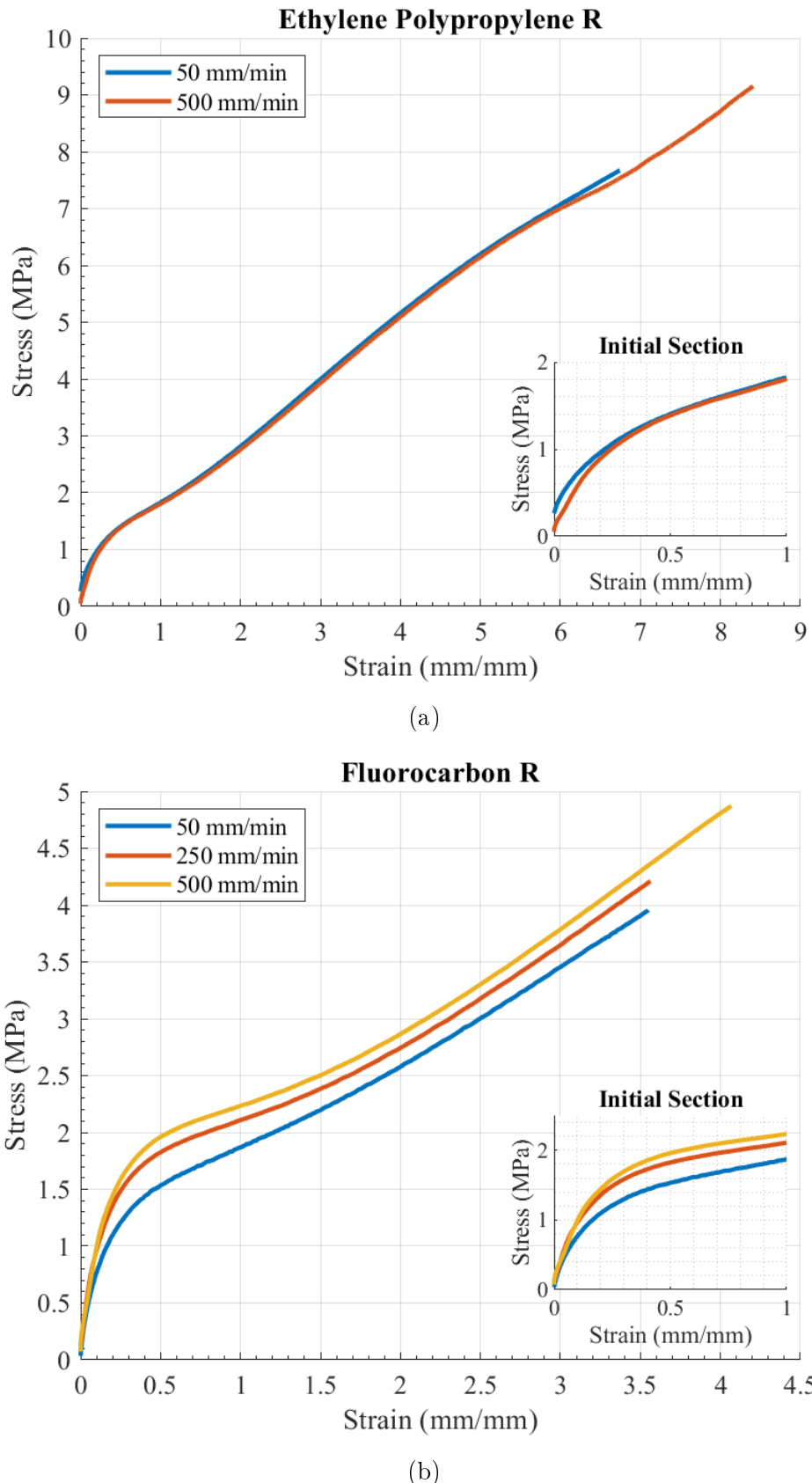


Figure 4.6: Stress-strain curves, during different strain rates, for the (a) EPR and (b) FR materials. On the bottom right, the initial section of the curve is presented.

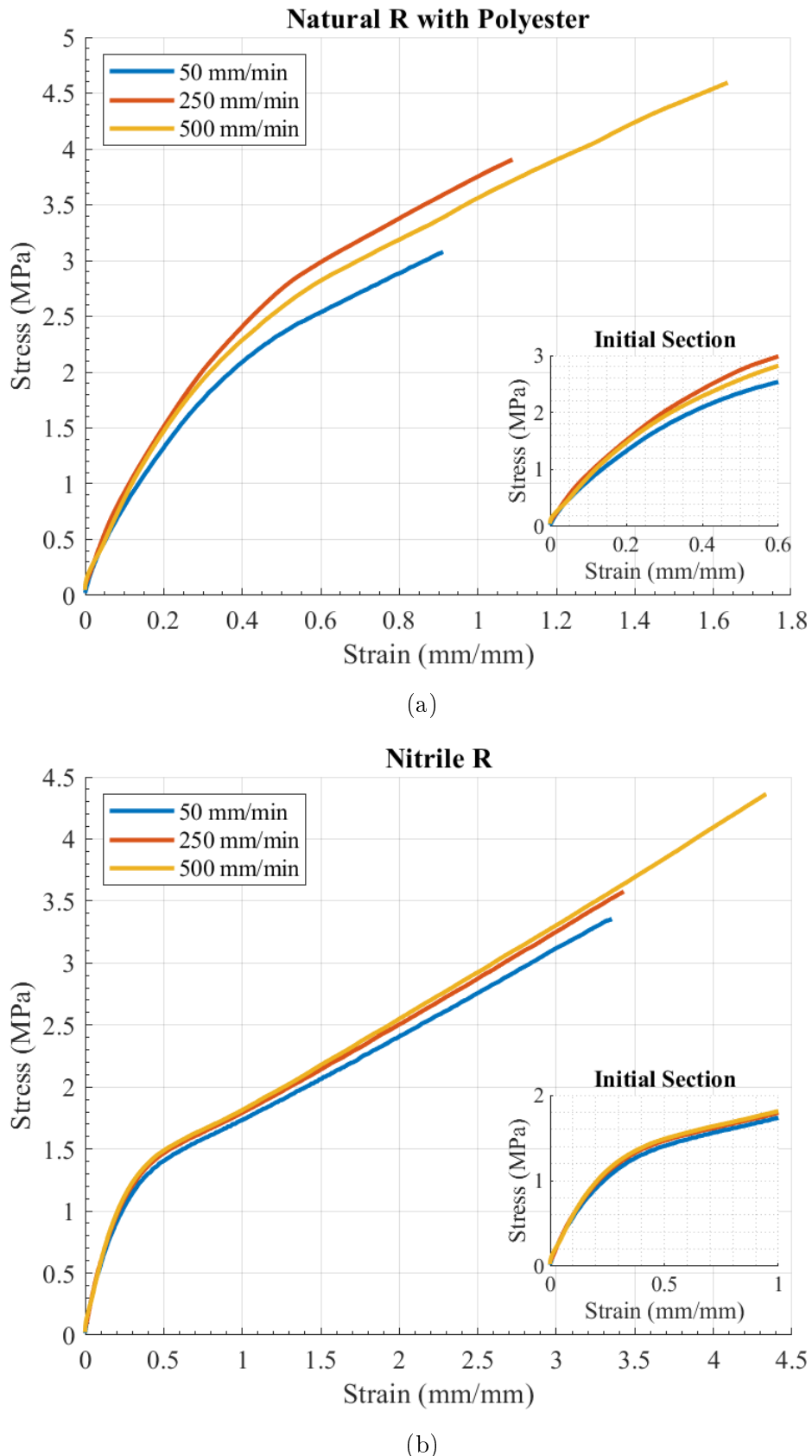
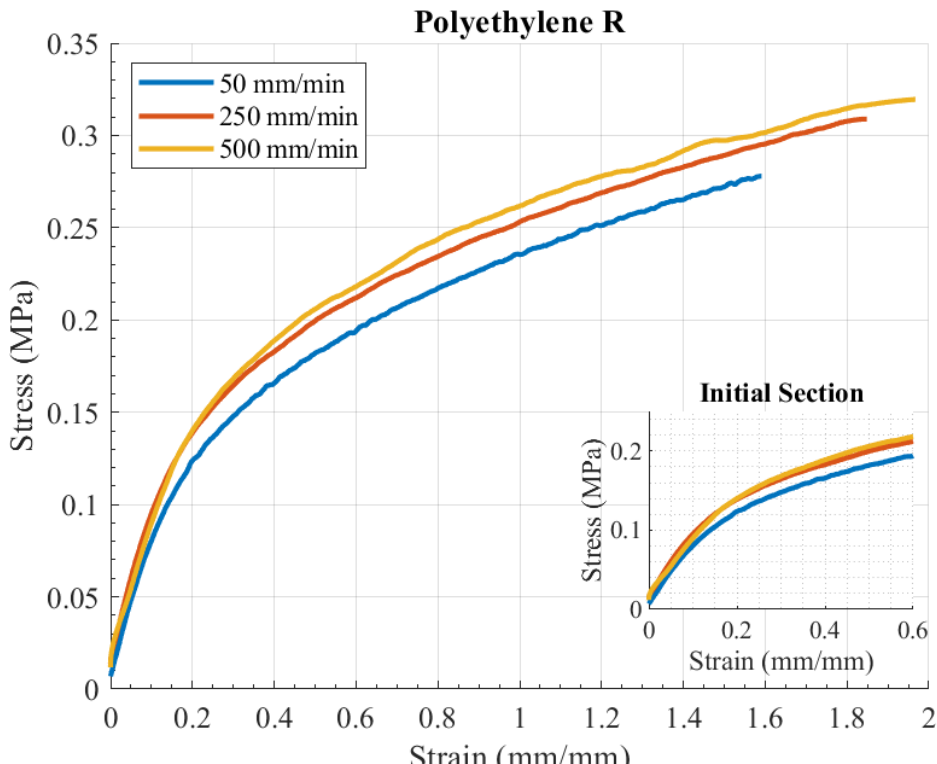
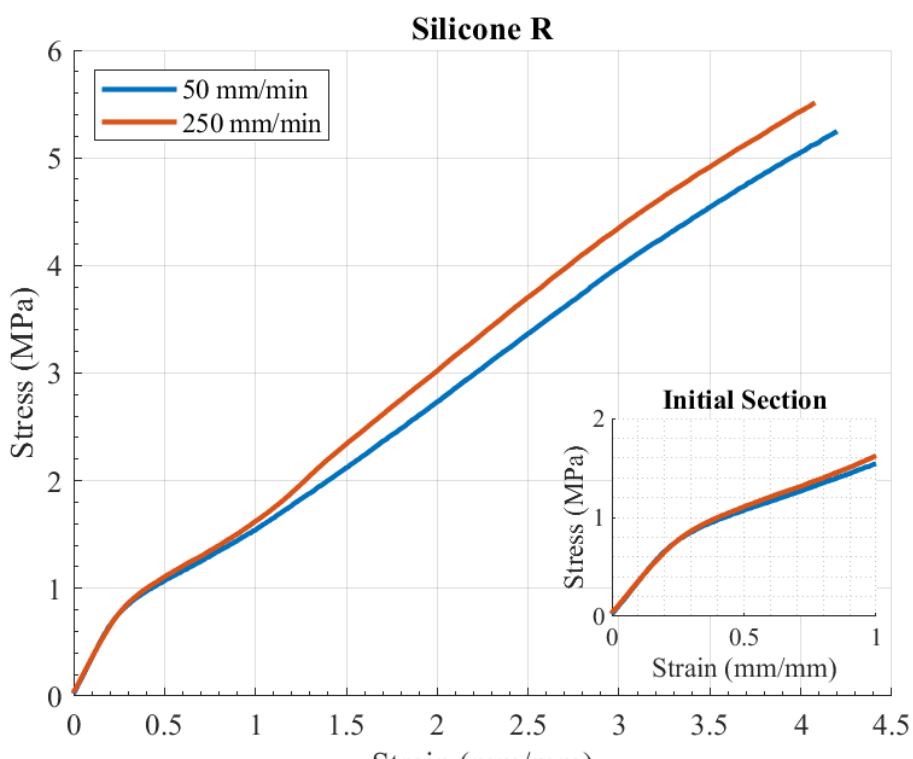


Figure 4.7: Stress-strain curves, during different strain rates, for the (a) NatPolR and (b) NR materials. On the bottom right, the initial section of the curve is presented.

4. CHARACTERIZATION OF THE MECHANICAL PROPERTIES OF SOFT MATERIALS



(a)



(b)

Figure 4.8: Stress-strain curves, during different strain rates, for the (a) PR and (b) SR materials. On the bottom right, the initial section of the curve is presented.

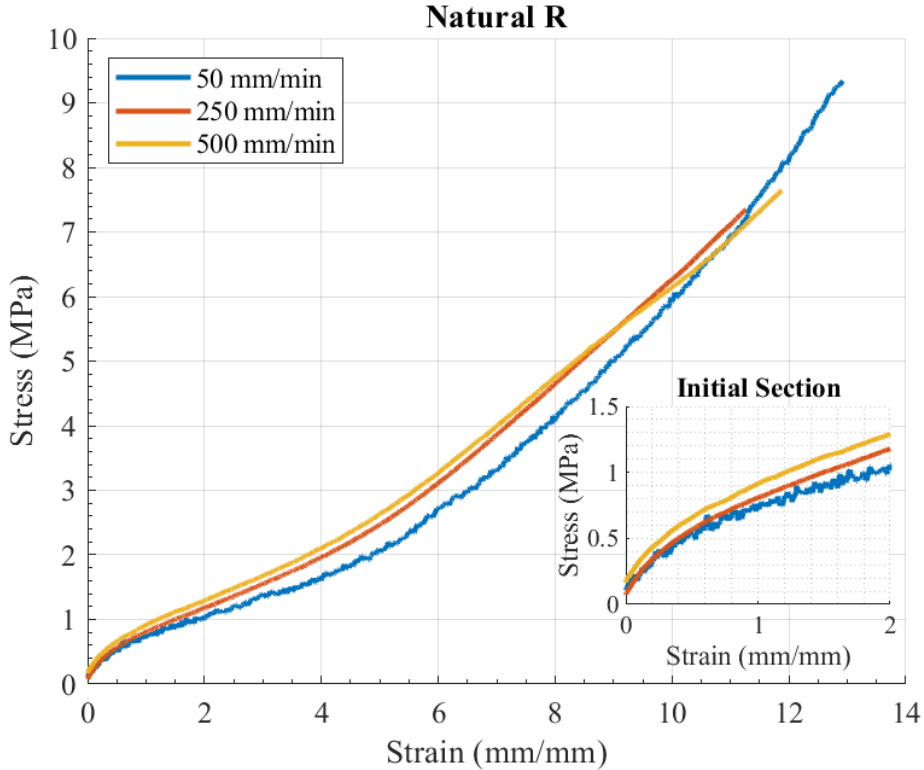


Figure 4.9: Stress-strain curve, during different strain rates, for the NatR. On the bottom right, the initial section of the curve is presented.

The velocity-dependency on the stress response of elastomers is also illustrated in Figures 4.6 to 4.9. In general, for larger strain rates, the materials exhibited a larger stress response. Moreover, a large difference in the ultimate values of the stress-strain curve of the Natural Rubber with Polyester material at 500 mm/min is observed in comparison to the other two curves (Figure 4.7a). This is a side effect from the unification step in the processing of the data, which is being amplified in here due to the small number of datasets involved in the tensile strength test for 500 mm/min (Table 4.1). Also, the Natural Rubber and Fluorocarbon materials showed signs of crystallization, a phenomenon that occurs when the internal molecular chains of the material are completely extended and greatly oppose to further deformation, hence the increase in stiffness just before the failure point [71].

Most of the materials have two regions in which the proportionality between the stress and strain appears to be constant. This is inline with the expected nonlinear behaviour from elastomers previously described. The slope of these regions, i.e. the stiffness, can be approximated by linear regression. A method such as the yield offset strength can be used to separate these regions into an initial and small elastic region, and a final and large elastic region. Therefore, the offset yield strength, σ_y and ε_y , is obtained and illustrated in Figures 4.10 to 4.16.

4. CHARACTERIZATION OF THE MECHANICAL PROPERTIES OF SOFT MATERIALS

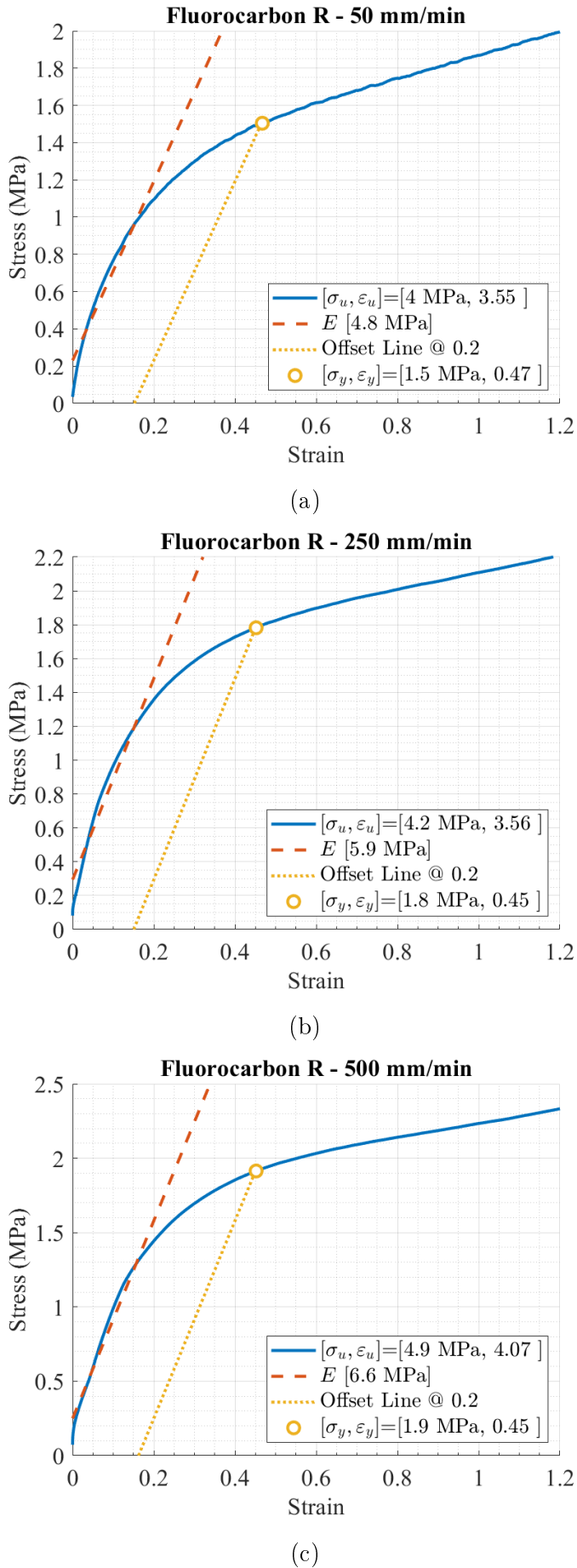
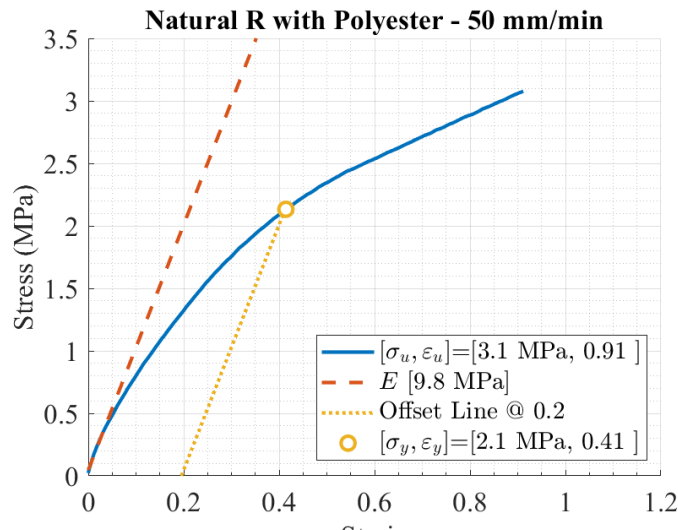
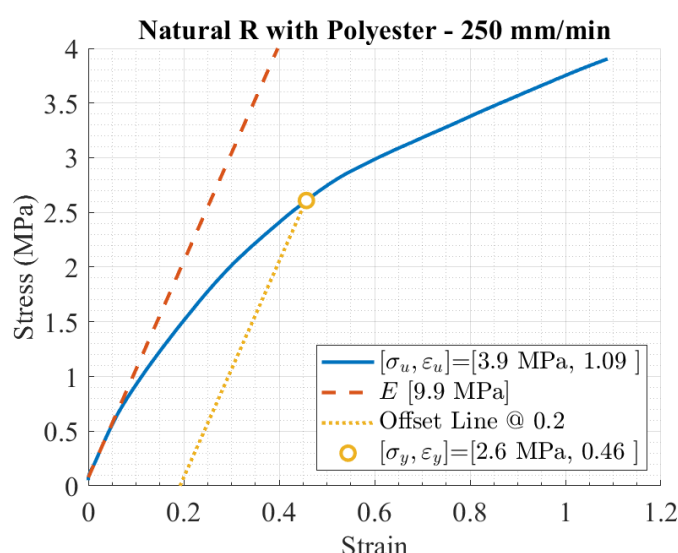


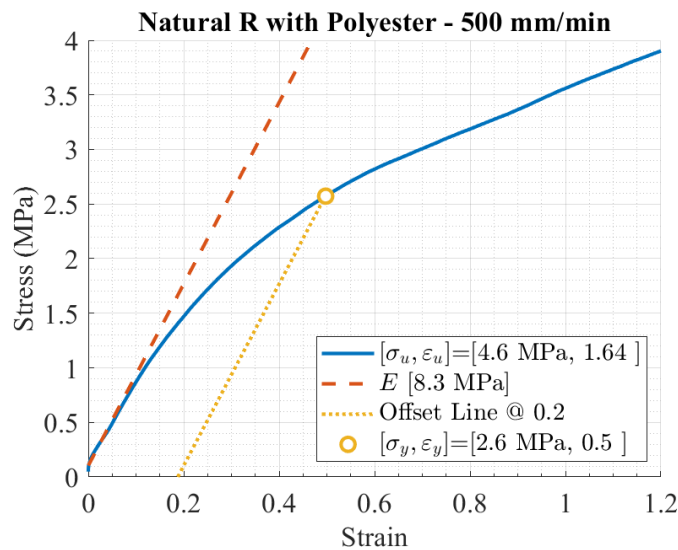
Figure 4.10: Offset Yield Strength for the FR material



(a)



(b)



(c)

Figure 4.11: Offset Yield Strength for the NatPolR material

4. CHARACTERIZATION OF THE MECHANICAL PROPERTIES OF SOFT MATERIALS

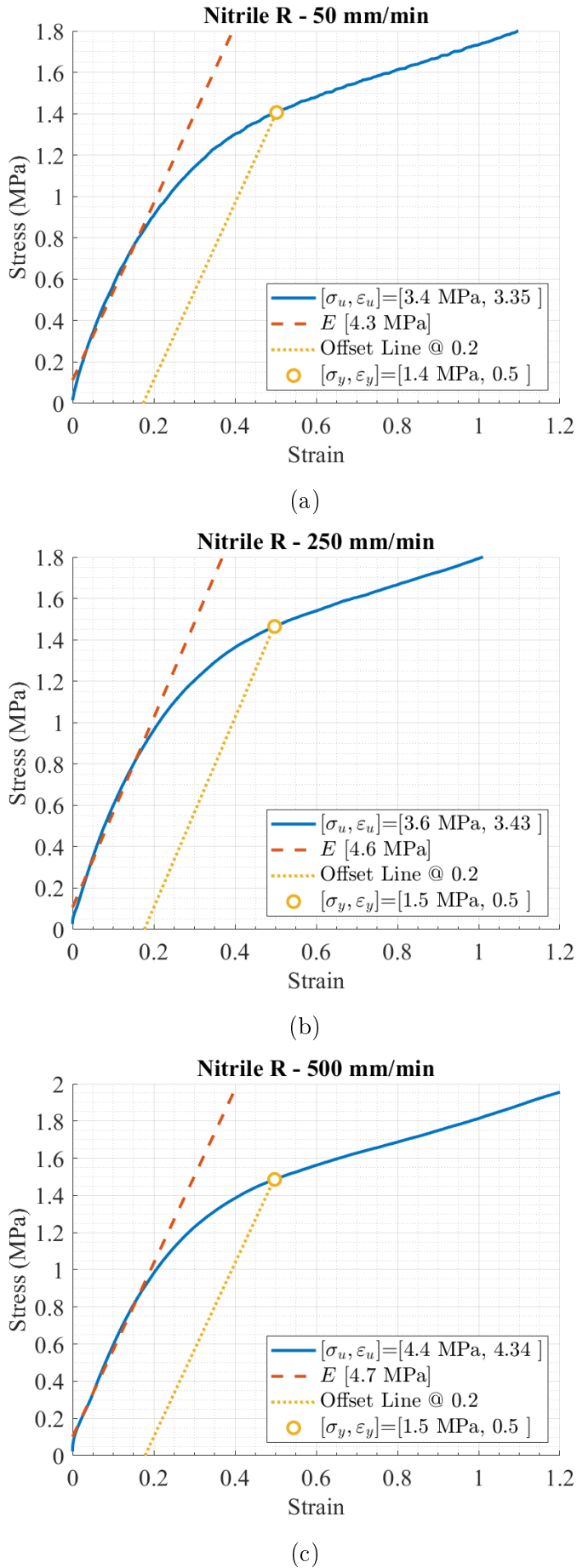


Figure 4.12: Offset Yield Strength for the NR material

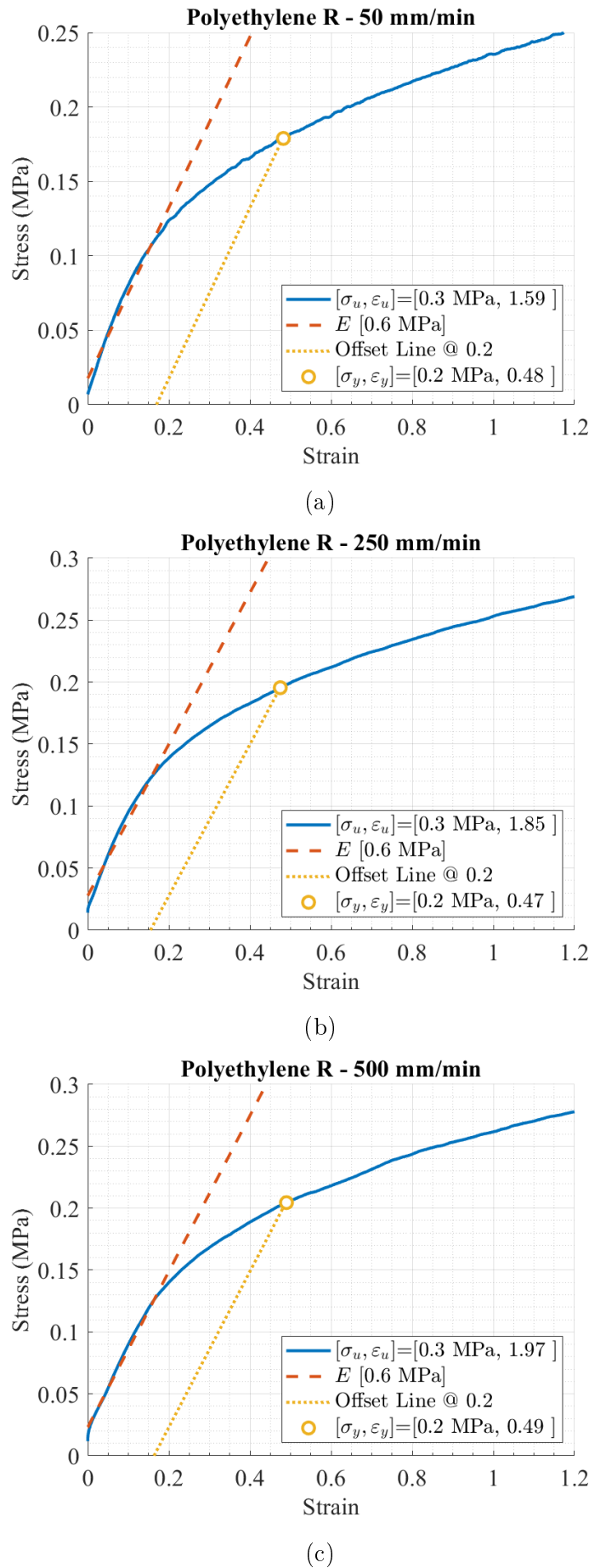
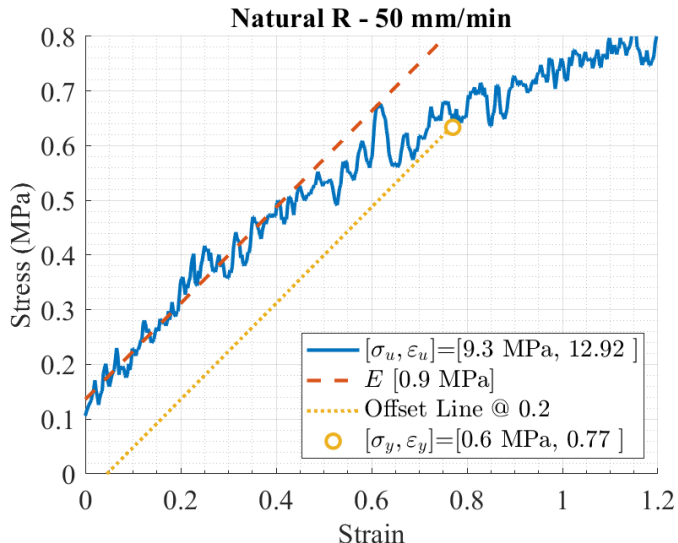
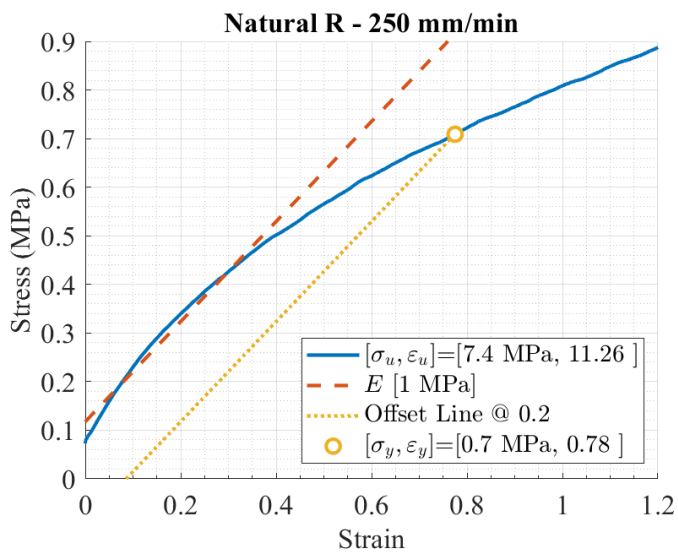


Figure 4.13: Offset Yield Strength for the PR material

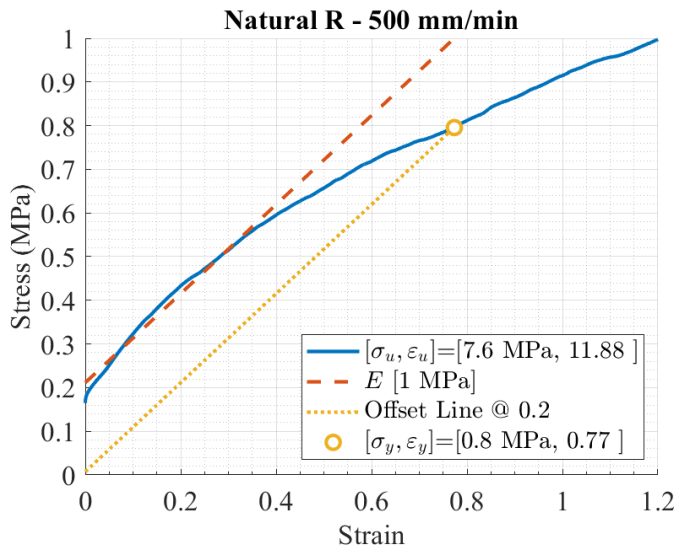
4. CHARACTERIZATION OF THE MECHANICAL PROPERTIES OF SOFT MATERIALS



(a)

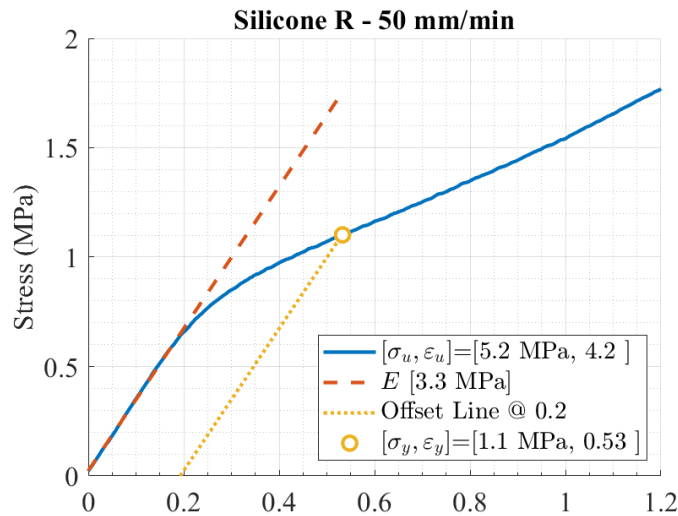


(b)

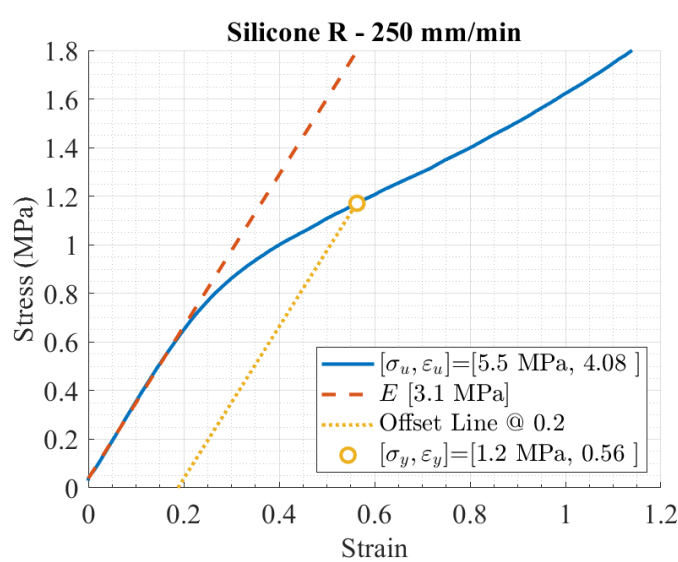


(c)

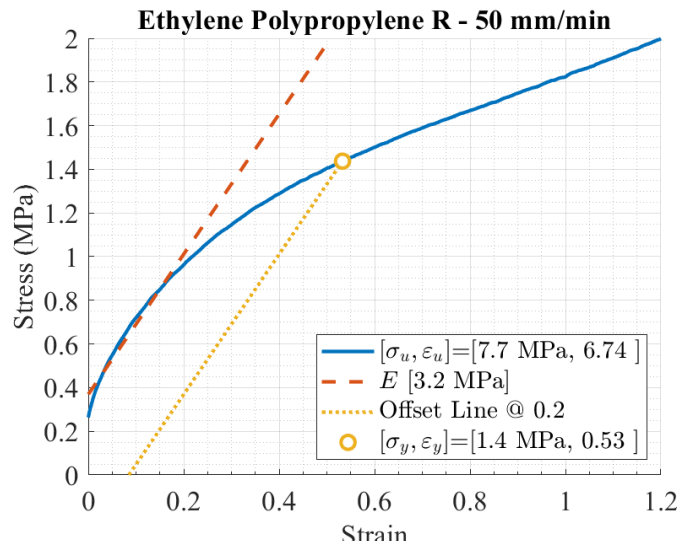
Figure 4.14: Offset Yield Strength for the NatR material



(a)



(b)



(c)

Figure 4.15: Offset Yield Strength for the SR and EPR (50mm/min) material.

4. CHARACTERIZATION OF THE MECHANICAL PROPERTIES OF SOFT MATERIALS

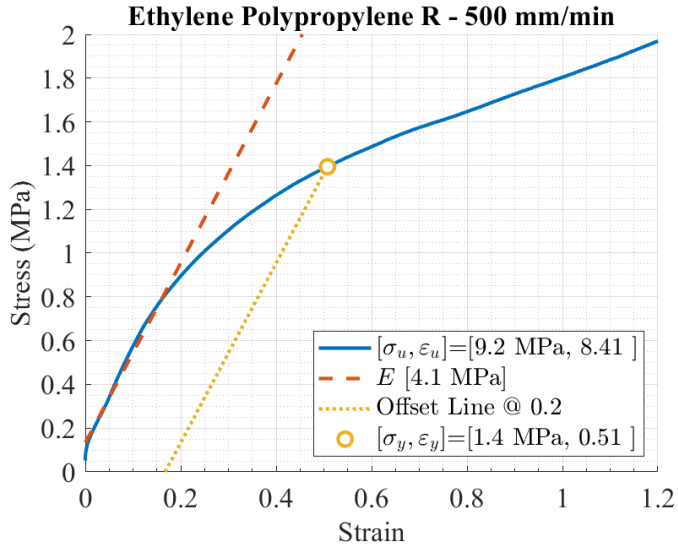


Figure 4.16: Offset Yield Strength for the EPR (500mm/min) material

In Figures 4.10 to 4.16, the elastic region is approximated by using the offset yield strength parameter, described previously. The values for the ultimate strength, yield strength, and the elastic modulus at the elastic region, are also provided. Any value below the offset yield strain can be assumed to be inside the elastic region of the material, hence the material will recover its original shape after undergoing any deformation inside this range of values. Having delimited the elastic region and its elastic modulus (now E_{small}), the slope of the second linear portion of the curve, i.e. the elastic modulus E_{large} , can be approximated.

The elastic properties of the material are compiled in Table 4.2. The ultimate values σ_{ue} and ε_{ue} are reported as the median value from all the specimens of a specific test type. The yield values σ_y and ε_y are obtained using the offset yield strength method. The parameters E_{small} and E_{large} are the elastic modulus at the initial section, and middle section of the stress-strain curve. Also, E_{small} is the most useful parameter for assessing the performance of a material in a real robotic application, because it describes the stiffness of a material inside the elastic region, i.e. safe working conditions. In this regards the PR material has the smallest value, whereas the NatR material has the largest.

4.3.2 Stress Relaxation Test

The stress relaxation test allows the extraction of the viscoelastic properties of the materials, i.e. the time-dependent properties. In this test, a predefined and constant elongation, also called initial strain ε_o is applied to the material specimen. The material is held in place for the whole duration of the test and the stress response is

Table 4.2: Elastic properties of the selection of soft materials. The materialas are: Polyethylene Rubber (PR), Ethylene Polypropylene Rubber (EPR), Natural Rubber with Polyester (NatPolR), Natural Rubber (NatR), Silicone Rubber (SR), Fluorocarbon Rubber (FR), and Nitrile Rubber (NR).

Materials	Speed mm/min	σ_{ue} MPa	ε_{ue}	σ_u MPa	ε_u	σ_y MPa	ε_y	E_{small} MPa	E_{large} MPa
EPR	50	8.48	7.56	7.67	6.74	1.44	0.54	3.23	0.99
	500	9.59	8.84	9.16	8.41	1.39	0.51	4.16	1.1
FR	50	4.36	3.97	3.96	3.56	1.5	0.47	4.83	0.65
	250	4.41	3.93	4.22	3.57	1.78	0.45	5.95	0.58
	500	5.35	4.29	4.87	4.07	1.91	0.45	6.78	0.61
NatPolR	50	3.57	1.19	3.08	0.91	2.12	0.41	9.97	2.05
	250	4.06	1.19	3.91	1.09	2.51	0.43	10.74	2.28
	500	4.59	1.64	4.59	1.64	2.52	0.48	8.77	1.9
NR	50	3.55	3.57	3.36	3.36	1.41	0.5	4.29	0.64
	250	3.65	3.62	3.58	3.43	1.47	0.5	4.63	0.69
	500	4.62	4.61	4.37	4.34	1.48	0.5	4.72	0.72
PR	50	0.3	1.87	0.28	1.59	0.18	0.48	0.58	0.11
	250	0.33	1.97	0.31	1.83	0.19	0.45	0.66	0.1
	500	0.32	1.97	0.32	1.97	0.2	0.49	0.64	0.1
SR	50	6.03	5.77	5.26	4.22	1.1	0.53	3.26	1.08
	250	5.68	4.27	5.52	4.08	1.15	0.54	3.26	1.35
NatR	50	9.43	13.02	9.37	12.93	0.61	0.69	1.01	0.33
	250	15.88	12.11	7.38	11.27	0.69	0.74	1.11	0.41
	500	11.93	12.26	6.61	11.22	0.73	0.71	1.19	0.43

recorded. The material will relax over time, i.e. the stress response will decrease. Similarly as for the tensile strength test, different combinations of test duration and initial strain values are chosen for the tests. Also, a varying number of specimens are included in each test. Some of these combinations are based on similar characterization processes available in the literature in where the duration time is no longer than 200 minutes [110, 111]. Nonetheless, a second test is proposed with a shorter duration. The diverse parameters used in the tests are aimed to create a richer dataset. As a recommendation, the value for the applied ε_o must fall bey-

4. CHARACTERIZATION OF THE MECHANICAL PROPERTIES OF SOFT MATERIALS

ond the elastic region of the material to avoid plastic deformation, i.e. irreparable damage. However, for highly elastic materials, such as elastomers, large values of ε_o are used in the literature. Also, the material must be elongated from zero strain to the value of ε_o as fast as possible. Therefore, the strain rate chosen for this test is 500 mm/min. With this in mind, the first test is performed using relatively large values of ε_o which are beyond the elastic region of the materials, identified in Section 4.3.1.2. For this case, the test duration is the longest, of 180 minutes. A second test is performed using ε_o values inside the elastic region of the materials and with a shorter duration of 15 minutes. The parameters for the performed tests are compiled in Table 4.3.

Table 4.3: Stress relaxation tests parameters and total collected datasets.

Test	Parameters	EPR	FR	NatPolR	NR	PR	SR	NatR
1	ΔL_o (mm)	5	5	7	6	3	6	40
	ε_o	0.15	0.15	0.21	0.18	0.09	0.18	1.21
	Duration (minutes)	15	15	15	15	15	15	15
Datasets		5	5	5	5	5	5	2
2	ΔL_o (mm)	20	10	6	5	4	15	-
	ε_o	0.61	0.3	0.18	0.15	0.12	0.45	-
	Duration (minutes)	180	180	180	180	180	180	180
Datasets		1	1	1	1	1	1	-

Similar to the tensile strength tests, the collected data is processed prior to the extraction of the relevant parameters. The data of interest is the one found after the machine has reached the predefined ε_o value. In here, several smoothing algorithms such as, moving average, Gaussian-weighted moving average, and the Savitzky-Golay algorithm, are analysed. During testing of these algorithms, a direct relationship between the decrease in the value of the initial stress σ_o , and the selected window size, is observed. The selected window size is based on the sampling frequency and the duration of the test. The Savitzky-Golay algorithm has the least impact on the initial stress σ_o in relation to the achieved smoothing. Therefore, this algorithm is chosen for the smoothing of the stress relaxation curve.

4.3.2.1 Stress Relaxation Properties

The stress relaxation test is useful for approximating the time relaxation constants of the materials. Commonly, viscoelastic materials have more than one relaxation constant. This is caused by the many number of internal molecular chains which relax at different rates. The stress relaxation curve of viscoelastic materials has a decaying exponential behaviour. This known mathematical function, in combination with the Linear Viscoelastic Models (LVMs), can be used to approximate the time relaxation constants of the materials. The LVMs have the flexibility to get as complex as required by adding extra elements to the model. The number of relaxation constants that can be extracted from the stress relaxation curve is directly proportional to the number of exponential functions contained in the LVM. This is described in detail in Chapter 5. The stress at the starting and ending points of the test, σ_o and σ_{end} , respectively, are the minimum required parameters to approximate one relaxation constant of the material using a LVM. Another parameter of interest is the achieved stress relaxation, which is defined as follows:

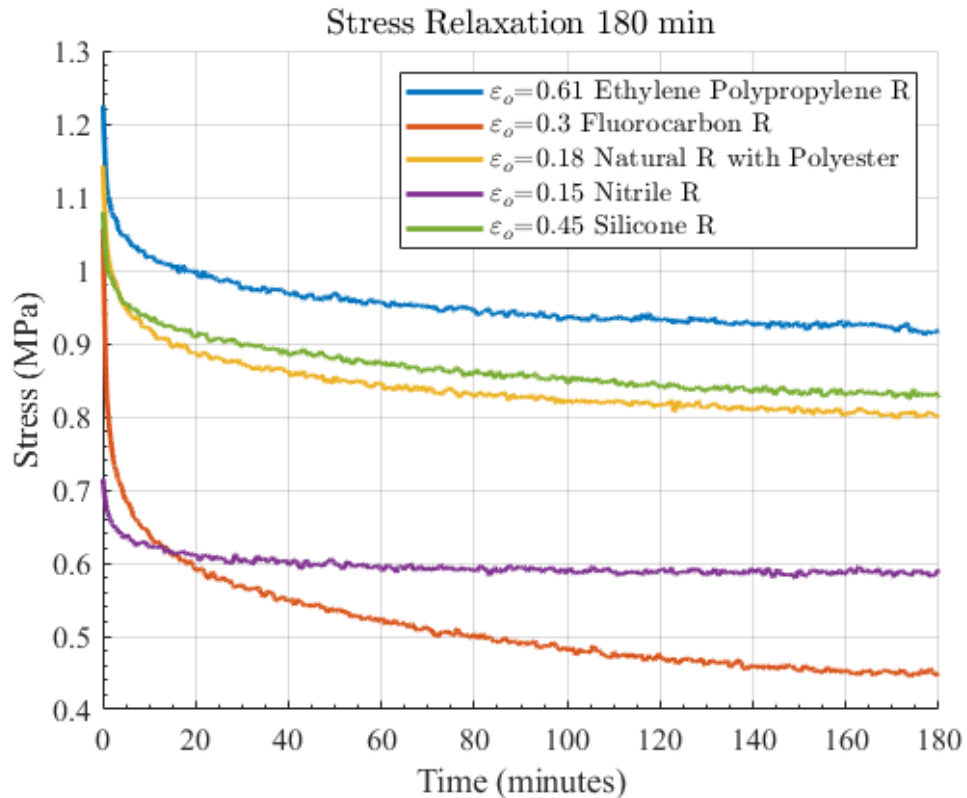
$$S.R. = 100 \left(\frac{\sigma_o - \sigma_{end}}{\sigma_o} \right) \quad (4.1)$$

The parameters extracted from the stress relaxation test are compiled in Table 4.4. The obtained stress relaxation curves of all the materials are illustrated in Figures 4.17 and 4.18. The values of σ_o and σ_{end} are obtained by finding the median value of all tests included in each scenario, using the collected raw data. The values of the *S.R.* are very similar in both tests, in terms of the duration of the test and the chosen value for ε_o . This means most of the *S.R.* happens very early into the test, and that only one relaxation time constant is required to model the stress relaxation of these materials.

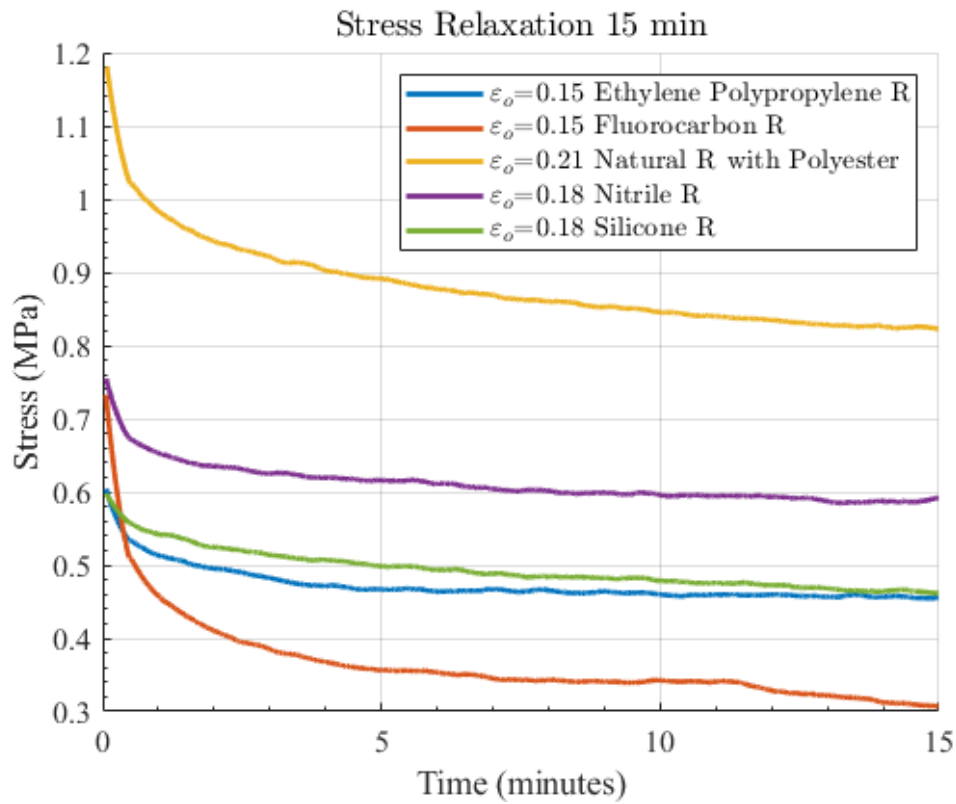
Table 4.4: Stress relaxation parameters for the selection of soft materials.

Test	Properties	EPR	FR	NatPolR	NR	PR	SR	NatR
1	σ_o (MPa)	0.61	0.84	1.22	0.77	0.06	0.61	2.15
	σ_{end} (MPa)	0.42	0.27	0.80	0.55	0.02	0.43	1.82
	<i>S.R.</i> (%)	32	67	35	29	63	31	15
2	σ_o (MPa)	1.28	1.13	1.18	0.72	0.07	1.11	
	σ_{end} (MPa)	0.89	0.41	0.76	0.55	0.03	0.80	
	<i>S.R.</i> (%)	31	63	36	24	51	28	

4. CHARACTERIZATION OF THE MECHANICAL PROPERTIES OF SOFT MATERIALS

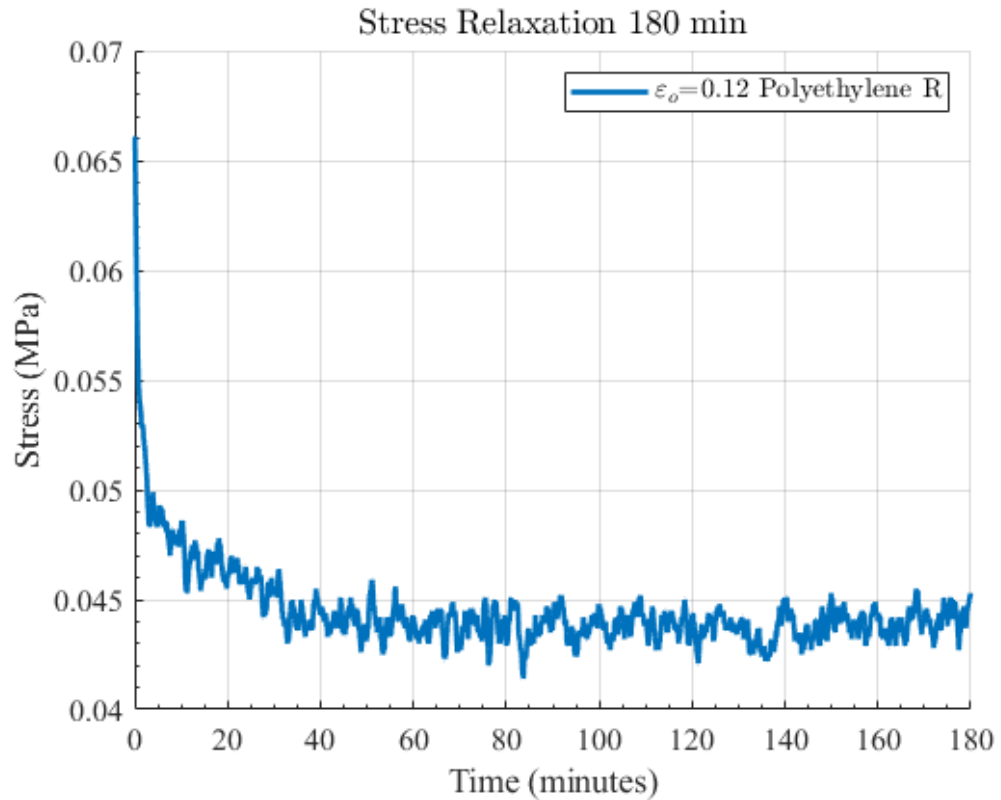


(a) Caption

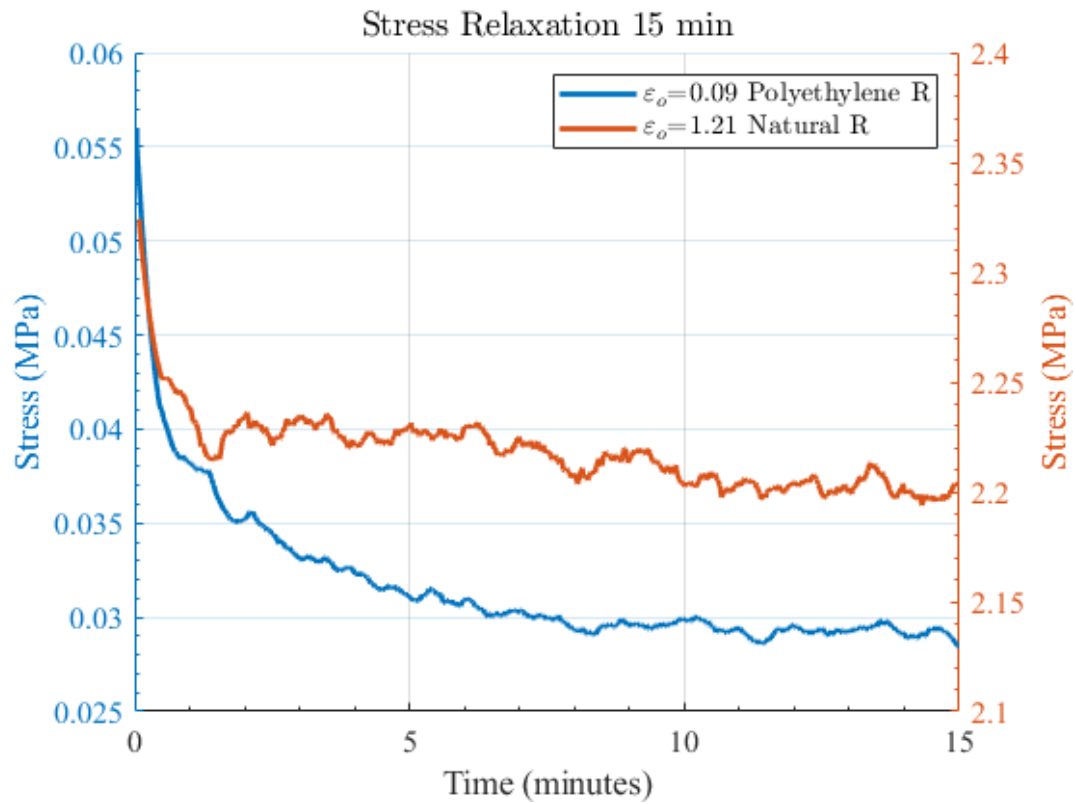


(b) Caption

Figure 4.17: Stress Relaxation curves for (a) 180 minutes and (b) 15 minutes, of the EPR, FR, NatPolR, NR and SR materials. Different values of ε_o are investigated.



(a) Caption



(b) Caption

Figure 4.18: Stress Relaxation curves for (a) 180 minutes and (b) 15 minutes, of the PR, and NatR materials. Different values of ε_o are investigated.

4. CHARACTERIZATION OF THE MECHANICAL PROPERTIES OF SOFT MATERIALS

4.4 Summary

In this chapter, the characterization process of the viscoelastic mechanical properties of a selection of seven different thermoplastic elastomers (TPEs) is presented. For this, the mechanical tests of tensile strength and stress relaxation are performed. In the tensile strength test, the materials are elongated until failure using up to three different strain rates. This decision is aimed to capture the velocity-dependent stress response of the materials and to create a richer dataset for the modelling stage. The algorithm used to condition the collected data is included is also described. The smoothing algorithm applied to both mechanical tests is the Savitsky-Golay algorithm. In the case for the Natural Rubber material, inconsistencies in the measured thickness of a type of band, from one batch to the other, are detected. Nevertheless, the mechanical behaviour of the material is captured accurately in the stress-strain curves. This suggests a linear proportionality between the thickness of the material and the strength of the material. The elastic region of the materials cannot be easily identified due to the non-linear stress-strain curve of the materials. Therefore, the elastic region is approximated using the offset yield strength parameter. This region is very important to delimit the working conditions of the soft materials in a real robotic application. Finally, the ultimate values of strain and stress, the elastic region location, the elastic modulus in two distinctive regions of the curve, and the offset yield strength parameters, are reported. The E_{small} is the most useful parameter for assessing the performance of a material in a real robotic application, because it describes the stiffness of a material inside the elastic region, i.e. safe working conditions, in contrast to the ultimate strength values. In this regard the PR material has the smallest value, whereas the NatR has the highest.

The performed stress relaxation tests can be divided into two sets. One with a low deformation, and low duration. The other, with large deformation, large duration. Regarding this, the achieved stress relaxation of the materials is very similar for both cases. Knowing the resemblance of the stress relaxation curve with an exponential decaying function, the latter finding suggests that only one time relaxation constant is responsible for the majority of the *S.R.* achieved. This hypothesis will be explored in the modelling stage.

CHAPTER 5

Soft Materials Modelling: Linear
Viscoelastic Models

5.1 Introduction

In this chapter, two modelling tools, based on mathematical models, for the prediction of the viscoelastic properties of seven soft materials are developed. These models are the PL-SLS model and the PL-Wiechert model. The work carried out in this chapter is inspired on the piecewise linearisation (PL) method described by Austin et al. [86]. The PL method has been proven successful in enabling the Standard Linear Solid (SLS) model to account for the strain-dependent stress response of soft materials. The model developed in Austin et al. work is called the Standard Linear Solid model with Strain-Dependent Stiffness (Std. Lin. SDS). The capabilities of the Std. Lin. SDS of accounting for velocity-dependent stress responses have not been assessed in the literature. This is investigated in this chapter.

The PL method implemented in this work is improved to maximize the prediction performance of the models. Due to this, the developed models in here differ from the ones available in the literature and represent a direct improvement to current modelling approaches. Two LVMs are studied in here, the SLS model and the Wiechert model. The PL method is applied to both, yielding the PL-SLS and the PL-Wiechert models. The Wiechert model is of interest due to its better capabilities of accounting for velocity-dependent stress responses, in comparison to the simpler SLS model. These additional capabilities of the Wiechert model translates into additional computational and mathematical complexity. Nonetheless, the PL method is capable of reducing this complexity.

In contrast with the fitting process described in the literature [86], the stress relaxation test is used to extract the relevant parameters for the SLS and Wiechert models. Subsequently, the PL method is applied to both models, allowing them to account for strain-dependent stress responses. The performance of both models is assessed using the stress-strain curves of the characterized soft materials: ethylene polypropylene rubber (EPR [11]), fluorocarbon rubber (FR [12]), nitrile rubber (NR [13]), natural rubber with polyester (NatPolR [14]), polyethylene rubber (PR [15]), silicone rubber (SR [16]), and natural rubber (NatR [17]).

Three mains analyses are performed. Firstly, the relationship between the PL method prediction accuracy and required complexity is assessed. A tolerance criteria is proposed in here, which establishes a proportional relationship between the complexity of the soft material stress-strain curve, and the required complexity of the PL method. Secondly, the maximum prediction accuracy of both models is assessed. The results indicate that both models can accurately predict the stress-strain

5. SOFT MATERIALS MODELLING: LINEAR VISCOELASTIC MODELS

curve of the soft materials under a single strain rate. Thirdly, the capabilities of both models to account for the velocity-dependent stress response of the materials are investigated. The results indicate the superiority of the PL-SLS model and the PL-Wiechert model in comparison to the Std. Lin. SDS model documented in the literature. The models developed here achieved normalized root mean square values of 5% in comparison to the 13.6% achieved by the Std. Lin. SDS model. In general, the PL-Wiechert model performs better for soft materials with moderate to high viscous properties, whereas the PL-SLS model performed better for soft materials with high elastic properties. In conclusion, the improved implementation of the PL method resulted in an improved modelling tool for the prediction of the nonlinear, strain-dependent, and time-dependent stress response of soft materials.

5.2 The Linear Viscoelastic Models

Thermoplastic elastomers have nonlinear and viscoelastic mechanical properties which cannot be easily described by mathematical models. The latter represents an important challenge for current soft robotic developments. However, the benefits of using soft materials are many: energy storing, passive compliance and safe human-robot interaction. This has motivated their implementation in robotic applications, as well as the development of robust modelling tools capable of describing their viscoelastic properties [112].

The natural property of the human skeletal muscle system of storing and releasing energy, has motivated the inclusion of elasticity in robotic applications. Series-elastic actuators (SEAs) are the most commonly used technology. The addition of an elastic element between the actuator and the load greatly simplifies the controller design. The deformation of the elastic element can provide an indirect measurement of the applied force to the load, essentially transforming a force-control problem into a displacement-control problem [113].

Traditional SEAs use metallic springs, considered as purely elastic. However, the human skeletal muscle system exhibits viscoelastic behaviour. In the literature, attempts of adding viscoelasticity to SEAs by using soft materials instead of metallic springs, are documented. In fact, viscoelasticity has the potential to address many of the limitations found in series-elastic actuators, such as: low torque resolution and low bandwidth [85, 114, 115].

The mechanical behaviour of a rigid element (metallic spring) can be accurately

described by known mathematical models. This is not the case for soft materials which have nonlinear and viscoelastic properties. The benefits of adding viscoelasticity to SEAs can only be fully exploited by developing a reliable modelling tool. Substantial research has been done on this. However, the most accurate models are mathematically complex and computationally expensive [72, 74, 75]. Nonetheless, even these complex models cannot account for all the different factors which modify the materials properties, such as the manufacturing process and internal weakening of the material after being loaded for the first time [110]. The latter highlights the difficulty of developing mathematical models which account for both microscopic and macroscopic aspects of the materials. This has motivated researchers to implement alternative methods for characterizing a material, such as Finite Element Analysis (FEA).

In robotic applications, where the controller can compensate inefficiencies in the system, a simple and fairly accurate modelling tool is preferred over a very accurate and highly complex one. For this reason, a known set of mathematical models, the Linear Viscoelastic Models (LVMs) are commonly used for the prediction of viscoelasticity in soft materials. In contrast to the mechanical model for Hooke's Law, which is based on a single spring, the LVMs are based on two fundamental mechanical components, a spring and a dashpot, which can be arranged in different configurations and quantities. This is illustrated in Figure 5.1, where the parameters k and η represent the spring stiffness and the dashpot viscous constant, respectively.

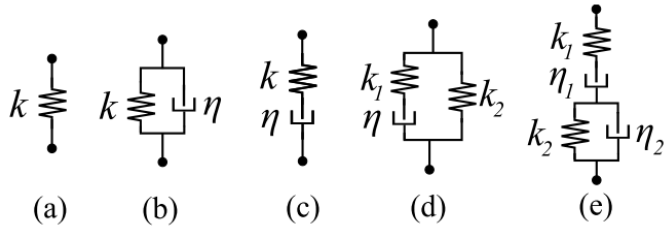


Figure 5.1: Hooke's Law and linear viscoelastic models: (a) Hooke's Law (b) Kelvin-Voigt, (c) Maxwell, (d) Standard Linear Solid, and (e) Burger. The parameters k and η represent the spring stiffness and the dashpot viscous constant, respectively [86].

In line with the mentioned approach of relying on the controller to compensate the limitations of simple models, the work performed by Austin et al. modifies the viscoelastic Standard Linear Solid (SLS) model by implementing a piecewise linearisation (PL) method [86]. The authors chose the SLS model instead of the

5. SOFT MATERIALS MODELLING: LINEAR VISCOELASTIC MODELS

more complete, hence more complex, Burger model to keep the modelling process as simple as possible. The implementation of the PL method allowed the SLS model to account for the nonlinear properties of the material stress response in proportion to the applied strain. Due to this, the developed model is called the Standard Linear Solid model with Strain-Dependent Stiffness (Std. Lin. SDS). Unfortunately, the developed model is still incapable of accounting for the material hysteresis. Due to hardware limitations, the velocity-dependent stiffness effects are not validated. Nonetheless, experimental tests validated the changes on the material stiffness depending on the velocity of the applied deformation.

The PL method has proven to be a successful way to improve the prediction capabilities of traditional LVMs. Although it still has some limitations. The latter is addressed in this chapter by implementing the PL method in a more complex member of the LVMs, the Wiechert model.

5.3 The Piecewise linearisation Method

The SLS model is frequently used when modelling viscoelastic materials, mainly due to its mathematical simplicity and its capability of accounting for the creep and stress relaxation phenomena of the materials (time-dependent properties). The SLS model can be viewed as a Maxwell model (also known as Maxwell branch) with an extra spring connected in parallel. The simplicity of the SLS model is also its main limitation. Viscoelastic materials are known to have more than one relaxation time constant, i.e. more than one Maxwell branch. In the family of LVMs, the relaxation time constant depends on the viscous elements, i.e. dashpots. The Wiechert model, which is essentially a SLS model with j Maxwell branches, is able to account for j relaxation time constants (Figure 5.2). The time-dependent behaviour of any viscoelastic material can be fully described by this model, given enough numbers of elements. However, the complexity of the model increases in proportion to the number of extra branches. Mathematically, each extra branch increases the derivative order of the model since more equations are required to account for the extra variables [73, 77].

As previously described in Section 4.2, in addition to time-dependent and history-dependent properties, elastomers also have a nonlinear stress response. This can be partially described by the LVMs. The relaxation time constant of the dashpots in these models describes the nonlinear and time-dependent stress response of the

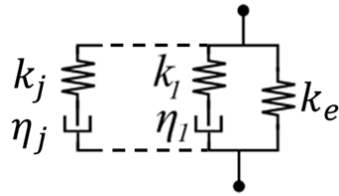


Figure 5.2: Wiechert Model. The components k_1 , η_1 , and the equilibrium spring k_e , together represents the SLS model. The components k_j , and η_j represents the Maxwell Branch. The Wiechert model can contain as many branches as required, this is symbolised by the subscript j .

material. Nonetheless, LVMs cannot account for the strain-dependent response of materials. The latter can be addressed by the PL method as described in [86].

The spring in parallel with the other elements, in both the SLS model and the Wiechert model, is known as the equilibrium spring, and its stiffness k_e , is assumed constant. In reality, the stiffness k_e of most elastomers is strain-dependent. Early attempts of modelling a strain-dependent stress response in viscoelastic materials are described by Schepelmann et al. in [85], where the stress-strain curve of a nonlinear rubber spring is approximated with an exponential model. In subsequent works, Austin et al. describe a piecewise linear regression fitted to the stress-strain curve of a material, in combination with the SLS model [86].

The slope of the stress-strain curve represents the material's Young Modulus which is proportional to the material stiffness. During a tensile strength test the material is deformed at a constant rate, i.e. $\dot{\varepsilon}$ is constant. The stress response of a viscous element is proportional to the strain rate $\dot{\varepsilon}$. Therefore, it can be safely assumed that the observed nonlinear stress response on the stress-strain curve is solely caused by changes in the equilibrium spring stiffness k_e .

Using the PL method, the nonlinear behaviour of the equilibrium spring is approximated by considering it as several springs in parallel which “engage” in sequence as the material strain increases. This is modelled by a summation of Heaviside functions centred in the desired strain in which each of the mentioned springs “engage” and contributes to the total stress response of the material. In other words, the stress-strain curve of the material is segmented in several sections which relates a single stiffness to a range of strains (Figure 5.3).

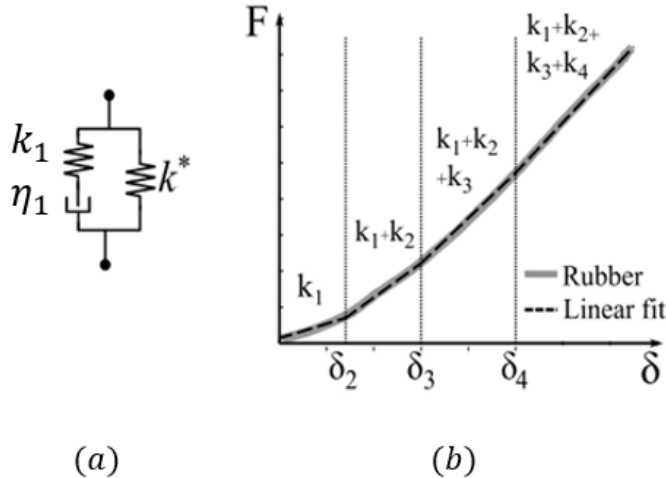


Figure 5.3: (a) Standard Linearized Solid model with Strain-Dependent Stiffness. (b) Piecewise linearisation method applied to the slope of the material load-displacement curve. This is analogous to many parallel springs which contribute to the material response depending on the material strain [86].

5.4 Model fitting

The mathematical expression for the SLS model and the Wiechert model can be simplified when considering a constant strain input (stress relaxation test). This simplification allows these models to be fitted into the stress relaxation curve and to approximate the parameters of interest, k and η [77]. The mathematical expression for the Wiechert model under a constant strain input is given by:

$$\sigma(t) = \left(k_e + \sum_j k_j e^{-t/\tau_j} \right) \varepsilon_o \quad (5.1)$$

where σ is the stress at a given time, k_e is the equilibrium spring stiffness and ε_o is the initial strain. For the summation, $\tau_j = \eta_j/k_j$ is the relaxation time constant, k_j and η_j are the spring stiffness and viscous constant of the elements in the j^{th} Maxwell branch, respectively. For the specific case when $j = 1$, the resulting equation describes the SLS model under a constant strain input, which is as follows:

$$\sigma(t) = (k_e + k_1 e^{-t/\tau}) \varepsilon_o \quad (5.2)$$

In (5.2), the three main parameters of the SLS model, i.e. the equilibrium spring stiffness k_e , the dashpot viscous constant $\eta = \tau k_1$, and the spring stiffness in the Maxwell branch k_1 , can be obtained from the stress relaxation curve by analysing

three significant points: $t = 0$, $t = \tau$, and $t = \infty$ (Figure 5.4). Due to the decaying exponential nature of this curve, the time constant τ can be related to the point in time t where the stress has decayed to approximately 36.8% of its initial value σ_0 . The longer the duration of the test, the better the approximation of k_e .

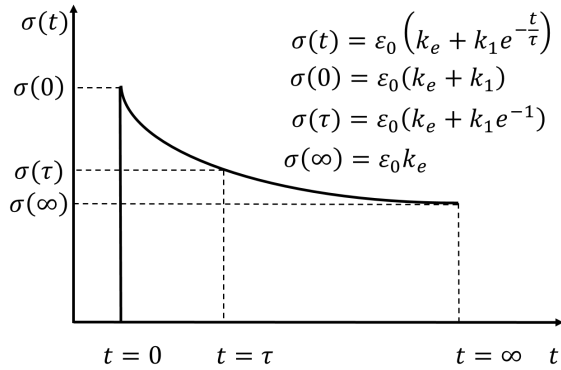


Figure 5.4: SLS model fitted to a typical stress relaxation curve of a viscoelastic material. The parameters k_e , k_1 and η can be obtained by analysing three points in the curve: $t = 0$, $t = \tau$, and $t = \infty$. The variable τ is the time constant of the exponential decaying curve.

The process to extract the parameters of the Wiechert model is more complicated due to its extra Maxwell branches, i.e. there are more than three points in time to be analysed. These points can be selected using a collocation technique [77, 116]. In the reviewed literature, the points of interest are linearly scattered throughout the whole duration of the stress relaxation curve. Nevertheless, the decaying exponential term in (5.1) is better approximated by selecting the points of interest using a logarithmic scale. This is possible with the MATLAB function `logspace` which spreads evenly the desired number of points between the allowable decades. This is best described in the following example. A Wiechert model with six branches, $j = 6$, is to be fitted into a stress relaxation curve with four decades of duration ($t = 10^4$ seconds). In total, it would be required seven points in time, one for each branch and one for $t = 0$. These points are spread as evenly as possible, using the total duration of the test, by the function `logspace`.

Similar to the process illustrated in Figure 5.4, each point in time represents a time constant τ_j for which there is a known stress σ_j from the experimental data. This can be rearranged into an system of j equations with k_j as the unknown variable as follows [116]:

5. SOFT MATERIALS MODELLING: LINEAR VISCOELASTIC MODELS

$$\begin{aligned}
k_e + k_1 e^{-\tau_1/\tau_1} + k_2 e^{-\tau_1/\tau_2} \dots + k_j e^{-\tau_1/\tau_j} &= \frac{\sigma(\tau_1)}{\varepsilon_0} \\
k_e + k_1 e^{-\tau_2/\tau_1} + k_2 e^{-\tau_2/\tau_2} \dots + k_j e^{-\tau_2/\tau_j} &= \frac{\sigma(\tau_2)}{\varepsilon_0} \\
&\vdots \\
k_e + k_1 e^{-\tau_j/\tau_1} + k_2 e^{-\tau_j/\tau_2} \dots + k_j e^{-\tau_j/\tau_j} &= \frac{\sigma(\tau_j)}{\varepsilon_0}
\end{aligned} \tag{5.3}$$

Prior to this step, k_e can be obtained using the equation for $\sigma(\infty) = \varepsilon_0 k_e$, as illustrated in Figure 5.4. Subsequently, the Wiechert model in (5.1) can be completely described by solving the system of equations described in (5.3). Finally, after obtaining all the k_j , the value of k_1 is corrected by analysing the point in time $t = 0$, as described in [77].

The previous process allows the Wiechert model equation to be fitted into the stress relaxation curve for a defined number of branches j . However, to obtain the optimal number of branches for each material, an iterative algorithm to find the smallest root mean square error (RMSE) between the Wiechert model response and the experimental data after testing a different number of branches in the range of $j = [1, 10]$ is implemented. The obtained optimal number of branches for each material varies between the range $j = [5, 8]$. A higher number of branches have a meaningless improvement on the RMSE. Furthermore, beyond the number of branches $j = 20$ the Wiechert model response shows an oscillatory behaviour, hence a higher RMSE.

Having obtained the parameters of interest for the SLS and the Wiechert model, their stress response under a constant strain is compared against the experimental data in Figure 5.5. In this figure the superior accuracy delivered by the extra Maxwell branches in the Wiechert model in comparison to the simpler SLS model is observed.

As previously mentioned, (5.1) is a simplification helpful to approximate the parameters of both models, but it is only applicable when the strain input is constant. The mathematical expression for the Wiechert model which describes the stress response under an unknown strain input, also called the constitutive equation, in the Laplace domain, is as follows [77]:

$$\bar{\sigma} = \bar{\sigma}_e + \sum_j \bar{\sigma}_j = \left\{ k_e + \sum_j \frac{k_j s}{(s + \frac{1}{\tau_j})} \right\} \bar{\varepsilon} \tag{5.4}$$

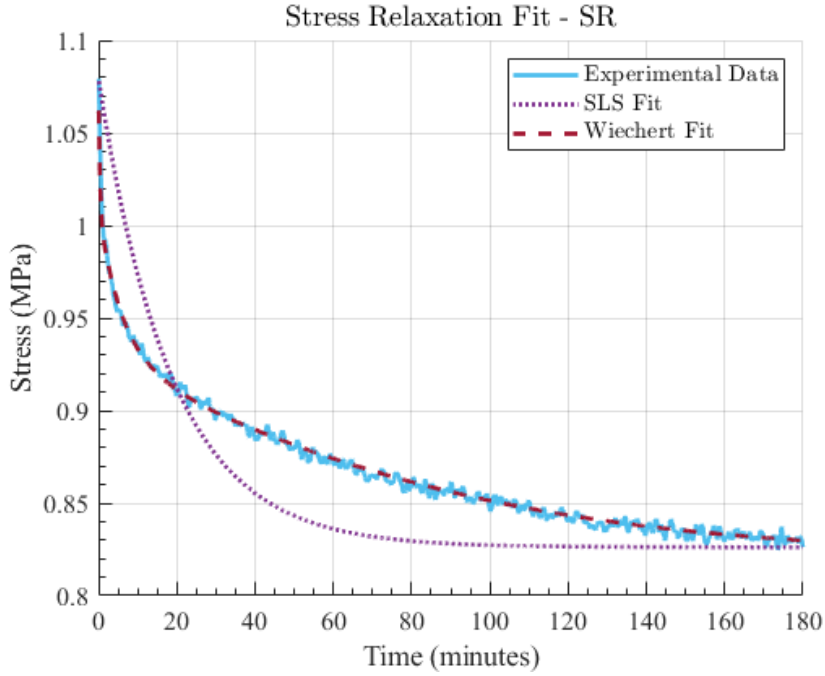


Figure 5.5: Obtained fit from the Standard Linear Solid (SLS) and Wiechert model of the stress relaxation curve of the Silicone Rubber material. The obtained optimal number of branches of the Wiechert model fit is $j = 8$.

where $\bar{\sigma}$ is the total stress, $\bar{\sigma}_e$ is the stress of the equilibrium spring, $\bar{\sigma}_j$ is the stress of the Maxwell branches, and $\bar{\varepsilon}$ is the strain function. All these variables are in the Laplace domain. Similarly, the constitutive equation for the SLS model, i.e. $j = 1$, in its time domain, is as follows:

$$\dot{\sigma} + \frac{\sigma}{\tau_1} = (k_e + k_1)\dot{\varepsilon} + \frac{k_e\varepsilon}{\tau_1} \quad (5.5)$$

where ε , $\dot{\varepsilon}$, and $\dot{\sigma}$ are the strain, the strain rate and the stress rate, respectively (for the detailed procedure refer to [77]). Notice that the previous procedure will yield into a higher derivative order equation when applied to the Wiechert model due to its extra branches. A higher number of branches will increase the model accuracy at the cost of increasing its mathematical complexity. The constitutive equation of a Wiechert model with j branches would result in a j^{th} order differential equation similar to (5.5). The aim of this chapter is to apply the PL method to the Wiechert model and evaluate its performance. Therefore, dealing with differential equations is out of the scope. Nonetheless, the Wiechert model can be evaluated by transforming it into a finite-differences equation yielding the following equation [77]:

5. SOFT MATERIALS MODELLING: LINEAR VISCOELASTIC MODELS

$$\sigma^t = k_e \varepsilon^t + \sum_j \frac{k_j (\varepsilon^t - \varepsilon^{t-1}) + \sigma_j^{t-1}}{\left(1 + \frac{\Delta t}{\tau_j}\right)} \quad (5.6)$$

where the superscript $t - 1$ and t refers to values before and after a small time step Δt have passed. Once again, making $j = 1$ in (5.6) yields the finite difference version of the SLS model.

The next step of the fitting process is focused on the tensile strength test. In this test, the strain rate is constant, hence the resulting stress for both models is dependent on both the equilibrium spring and the Maxwell branches. At this stage of the model fitting process, the parameters of the Maxwell branches in both models are known and their stress response can be calculated. The stress response in the equilibrium spring k_e can be isolated by subtracting the stress response of the Maxwell branches to the stress measured in the tensile strength test.

After isolating the stress response of k_e , the final step in the fitting process is to implement the PL method to both models and compare their response against the experimental data. Firstly, the stress-strain curve from the tensile strength test is divided into n segments. As previously explained, k_e is considered as a group of parallel springs which “engage” as the strain increases. This means, each subsequent stiffness is a combination of the ones found in previous segments of the stress-strain curve (Figure 5.3). Lastly, a linear regression is applied to the stress-strain curve for the desired n strain segments to find the slope of the curve. This slope represents the stiffness of the equilibrium spring in each segment. By combining the n obtained stiffness, the stress response of the strain-dependent stiffness k_i^* is defined as follows:

$$\sigma^{*t} = \sum_i^n k_i^* H_{\varepsilon-\varepsilon_i}(\varepsilon^t - \varepsilon_i) \quad (5.7)$$

where n is the desired number of strain intervals to fit, ε_i represents the strain value at which the i^{th} spring starts contributing to the stress response, the $H_{\varepsilon-\varepsilon_i}$ is the Heaviside or unitary step function centered at ε_i , i.e. the function output goes from 0 to 1 when $\varepsilon - \varepsilon_i = 0$. By substituting (5.7) into (5.5), the Standard Linear Solid model with Strain-Dependent Stiffness is obtained [86].

The LVMs describe a nonlinear relationship between the applied strain and the resulting stress in a material. However, they only account for a linear stress response of the equilibrium spring. In reality, the relocation of internal molecular chains causes viscoelastic materials to exhibit a nonlinear and strain-dependent stress response. This can be solved by applying the PL method to (5.6). The equilibrium

spring stiffness k_e is replaced by the strain-dependent stiffness k_i^* , yielding the linearized Wiechert model (PL-Wiechert) in (5.8). Subsequently, the Std. Lin. SDS model, found in [86], is transformed into a finite difference equation, yielding the PL-SLS model described in (5.9).

$$\sigma^t = \sigma^{*t} + \sum_j \frac{k_j(\varepsilon^t - \varepsilon^{t-1}) + \sigma_j^{t-1}}{\left(1 + \frac{\Delta t}{\tau_j}\right)} \quad (5.8)$$

$$\sigma^t = \sigma^{*t} + \frac{k_1(\varepsilon^t - \varepsilon^{t-1}) + \sigma_m^{t-1}}{\left(1 + \frac{\Delta t}{\tau_1}\right)} \quad (5.9)$$

The linearized SLS model (5.9) is labelled as the Piecewise Linearized SLS (PL-SLS) model, differentiating it from the Std. Lin. SDS model due to the many optimizations performed to the PL method. The latter included using the stress relaxation curve of the materials. The optimization performed on the number of branches delivered a range from $j = 5$ to $j = 8$. Lastly, the process of fitting the Piecewise linearisation method to the SLS and the Wiechert model to create the PL-SLS and the PL-Wiechert model is described in Figure 5.6.

5.5 Findings

The following section describes the findings obtained from three individual analyses about the PL method performance and capabilities. The latter is organized into three subsections. Section 5.5.1 is focused on analysing the trade-off between the number of strain segments fitted to the stress-strain curve, i.e. complexity, and the achieved accuracy, when being applied to the PL-SLS model and the PL-Wiechert model. Section 5.5.2 is focused on analysing the accuracy of the PL-SLS model and the PL-Wiechert model in terms on the achieved normalized mean square error (NRMSE). Lastly, Section 5.5.3 is focused on analysing the capabilities of both models to account for the velocity dependency of the materials stress response. In other words, the generalization capabilities of both models are assessed.

The stress-strain curves from the materials studied in this section are from the tensile strength test with 500 mm/min strain rate. With the exception of the SR material, for which the 50 mm/min stress-strain curve is used. The available data for each soft material is described in Table 4.1.

5. SOFT MATERIALS MODELLING: LINEAR VISCOELASTIC MODELS

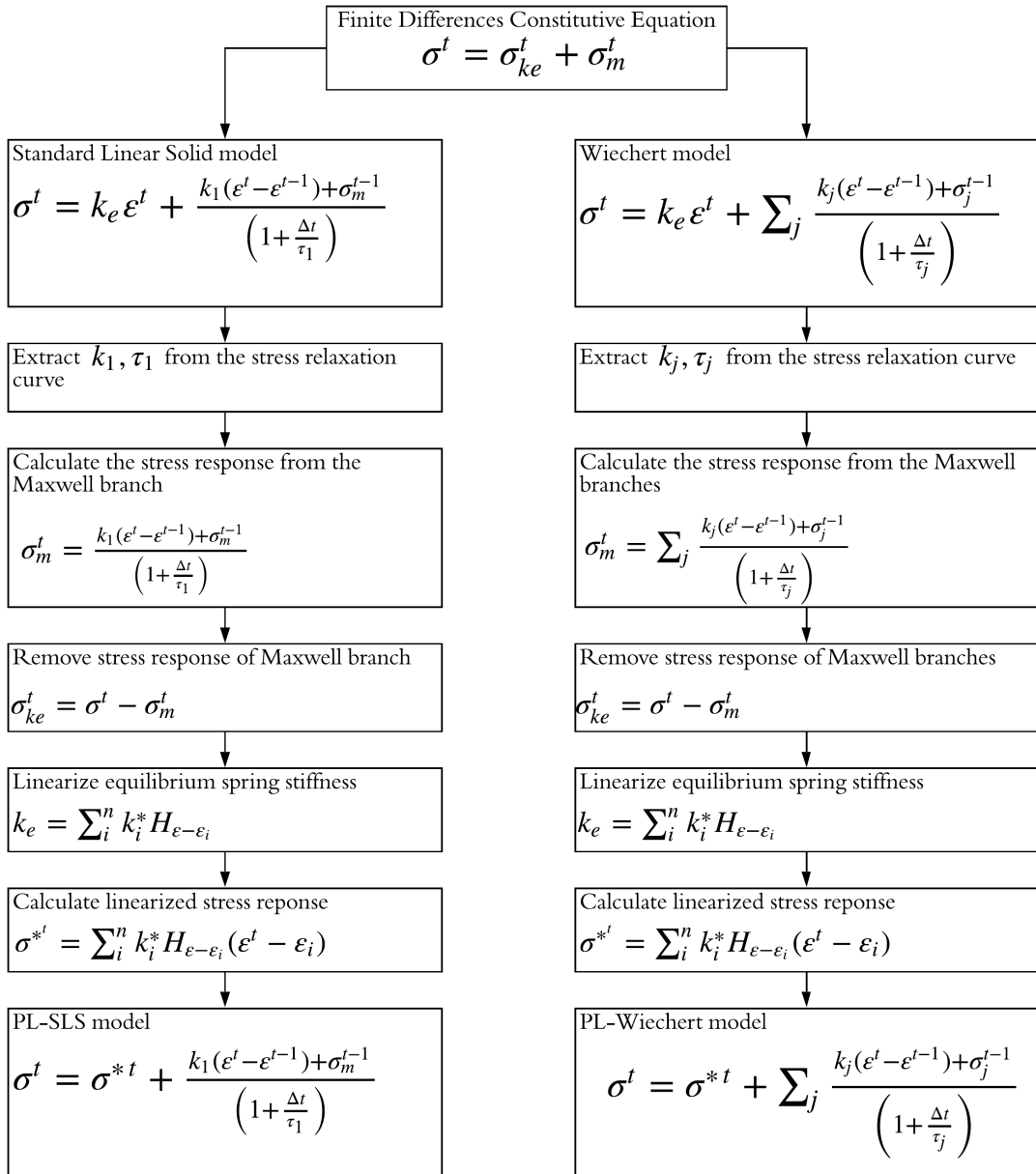


Figure 5.6: Description of the implemented Piecewise linearisation method.

5.5.1 Analysis of the Optimal Number of Strain Segments

The amount of strain segments and their proper collocation have an impact on the PL method accuracy. In the work presented by Austin et al. there is no explanation about the criteria used to select the strain segments. Nonetheless, the implementation of a linear collocation approach can be inferred from the description provided [86].

In here, the variation of the slope of the stress-strain curve is proposed as a

selection criteria for obtaining the right number of strain segments to fit to the stress-strain curve of the materials. Hence, an algorithm is developed to automatically collocate a new strain segment when the curve's slope exhibits a variation greater than a proposed tolerance value. In the optimization process the testing of different tolerance values in the range of 10 to 100 % is performed. This process is described in Figure 5.7.

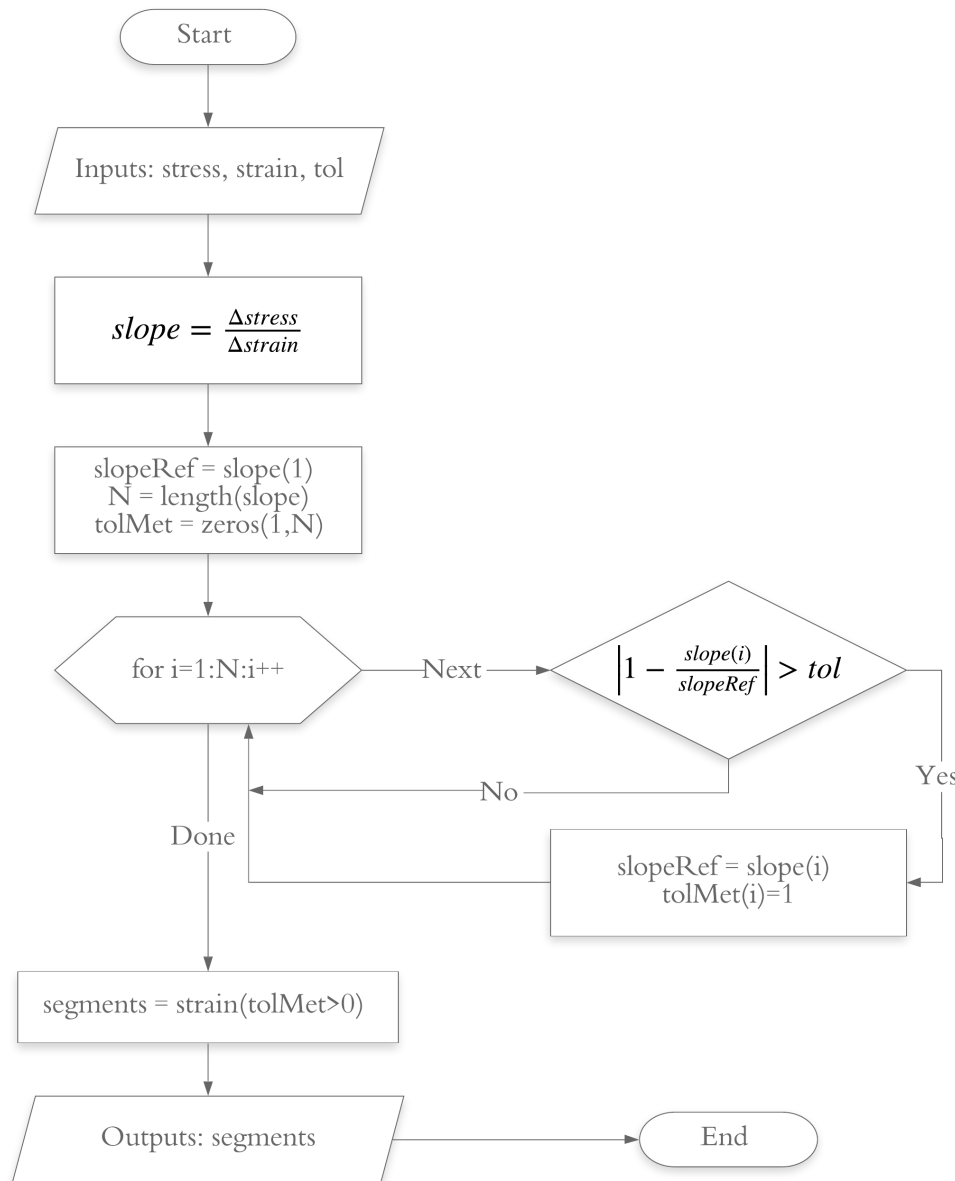


Figure 5.7: Algorithm for obtaining the right number of strain segments to be fitted based on the variation of the stress-strain curve slope.

The slope is calculated by numerical differentiation of the stress-strain curve.

5. SOFT MATERIALS MODELLING: LINEAR VISCOELASTIC MODELS

Then, the first calculated value of the slope is used as reference to monitor the variation of the slope along the stress-strain curve. When the variation is greater than the defined tolerance two things happen: a new strain segment is created, and the slope at this point becomes the new slope reference. This process is repeated until the complete stress-strain curve is scanned.

The proposed tolerance criteria establishes a proportional relationship between the nonlinearity of the stress-strain curve and the complexity of the Piecewise linearisation method. In other words, highly nonlinear soft materials will require more strain segments to be collocated. In a similar way, the tolerance criteria is inversely proportional to the obtained number of strain segments. In other words, the smaller the tolerance the larger the number of strain segments.

The performance of the PL method can be analysed with the optimization process described. Specifically, the relationship between the complexity and accuracy of the PL method. The complexity of the PL method is measured in terms of the number of strain segments fitted to the stress-strain curve. Whereas, the accuracy of the PL method is measured in terms of the normalized root mean square error (RMSE) [117], described as follows:

$$\text{NRMSE} = \sqrt{\frac{\langle(\sigma^{pred} - \sigma^{exp})^2\rangle}{\langle\sigma^{exp2}\rangle}} \quad (5.10)$$

where the $\langle \dots \rangle$ represents the arithmetic mean, σ^{pred} and σ^{exp} represent the predicted and experimental values of the stress response of the material, respectively. The results of the optimization process are illustrated in Figures 5.8 to 5.11. In these figures, the inversely proportional relationship between the number of strain segments and the tolerance is demonstrated. In other words, the smaller the tolerance value the greater the number of strain segments. In general, the relationship between these two parameters is inversely exponential for both the PL-SLS model and the PL-Wiechert model. This is consistent with all but one of the studied soft materials, the SR material. In this case, the relationship between the tolerance value and the number of strain segments, for both models, is more linear than exponential. There is in fact a complex relationship between the number of strain segments, the tolerance criteria, the achieved accuracy and the model used.

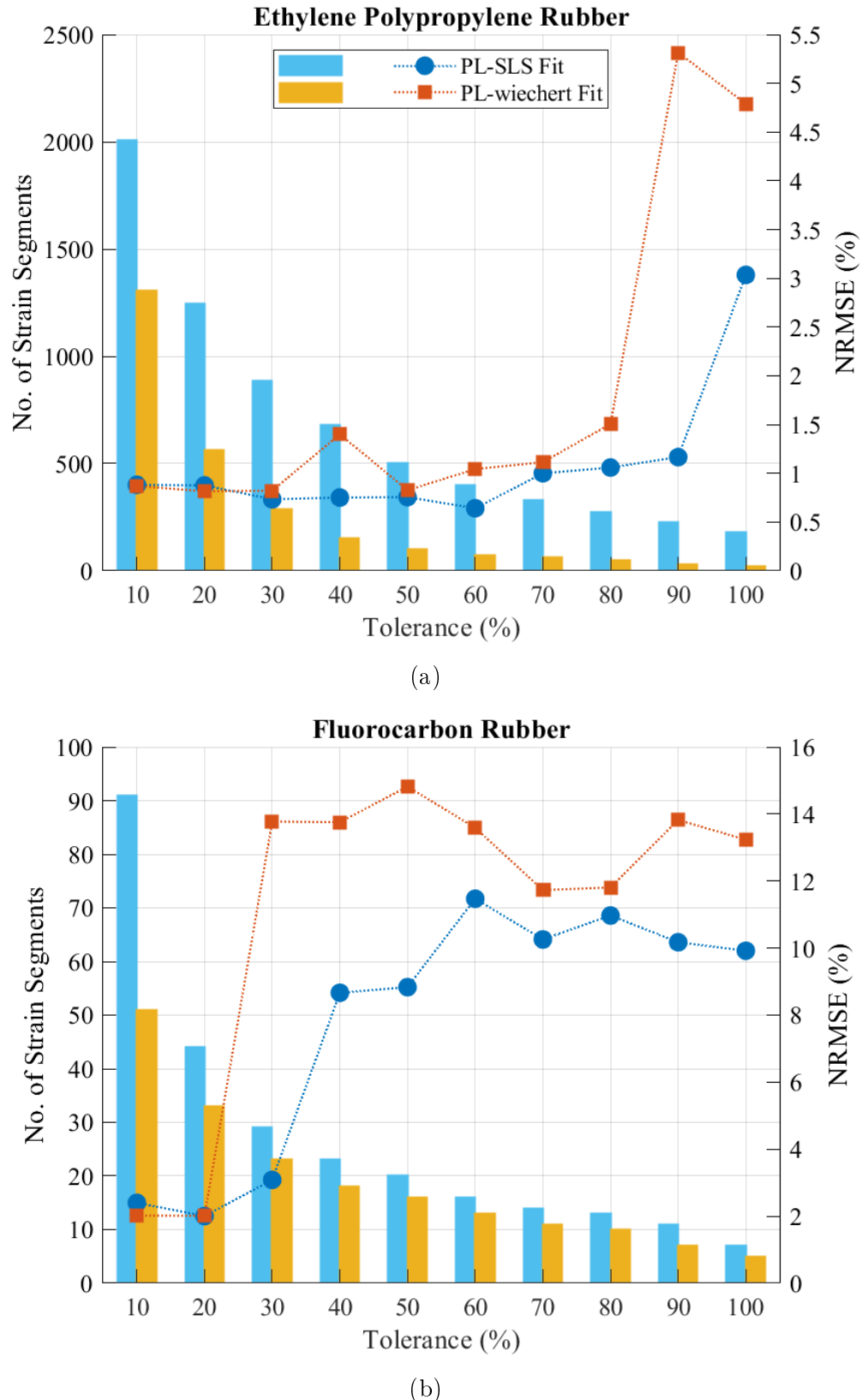


Figure 5.8: Impact of the proposed tolerance criteria on the relationship between the number of strain segments and the achievable accuracy of the PL method. (a) EPR material (b) FR material.

5. SOFT MATERIALS MODELLING: LINEAR VISCOELASTIC MODELS

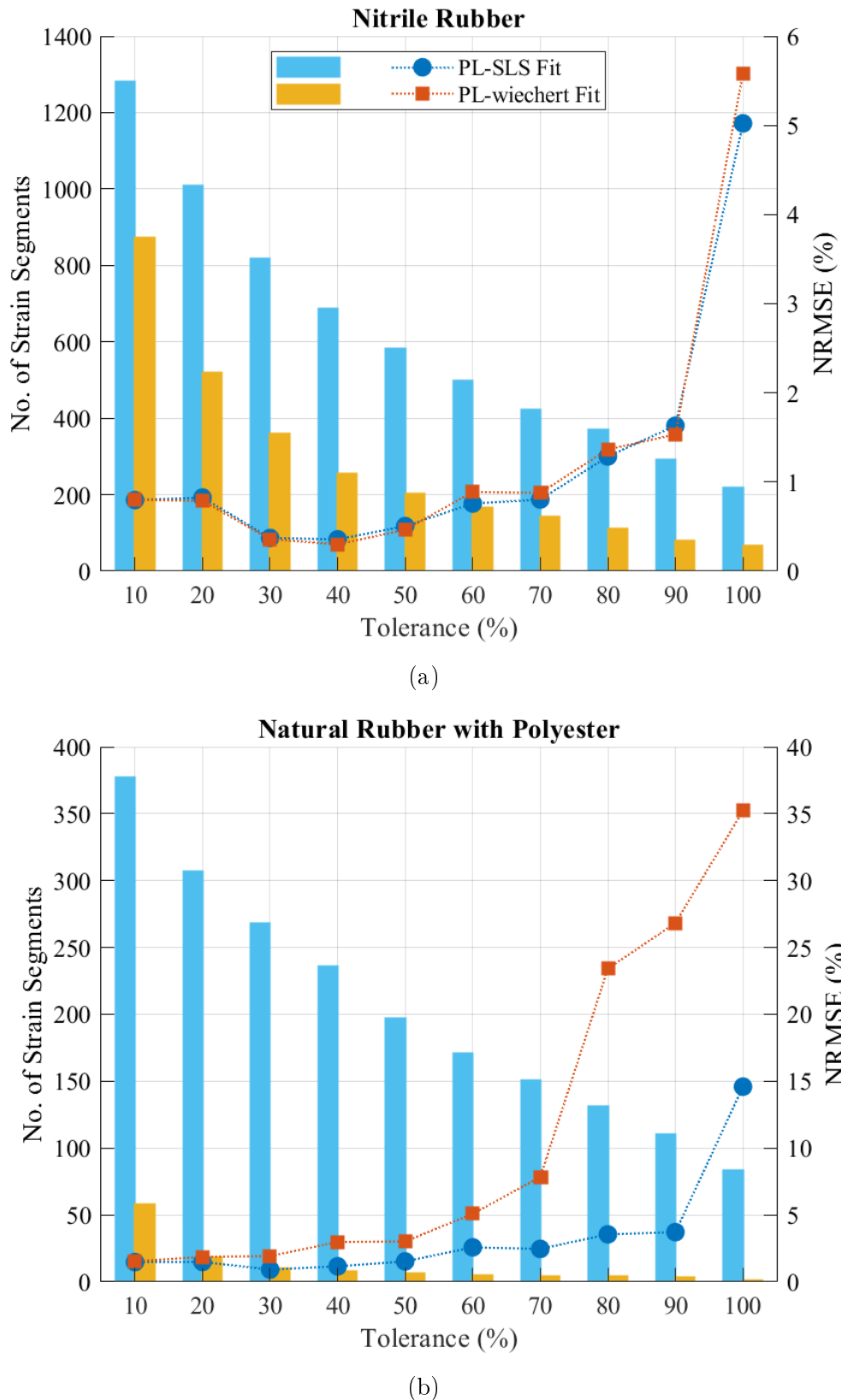


Figure 5.9: Impact of the proposed tolerance criteria on the relationship between the number of strain segments and the achievable accuracy of the PL method. (a) NR material (b) NatPolR material.

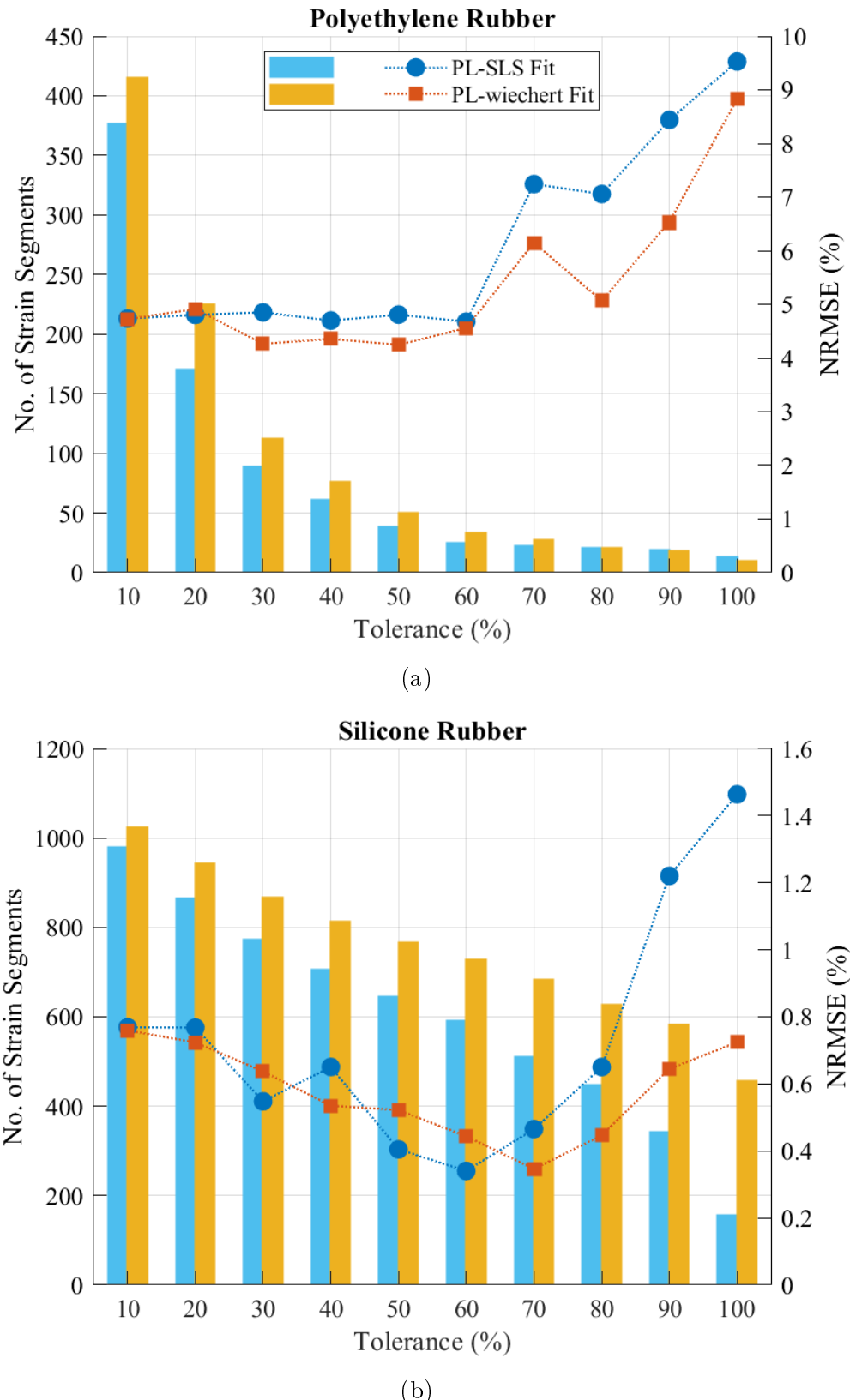


Figure 5.10: Impact of the proposed tolerance criteria on the relationship between the number of strain segments and the achievable accuracy of the PL method. (a) PR material (b) SR material.

5. SOFT MATERIALS MODELLING: LINEAR VISCOELASTIC MODELS

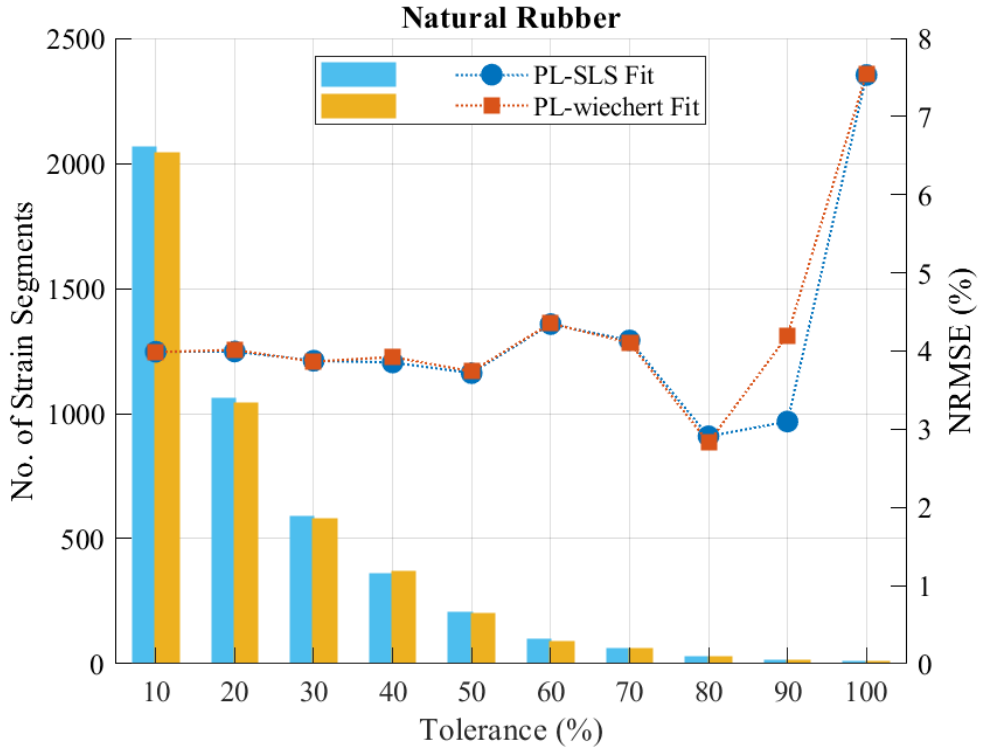


Figure 5.11: Impact of the proposed tolerance criteria on the relationship between the number of strain segments and the achievable accuracy of the PL method. NatR material

In general, there is no substantial difference in the best obtained accuracy of both models. The main difference between the models is the number of strain segments required to achieve this accuracy. In most of the cases, the PL-Wiechert model requires fewer strain segments than the PL-SLS model. This is the case for the EPR, FR, NR, NatPolR and NatR materials (Figures 5.8, 5.9 and 5.11). In these cases, the benefit of isolating the stress response of the equilibrium spring stiffness k_e by subtracting the stress response of the Maxwell branches from the stress-strain curve of the materials is appreciated. The latter, essentially split the stress response of the material in two parts: the time dependent stress response and the nonlinear strain-dependent stress response. The PL-Wiechert model, which has a larger number of Maxwell branches, is expected to describe the time dependent stress response more accurately than the PL-SLS model. This allows the PL method to be more effective in modelling the nonlinear strain-dependent stress response. The effectiveness of the latter process is dependent on the properties of the soft material in turn. The materials with dominant viscoelastic properties are benefited the most when using the PL-Wiechert method. In fact, it is possible to categorize

the studied soft materials into: highly elastic (Figures 5.10 and 5.11), viscoelastic (Figures 5.8b and 5.9a), and highly viscous (Figures 5.8a and 5.9b), by analysing the difference on the required number of strain segments between the PL-SLS model and the PL-Wiechert model.

Another important finding is the speed in which both models converge to the smallest NRMSE value. In this scenario, the PL-SLS model is faster than the PL-Wiechert model. In general, it is safe to assume that the smallest tolerance criteria does not always yield the best accuracy for both models. In other words, there is a tolerance value which delivers the best accuracy for each individual model. The latter is analysed in the following section. In summary, the analysis performed in this section describes the relationship between the complexity of the PL method and its accuracy when being applied to the LVMs.

5.5.2 Analysis of the Model Fit Accuracy

In this section, the goodness of fit of both developed models is analysed. In general, both the PL-SLS model and the PL-Wiechert model converge to very similar NRMSE values when enough number of strain segments are used. The main difference between the models is the number of strain segments required for convergence. In most cases, the PL-SLS model requires fewer strain segments to converge than the PL-Wiechert model. This is illustrated in the previous section (Figures 5.8 to 5.11). In this section, the best case performance of both models is analysed. The latter aims to test the hypothesis that a better model can be developed by implementing the PL method to more complex LVMs, i.e. the Wiechert model. The latter can be tested by calculating the increment or decrement achieved by the PL-Wiechert model with respect to the PL-SLS model, for both the accuracy and number of strain segments, as follows:

$$\Delta Accuracy = 100 \left(1 - \frac{NRMSE_{Wiechert}}{NMRSE_{SLS}} \right) \quad (5.11)$$

$$\Delta Complexity = 100 \left(\frac{Segments_{Wiechert}}{Segments_{SLS}} - 1 \right) \quad (5.12)$$

where $\Delta Accuracy > 0$, and $\Delta Complexity < 0$, represents the degree of improvement achieved by the PL-Wiechert model with respect to the PL-SLS model. In Table 5.1, the best performance case for both models is compiled. In here, the performance of the PL-Wiechert model is compared against the performance of the PL-SLS model.

5. SOFT MATERIALS MODELLING: LINEAR VISCOELASTIC MODELS

Table 5.1: Best accuracy of the PL-SLS model (1), the PL-Wiechert model (2), and the degree of improvement achieved by the PL-Wiechert model.

Model	Parameters	EPR	FR	NatPolR	NR	PR	SR	NatR
1	NMRSE (%)	0.64	2	0.91	0.35	4.67	0.34	2.90
	Segments	400	44	268	686	25	592	27
	Tolerance (%)	60	20	30	40	60	60	80
2	NMRSE (%)	0.81	2.01	1.53	0.29	4.24	0.34	2.82
	Segments	561	33	58	255	50	684	28
	Branches	7	8	7	5	7	6	5
3	Tolerance (%)	20	20	10	40	50	70	80
	ΔAccuracy (%)	-27	0	-68	16	9	-2	3
	ΔComplexity (%)	40	-25	-78	-63	100	15	4

The soft materials for which the PL-Wiechert model performs better than the PL-SLS model are the FR and the NR materials. Therefore, choosing the PL-Wiechert model over the PL-SLS model can be justified for these soft materials. Strictly speaking, the only case in which the PL-Wiechert model outperforms the PL-SLS model by a considerable percentage is for the NR material. In the case of the NatR material, the performance of both models is very similar. Hence, either model can be chosen. Lastly, the PL-Wiechert model performs worse than the PL-SLS model for the EPR, NatPolR, PR and SR materials. Hence, the PL-SLS model is a better choice.

The analysis performed in this section provides useful guidelines for choosing the right model to implement depending on the soft material of interest. Nonetheless, the complexity of the PL-Wiechert calculated in here is based on the PL method complexity and does not take into account the complexity added from having a higher number of Maxwell branches than the PL-SLS model. There is the possibility that when taking these two factors into account, the resulting added complexity of using the PL-Wiechert model overcomes the accuracy increment. In this scenario the PL-SLS model is a safer choice. Finally, the models best fit on the stress-strain curve on the soft materials is illustrated in Figures 5.12 to 5.15.

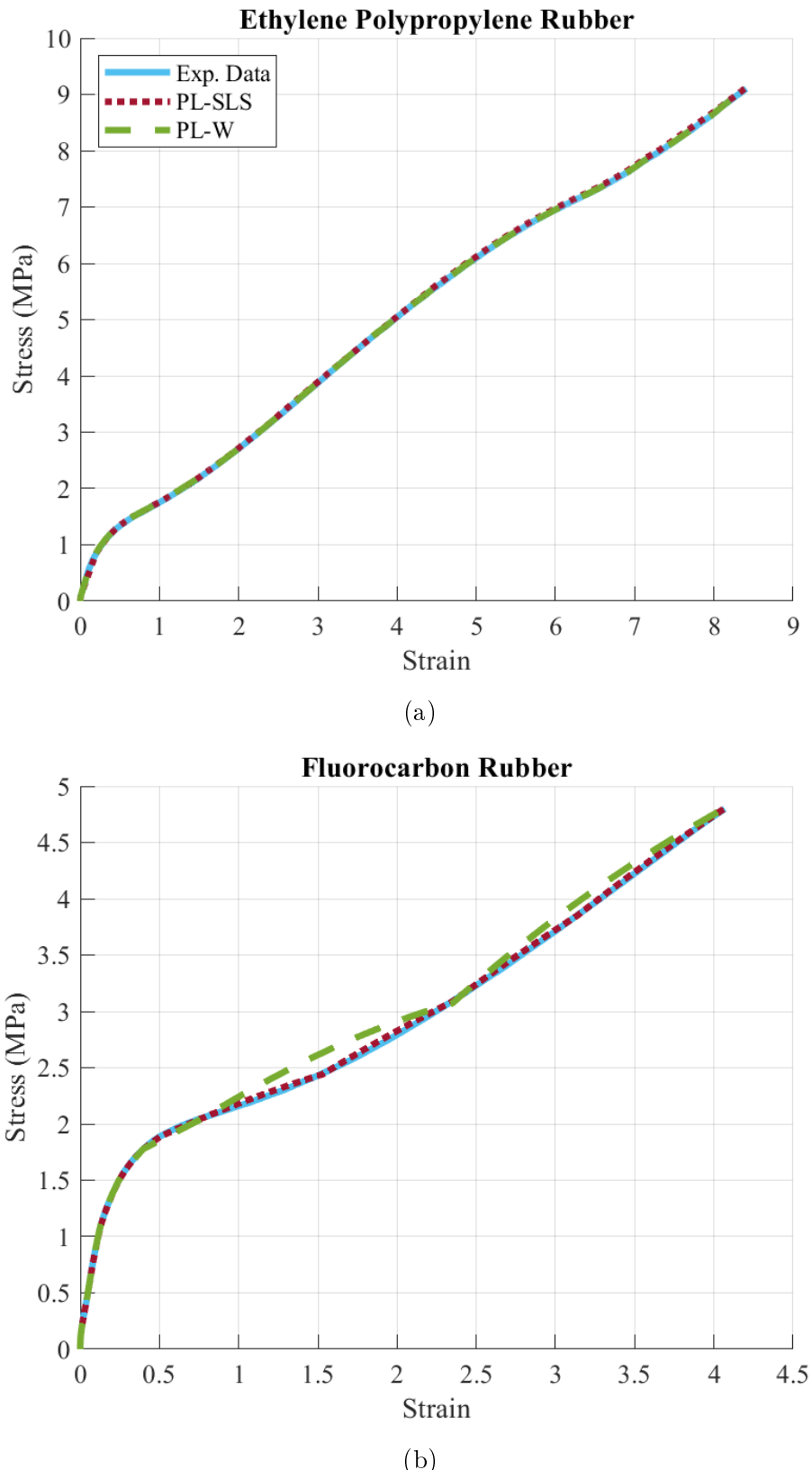
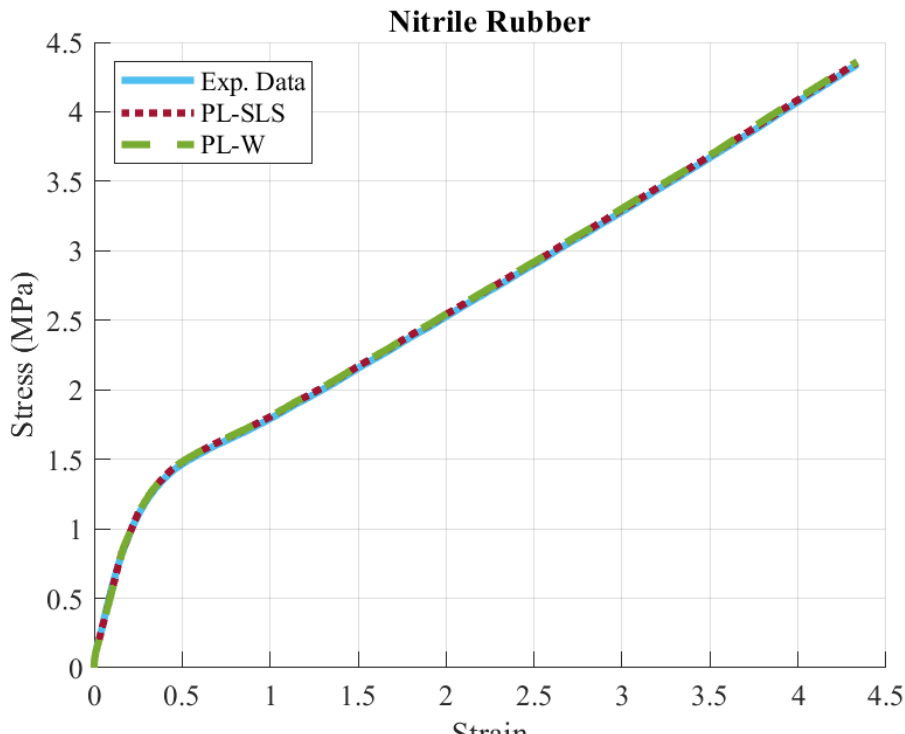
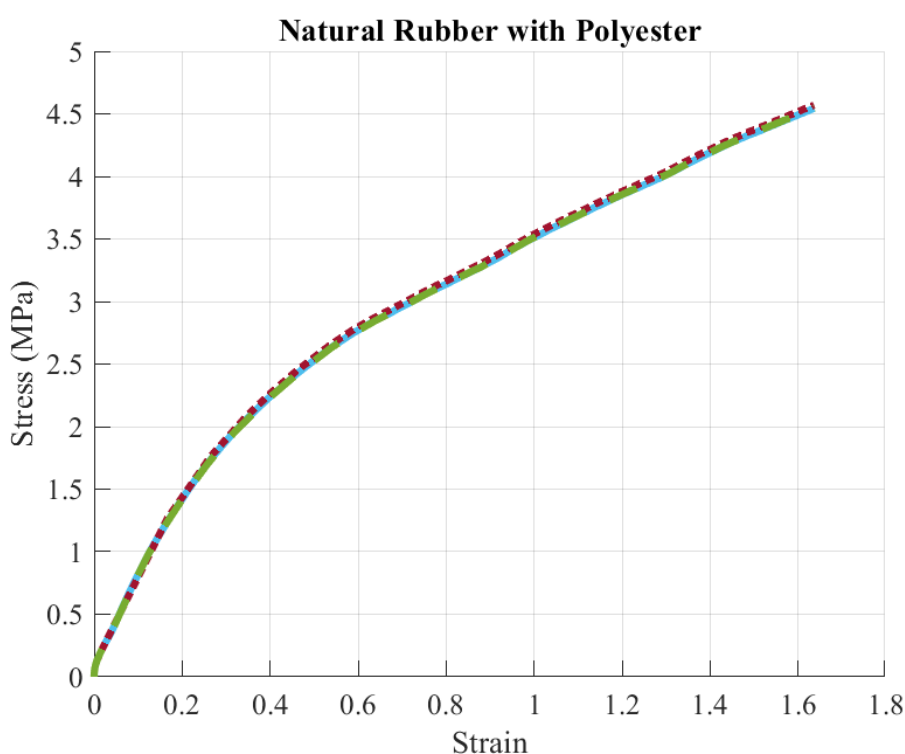


Figure 5.12: Best fit for the PL-SLS and PL-Wiechert models on the stress-strain curve of (a) EPR material (b) FR material. The parameters required for this fit can be found in Table 5.1.

5. SOFT MATERIALS MODELLING: LINEAR VISCOELASTIC MODELS



(a)



(b)

Figure 5.13: Best fit for the PL-SLS and PL-Wiechert models on the stress-strain curve of (a) NR material (b) NatPolR material. The parameters required for this fit can be found in Table 5.1.

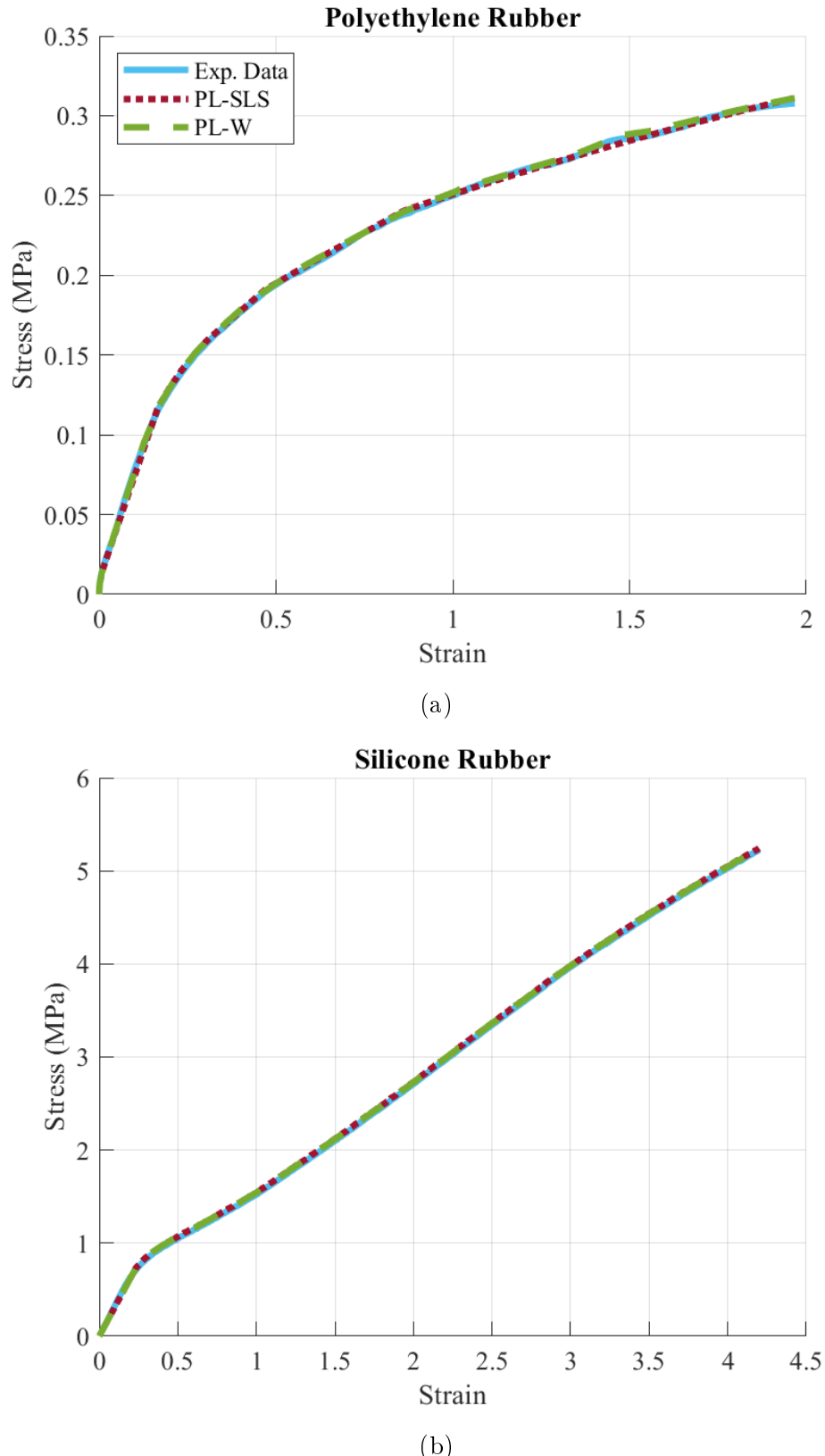


Figure 5.14: Best fit for the PL-SLS and PL-Wiechert models on the stress-strain curve of (a) PR material (b) SR material. The parameters required for this fit can be found in Table 5.1.

5. SOFT MATERIALS MODELLING: LINEAR VISCOELASTIC MODELS

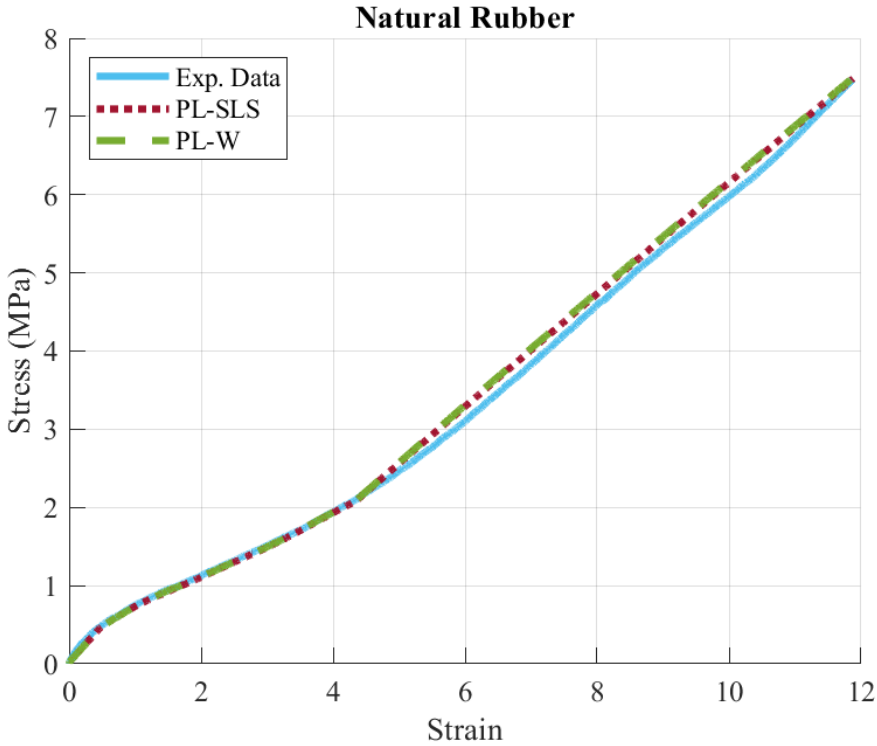


Figure 5.15: Best fit for the PL-SLS and PL-Wiechert models on the stress-strain curve of NatR material. The parameters required for this fit can be found in Table 5.1.

5.5.3 Analysis of the Velocity-dependent Stress Response

In previous sections, the performance of both the PL-SLS model and PL-Wiechert model is found to be very similar in all the studied soft materials. The main difference between the models is the required complexity to achieve said accuracy. In this section, the capability of both models to account for the velocity-dependent stress response of the soft material is analysed. The result of this analysis can provide a better way to determine which of the developed models is the best choice for each soft material. Moreover, the PL-SLS and the PL-Wiechert models are inspired by the work of Austin et al. where a similar model, the Std. Lin. SDS model was developed [86]. In the previous work, the capabilities of the Std. Lin. SDS model of accurately describing the velocity-dependent stress response of the soft material used was not assessed due to hardware limitations. Due to this, the latter property is investigated in this section.

The PL-SLS model and the PL-Wiechert model analysed so far are the result of applying the PL method to the stress-strain curve of the soft materials obtained

from the tensile strength test. The strain rate used in these tests varies from one material to the other. Almost in all cases the 500 mm/min strain rate is used for the fitting process. The only exception is the SR material where the strain rate of 50 mm/min is used instead. The dataset of the studied soft materials contains up to three different strain rates per material, as described in Table 4.1.

The strain-dependent stiffness k^* is the result of fitting the PL method to the SLS and the Wiechert models. This parameter is the linearized version of the equilibrium spring stiffness contained in both LVMs. The obtained k^* for each soft material is specific to one strain rate. In the following analysis, the strain-dependent stiffness of the equilibrium spring k^* has a major role. Therefore, the analysis in this section investigates the performance of the PL-SLS model and the PL-Wiechert model when using the obtained k^* under different strain rates.

In Sections 5.5.1 and 5.5.2, the NRMSE and the number of strain segments are used to measure the performance of both the PL-SLS and the PL-Wiechert models. There is a clear trade-off between the achieved accuracy and the required model complexity. In these analyses, the case for which the NRMSE value is the smallest do not reflect the best fit for the task of accounting for the velocity-dependent stress response of the soft materials. In fact, this can cause the fitted model to only perform well for a specific set of data, or in this case, a specific strain rate. Therefore, the main focus of the analysis performed in this section is to obtain the number of strain segments, i.e. a k^* , for each material that allows the PL-SLS model and the PL-Wiechert model to predict the stress-strain curve of the materials for different strain rates. The latter also assesses the generalization capabilities of the developed models.

The analysis performed in here is an extension of the one performed in Section 5.5.1. In here, the prediction of the models for the strain rates of 50 min/mm, 250 min/mm, and 500 min/mm is obtained. The same range of tolerance values is used in here. Similarly, the NRMSE is used to measure the models accuracy. The results are illustrated in Figures 5.16 to 5.19. In addition to this, the generalization error of both models is calculated as the mean NRMSE value along all strain rates for a single tolerance value, as follows:

$$GE = \frac{1}{N} \sum_{j=1}^N NRMSE_j \quad (5.13)$$

where N is the total number of strain rates cases, up to 3, and the subscript j is the individual strain rate case.

5. SOFT MATERIALS MODELLING: LINEAR VISCOELASTIC MODELS

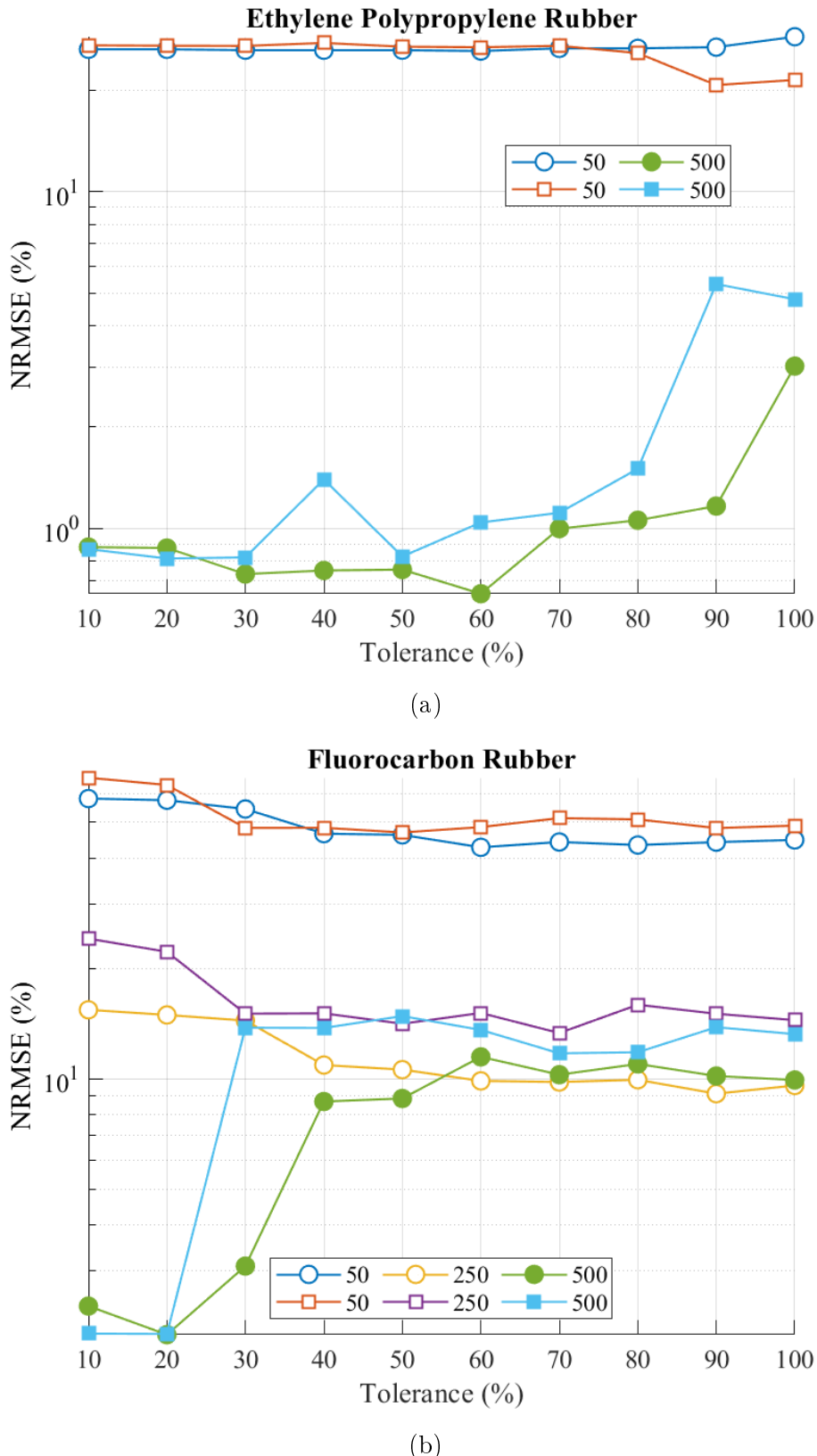


Figure 5.16: Prediction of the PL-SLS (circles) and the PL-Wiechert (squares) model under different strain rates for the (a) EPR material (b) FR material. Strain rates are in millimetres per minute. Filled markers indicate the strain rate used to extract the strain dependent stiffness k^* .

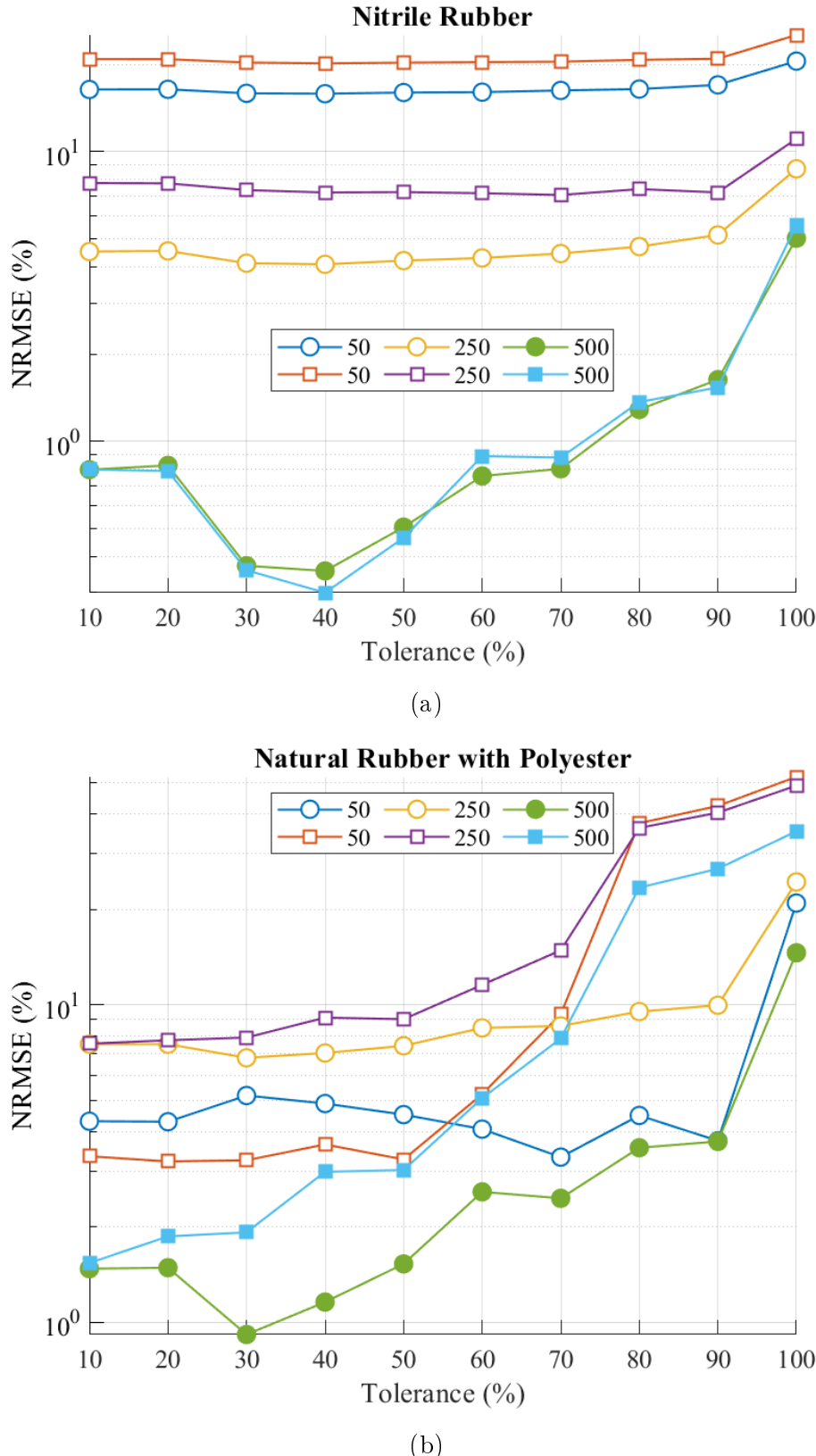


Figure 5.17: Prediction of the PL-SLS (circles) and the PL-Wiechert (squares) model under different strain rates for the (a) NR material (b) NatPolR material. Strain rates are in millimetres per minute. Filled markers indicate the strain rate used to extract the strain dependent stiffness k^* .

5. SOFT MATERIALS MODELLING: LINEAR VISCOELASTIC MODELS

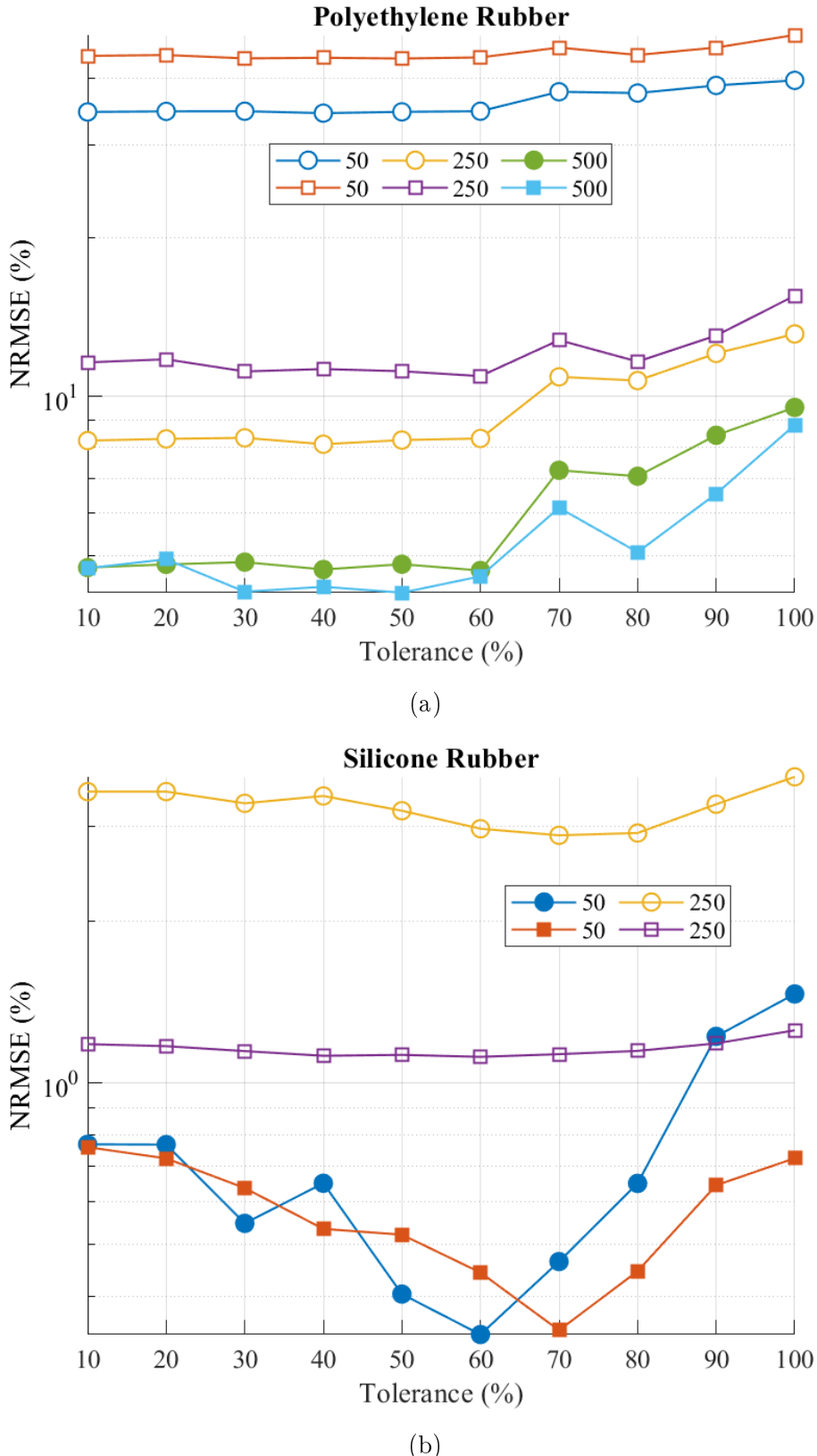


Figure 5.18: Prediction of the PL-SLS (circles) and the PL-Wiechert (squares) model under different strain rates for the (a) PR material (b) SR material. Strain rates are in millimetres per minute. Filled markers indicate the strain rate used to extract the strain dependent stiffness k^* .

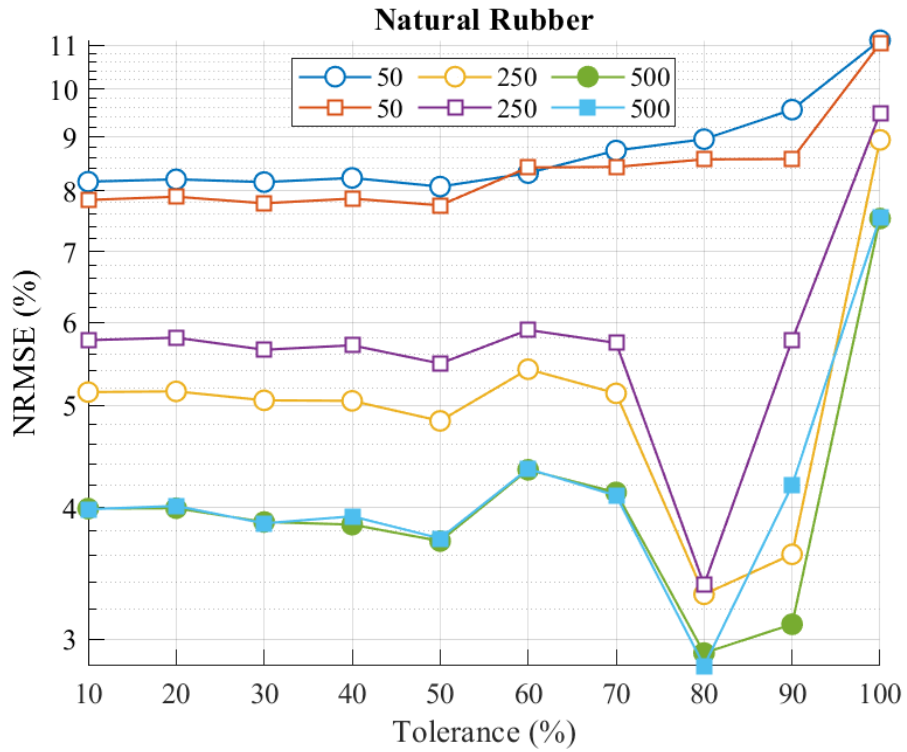


Figure 5.19: Prediction of the PL-SLS (circles) and the PL-Wiechert (squares) model under different strain rates for the NatR material. Strain rates are in millimetres per minute. Filled markers indicate the strain rate used to extract the strain dependent stiffness k^* .

From previous figures, an interesting tendency is revealed. For the cases in which the strain rate of 500 mm/min is used to obtain the strain dependent stiffness k^* , the accuracy of both models decreases in proportion to the difference between the predicted strain rate and the strain rate used for fitting. In contrast, for the cases in which the strain rate of 50 mm/min is used for fitting, i.e. for the SR material, the accuracy of both models behaves differently (Figure 5.18b). In this scenario, the PL-Wiechert model outperforms the PL-SLS model. The latter finding could suggest that using a slower strain rate for extracting the k^* delivers better results. Although, there are some variables to take into account before jumping to any conclusion, such as the type of material, and overall complexity of the model used. Nonetheless, considering the velocity-dependency stress response of the elements on the Maxwell branches for both models, using a slower strain rate has the potential to better isolate the stress response of the equilibrium spring k_e . In other words, this approach has the potential to improve the PL method fitting process.

In almost all cases, the PL-SLS model achieved smaller NRMSE values than the

5. SOFT MATERIALS MODELLING: LINEAR VISCOELASTIC MODELS

PL-Wiechert model, with the exception of the SR and NatR materials (Figures 5.18b and 5.19). Nonetheless, the overall performance of each model is best assessed using the generalization error, GE . Therefore, the tolerance value which yielded the smallest GE is calculated and reported in Table 5.2.

Table 5.2: Best generalization error of the PL-SLS (1) and the PL-Wiechert (2) models.

Model	Parameters	EPR	FR	NatPolR	NR	PR	SR	NatR
1	Gen. Error (%)	13.04	3.03	2.27	1.36	2.70	1.44	1.10
	Tolerance (%)	60	90	30	40	40	70	80
2	Gen. Error (%)	10.34	4.44	2.51	2.36	3.64	0.55	1.12
	Tolerance (%)	90	70	10	70	60	60	80

The obtained best case generalization errors are in line with the best case NRMSE values reported in Table 5.1. In here, the PL-SLS model outperforms the PL-Wiechert model for all but two materials, the EPR and the SR materials. For the specific case of the SR material, the PL-Wiechert model performs much better than the PL-SLS model. The reason for this is the small value of strain rate used for fitting the PL method to the stress-strain curve of the SR material. In all cases, both models achieve a GE value smaller than 5% which indicates that the models are capable of accounting for the velocity-dependent stress response of the studied soft materials. The exception to this is the EPR material which delivered a very large GE value in comparison to the other materials. The larger GE value in here can be attributed to the absence of a dataset for the strain rate of 250 mm/min. This creates a larger gap between the prediction at 50 mm/min and the prediction at 500 mm/min, which is reflected when calculating the mean NRMSE along all strain rates, i.e. the GE described in (5.13). On top of this, the potential disadvantage previously described of using the strain rate of 500/min can also be influencing the performance of both models for this particular soft material. Lastly, the models developed in here achieved a higher performance in comparison to the Std. Lin. SDS model documented in the literature. The reported relative RMSE value for the Std. Lin. SDS model is of 13.6%. The conditions in which the latter performance is achieved are comparable to the conditions in Section 5.5.2, where the reported NRMSE values for both models are between 0.34% to 4.67% (Table 5.1). Similarly, the generalization error GE obtained in this section further validates the

much better performance achieved by the PL-SLS and the PL-Wiechert models.

Summarizing, in this section the capabilities of the PL-SLS and the PL-Wiechert model of accounting for the velocity-dependent stress response of the soft materials are assessed. This is measured using the generalization error GE , described in (5.13). The results indicate that both models are capable of predicting the stress response of the soft materials under different strain rates with reasonable accuracy. In other words, they are capable of accounting for the velocity-dependent stress response of the soft materials. The only exception to this conclusion is the EPR material, where a larger GE value was obtained. The potential causes of this isolated case are the larger gap between the strain rate used in the fitting process and the predicted strain rate, and the potential limitations of using 500 mm/min instead of 50 mm/min as the strain rate in the fitting process. Using the strain rate of 50 mm/min is found to be beneficial for the performance of both models as observed in the results for the SR material.

5.6 Summary

In this chapter, the development process of the PL-SLS and the PL-Wiechert models is described. The fitting process of both models is very similar, as described in Figure 5.6. The main differences between the developed models in here and the Std. Lin. SDS model found in the literature [86] are the following optimizations:

- Transformation of the constitutive differential equations of both models into their finite differences form. This allowed the PL method to be easily implemented in both models.
- Implementation of a logarithmic time collocation approach to extract the values of k_j and τ_j from the stress relaxation curve.
- Removal of the stress response of the components in the Maxwell branches.
- Proposed tolerance criteria to determine the number of strain segments to be fitted based on the variation of the stress-strain curve.

In addition to the latter differences, several aspects of the Piecewise linearisation method are investigated in this section. Firstly, the relationship between the complexity and the accuracy of the PL method is described in Section 5.5.1. The latter is achieved due to the proposed tolerance criteria which is based on the slope

5. SOFT MATERIALS MODELLING: LINEAR VISCOELASTIC MODELS

variation of the stress-strain curve. The obtained results, illustrated in Figures 5.8 to 5.11, describe the relationship between the required complexity and the achieved accuracy for both the PL-SLS and the PL-Wiechert models. Both models behave different depending on the soft material. The latter can be used to categorize the studied soft materials in highly elastic, viscoelastic, and highly viscous. The PL-SLS model performs better for soft materials in the highly elastic category, where the PL-Wiechert model performs better for soft materials in the viscoelastic and highly viscous categories. The latter is in line with the fundamentals behind each model where the PL-Wiechert model has many Maxwell branches to describe many time constants of the material, i.e. many viscous constants.

Secondly, in Section 5.5.2 the performance of both developed models is investigated. The obtained results are compiled in Table 5.1, where the PL-SLS model is suggested as the best choice for most cases. The additional complexity of using the PL-Wiechert model does not justify the performance improvement. Nonetheless, in this analysis the models are only assessed in their capabilities of fitting the stress-strain curve for a single strain rate. This conclusion changes when considering the models capability of accounting for different strain rates.

Thirdly, the analysis described in Section 5.5.3 is focused on assessing the capabilities of the developed models of accounting for the velocity-dependent stress response of the soft materials. In other word, the generalization capabilities of the developed models are assessed. In here, the obtained strain dependent stiffness k^* is used to predict the stress-strain curve of the soft materials under different strain rates. Up to three different values of strain rates are evaluated: 50, 250, and 500 mm/min. The performance of the models is assessed using the generalization error GE described in (5.13). In general, the PL-SLS model outperforms the PL-Wiechert model for all but two materials, the EPR and the SR materials. For the specific case of the SR material, the PL-Wiechert model performs much better than the PL-SLS model. The differences in performance can be caused by the strain rate used for the extraction of the strain dependent stiffness k^* . The results are compiled in Table 5.2. In all cases, both models achieved a GE value smaller than 5% which prove the capability of the models to account for the velocity-dependent stress response of soft materials. The only isolated case in which the achieved GE is higher than 5% is for the EPR material. The potential cause for this is the strain rate used for the fitting process of the PL method. This further validate the hypothesis that using a small value of the strain rate is beneficial for the fitting process.

Finally, the PL-SLS and the PL-Wiechert models achieved a higher prediction accuracy in comparison to the Std. Lin. SDS model documented in the literature. The reported relative RMSE value for the Std. Lin. SDS model is of 13.6%. The conditions in which the latter performance is achieved are comparable to the conditions in Section 5.5.2, where the reported NRMSE values for both models are between 0.34% to 4.67% (Table 5.1). Similarly, the prediction accuracy of the models developed in here when accounting for different strain rates, reported as *GE* values in Table 5.2, further validates the much better performance achieved by the PL-SLS and the PL-Wiechert models in comparison to their predecessor the Std. Lin. SDS model. The performance of the Std. Lin. SDS model under this scenario was not assessed in the literature. The superiority of the PL-SLS and the PL-Wiechert models is due to the many optimizations performed to the PL method fitting process.

CHAPTER 6

Soft Materials Modelling: Artificial Neural Networks

6.1 Introduction

In the previous chapter, the development of two mathematical models for the prediction of viscoelastic behaviour in soft materials is described. The PL-SLS model and the PL-Wiechert model can describe the nonlinear, time dependent, and strain dependent stress response of seven soft materials. The main limitation of modelling tools based on mathematical models is their implementation in control systems for real robotic applications. Due to this, a different modelling approach is investigated in this chapter.

The field of machine learning provides reliable algorithms to tackle regression problems, such as artificial neural networks (ANNs). ANNs have been successful in extracting complex mechanical parameters of soft materials, and are now being used to model the stress-strain curve of many materials. Nonetheless, back in 2016 the literature on the latter subject was very scarce. It is until 2019, that a surge in research dealing with the implementation of different architectures of ANNs, in combination with Dynamic Mechanical Analysis (DMA), is being performed as an attempt to model the viscoelastic properties of soft materials. Nonetheless, there is still plenty of research to be done, such as implementing ANNs for the real-time prediction of the viscoelastic properties of soft materials. In this context, real-time prediction refers of deploying the trained ANN model into a control system, essentially replacing the mathematical model commonly used to estimate the stress-strain curve of elastic elements used in series-elastic actuators. This gap in the body of knowledge is addressed in this research.

In this work, a feedforward ANN model is developed. The Bayesian Regularization algorithm is used during the training process. The selection of inputs and outputs to be included to the network is optimized by observing the generalization capabilities of different combinations. The total number of neurons in the hidden layer is also optimized to minimize the risk of a common phenomenon known as over-fitting. The optimal number of neurons varies from one soft material to the other, but in any case exceeds 10 neurons.

Finally, the generalization error of the developed ANN is compared against the PL-SLS and the PL-Wiechert models. The results varies from one material to the other. In general, the developed ANN model can predict the nonlinear time-dependent stress response of the soft materials. The ANN model performed poorly for the single case of the NatR material. The reasons behind this might be related to the uneven dataset of this material. Lastly, the three developed modelling tools

6. SOFT MATERIALS MODELLING: ARTIFICIAL NEURAL NETWORKS

so far are suitable for the prediction of the complex behaviour of soft materials.

6.2 Artificial Neural Networks

Artificial Neural Networks (ANNs) are computational systems inspired in the structure and functionality of the biological nervous system. Neurons, a specific type of cell, are the basic components in the brain. They form connections with a vast number of other neurons, allowing us to remember, think, and apply previous knowledge to our present actions. The basic functionality of a neuron is to receive information in its inputs from many sources, to combine this information, to apply a nonlinear operation, and to output the end result. Moreover, neurons are capable of specializing for a specific task by amplifying or reducing the impact of their individual inputs. Neurons are also capable of reorganizing themselves in complex interconnected clusters in a three-dimensional space, called biological neural networks, where the information flows from one group of neurons to the other.

Similarly, Artificial Neural Networks are composed of many basic components working in parallel, known as artificial neurons. The clustering found in biological neural networks, can be replicated in ANNs by creating layers, containing many neurons, which can be interconnected between each other in different ways. The simplest structure of an ANN is composed of three layers: an input layer, a hidden layer, and an output layer. As the name suggest, the input and output layers interface the ANN with the outside world. The main learning process happens in the hidden layer. The way in which the interconnections between these three layers are formed are mainly dependent on the application. The strength of each interconnection depends on a weighting factor, enabling the artificial neuron to amplify or reduce the contribution of a specific input. The fine tuning of these weights, performed in a process called training, allows ANNs to specialize in a particular task, i.e. allow them to learn. The latter highlights the capability of ANNs to simulate two key functionalities of the human brain, which are: acquiring knowledge from the environment through a learning process, and storing this knowledge in the form of inter-neuron connection strengths, i.e. synaptic weights. The capability of learning from experience, i.e. experimental data, make ANNs particularly useful when dealing with complex scientific and engineering problems where an adequate analytical description is not available, or is too complex [118, 119].

Artificial Neural Networks can have as many layers as required, simulating the

clustering phenomenon found in biological neural networks. These type of multi-layered ANNs can be categorized depending on how the information flows inside it. For example, an ANN in which the information flows in one direction, from the input layer up to the output layer, is called Feedforward Neural Network (FFNN). This type of ANN is one of the most commonly used for function approximation, pattern recognition and classification (Figure 6.1a) [118].

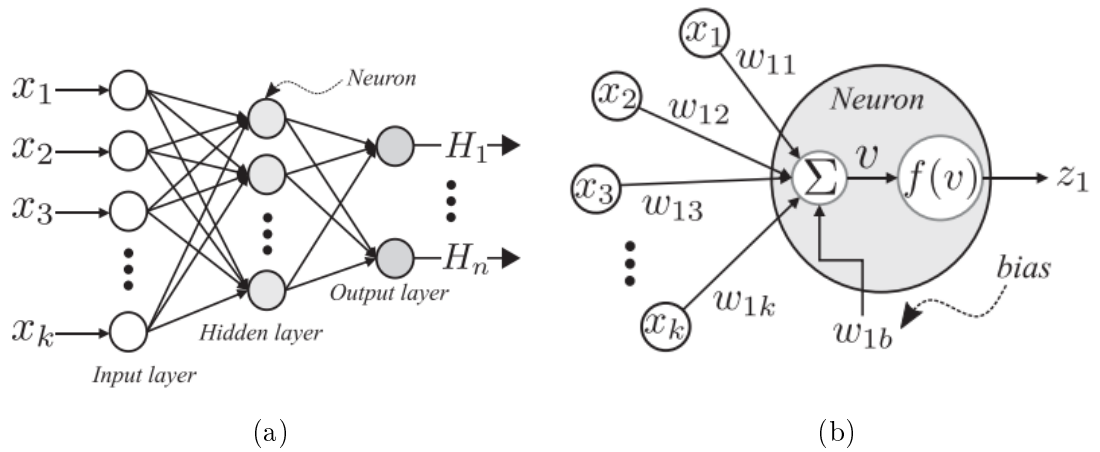


Figure 6.1: (a) Feedforward artificial neural network (b) Internal structure of an artificial neuron [120].

The variables illustrated in Figure 6.1a are as follows. The inputs of the ANN are represented by the variable \mathbf{x} , in the form of:

$$\mathbf{x} = [x_1, x_2, x_3, \dots, x_k] \quad (6.1)$$

where k represents the total number of inputs. Similarly, the outputs of the ANN are represented by the variable \mathbf{H} in the form of:

$$\mathbf{H} = [H_1, H_2, H_3, \dots, H_n] \quad (6.2)$$

where n represents the total number of outputs. Furthermore, the output of the neuron illustrated in Figure 6.1b, combines the individual weighted values of the input vector x with a bias value. Then, a nonlinear function is applied to the result of this sum. This is described as follows:

$$z_1 = f \left(\sum_{i=1}^k (x_i w_{i,j}) + w_{1,bias} \right) \quad (6.3)$$

6. SOFT MATERIALS MODELLING: ARTIFICIAL NEURAL NETWORKS

where $w_{1,1}$ to $w_{1,k}$ represents the weights of one neuron which interacts with all the inputs. The subscript i in $w_{i,j}$ indicates to which neuron this weight is interacting, whereas the subscript j indicates the input that this weight is related to.

In order for the ANN to learn, it must be trained first. In FFNN the most common approach for training is based on the backpropagation algorithm. The training process of ANN commonly involves dividing the available data into a training and a test subset. The former subset is used for training of the ANN, whereas, the latter is used for testing the prediction capabilities of the ANN after being trained. During training, the ANN is presented with known values of the output, called targets, which are related to a specific combination of inputs. In each training session the ANN will adapt slightly until its output is close to the target value. The backpropagation algorithm is based on minimizing the sum of square errors (SSE) between the target and predicted values, by modifying the weights and biases of the ANN [118]. This algorithm is so powerful in minimizing the error that it could cause the ANN to memorize the training dataset instead of generalizing it. This means that the ANN will not be able to provide accurate predictions when new data is presented to it. This issue is called over-fitting.

According to the literature, FFNN are capable of representing any functional relationship between a set of inputs and outputs, as long as the ANN has enough number of neurons in its hidden layers. However, having too many neurons increases the risk of over-fitting. As previously mentioned, over-fitting will prevent the ANN to generalize well. Therefore, when designing an ANN, it is better to use the minimum amount of resources which are able to provide a good fit. There are two main methods for preventing over-fitting from happening, i.e. improving generalization, during the training process: early stopping and regularization. On the one hand, in the early stopping method, a third subset of data is involved, called the validation subset. In general terms, when the error during the validation process increases over certain number of consecutive training sessions, then over-fitting is detected and the training process is stopped. On the other hand, in a regularization method the performance function used during training, commonly the SSE of the ANN prediction, is modified. For example, in the Bayesian Regularization method, the performance function has an additional condition, which is to minimize the SSE of the weights and biases of the ANN. This limits the correction power of the backpropagation algorithm, which allows the weights and biases to be fine-tuned rather than have large variations. There are many variables involved in the process of designing and

optimizing an ANN for a specific application. Therefore, the relevant works on implementation of ANNs for the modelling of soft materials are presented in the following section.

6.3 Soft Materials Modelling

Artificial Neural Networks have been implemented in a wide number of applications, such as: forecasting, control, power systems, robotics, signal processing, manufacturing, pattern recognition and optimization [121]. At the time of writing this document, the available literature about the implementation of ANNs for the modelling of the complex behaviour of soft materials, specifically elastomers, is scarce. Recently there has been an increase in the number of published papers focusing on modelling soft materials using ANNs which highlights the relevance of this field of research.

One of the earliest works in this field is documented in [122] by Zhang et al.. In here, a FFNN is developed to model the dynamic mechanical properties of short fibre reinforced materials. The trained ANN can predict the storage modulus and damping of the material for temperature values not used during the training process. Many properties of the material are provided as input to the network. The developed ANN had 25 neurons in its single hidden layer with a tan-sigmoidal transfer function, whereas the output layer had a linear transfer function. The Bayesian Regularization algorithm was used for training. The prediction capabilities of the ANN were assessed using the percentage of correct predictions, in which a prediction with an R^2 value greater than 0.9 is considered correct. The ANN was tested 50 times with a randomized test set each time. Moreover, the authors found a proportional relationship between the complexity of the parameters to model, and the amount of data required for training to achieve a good accuracy.

The review paper of Zhang et al. about the implementation of ANNs in polymer composite applications states that the available literature on the subject was scarce at that time [118]. Moreover, the documented applications ranged from modelling of the fatigue life of the material, to prediction of tribological and dynamic mechanical properties of composite materials [122, 123]. This review paper provided very insightful evidence of the potential of ANNs for applications such as: design of new composite materials, optimization of the manufacturing process, and modelling the relationship between different manufacturing parameters. From the reviewed works,

6. SOFT MATERIALS MODELLING: ARTIFICIAL NEURAL NETWORKS

the authors were able to find a well defined sequence of actions which describes the process of implementing ANNs for the prediction of the mechanical properties of composite materials:

1. **Data collection:** the first step in designing an ANN is to collect enough data from experimentation. On top of this, processing of the collected data, mainly to filter out noise, might be required.
2. **ANN design and training:** the second step is to design the ANNs depending on the application at hand. This involves deciding on the best parameters to use, in terms of: number of neurons, number of hidden layers, training algorithm and neuron's activation function. Also, this step involves the training of the proposed ANN.
3. **Test of the trained network:** this step is about assessing the prediction and generalization capabilities of the trained ANN. The former is commonly assessed by looking at the difference between predicted and experimental values, as a general rule, the lower the error, the better the prediction. The generalization of the network is assessed by statistical methods such as p-fold cross-validation and the coefficient of determination.
4. **Use of the trained network:** the last step is to use the trained network to simulate new data or for prediction.

The latter process highlights the large number of configurations available when tackling a modelling problem. Due to this, some works in the literature opt for a “trial and error” approach when investigating the potential of ANNs for a specific application. Nonetheless, many works do perform optimizations in more than one of the ANN hyper-parameters. For example, motivated by the limitations of traditional viscoelastic models, the viscoelastic behaviour of polymer composites is investigated by Al-Haik et al. in [124]. In here an ANN is developed to predict the stress relaxation characteristics of a polymer composite. The amount of data used in here is rather large, having 900 datasets covering different conditions of the stress relaxation process. The training algorithm used is the scaled conjugate gradient. In addition to this, the optimal brain surgeon algorithm is used to optimize the topology of the network. The latter algorithm assesses the contribution of each neuron to the final results, by removing neurons one by one. This process is also known as pruning. The developed ANN had two hidden layers with 45 and 39 neurons, respectively;

and was successful in modelling the stress relaxation characteristics of the material for ranges in which viscoelastic models were unsuccessful.

Initial works on this field of research were solely focused on one specific material. However, as the research matured, more materials were studied in a single work. This is the case for the work from Trebar et al. where a total of 12 different composite materials, natural rubber among them, were studied [119]. This work is more oriented towards assessing the generalization capabilities of ANNs for this specific selection of materials, having the previous knowledge of ANNs being successful for the modelling of viscoelastic materials. Therefore, more attention is given to the validation of the ANN prediction. This is done by using three different statistical parameters: (i) the root mean square error (RMSE), (ii) the normalized to the standard deviation, (iii) the mean absolute percentage difference (MAPE), and (iv) the percentage of correctly classified samples. In this case, the Levenberg-Marquardt algorithm, an early stopping method, was used to prevent over-fitting. The dataset was divided into training (80%) and testing (20%) subsets. The training subset was further subdivided, allocating 80% of the data for the actual training and 20% for the validation process required for the early stopping algorithm. Different number of neurons in the hidden layer were tested, ranging from three neurons to three times the number of inputs. The latter ratio has also been mentioned in [118], where three to four neurons per input node are found to be the optimal ratio. Although this is more a suggestion rather than a rule. Trebar et al. assessed the impact of using raw and preprocessed data for the training process. The preprocessed data consisted of the statistical parameters of the mechanical properties used as input, such as the standard deviation and mean values. The authors found that the developed ANN was in agreement with the experimental data of studied mechanical parameters of hardness and tensile properties.

Current implementations of ANNs in this field are focused more on using the ANN as an alternative to current mathematical models for the prediction of the stress relaxation and stress-strain curves of the materials. For example, in [125], the prediction capabilities of an ANN are compared against one of the LVMs, the Generalized Maxwell model, also known as the SLS model. A rather simple ANN was developed here, having only one input, the time, and one output, the stress. The back-propagation with declining rate algorithm was used for training. The performance of the ANN was assessed by the total sum of squared errors (TSSE) and by commonly used statistical parameters, such as the RMSE and R^2 coefficient.

6. SOFT MATERIALS MODELLING: ARTIFICIAL NEURAL NETWORKS

The optimal number of neurons was found by trial and error, keeping the learning rate, momentum and total number of epochs constant. In this case, the logarithmic sigmoid function was chosen due to the compatibility with the stress relaxation behaviour. The main difference between the latter function and the tan-sigmoid function is that the former have an output range of [0, 1], whereas the latter range is [-1,1]. In another work, the SLS model is again compared to an ANN [126]. In this case, many hyper-parameters, such as the number of neurons, number of hidden layers, and activation function in the hidden layers, are optimized by trial and error. Particular attention is put to the activation function of choice, which are tan-sigmoid (tansig) and logarithmic sigmoid (logsig). All combinations of using the latter function for a single and double layer network were assessed. The combination of using logsig and tansig in a double layered network was found to be the most optimal. The assessment of the performance of the ANN is based on the training time, overall training error and maximum error. The ideal network would have these parameters at its minimum values. This approach of minimizing the number of resources of the ANN was previously mentioned as a way to avoid over-fitting. Lastly, both mentioned works are good examples of the potential of ANN of replacing traditional mathematical models for the prediction of the stress relaxation of soft materials.

The literature on ANNs for the modelling of the stress-strain curve of soft materials is very scarce and fairly recent, in comparison to the literature available for metals [127–129]. Nonetheless, one of the earliest attempts of modelling the stress-strain curve of non-metal materials is documented in [130]. In this work, polymer composite materials are studied. The ANN developed in here follows the same trend of using FFNN. However, the number of neurons and hidden layers are larger than in previous applications. In this work, up to three hidden layers and up to 45 neurons, are investigated. The aim of this work was to analyse the effect of polymer blending ratio in the stress-strain curve of these materials. Current mathematical models were only effective, for the previously mentioned task, inside the elastic range of the material. The developed ANN was capable of overcoming this limitation. Moreover, a logsig activation function was used, together with a backpropagation training algorithm. No information is given on the reasoning behind the selection of neurons and hidden layer, therefore a trial and error approach must have been adopted.

More recent works specifically investigates the performance of ANNs for the modelling of soft materials such as elastomers and thermoplastic elastomers (TPEs). An

example of this is documented in [131]. The aim of this work is to model the temperature dependency on the dynamic mechanical properties of TPEs. Therefore, the materials are characterized using a Dynamic Mechanical Analysis (DMA), which describes the stress response of the material on a range of frequencies or strain rates. Nonetheless, the study is focused on a single frequency of 1 Hz. This particular work is closely related to the research presented in this thesis. Therefore, the methodology implemented by the authors is of interest. The work focuses on thermoplastic polyurethanes (TPUs). Again, the FFNN architecture is chosen for the developed ANN. The temperature history is presented as input to the network, whereas the storage modulus, damping factor, and loss modulus are the desired parameters to predict. Three individual ANNs were developed, one for each parameter. The latter parameters describes the viscoelastic properties of materials. In terms of the activation functions, the commonly used configuration of having a tangent-sigmoid function in the hidden layer and a linear function (purelin) in the output layer is chosen. The Levenberg-Marquardt back-propagation minimization algorithm was implemented. No particular measurements, besides the already provided by the training algorithm, were implemented to ensure good generalization capabilities of the network. Among the three developed ANN, no more than 15 neurons were used.

Kopa et al. continued the latter research in a recently published paper [132], this time focusing on predicting the uni-axial tensile response of vulcanized rubber. Again, a FFNN is developed. The inputs were the engineering strain and the content of carbon black in the rubber blend. The output was the engineering uni-axial stress. The optimal number of neurons was found by trial and error, being six the optimal number of neurons. Similarly to previous applications, the tansig-purelin combination of transfer function was chosen. The Levenberg-Marquardt algorithm was also used. The main contribution of this work is the validation approach implemented, which is based on knowing the relationship between the material stress-strain ultimate values, and the carbon black content of the material. A quadratic regression can describe the latter with adequate accuracy. This is a simpler approach in comparison to fit the whole stress-strain curve of a material with a LVM. In summary, the ANN was presented with unknown values of carbon content, obtained from the regression model. The validation was successful since the ANN was capable, not only of agreeing with the ultimate strain-stress values corresponding to that carbon black content, but also of describing the whole stress-strain curve.

Lastly, the most recent work on this research field was performed by Rodriguez

6. SOFT MATERIALS MODELLING: ARTIFICIAL NEURAL NETWORKS

et al. in [120]. Many thermoplastic elastomers are studied in this work. Their stress/strain curves are extracted from an available dataset, hence no mechanical characterization is performed. The developed ANN is aimed to model the stress-strain curve of many thermoplastic elastomers under different values of temperature. In comparison to previous works, several optimizations are performed in this one. For example, the training process of the ANN consist of two steps. Initially, the Simulated Annealing (SA) algorithm is used to explore initial solutions for the weights of the network prior to applying the greedy gradient-based Levenberg-Marquardt (GGLM) algorithm. The main objective of the SA algorithm is to prevent the weights, tuned by the GGLM algorithm, to fall into a local minimum. The latter is a well-known side effect of Levenberg-Marquardt-based algorithms. Furthermore, the ANN developed in here is a FFNN with 10 neurons in its single hidden layer. The process of finding the optimal number of neurons involved the training and test of many ANNs with different number of neurons ranging from 1 to 20 neurons. The decision of using 10 neurons is based on the small improvement of the achieved prediction error when further increasing the number of neurons. No explicit mention of the activation function used in either of the ANN layers is given. The authors opted to use the Neural Lab software to developed the ANN, instead of the commonly used Neural Network Toolbox from Matlab®. The temperature and strain values were used as inputs, and the stress response as output. This work implements similar methods as the one found in the literature for data division, measurement of performance, and validation of the ANN prediction capabilities. Nonetheless, the validation process implemented is extensive because five different hyper-elastic models, and a Probabilistic Neural Network are used for comparison. The validation process was mainly focused on the prediction error rather than the generalization capabilities of the developed ANN. The latter was assessed using the Normalized Absolute Difference (NMAD) and the R^2 coefficient. An extra validation step was performed which consisted of retraining the ANN using the data from another material from the same type. In this case, the prediction error was slightly higher but still adequate, considering that no further optimizations were performed in this test.

Summarizing, the implementation of ANNs for the modelling and prediction of soft materials, such as composite materials, is still in its early stages. The available literature is very limited for the specific application of modelling the stress-strain curve of soft materials. Available works are focused on the effect of the temperature. Moreover, works focusing on the effect of the strain rate, hence the velocity-

dependency, of the stress response of the soft materials are currently not available in the literature. The latter is addressed in this thesis. Nonetheless, the potential of ANNs for this application has been proven in the documented works. Despite the many differences in the selection of hyper-parameters for the developed ANNs, the architecture of choice has been the same, feedforward neural networks. Moreover, a very comprehensive review can be found in [133] which includes information about the commonly used validation methods, measurement of performance, sample size, and the type of statistical models, implemented in engineering applications. More detailed information on the specific statistical methods for the validation of the developed ANN, such as the p-fold cross-validation method can be found in [134, 135]

6.4 Model Development

As previously discussed in Chapter 2, modelling the nonlinear, time dependent, and strain dependent stress response of soft materials is critical for the implementation of reliable control systems in soft robotic applications. This has been attempted in many ways, and is also attempted in this thesis with the development of the PL-SLS and the PL-Wiechert models described in Chapter 5. The obtained results highlight the capabilities of these models of predicting the mechanical behaviour of soft materials. Nonetheless, the main limitation of modelling tools based on mathematical models is the high complexity required to achieve adequate accuracy. The latter is amplified when these models are deployed in hardware with limited computing power. This situation is not present in machine learning models where the high computational complexity happens during training only. The computational cost of a deployed model is minimum.

In line with the work available in the literature, a feed-forward back-propagation neural network is developed in here. Nonetheless, the optimization of many of its hyper-parameters is performed to increase its generalization capabilities. These hyper-parameters include: the number of neurons in the hidden layer and the selection of inputs. The remainder hyper-parameters used in here are based on successful implementations from the literature. Table 6.1 provides a summary of the hyper-parameters to be optimized and the hyper-parameters chosen based on the literature.

In this work, the training function `trainbr` is used to train the ANNs, which is based on the Bayesian Regularization (BR) algorithm. This is one of the two most

6. SOFT MATERIALS MODELLING: ARTIFICIAL NEURAL NETWORKS

Table 6.1: Summary of proposed and optimized hyper-parameters.

Proposed Hyper-parameters	
Topology	Feedforward Neural Network
No. of Hidden Layers	1
Hidden Layer Activation Function	Hyperbolic Tangent Sigmoid (tansig)
Output Layer Activation Function	Linear (purelin)
Training Algorithm	Bayesian Regularization (BR)
Cost Function	Mean Squared Error (MSE)
Output	Stress (σ)
Dataset Size	All available data
Dataset Division Function	Random Division
Validation Error Measurement	Normalized Root Mean Squared Error (NRMSE)
Validation Method	Multiple Training Sessions (5)
Optimized Hyper-parameters	
Number of Neurons	1 - 20
Inputs	1 - 3

commonly implemented methods to avoid overfitting in ANNs. The BR algorithm is more computational demanding than the Levenberg-Marquardt algorithm, which is commonly implemented as an early stopping training algorithm. Nevertheless, the BR algorithm performs better for function approximation applications, and when the dataset is small [136]. These characteristics are inline with the dataset used in this research. The characteristics of the available dataset for each material is presented in Table 6.2.

Table 6.2: Total number of training samples per soft material for the number of neurons optimization. In here, the total number of training samples represents the 100% of the whole dataset.

Test Type	EPR	FR	NatPolR	NR	PR	SR	NatR
50 mm/min	45294	11675	4675	11592	8788	24810	3768
250 mm/min	-	11675	2129	10143	4735	11578	124344
500 mm/min	14154	8754	425	8694	676	-	41450
Total	59448	32104	7229	30429	14199	36388	169562

The analyses presented in the following sections summarizes the large exploration process, initially based on a trial and error approach, performed as part of assessing the capabilities of ANNs for the prediction of the viscoelastic properties of the soft materials included in this research. These tests provided with enough evidence on the capabilities of ANNs for the mentioned application. Lastly, the optimization processes performed to some of the ANN hyper-parameters are described in detail in the following sections.

6.4.1 Analysis of the Model Inputs Selection

The first hyper-parameter to optimize is the selection of inputs. For this application, in which the modelling of the velocity-dependent stress response of the material is desired, the decision to include both the strain and the strain rate as inputs of the ANN models, is made. However, in the scenario where the developed ANN is deployed as part of a control system in a real application, having a derivative term and the peaks associated with rapid changes in the input can cause the ANN model to behave unexpectedly. An alternative to circumvent this limitation without preventing the ANN model to learn the time-dependent properties of the stress response, is to use the current and past values of the strain as inputs, i.e. the strain history, allowing the network to learn the time dependency of the stress response without having to differentiate any input. The latter configuration describes a very basic form of a Recurrent Neural Network.

In this work, both described scenarios are analysed. On the one hand, the proposed ANN architectures which have derivative terms in its inputs is considered rate-dependent. On the other hand, the ANN architecture which has current and past values of their inputs, instead of a derivative term, is considered rate-independent. The proposed combination of inputs used to create the ANN models studied in this section, are described in Table 6.3.

As previously mentioned, the inputs and outputs listed in Table 6.3 must be presented to the ANN in the form described in Equations (6.1) and (6.3), yielding:

$$\mathbf{X} = \begin{bmatrix} \varepsilon_{t_1} & \varepsilon_{t_2} & \varepsilon_{t_3} & \dots & \varepsilon_{t_n} \\ \varepsilon_{t-1_1} & \varepsilon_{t-1_2} & \varepsilon_{t-1_3} & \dots & \varepsilon_{t-1_n} \end{bmatrix} \quad (6.4)$$

$$\mathbf{H} = \begin{bmatrix} \sigma_{t_1}^{pred} & \sigma_{t_2}^{pred} & \sigma_{t_3}^{pred} & \dots & \sigma_{t_n}^{pred} \end{bmatrix} \quad (6.5)$$

$$\mathbf{T} = \begin{bmatrix} \sigma_{t_1}^{exp} & \sigma_{t_2}^{exp} & \sigma_{t_3}^{exp} & \dots & \sigma_{t_n}^{exp} \end{bmatrix} \quad (6.6)$$

6. SOFT MATERIALS MODELLING: ARTIFICIAL NEURAL NETWORKS

Table 6.3: Proposed ANN architectures. The architectures FFRI1, FFRI2 and FFRI3 are rate-independent, whereas the architecture FFRD4 is rate-dependent.

	FFRI1	FFRI2	FFRI3	FFRD4
Inputs	ε_t	ε_t	ε_t	ε_t
		ε_{t-1}	ε_{t-1}	$\dot{\varepsilon}_t$
			ε_{t-2}	
Output	σ_t	σ_t	σ_t	σ_t

where \mathbf{X} , \mathbf{H} , and \mathbf{T} are the inputs, outputs, and targets matrices. The variables σ^{exp} and σ^{pred} represent the experimental and predicted values of the stress response of the material for a given strain, respectively. The subscript n refers to the total number of samples in each matrix. The assessment of the best combination of input parameters is based on a 10-fold cross-validation approach which includes the execution of several training sessions. During each training session, up to 10 sessions, the training dataset is randomized prior to be presented to the ANN. Due to the 90-10 proportion used to create the training and test subset, the latter means that the ANN will learn from a different 90% of the data and at the same time, it will be tested with a different 10% of the data, at random. Also, the initial weights of the ANN are randomized in each training session. By default, the measurement of performance used during training is the mean square error (MSE). However, the normalized root mean square error (NRMSE), between the ANN prediction and the experimental data, is extracted from each training session and used for validation (5.10) [117]. Finally, the generalization error is defined as the mean NRMSE value from all the training sessions. The architecture with the lowest generalization error is considered as the best candidate.

Due to the findings from Chapter 5, where the performance of the developed PL-SLS and PL-Wiechert models can be correlated to the properties of the soft materials, i.e. highly elastic, viscoelastic or highly viscous, the decision to optimize the selection of inputs presented to the ANN on the remainder of the studied soft materials is made. In other words, it is not safe to assume a “one fits all” approach due to the differences between the materials properties.

In Table 6.4, the hyper-parameters chosen for this optimization are described. This is intended to isolate the impact of the different inputs presented to the ANN. Similarly, the impact of the amount of data used during training is isolated by using

Table 6.4: Proposed parameters for the selection of best inputs

Fixed Hyper-parameters	
Number of Neurons	20
Dataset Size	10% of available data
Data Division	90% for training, 10% for testing
Error Measure	NRMSE and Generalization Error
Validation Method	10-fold Cross Validation

only 10% of all the complete dataset previously described in Table 6.2. Subsequently, the data is divided into training and testing subsets, containing 90% and 10% of the data, respectively. The size of the testing set is based on the number of training session to perform, which is 10. The Matlab function `cvpartition` is used to obtain 10 nonstratified subsets of data which guarantees a unique subset of data is used for each training session. The testing subset is used to validate the generalization capabilities of the ANN when unknown data is presented to it. Similarly, a relatively large number of neurons is used in this optimization to avoid limiting the performance of the ANN models. Finally, the results are illustrated in Figures 6.2 and 6.3. The obtained charts indicates that the FFRD4 architecture is the one with the best generalization capabilities, i.e. smallest generalization error. In some cases, such as the EPR and NR materials, the achieved error of the FFRI1 and FFRD4 architectures are very similar. The difference between the achieved errors are minor. Hence, the FFRD4 architecture is selected as the best candidate.

Another important observation is the relationship between the achieved error and the complexity of the rate-independent architectures. In other words, presenting the ANN models with more inputs, in the form of past values of the strain, does not always yield in a performance increase. This is the case for the FR, NR, and SR materials. These results could be related to a weak velocity-dependency of the previously mentioned materials. Presenting the ANN models with additional inputs, aimed to account for velocity dependencies in the materials stress response, can harm the learning process rather than aid it.

As part of this analysis, the concept of having past values of the material stress response as input to the ANN model was also investigated. The achieved generalization error of this architecture is at least one order of magnitude lower than the other four architectures. Nonetheless, this concept is later dropped due to its incom-

6. SOFT MATERIALS MODELLING: ARTIFICIAL NEURAL NETWORKS

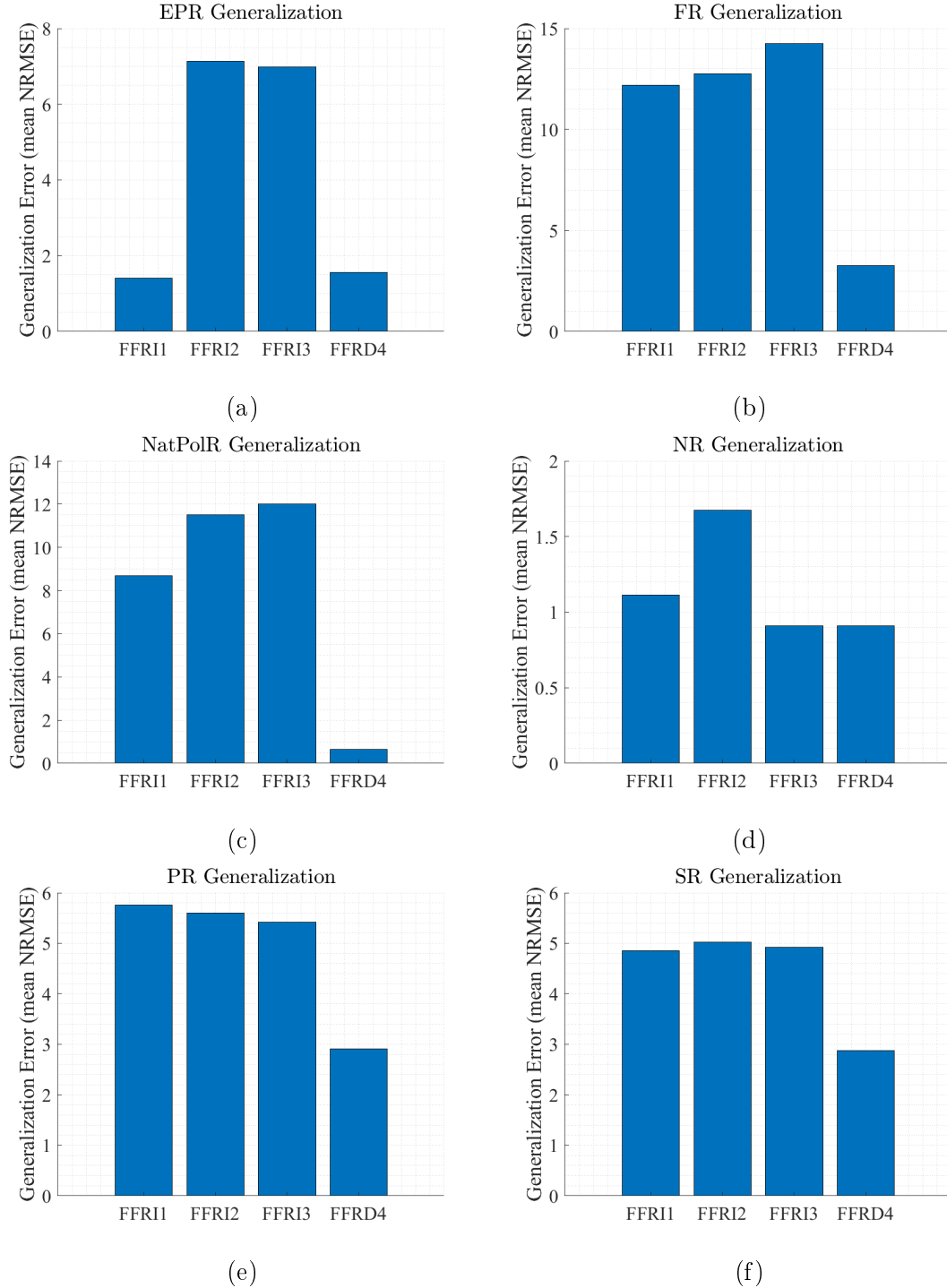


Figure 6.2: Generalization error, based on a 10-fold cross-validation, for the (a) EPR, (b) FR, (c) NatPolR, (d) NR, (e) PR, and (f) SR materials. The best input combination is the one with the smallest generalization error, which in most cases is the FFRD4 configuration.

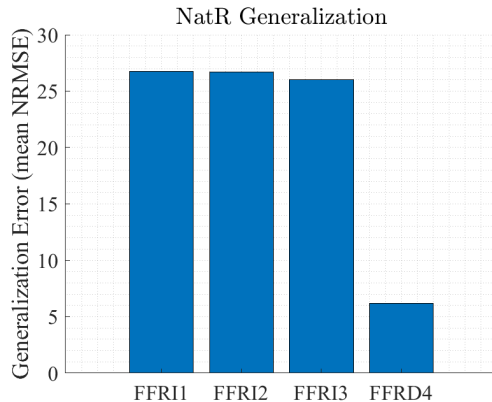


Figure 6.3: Generalization error, based on a 10-fold cross-validation, for the NatR material. The best input combination is the one with the smallest generalization error, i.e. the FFRD4 configuration.

patibility with a real robotic application. In other words, having the stress response of the material as input to the ANN model would translate into adding a load cell to the application. This cancels out one of the main benefits behind series-elastic actuators, which is transforming the force control problem into a position control problem. In other words, using a modelling tool to predict the stress response of the material based on the measured deformation of the material. Finally, the optimization performed in here showed that a rate-dependent architecture, such as the FFRD4, is more suitable for accounting the velocity-dependency of the stress-strain curve of soft materials.

6.4.2 Analysis on the Optimal Number of Neurons

In the literature, having two to three neurons for each input of the ANN is recommended. This recommendation seems to be in accordance to the number of neurons used in the documented implementations [120, 129, 132]. Nonetheless this is not true for all implementations [130, 131]. Moreover, the number of neurons must be kept at its minimum to avoid the ANN to over-fit the training dataset. Therefore, it is desirable to search for the optimal number of neurons which allows the developed ANN models to achieve a desired accuracy. In here, the latter search is performed, initially, for a range of 1 to 20 neurons. The coefficient of determination, R^2 value, is used to assess the performance of the ANNs. In addition to this a 10-fold cross validation is performed. The latter is done by firstly dividing the whole training dataset into 10 subsets. Then, multiple training sessions are performed. In each

6. SOFT MATERIALS MODELLING: ARTIFICIAL NEURAL NETWORKS

training session, 1 out of the 10 available subsets becomes the test set and the remainder 9 subsets become the training set. In this way, each training session use a different section of the whole dataset during the training. On top of this, the range from 1 to 20 neurons is investigated. This means, a total of 200 ANN models are trained per soft material. The main objective of this optimization process is to limit the resources of the developed ANN models, i.e. to avoid over-fitting. The training session with the minimum number of neurons that has a value of $R^2 > 99.9\%$ is considered as the best candidate. A similar process to this, but using the percentage of correct prediction, is documented in [122].

In this optimization, the complete dataset available for each material is subdivided to allocate 90% of the data for training and 10% for testing. As previously mentioned, no validation subset is required when using the Bayesian Regularization algorithm. Therefore, the training set is no further subdivided. The list of hyper-parameters used in this case is compiled in Table 6.5, and the total number of training samples for each soft material is compiled in Table 6.2.

Table 6.5: Proposed hyper-parameters for the number of neurons optimization

Fixed Hyper-parameters	
Architecture	FFRD4 (see Table 6.3)
Number of Neurons	1 to 20
Error Measure	R^2 value
Validation Method	10-fold Cross Validation
Data Division	90% for training, 10% for testing
Data Set Size	100% of available data

The achieved generalization errors (Gen. Error) and the R^2 values obtained from this optimization are illustrated in Figures 6.4 to 6.6. The calculation of the Gen. Error is based on the mean value of the NRMSE values obtained during the 10 training sessions, as follows:

$$\text{Gen.Error} = \frac{1}{N} \sum_{j=1}^N \text{NRMSE}_j \quad (6.7)$$

where N is the total number of training sessions, 10, and the subscript j represents the NRMSE value obtained in each individual training session. It is important to mention that the training set is different from one training session to the other, but it is constant among the different number of neurons tested.

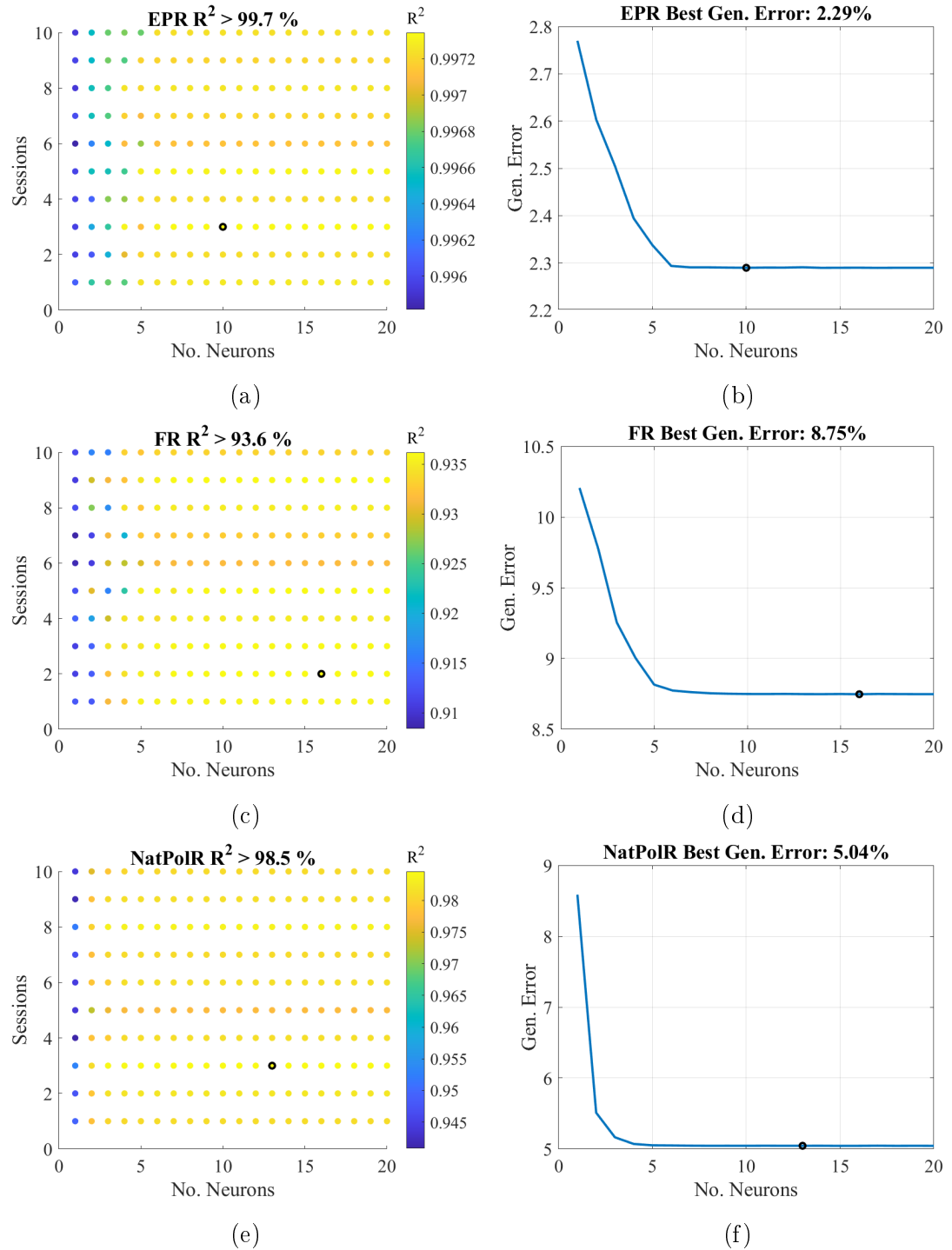


Figure 6.4: Impact of the number of neurons on the R^2 value (a), (c), (e), and the Generalization error (b), (d), (f), for the EPR, FR, and NatPolR materials. A total of 200 ANN models are trained per soft material. The best R^2 value is circled in (a), (c), (e). The optimal number of neurons is circled in (b), (d), (f).

6. SOFT MATERIALS MODELLING: ARTIFICIAL NEURAL NETWORKS

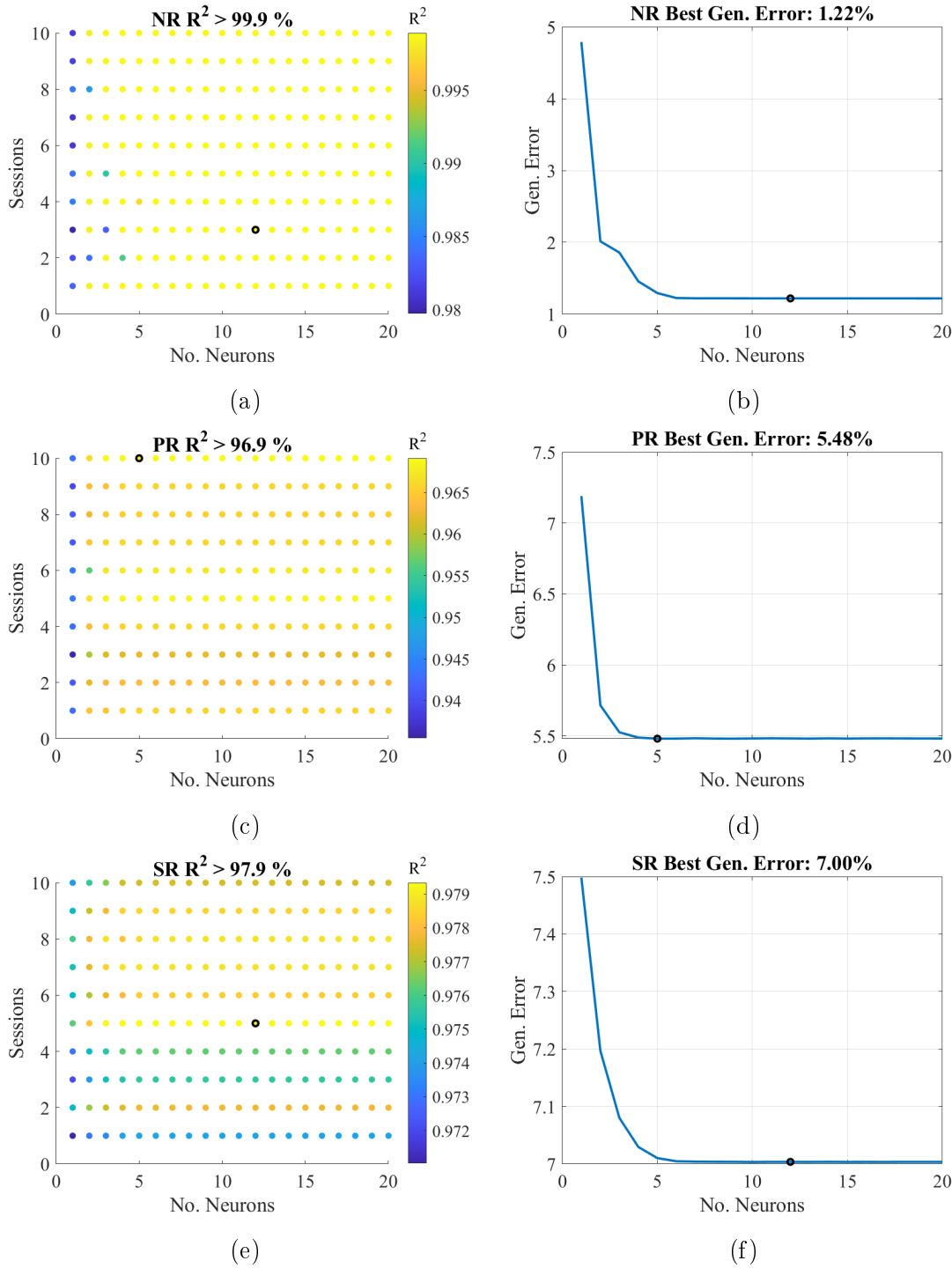


Figure 6.5: Impact of the number of neurons on the R^2 value (a), (c), (e), and the Generalization error (b), (d), (f), for the NR, PR, and SR materials. A total of 200 ANN models are trained per soft material. The best R^2 value is circled in (a), (c), (e). The optimal number of neurons is circled in (b), (d), (f).

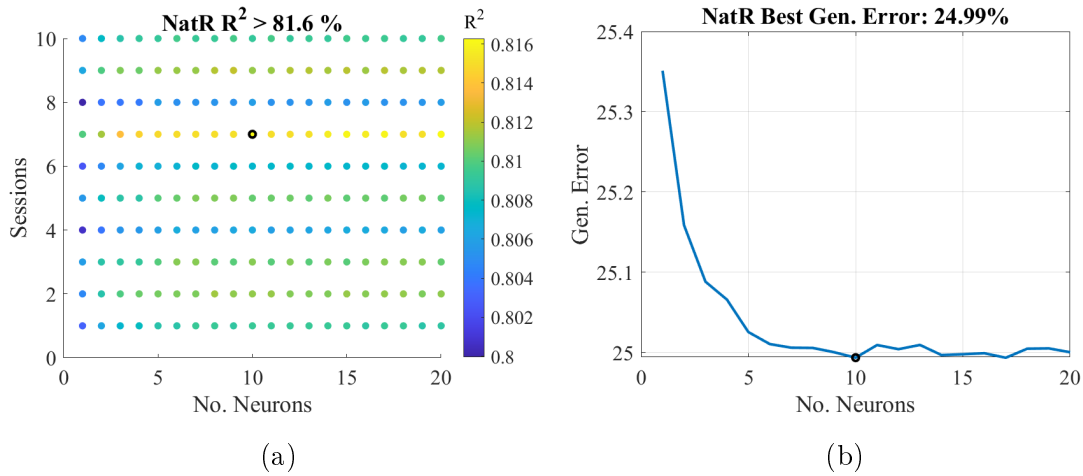


Figure 6.6: Impact of the number of neurons on the R^2 value (a) and the Generalization error (b), for the NatR material. A total of 200 ANN models are trained per soft material. The best R^2 value is circled in (a). The optimal number of neurons is circled in (b).

The R^2 value, or coefficient of determination, indicates the fraction of the data variation which is explained by the ANN models. Traditionally, a R^2 value closer to 1 indicates a very good model fit. However, in the field of ANNs, a very high R^2 value could actually indicate over-fit in the developed ANN. In general, most of the achieved R^2 values are below the desired threshold of $R^2 > 99.9\%$. Only the ANN model NR material is able to meet the latter threshold. In contrast, the lowest R^2 value achieved among all materials is reported for the NatR material as $R^2 > 81.6\%$.

The ANN models with the optimal number of neurons must have the right combination of good accuracy (small NRMSE), low number of neurons, and high R^2 values. The first parameter to consider is the R^2 value. For the training sessions with a $R^2 > 99.9\%$, the optimal candidate is the one with the lowest number of neurons. For the cases in which the threshold is not achieved, the maximum achieved R^2 value is taken as reference. Following these conditions, the optimal number of neurons per soft material are extracted and presented in Table 6.6. In here, the PL-SLS and the PL-Wiechert models are also compared against the developed ANN model.

The values of the generalization error for all the three models are very similar. The calculation of this parameter is different between the ANN models (6.7) and the PL models (5.13). Nonetheless, in both cases, the generalization error measures the capabilities of the models for accounting the non-linear velocity-dependent stress response of the studies soft materials.

6. SOFT MATERIALS MODELLING: ARTIFICIAL NEURAL NETWORKS

Table 6.6: Comparison between the performance of the best case ANN model, the PL-SLS model, and the PL-Wiechert model. The generalization error, Gen. Error (6.7), is based on the mean NRMSE value from all training sessions, whereas the *GE* (5.13), is based on the mean NRMSE among all available strain rates as described in Chapter 5.

	EPR	FR	NatPolR	NR	PR	SR	NatR
ANN model							
Gen. Error (%)	2.29	8.75	5.04	1.22	5.48	7	24.9
R^2	99.7	93.6	98.5	99.9	96.9	97.9	81.6
No. of Neurons	10	17	13	12	5	12	10
PL-SLS model							
<i>GE</i> (%)	13.04	3.03	2.27	1.36	2.70	1.44	1.10
Tolerance (%)	60	90	30	40	40	70	80
PL-Wiechert model							
<i>GE</i> (%)	10.34	4.44	2.51	2.36	3.64	0.55	1.12
Tolerance (%)	90	70	10	70	60	60	80

In general, the generalization error values of the developed ANN models are slightly higher than the values reported for the PL models. This is expected due to the selection criteria when choosing the optimal number of neurons. In other words, this is the potential effect of constraining the number of neurons to avoid over-fitting from happening. Nonetheless, the NatR material is identified as an outlier. This material reported a significantly different Gen. Error value of 24.9% which is also not aligned with the generalization errors reported for the PL models. The potential cause of this is the uneven dataset available for this material in which much of the data is concentrated in the strain rates of 250 and 500 mm/min. Another potential cause of this is the limited number of neurons used, in comparison to the size of the dataset available for this soft material, which is the largest among all the studied materials. This hypothesis is further verified by looking at Figure 6.3 from the selection of inputs optimization where only 10% of the whole dataset is used. In this scenario, the Gen. Error achieved by the ANN model is around 5%, a value closer to the Gen. Error values reported in Table 6.6.

Interestingly enough, the ANN models performed better for the case of the EPR material, where the PL models performed the worst. Again, this can be related to

the characteristics of the dataset. For this material, there is no available data for the strain rate of 250 mm/min. In addition to this, the stress-strain curves of this material for the strain rates of 50 and 250 mm/min are very similar (Figure 4.6a). Due to this, a small Gen. Error in this scenario could in fact indicate over-fitting. Nonetheless, the developed ANN models performed better than Std. Lin. SDS model, the reference which has been used along this thesis, where the reported relative RMSE is of 13.6%. Therefore, the developed ANN models are also suitable for the prediction of the non-linear, time dependent, and strain dependent stress response of viscoelastic materials. Lastly, the performance of the developed ANN models is further validated under simulated real-time conditions, replicating as much as possible the conditions expected in a real robotic application.

6.5 Summary

In this chapter, a feedforward artificial neural network model is developed and tested as an alternative to traditional modelling approaches based on the LVMs, such as the PL models developed in Chapter 5, which can be very computationally costly. Artificial neural networks have been successfully implemented in many applications, but the literature available on the prediction of the viscoelastic properties of soft materials is still scarce. The developed ANN models are aimed to be used in real robotics applications, specifically to predict the mechanical behaviour of the viscoelastic element found in a recent actuation technology, the series-viscoelastic actuator.

The process of developing the ANN models involved the optimization of the number of neurons in the hidden layer and the most appropriate selection of inputs and outputs, to account for the viscoelastic properties of the studied soft materials. The optimal number of neurons varied from one material to the other but it does not exceed 20 neurons. The inputs of the ANN models are defined as the strain and the strain rate of the materials. As the output, the ANN models are aimed to predict the stress response. In order to avoid over-fitting, the Bayesian Regularization algorithm is used instead of a traditional early stopping method such as the Levenberg-Marquardt algorithm.

The generalization capabilities of the ANN models are assessed using a k-fold cross validation approach together with multiple training sessions. In this way, the network is trained and tested with unique data subsets in each training sessions. The mean NRMSE from these training sessions is defined as the generalization error

6. SOFT MATERIALS MODELLING: ARTIFICIAL NEURAL NETWORKS

of the ANN models. In general the ANN models outperformed the Std. Lin. SDS model documented in the literature, which has been used as reference in this thesis. When comparing the performance of the ANN models to the PL models, two outliers are detected. On the one hand, the ANN model for the EPR material outperformed the developed PL models. On the other hand, the ANN model for the NatR material performed worse than the PL models. The differences in performances could be caused by the characteristics of the dataset of each of these materials. This however, do not disregard the capabilities of the ANN models to account for the non-linear velocity-dependent stress response of soft materials. Nonetheless, the performance of these modelling approaches when being implemented as part of a control system is still unknown. This is investigated in the following chapter.

CHAPTER 7

Modelling a bio-inspired series-viscoelastic actuator

7. MODELLING A BIO-INSPIRED SERIES-VISCOELASTIC ACTUATOR

7.1 Introduction

In the previous chapters, the development of two modelling tools based on the LVMs, and one modelling tool based on machine learning algorithms is described. The three developed models are capable of accounting for the nonlinear velocity-dependent stress response of the studied soft materials with adequate accuracy. Due to the measurement of performance used for evaluating the ANN models, further validation is desired. Specifically, under a simulated real-time scenario, which replicates the conditions expected in a real robotic application. This is in line with the motivation of this research of addressing the current limitations of traditional modelling tools when being deployed as part of a control system, such as: high complexity and large computational power requirements.

In this chapter, the performance of the ANN model is assessed under a simulated real-time scenario. This is done by assessing the prediction performance of the ANN model under different types of strain inputs, such as a sine wave, and using a simplified model of a series-viscoelastic actuator. This study is performed in Simulink. The developed PL models are not included in this analysis due to their formulation which make use of past values of the stress response of the material. This contradicts the principles and benefits of series-elastic actuators.

Also included in this chapter is the investigation about the similarities between the human tendon and the studied soft materials. This is a crucial part for selecting the best soft material to be implemented as part of the model of a series-viscoelastic actuator.

Results highlight an unexpected limitation of the developed ANN model which is not capable of performing well under a variable strain rate input. This can be circumvented by keeping the strain rate input constant. However, this is a limitation which must be addressed for the ANN model to be reliable in real robotics applications.

In summary, the design process presented in here consists of: the selection of the best soft material to match the human tendon properties; the selection of the electric motor and gearbox combination suitable to deliver 50% assistance, based on the knee torque requirements during walking activities; the evaluation of the ANN model in simulated real-time under different strain input signals; and the 3D design of a clamping device aimed to hold several pieces of soft materials in a bundle-form.

7.2 Matching the Human Tendon Properties

In line with the aim of implementing the human skeletal muscle system functionality in soft robotic applications in the form of a bio-inspired soft actuator, this section presents a comparison analysis between the mechanical properties of the seven studied soft materials, and the human tendons and ligaments involved in the motion of the knee joint. The latter is motivated due to the large contribution of this joint on the activities of daily living, as described in Chapter 3. Due to the limited availability of clinical studies focusing on the tensile strength and stress relaxation properties of the tendons and ligaments involved in the human knee joint, a selection of three separate clinical studies is made. The first study is solely focused on the tensile strength properties of the patellar tendon [137], the second one is focused on the stress relaxation properties of the quadriceps ligaments [70], and the third study is focused on the tensile strength properties of both the patellar tendon and the quadriceps ligaments [138]. The aim of this comparison analysis is to identify which of the studied soft materials can match the human tendon mechanical properties. Due to this, the viscoelastic properties of the human patellar tendon and the quadriceps ligaments are compiled in Table 7.1, alongside the mechanical properties of the studied soft materials for direct comparison.

Table 7.1: Viscoelastic properties of the patellar tendon and the quadriceps ligament [70, 137, 138], compared against the viscoelastic properties of the studied soft materials (Tables 4.2 and 4.4).

	Human Tendon	EPR	FR	NatPolR	NR	PR	SR	NatR
Tensile Strength								
σ_{ue} (MPa)	33.6	8.48	4.36	3.57	3.55	0.3	6.03	9.43
ε_{ue}	0.14	7.56	3.97	1.19	3.57	1.87	5.77	13.02
E_{small} (MPa)	303.9	3.23	4.83	9.97	4.29	0.58	3.26	1.01
Stress Relaxation								
$S.R$ (%)	41	32	67	35	29	63	31	15

In Table 7.1, the large difference between the elastic properties of the quadriceps tendon and the studied soft materials, specifically for the elastic modulus E_{small} , can be appreciated. Nonetheless, the achieved stress relaxation in the human tendon is

7. MODELLING A BIO-INSPIRED SERIES-VISCOELASTIC ACTUATOR

very similar to the one found in the soft materials. Therefore, they share similar viscous properties. This is a positive finding, because the elastic properties, of stress and strain, are structural parameters which depends on the dimensions of the material Section 4.3. The stress is inversely proportional to the cross-sectional area of the material. Moreover, the stress has a nonlinear relationship with the material strain. Hence, a material with larger cross-sectional area will require a larger force to achieve the same deformation. With this in mind, a new questioning arises regarding the cross-sectional area increment required for the soft materials to match the properties of the human tendon.

The latter questions must be answered considering the end application of the soft materials. As previously mentioned, these are intended to be used as part of a series-viscoelastic actuator. Having this in mind, the way in which the soft materials match the human tendon properties by an increase in their cross-sectional area can be better visualized. The implementation of a bundle of many strips of a soft material is proposed. The dimensions of each strip must be in line with the dimensions in which the material is available from the manufacturer. As previously mentioned, they all come in a rectangular shape. The thickness among all the studies soft materials vary from one to the other. Moreover, it is useful to think in the end application of the soft actuator itself, which is human assistance. According to the literature, a robotic wearable device for rehabilitation applications must deliver an assistance of 60% of the peak torque required [139]. Due to this, an objective assistance percentage of 50% is proposed in here as design guidelines for the selection of the motor-gearbox combination. In addition to this, the safe working conditions of the studied soft materials, i.e. the elastic region, are considered. The approximated elastic region of each studied, using the offset-yield strength, is compiled in Section 4.3. Lastly, all this information is considered in the matching factor calculation, in which the elastic modulus E_{small} of the human tendon is desired to be matched by the soft materials.

The matching factors described in Table 7.2 are obtained using a two-fold process. Firstly, the cross-sectional area of each soft material is matched with the cross-sectional area of the human tendon. Secondly, the elastic modulus of the human tendon is matched, considering the previous increase in the cross-sectional area of the materials. As previously mentioned, the materials thickness is defined by the manufacturer, therefore fixed. Nonetheless, many strips can be extracted from the material rectangular sheet using laser cutting. The width of these strips can be

Table 7.2: Matching factors required for the soft materials to achieve the human tendon E_{small} value. The width proposed for the material strips is 66 mm.

	EPR	FR	NatPolR	NR	PR	SR	NatR
Matching factors							
A_o	7	7	7	7	2	7	12
E_{small}	77	52	25	58	375	76	248
E_{small} @ 50%	39	26	12	29	188	38	124
Material Dimensions							
Old A_o (mm^2)	9	9	9	9	36	9	5.22
New A_o (mm^2)	4852	3245	1572	3653	27020	4807	15517
New A_o @ 50% (mm^2)	2426	1622	786	1827	13510	2404	7758
Strip Width (mm)	66	66	66	66	66	66	66
No. of strips	49	33	16	37	68	49	270
No. of strips @ 50%	25	16	8	18	34	24	135

modified to increase the cross-sectional area of the material. Hence, a width of 66 mm is proposed for the latter calculations. The latter is decided taking into consideration the application in which the bundle of strips will be implemented. That is, bio-inspired actuator. Moreover, this actuator is aimed to be used to assist the knee joint. This in fact puts a limit to the width of the bundle of strips, and that is the dimensions of the human shank. Taking this into consideration, and the relationships between the required number of strips and the strips width. The previously mentioned value of 66 mm is adequate. In theory, it is possible for all the materials to match the human tendon elastic modulus as long as enough strips are used. The exact number is stated in Table 7.2. Finally, by analysing the obtained matching factor in combination with the stress relaxation properties of the human tendon, the soft material with the closest properties is identified to be the NatPolR material.

7.3 Validation in Simulated Real-time

In this validation, the developed PL models are not included because its formulation makes use of past values of the stress response. This contradicts the benefits of implementing a SEA in the first place, which is to use the deformation of the elastic

7. MODELLING A BIO-INSPIRED SERIES-VISCOELASTIC ACTUATOR

element as an indirect way to measure the stress response. The same principle apply for series-viscoelastic actuators (SVAs).

The developed ANN models, takes two inputs, the strain and strain rate, and outputs the stress response of the material in MPa. Therefore, particular care must be taken with regard to the conversion to avoid undesired results. As previously mentioned the stress is defined as $\sigma = F/A_o$, whereas the strain is defined as $\varepsilon = \Delta L/l_o$. The value of $l_o = 33\text{mm}$ applies to all soft materials studied in here. The cross-sectional area A_o varies from one material to the other. The units from the stress output (MPa) and A_o (mm^2) are compatible and can be used as they are in the conversion.

The simulation environment is based on the model of a soft SVAs. Commonly, these actuators are cable-driven. In simple terms, this means that an electric motor is connected in series to a viscoelastic element, and this element to a load. In here, many assumptions are made to simplify the model of the actuator and isolate the performance of the ANN model. These assumptions are as follows:

- The electric motor is replaced with a simple sine wave block which represents the strain. The derivative of this input signal is the strain rate.
- The viscoelastic element is connected to the motor in one end, and is fixed on the other end. Hence, no load is connected to this element.
- The concept of implemented multiple pieces of the same material is implemented by a gain block.

Having defined the conditions of the simulation, the developed Simulink model is illustrated in Figure 7.1, as follows:

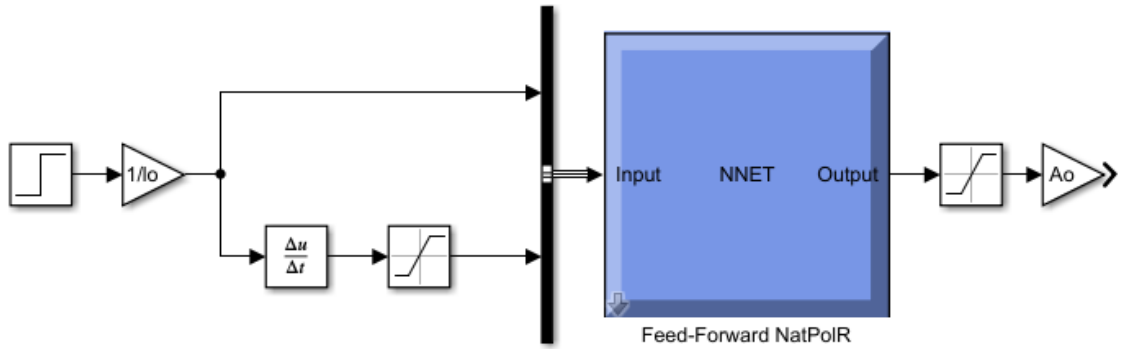


Figure 7.1: Simulink implementation of the ANN model. The ANN model takes the strain and strain rate as inputs, and delivers the stress response of the material in MPa as output. The gain blocks ensure that the units are consistent.

In Table 7.2, the NatPolR material is identified as the best candidate to imitate the mechanical properties of the human tendon. Due to this, the NatPolR material is selected for this simulation. The parameters of the generated sine wave must be inside the working conditions of this soft material. The latter is reported in Table 4.2. The elastic limit ε_y of the NatPolR varies from 0.41 to 0.48 strain. Similarly, the stress response of the material in this range of deformation goes from 2.12 to 2.52 MPa. Moreover, the prediction capabilities of the ANN models have been assessed for the three available strain rates of 50, 250, 500 mm/min. Therefore, the frequencies of the generated sine wave must be inside this range as well. For consistency, these values are changed to mm/sec when defining the sine wave. Inside the block diagram, the generated sine wave is divided by the initial length of the material $l_0 = 33\text{mm}$, yielding the units of the strain (mm/mm) per second. The generated sine wave must have positive values of the strain only. This is in line to the training set where only positive values of the strain are available. The generated sine waves follow the basic formula $f(t) = A\sin(\omega t + \beta) + C$. For simplicity, only the amplitude A and the offset C are varied. Changing these two parameters allows each sine wave to have different values of strain rates, measured as the difference between the maximum and minimum values of the sine wave that are spaced by one second due to the chosen frequency.

A total of four different sine waves are generated to represent a varying strain inputs. The strain rate input is the derivative of the sine wave, i.e. a cosine wave. Each one is aimed to assess a specific scenario. The sinewaves with the strain rate of 100 mm/min and 400 mm/min are aimed to assess the response of the model for

7. MODELLING A BIO-INSPIRED SERIES-VISCOELASTIC ACTUATOR

positive values of the strain and the strain rates which are unknown to the ANN model, i.e. they are not included in the training set. The sinewave with a strain rate of 50 mm/min is aimed to assess the response of the ANN model when negative values of both the strain and strain rate are included. In reality, negative values of the strain, i.e. compressing the material, do not produce any stress response. Nevertheless, this behaviour must be considered when deploying the ANN model in a control system. Lastly, the sine wave with a strain rate of 500 mm/min is aimed to assess the response of the ANN model when the strain rate is saturated, i.e. negative values of the strain rate are replaced with zero. The results of the simulation are illustrated in Figure 7.2.

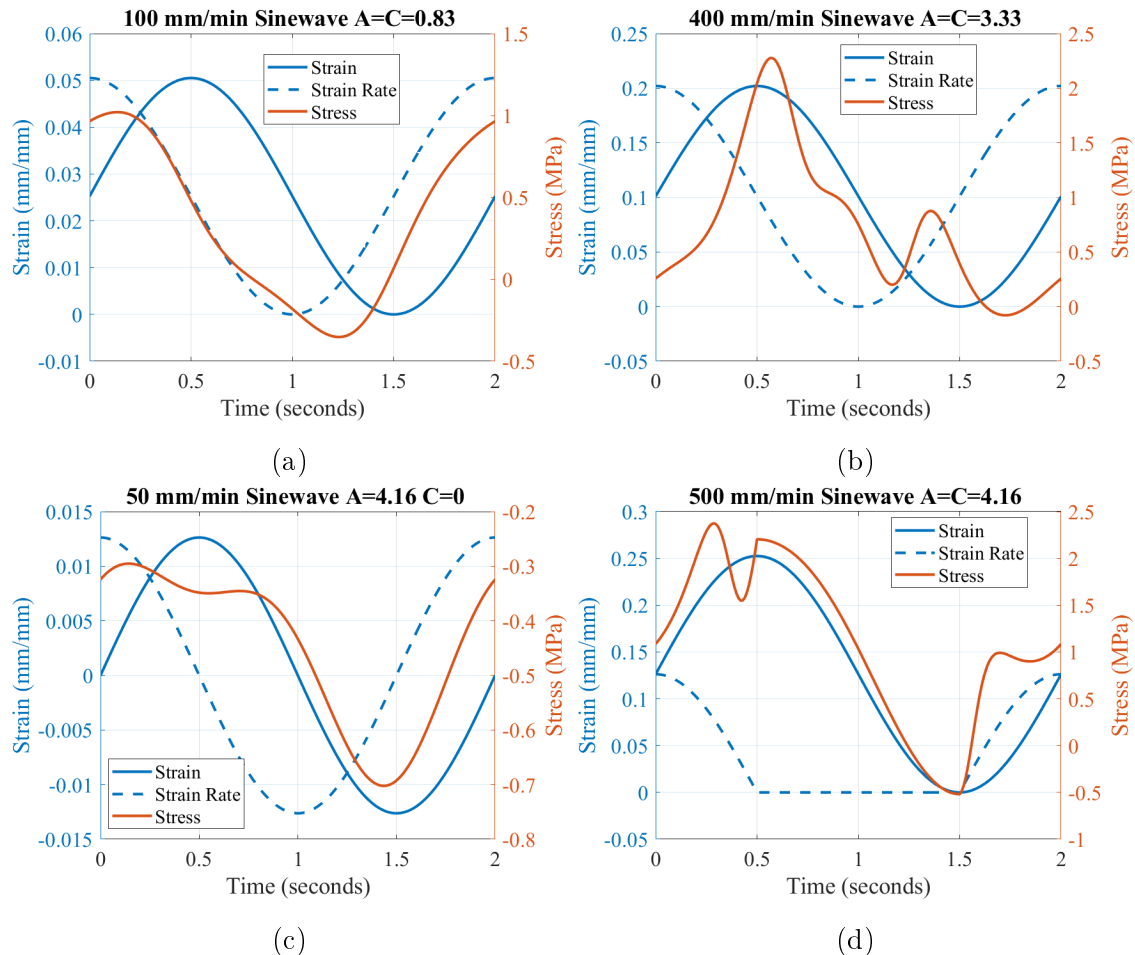


Figure 7.2: ANN model stress response to a sine wave strain input. The solid and dotted blue line are the strain and strain rate, respectively. (a) and (b) positive and unknown strain rate values, (c) negative values of the strain and strain rate, (d) strain rate saturated to avoid negative values.

The prediction of the ANN model under scenario (a) is not entirely accurate

since negative values of the stress response are present (Figure 7.2a). This is an unexpected behaviour because both the strain and strain rate are positive and are inside the elastic limit of the material. This behaviour can be caused by the steep decaying rate of the cosine wave in the 0.5 to 1.5 seconds interval. Nonetheless, the stress response of the ANN model is even more unstable when using a larger value for the strain and strain rate as shown in scenario (b) (Figure 7.2b). In here, the response of the ANN model do not reach negative values. In scenario (c), the response of the model looks very stable. However, the stress response is always negative (Figure 7.2c). This scenario is initially out of the ordinary due to the negative values of the strain and strain rate which are not expected to be present in a real application. Due to this, the obtained stress response if expected to be inaccurate. Lastly, in scenario (d) the response of the ANN model oscillates between positive and negative values despite the saturation implemented to the strain rate signal (Figure 7.2d). In summary, the scenario in which the ANN model performed the best is in (a). Although, the obtained negative values of the stress response are undesired.

The unstable response of the ANN model can be caused by the limited number of strain rates included in the training set. Moreover, the strain rate in these scenario is changing over time, whereas the strain rate in the training set is fixed between three different values. Due to this, the four scenarios are tested again, this time using a positive and constant strain rate of 250 mm/min. The results are illustrated in Figure 7.3.

The response of the ANN model when a constant strain rate is used is very stable (Figure 7.3). This further indicates that the main limitation of the developed ANN models, i.e. their performance relies heavily on the training set. This can be improved by adding the unloading stage of the stress-strain curve of the material. In this way, the concept of a decreasing strain rate can be learned by the ANN model.

Summarizing, the analysis performed in this section provided useful information about the behaviour of the ANN model in simulated real-time conditions. An important limitation is found, which is the erratic prediction of the ANN model when the strain rate varies over time. The lack of a bigger and richer training set is identified as the potential cause. The relevance of understanding the role of the strain rate on the stress response of soft materials has been recently highlighted in the literature. In the work performed by Xu et al. in 2019, the development of an ANN model capable of predicting the elastic modulus of soft materials under differ-

7. MODELLING A BIO-INSPIRED SERIES-VISCOELASTIC ACTUATOR

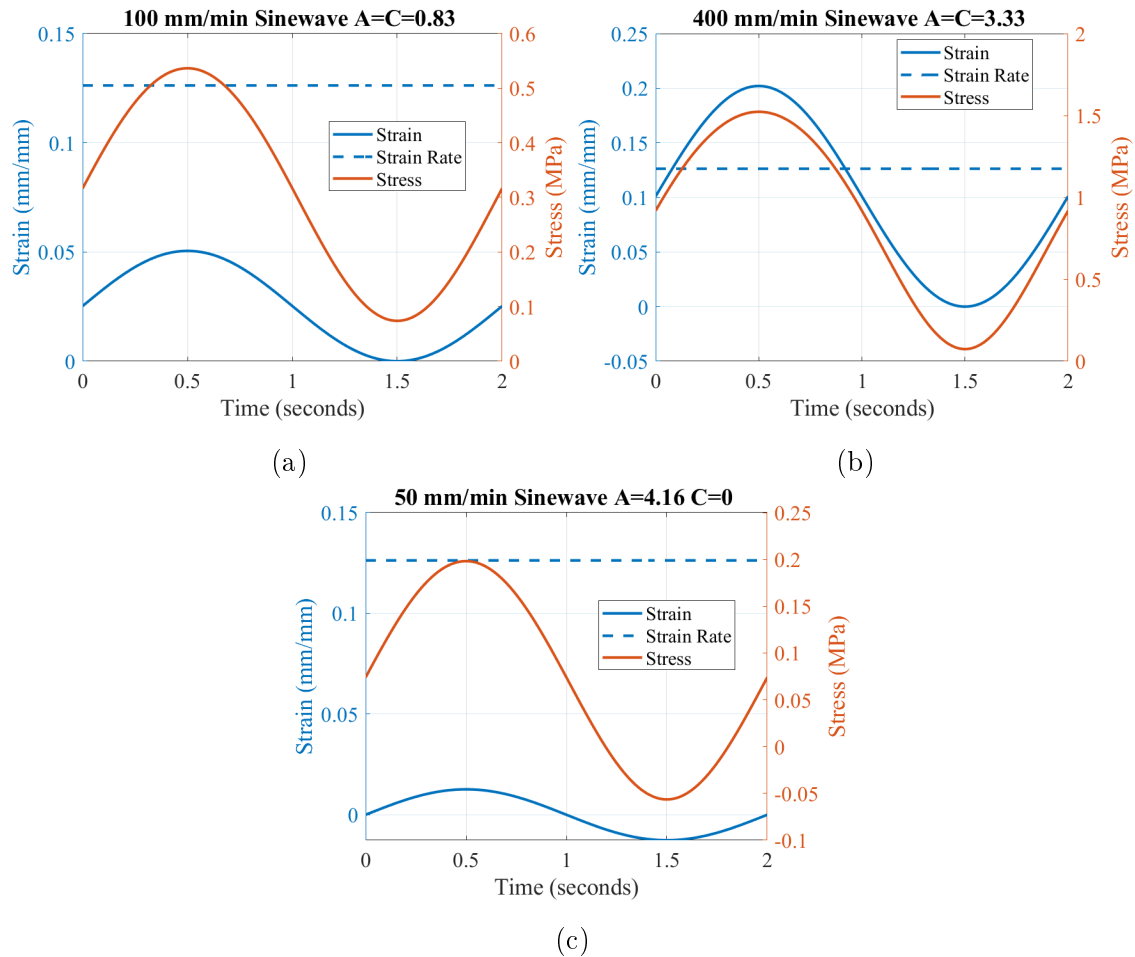


Figure 7.3: ANN model stress response to a sine wave strain input and a constant strain rate. The solid and dotted blue line are the strain and strain rate, respectively. (a-b) positive and unknown strain values, (c) negative values of the strain.

ent strain rates is described [140]. The studied material in this case is a graphene reinforced composite, and is characterized using a dynamic mechanical analysis over a range of frequencies and temperatures. These ranges of values are the input of the ANN model which in fact, does not directly predict the stress response of the material, and instead, predicts the storage modulus of the material which is a parameter related to the viscoelasticity of materials. Using this parameter in combination with known mathematical equations, the stress response of the material can be extracted. Ongoing research about the modelling of soft materials using ANN models highlights the relevance and feasibility of the research presented in this thesis.

7.4 Series-viscoelastic Actuator: Design Concept

Series and parallel elastic actuators have been implemented in human assistance applications to achieve a muscle-like performance and increase the assistance capability of robotic wearable devices. Traditionally, the mechanical element used to provide elasticity in actuators is a metallic spring. However, the idea of replacing the metallic spring with a soft material, such as rubber, is being researched now. The works performed by D. Rollinson has proved this idea to be beneficial for series-elastic actuators (SEAs) by developing a rotational spring based on natural rubber [83, 141]. In fact, the latter research gave birth to HEBI Robotics and to the first SEA implementing a soft material as the elastic element [142]. In addition to this, other SEA concepts implementing rubber [86], dielectric elastomer [143] and polyurethane [114] are being researched.

The benefits of series and parallel elasticity have been demonstrated in many works both with rigid and soft materials as the elastic element. However, there is only one actuator concept documented in the literature which implements both series and parallel elasticity in the same actuator, creating a series-parallel-elastic actuator (SPEA) [144]. This actuator implements rigid springs and is based on the variable recruitment process observed in human muscles, which means that depending on the required torque and displacement, more springs are engaged.

As previously mentioned, an objective assistance of 50% of the required peak torque is proposed. Moreover, the research is focused on the human knee joint due to its major role in the activities of daily living. In line with this, the required peak torque and angular speed range for the knee joint during normal walking is found to be 29 Nm and ± 50 rpm respectively [139, 145]. Therefore, the peak torque aimed to be delivered to achieve a 50% assistance is 15 Nm. The previous parameters will be used as guidelines when selecting the electric motor/gearbox combination to be used in the simulation. In addition to this, the working range of the soft materials is also important. The latter is indicated by the elastic region of the material, which is approximated using the offset yield strength in Section 4.3. In summary, the parameters aimed to be used in a future experimental validation are presented in Table 7.3.

As part of the preliminary design of the series-viscoelastic actuator, and in line with using a bundle of soft materials to match the human tendon mechanical properties, a clamping device is designed in SolidWorks® (Figure 7.4). The width of the clamp is in line with the end application, which is an assistive wearable device

7. MODELLING A BIO-INSPIRED SERIES-VISCOELASTIC ACTUATOR

Table 7.3: Simulation parameters

Soft Material	Natural Rubber with Polyester (NatPolR)
Working Range	Up to 0.5 strain (16.5 mm)
Strip Width	20 mm
Strip length	33 mm
A_o	9 mm ²
No. of strips	8
Torque reference	Knee joint motion capture data
Position reference	Knee joint motion capture data
Electric motor	Maxon RE53-323891 [146]
Nominal Voltage	24 V
L_a	0.191 mH
R_a	0.583 Ω
K_a	29.2 mNm/A
K_b	0.029 V/(rad/s)
J_m	79.2 g/cm ²
Gearbox	Maxon GP 42 C-203124 [147]
n	1/81

for the human knee joint. The idea behind this design is to stack several pieces of the same material on top of each other and then clamp them together to create a bundle of soft materials. This design is similar to the one used in the literature when dealing with rubber materials and cable-driven actuators [86].

The clamp mechanism of Figure 7.4 is designed to be detachable. This is achieved by having a T-shape element which can be glued to a bundle of materials strips. Each soft material strip must also be glued to each other to allow for even deformation of the whole bundle. The T-shape attachment, which resembles a “plug and play” device, fits inside the clamp base (Figure 7.4a) and also in the clamp top element. This allows the quick testing of different bundles of soft materials. Once in place, the clamp mechanism can be secured with bolts going through the holes added to the clamp base and top parts. This is illustrated in Figure 7.4b. This design is inspired in the one used in [86], with the addition of designing it as detachable clamping mechanism to allow the test of different soft materials bundles, when being used as part of a test bench.

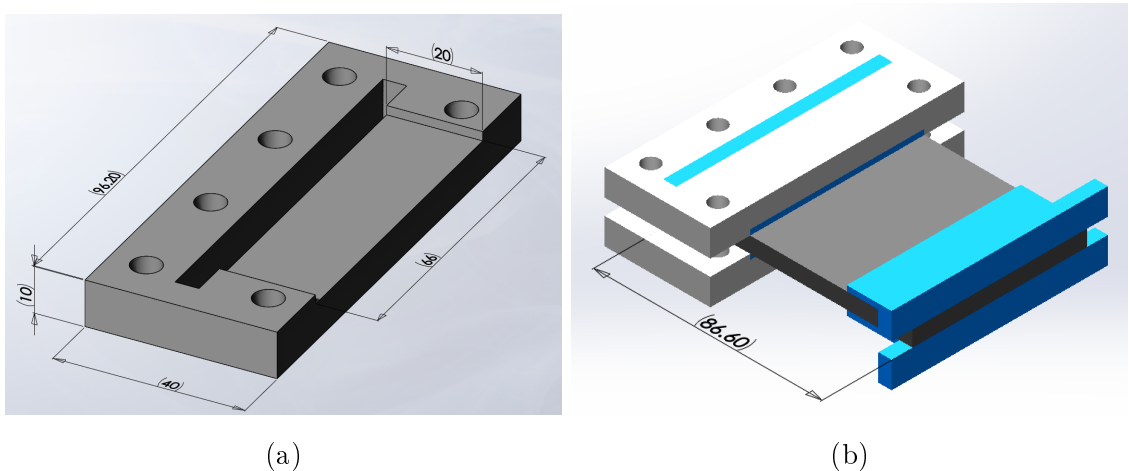


Figure 7.4: CAD Design of the detachable clamping device (a) Bottom part, (b) Final assembly, the soft material is coloured in black, and the T-shape attachment in blue. Units are in millimetres.

7.5 Summary

In this chapter, the preliminary design concept of a series-viscoelastic actuator is presented. As the very first step in the design process and in line with the aim of mimicking the human muscle skeletal system, the comparison of the human tendon mechanical properties against the properties of the soft materials is made. In addition to this, the validation of the ANN model performance under simulated real-time conditions is investigated. The results are unexpected due to the erratic stress response prediction of the ANN model. The latter is directly related with the fact that only up to three different strain rates are included in the training set. Moreover, the stress response of the ANN model is also affected by the selection of frequency and amplitude of the strain input. Nonetheless, the prediction performance of the ANN model is very stable when the strain rate is positive and constant. This highlight the necessity of a richer dataset which includes the unloading stage of the stress-strain curve of the materials. Also, information about a decreasing strain rate can improve the performance of the ANN model described in here. Finally, the work related to the design process of the series-viscoelastic actuator is presented, which includes: the selection of actuator technologies, selection of the best soft material to match the human tendon properties, and design of a clamping device to hold a bundle of stacked soft material pieces.

CHAPTER 8

Summary, Conclusions, and Future Work

8. SUMMARY, CONCLUSIONS, AND FUTURE WORK

8.1 Summary

The aim of this research, is to investigate the concept of implementing viscoelasticity, a property found in the human skeletal muscle system, in soft robotics applications for the assistance of the human lower limb. Narrowing this a little further, special focus is put into the human knee joint and the concept of a series-viscoelastic actuator. In addition to this, this research aims to address current limitations on the modelling of soft materials. Specially the nonlinear, time dependent, and strain dependent stress response of soft materials is of interest. The latter is systematically investigated by developing three modelling tools. Two of them are based on the Linear Viscoelastic Models, whereas the third one is based on artificial neural networks (ANNs). The motivation behind investigating different modelling approaches is to address the known limitations of traditional modelling tools, based on mathematical models, when being deployed as part of a control system. These limitations are high complexity and large computational power requirements. Due to the latter, the performance of the developed ANN model is assessed in a simulated real-time environment using Simulink. The simulation is based on the simplified model of a bio-inspired series-viscoelastic actuator (SVA). The main difference between a SVA and traditional series-elastic actuators is in the type of elastic element implemented. In here, the aim is to implement a bundle of strings made of a specific soft material. Lastly, this last chapter of the thesis provides a summary of the actions taken towards completing the aims and objectives presented in Chapter 1, as follows:

Survey the literature to identify: the terminology related to the biomechanics of the human lower limb, and the current soft robotic developments for the field of human assistance.

The tendency of mimicking the human muscle skeletal system functionality when developing soft robotic applications for human assistance, is presented in Chapter 2. Furthermore, the most matured soft actuation technologies commonly used are identified as: pneumatic/hydraulic artificial muscles, and cable-driven actuators. The benefits and limitations of these technologies are described. In the field of soft sensing applications, the literature is mainly focused on elastomers with embedded micro-conductive channels. The lack of literature describing the modelling of the soft materials used for these applications is detected as a research opportunity. Lastly, the implementation of soft actuation technologies as a way to imitate the functionality of the muscle-tendon component is mainly focused on the contractile

element rather than the elastic element. Polymer materials are identified as potential candidates to be used as part of a bio-inspired actuator due to the similarities of these materials with the mechanical properties of the human tendon, and due to the medical application in which they have been used, e.g. tendon reconstruction. Lastly, viscoelasticity, a property of most soft materials, is now being researched as an alternative to improve mature actuation technologies, such as series-elastic actuators. The concept of a series-viscoelastic actuator is very recent and further validates the feasibility of this research.

Investigate the biomechanics of the human lower limb during activities of daily living.

In Chapter 3, kinetic and kinematic parameters of the human lower limb during activities of daily living are presented. Special attention is given to the mechanical model commonly used in soft robotic applications, the Hill's model, when mimicking the functionality of the human skeletal muscle system. The potential of using the compiled data is identified and a conference paper is produced from the work performed in this chapter. The latter paper presents several visualization techniques which can be useful for the design phase of any soft robotic application for human assistance of the lower limb. The complete collected dataset is presented in Appendix A in the form of charts.

Characterize the viscoelastic properties of suitable soft materials.

The characterization process of seven soft materials from the family of composite materials is presented in Chapter 4. The studied rubber-based materials are as follows: Polyethylene Rubber (PR), Ethylene Polypropylene Rubber (EPR), Natural Rubber with Polyester (NatPolR), Natural Rubber (NatR), Silicone Rubber (SR), Fluorocarbon Rubber (FR), and Nitrile Rubber (NR). The concept of elasticity and viscoelasticity are described in here. The mechanical tests of tensile strength and stress relaxation are performed. The processing of the collected data is described in detail. Moreover, particular attention is paid to find the elastic region of the studied materials since these regions dictates the safest working conditions for each material. This information is latter used for the design of a bio-inspired soft actuator.

Identify the soft materials with the most similar mechanical properties to the human tendon.

8. SUMMARY, CONCLUSIONS, AND FUTURE WORK

The motivation behind characterizing many composite materials is to identify the material with the most similar viscoelastic properties as the human tendon. This is another step towards implementing viscoelasticity in soft robotic applications for human assistance. The process to identify the best candidate is presented in Chapter 7, as part of the design process of a bio-inspired actuator. In this comparison, the human tendons involved in the motion of the knee joint are investigated. These are the patellar and quadriceps tendons. The results showed a large difference between the elastic properties of the materials and properties of the human tendon. Nonetheless, their viscoelastic behaviour is found to have similarities. Due to this, the calculation of a matching factor is performed. The idea is to combine several pieces of a material into a bundle to increase the effective cross-sectional area of the material, hence its elastic properties. Lastly, the soft material with the most similar properties as the human tendon, in terms of the achievable stiffness, is identified by looking at the obtained matching factors. This material is the Natural Rubber with Polyester material (NatPolR).

Address current limitations on modelling tools for the prediction of the viscoelastic behaviour of soft materials.

In Chapter 5 the current modelling approach for the prediction of stress response of soft materials is presented. In general, modelling approaches are based on the Linear viscoelastic Models (LVMs), which can describe any viscoelastic materials using a combination of two basic components: a spring and a dashpot. Nonetheless, the accuracy of these models is tightly linked to a high complexity and large computational power requirements. One of the recent methods described to circumvent the latter limitation is found in the literature as the Standard Linear Solid model with Strain-Dependent Stiffness (Std. Lin. SSD). This model can account for the nonlinear stress response of viscoelastic materials by implementing a piecewise linear regression on the equilibrium spring stiffness k_e found in the Standard Linear Solid model (SLS). Nonetheless, the model has not been validated when predicting the velocity-dependent properties of viscoelastic materials. Therefore, a case study is performed on this model, aimed to address its limitations. The latter is done by linearising the Wiechert model, a more complex model from the family of LVMs, using the Piecewise Linearisation method. The hypothesis behind this is that a more complex model might be capable of accounting for the time dependent stress response of the viscoelastic materials. The Piecewise Linearisation method implemented in this work is optimized in many aspects (Figure 5.6). Hence, the resulting

PL-SLS and PL-Wiechert models are different, and a direct improvement, from the Std. Lin. SSD. The proposed tolerance criteria, which takes the variation on the slope of the stress-strain curve to define the number of strain segments to collocate, provided crucial information about the benefits and limitations of the PL method. The models developed in here can account for the nonlinear, time dependent, and strain dependent stress response of soft materials, and in fact, outperformed the Std. Lin. SDS model. The work done in here is substantial enough to produce a second conference paper. In addition to this, a different modelling approach is investigated in Chapter 6. This model is based on machine learning algorithms, specifically on feedforward artificial neural networks (ANNs). The implementation of an ANN model for the prediction of the stress response of viscoelastic materials is poorly documented. Nonetheless, this area of research is rapidly growing due to the proven potential of ANNs to approximate complex functions. The data from the same seven materials is used for the training of the ANN models. The objective is to overcome the limitations of modelling tools based on the LVMs. These limitations are high complexity and computational cost. The performance of the ANN models is very similar to the PL methods. The latter is assessed by statistical parameters such as the root mean square error and the coefficient of determination. In summary, the three developed models outperforms the Std. Lin. SDS in the task of predicting the nonlinear, time dependent, and strain dependent stress response of soft materials.

Investigate the performance of current modelling tools under simulated real-time conditions.

The developed ANN model is chosen for further validation. In this case, the PL methods are not suitable due to their formulation which make use of previous values in time of the stress response of the material. This contradicts the main motivation behind using a viscoelastic element in series with a load. The real-time validation performed in Simulink highlighted the limitations of the developed ANN model, presented in Chapter 7. In summary, the ANN model is unstable due to the varying strain rate used for testing. For a constant strain rate, as the one used when validating the accuracy, the ANN model performed as expected.

Design a bio-inspired soft actuation for human-assistance applications

The design concept of a series-viscoelastic actuator is presented in Chapter 7. The proposed actuator is aimed to assist the knee joint, hence the torque knee

8. SUMMARY, CONCLUSIONS, AND FUTURE WORK

requirements of the joint during walking activities are used as guidelines for the selection of the electric motor and gearbox combination. Lastly, the design of a clamping device to be used in the experimentation is designed. The clamping mechanism was designed to be detachable and allow the testing of many materials without modifying the experimental setup.

8.2 Conclusions

In conclusion, in this research the development of three modelling tools is presented. They are the PL-SLS model, the PL-Wichert model, and the ANN model. All three of these models are successful in describing the nonlinear, time dependent, and strain dependent stress response of the studied soft materials. The accuracy of all models when predicting the stress-strain curve of the materials is better than the accuracy reported for the Std. Lin. SDS model. On the one hand, the Piecewise linearisation method implemented in here is optimized in many ways (Figure 5.6). Due to this, the models developed in here are differentiated from the Std. Lin. SDS and named as PL-SLS model and PL-Wiechert model. On the other hand, the ANN model, based on feedforward artificial neural networks also outperformed the Std. Lin. SDS. The optimization performed to the ANN models indicated that the architecture FFRD4 is the most suitable for the prediction of viscoelasticity. The inputs of this architecture are the strain and the strain rate. The output is the stress. Due to the addition of the strain rate, this type of architecture is categorized as rate-dependent. The ANN models are investigated under real-time simulation conditions. In this scenario, the ANN models performed poorly. The results indicate that a richer dataset is required for the ANN models to correctly predict a varying strain rate input.

Finally, the main contribution of this research to the field of soft robotic applications for human assistance is the development and assessment of three novel modelling tools. During this process, an improved way to implement the Piecewise linearisation method is proposed. Moreover, this research also provided a novel approach to adequately select the actuator technology when designing an assistive device, using the kinetic and kinematic parameters found in clinical studies. Furthermore, the research performed on series-viscoelastic actuators yielded a novel concept design for a clamping mechanisms which has the potential to reduce research and development times when studying soft materials, due its modular design.

8.3 Future Work

The findings of this research have allowed the identification of the following issues still needed to be addressed:

- Dynamic mechanical analysis can be used to characterize the soft materials under a wide range of frequencies to create a more comprehensive dataset to train ANN models.
- Further investigation on the concept of series and parallel elasticity in combination with soft materials.
- Validation of the ANN model when being deployed as part of a control system must be investigated.
- Further characterization of the viscoelasticity of soft materials could be done by extracting their hysteresis, creep and cyclic behaviour.
- Different input combinations for the ANN model could be explored, mainly the ones which do not have the strain rate of the material as input.
- Alternative types of ANNs could be investigated, such as Radial Basis Neural Networks and Recurrent Artificial Neural Networks.
- Alternative techniques, such as synthetic data creation, can be investigated to create a richer dataset without having to perform more experimental tests.
- Further investigation on the implementation of the concepts of co-contraction and variable recruitment could be performed for soft robotics applications.
- Further investigation on the field of the human skeletal system functionality, such as muscle redundancy, which is a compatible approach for cable-driven actuators.

Appendices

APPENDIX A

Characterization of the Human Body Lower Limb

A.1 Stacked Clustered Bar Charts

This appendix presents the compiled data from the reviewed gait analysis studies, in the form of charts as the ones presented in Section 3.2, for the hip, knee and ankle joints. The parameters of torque, angle and power, are extracted.

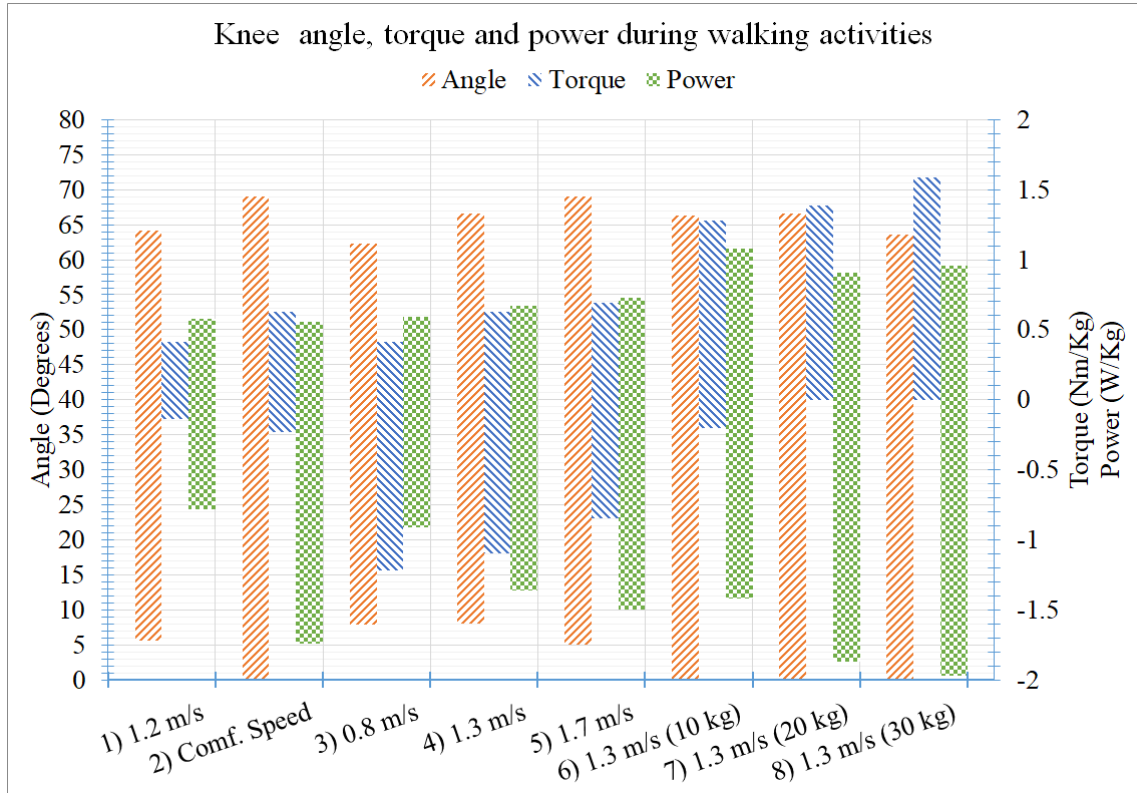


Figure A.1: Knee joint characteristics for walking over ground activities. The weight next to the name of some activities dictates the load carried by the subjects during the experiment [18]. Data collected from: (1) [90], (2) [89], (3-8) [91].

A. CHARACTERIZATION OF THE HUMAN BODY LOWER LIMB



Figure A.2: Ankle joint characteristics for walking over ground activities. The weight next to the name of some activities dictates the load carried by the subjects during the experiment [18]. Data collected from: (1) [90], (2) [89], (3-8) [91].

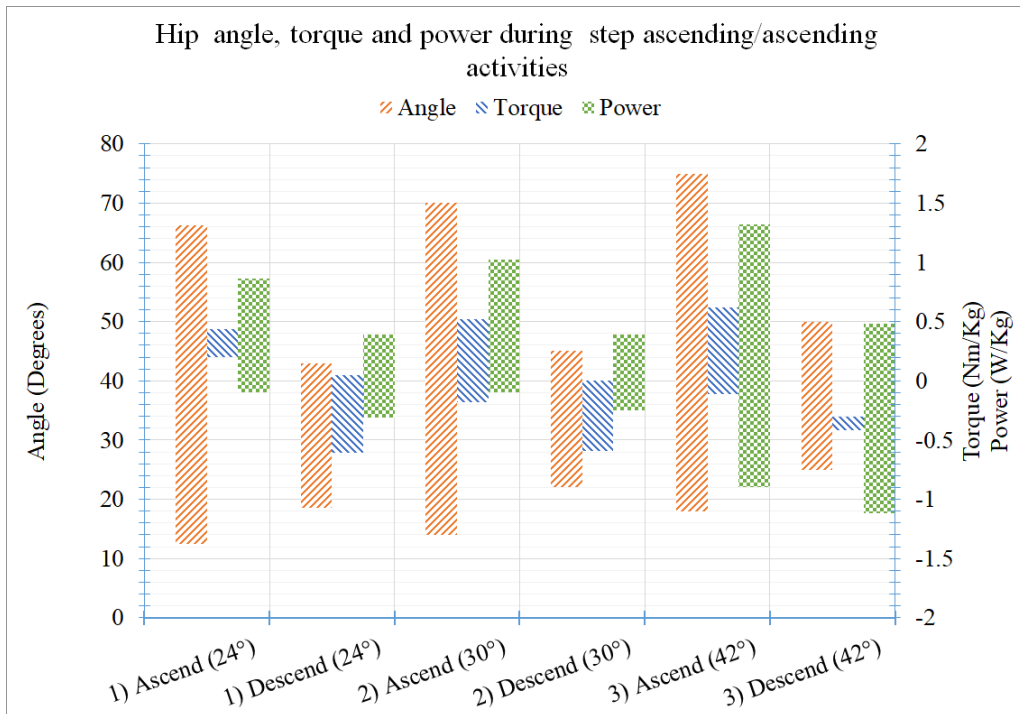


Figure A.3: Hip joint characteristics for step ascending/descending experiments [18]. Data collected from: (1) [94], (2) [95], (3) [99].

A.1 Stacked Clustered Bar Charts

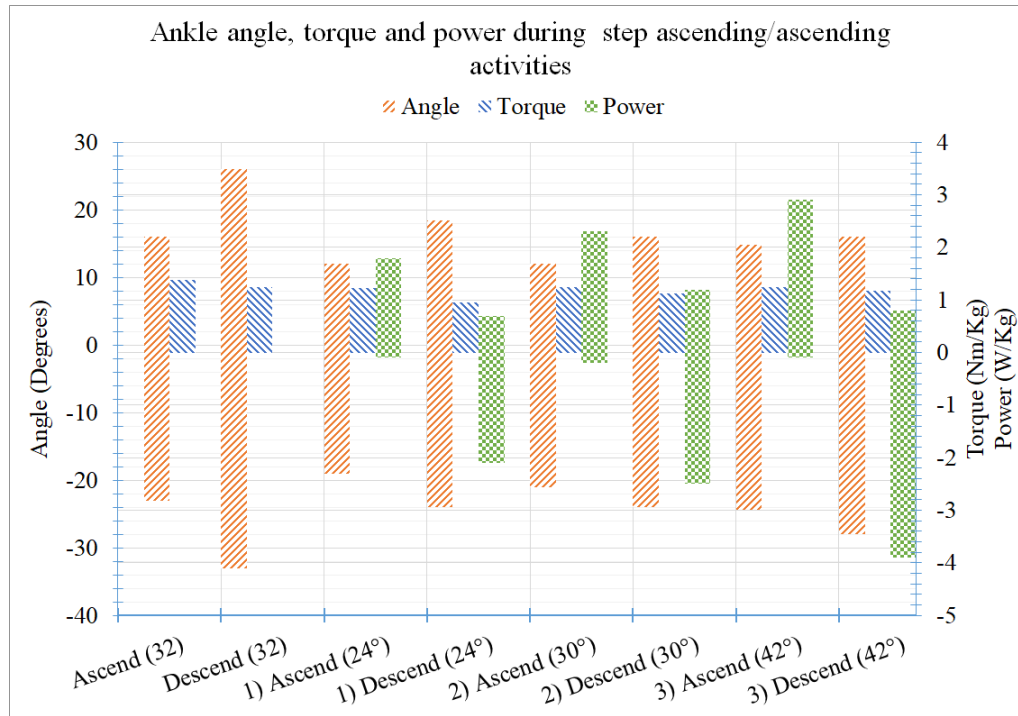


Figure A.4: Ankle joint characteristics for step ascending/descending experiments [18]. Data collected from: (1) [94], (2) [95], (3) [99].

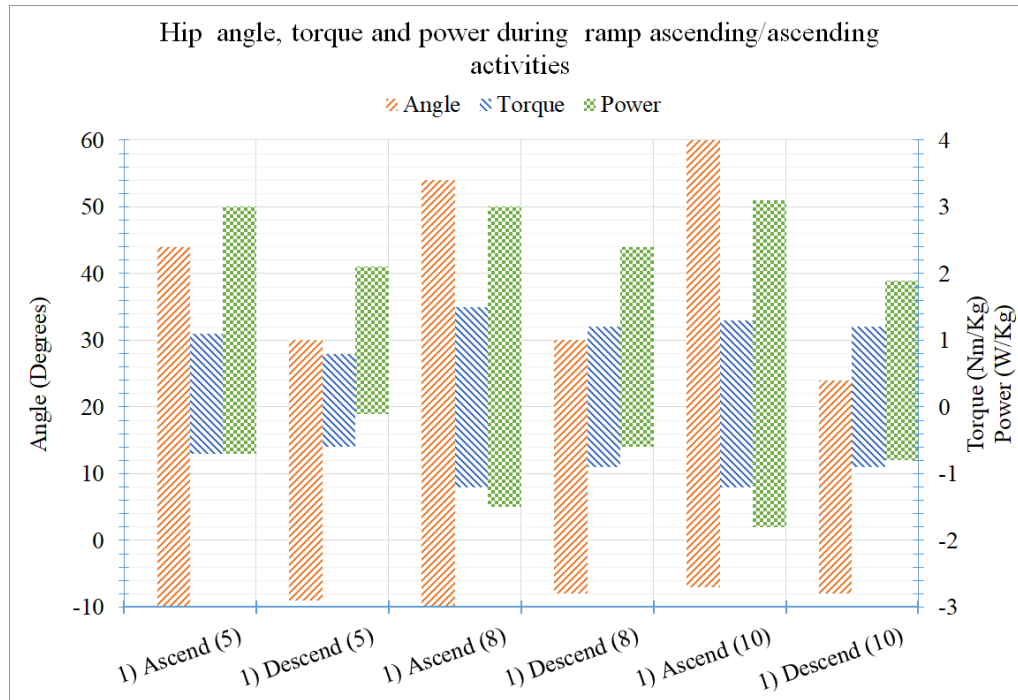


Figure A.5: Hip joint characteristics for ramp ascending/descending experiments [18]. Inclination in brackets. Data collected from [96]

A. CHARACTERIZATION OF THE HUMAN BODY LOWER LIMB

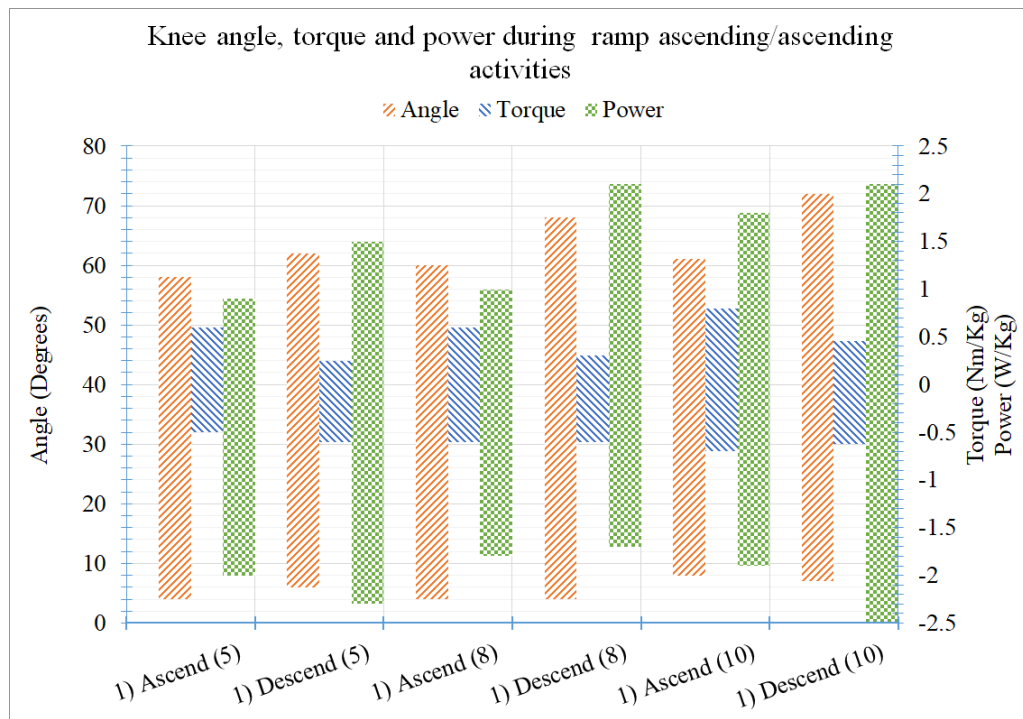


Figure A.6: Knee joint characteristics for ramp ascending/descending experiments [18]. Inclination in brackets. Data collected from [96].

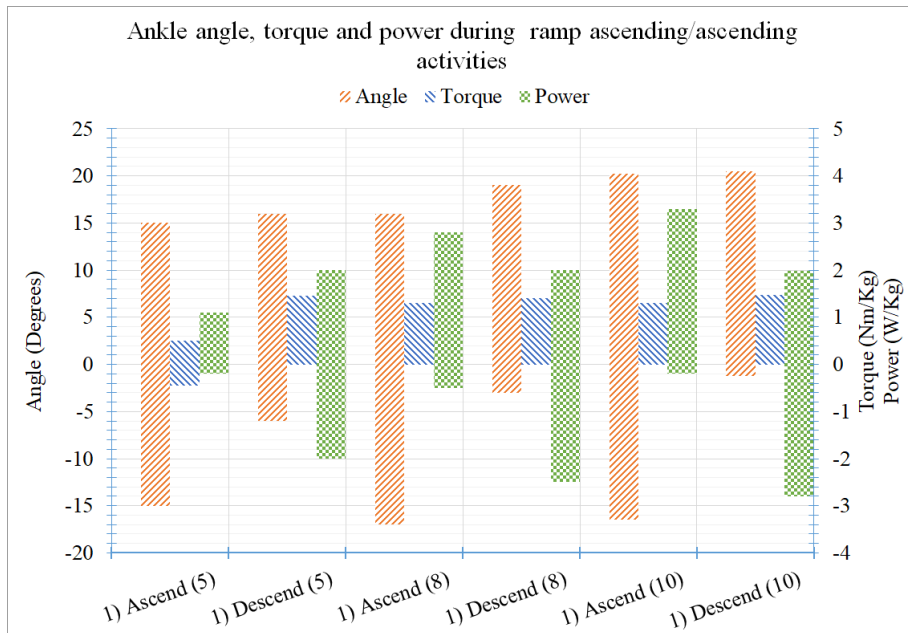


Figure A.7: Ankle joint characteristics for ramp ascending/descending experiments [18]. Inclination in brackets. Data collected from [96].

A.1 Stacked Clustered Bar Charts

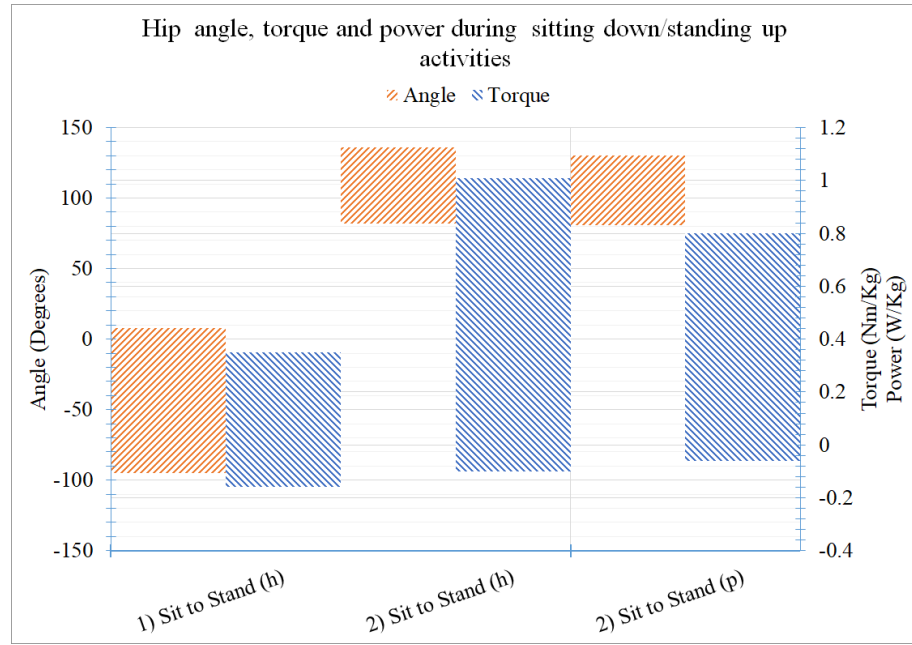


Figure A.8: Hip joint characteristics for sit to stand/stand to sit experiments [18]. In brackets (h) healthy subjects, and (p) subjects with Parkinson's. Data collected from: (1) [97], (2) [98].

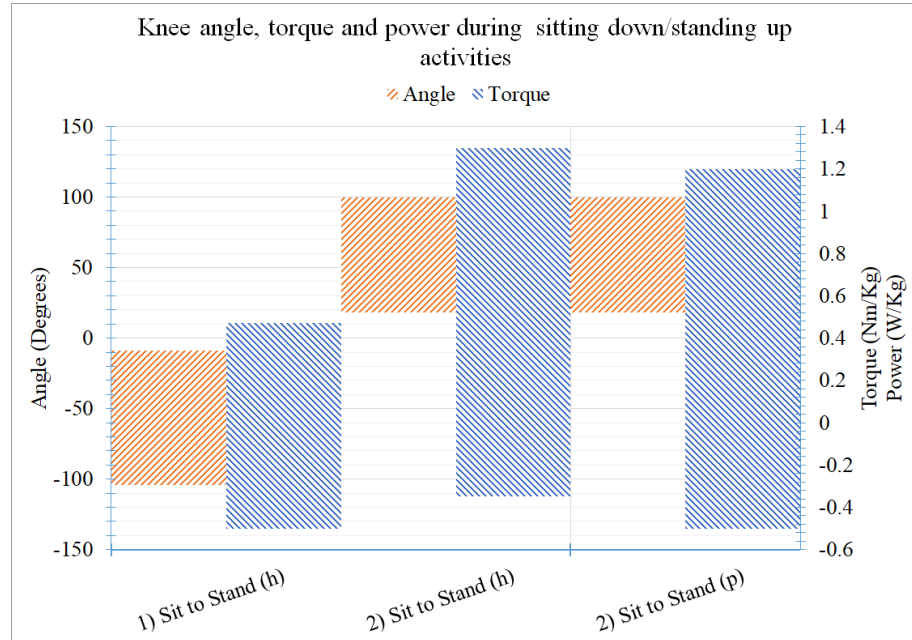


Figure A.9: Knee joint characteristics for sit to stand/stand to sit experiments [18]. In brackets (h) healthy subjects, and (p) subjects with Parkinson's. Data collected from: (1) [97], (2) [98].

A. CHARACTERIZATION OF THE HUMAN BODY LOWER LIMB

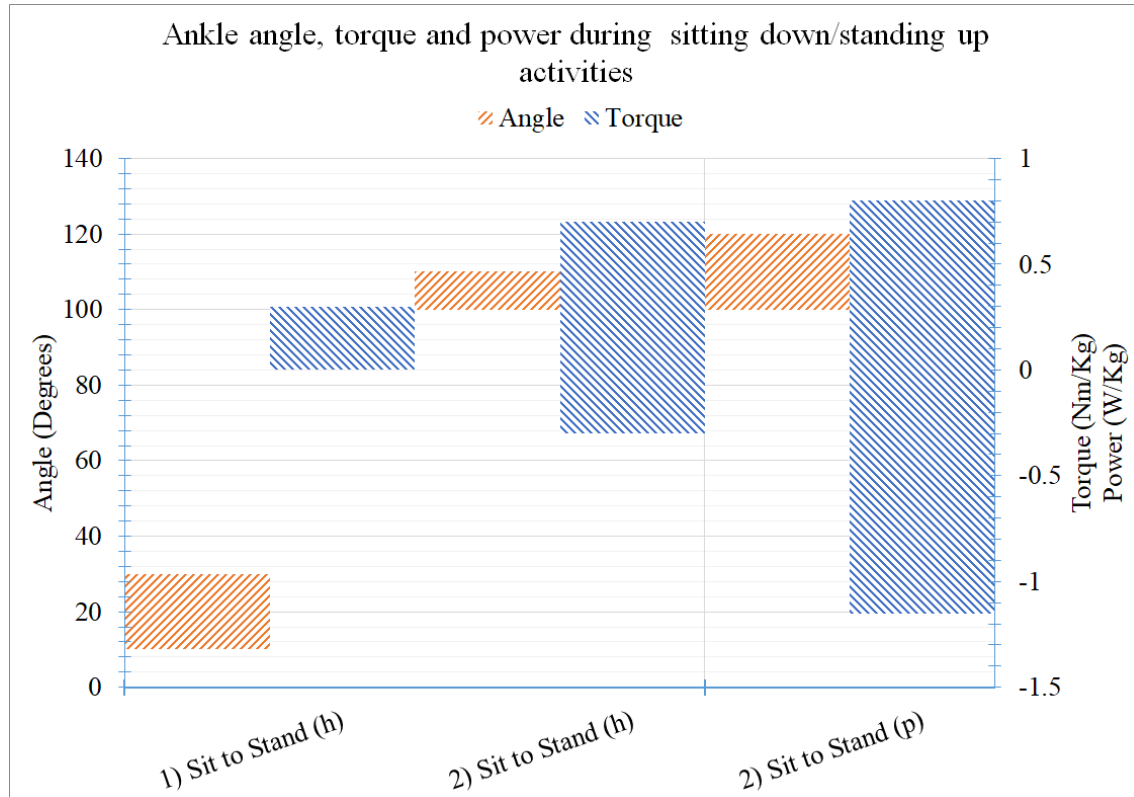


Figure A.10: Ankle joint characteristics for sit to stand/stand to sit experiments [18]. In brackets (h) healthy subjects, and (p) subjects with Parkinson's. Data collected from: (1) [97], (2) [98].

REFERENCES

- [1] Sangbae Kim, Cecilia Laschi, and Barry Trimmer. Soft robotics: a bioinspired evolution in robotics. *Trends in biotechnology*, 31(5):287–294, 2013.
- [2] C Laschi. Soft robotics: from scientific challenges to technological applications. In *Micro-and Nanotechnology Sensors, Systems, and Applications VIII*, volume 9836, page 983626. International Society for Optics and Photonics, 2016.
- [3] Deepak Trivedi, Christopher D Rahn, William M Kier, and Ian D Walker. Soft robotics: Biological inspiration, state of the art, and future research. *Applied bionics and biomechanics*, 5(3):99–117, 2008.
- [4] Fumiya Iida and Cecilia Laschi. Soft robotics: challenges and perspectives. *Procedia Computer Science*, 7:99–102, 2011.
- [5] Alan T Asbeck, Stefano MM De Rossi, Ignacio Galiana, Ye Ding, and Conor J Walsh. Stronger, smarter, softer: next-generation wearable robots. *IEEE Robotics & Automation Magazine*, 21(4):22–33, 2014.
- [6] Michael Wehner, Brendan Quinlivan, Patrick M Aubin, Ernesto Martinez-Villalpando, Michael Baumann, Leia Stirling, Kenneth Holt, Robert Wood, and Conor Walsh. A lightweight soft exosuit for gait assistance. In *2013 IEEE International Conference on Robotics and Automation*, pages 3362–3369. IEEE, 2013.
- [7] Yong-Lae Park, Bor-rong Chen, Néstor O Pérez-Arancibia, Diana Young, Leia Stirling, Robert J Wood, Eugene C Goldfield, and Radhika Nagpal. Design and control of a bio-inspired soft wearable robotic device for ankle–foot rehabilitation. *Bioinspiration & biomimetics*, 9(1):016007, 2014.

REFERENCES

- [8] Yong-Lae Park, Bor-rong Chen, Diana Young, Leia Stirling, Robert J Wood, Eugene Goldfield, and Radhika Nagpal. Bio-inspired active soft orthotic device for ankle foot pathologies. In *2011 IEEE/RSJ International Conference on Intelligent Robots and Systems*, pages 4488–4495. IEEE, 2011.
- [9] P. J. Colombo, M. E. Crawley, B. S. East, and A. R. Hill. Aging and the Brain. https://www.who.int/ageing/publications/global_health.pdf, 2012. [Online; accessed 28-Aug-2019].
- [10] Amelia Hill. Nearly one in seven Britons could live alone by 2039, study shows. <https://www.theguardian.com/society/2019/apr/04/nearly-one-in-seven-britons-could-live-alone-2039-study-shows>, 2019. [Online; accessed 28-Aug-2019].
- [11] RS Components Ltd. Black epdm rubber sheet. <https://uk.rs-online.com/web/p/ethylene-polypropylene-epdm-sheets/8405523/>, 2019. [Online; accessed 28-Aug-2019].
- [12] RS Components Ltd. Black fluorocarbon rubber sheet. <https://uk.rs-online.com/web/p/fluorocarbon-rubber-sheets/5062974/>, 2019. [Online; accessed 28-Aug-2019].
- [13] RS Components Ltd. White nitrile rubber sheet. <https://uk.rs-online.com/web/p/nitrile-rubber-nbr-sheets/5063242/>, 2019. [Online; accessed 28-Aug-2019].
- [14] RS Components Ltd. Black natural rubber sheet. <https://uk.rs-online.com/web/p/natural-rubber-sheets/5063078/>, 2019. [Online; accessed 28-Aug-2019].
- [15] RS Components Ltd. Black polyethylene foam. <https://uk.rs-online.com/web/p/polyethylene-rubber-sheets/7336690/>, 2019. [Online; accessed 28-Aug-2019].
- [16] RS Components Ltd. White silicone rubber sheet. <https://uk.rs-online.com/web/p/silicone-rubber-sheets/5063264/>, 2019. [Online; accessed 28-Aug-2019].
- [17] COREZONE Sports. Resistance loop bands. <https://www.corezonesports.co.uk/collections/resistance-bands/products/resistance-loop-bands-6-pack>, 2019. [Online; accessed 28-Aug-2019].

- [18] Rodrigo D Solis-Ortega, Abbas A Dehghani-Sanij, and Uriel Martinez-Hernandez. Characterization of kinetic and kinematic parameters for wearable robotics. In *Annual Conference Towards Autonomous Robotic Systems*, pages 548–556. Springer, 2017.
- [19] Rodrigo D Solis-Ortega, Abbas A Dehghani-Sanij, and Uriel Martinez-Hernandez. The assessment of viscoelastic models for nonlinear soft materials. In *2018 7th IEEE International Conference on Biomedical Robotics and Biomechatronics (Biorob)*, pages 1274–1279. IEEE, 2018.
- [20] Daniela Rus and Michael T Tolley. Design, fabrication and control of soft robots. *Nature*, 521(7553):467, 2015.
- [21] Roberto Filippini, Soumen Sen, and Antonio Bicchi. Toward soft robots you can depend on. *IEEE Robotics & Automation Magazine*, 15(3):31–41, 2008.
- [22] Tomoyuki Noda, Tatsuya Teramae, Barkan Ugurlu, and Jun Morimoto. Development of an upper limb exoskeleton powered via pneumatic electric hybrid actuators with bowden cable. In *IEEE Int. Conf. Intell. Robot. Syst.*, pages 3573–3578, 2014.
- [23] Guido Belforte, Gabriella Eula, Alexandre Ivanov, and Silvia Sirolli. Soft Pneumatic Actuators for Rehabilitation. *Actuators*, 3(2):84–105, 2014.
- [24] Juan Manuel Florez, Benjamin Shih, Yixin Bai, and Jamie K. Paik. Soft pneumatic actuators for legged locomotion. In *2014 IEEE Int. Conf. Robot. Biomimetics, IEEE ROBIO 2014*, pages 27–34, 2014.
- [25] John Morrow, Hee-sup Shin, Jacob Torrey, Riley Larkins, Steven Dang, Calder Phillips-grafflin, Yong-lae Park, and Dmitry Berenson. Improving Soft Pneumatic Actuator Fingers through Integration of Soft Sensors , Position and Force Control , and Rigid Fingernails, 2015.
- [26] Harshal Arun Sonar and Jamie Paik. Soft Pneumatic Actuator Skin with Piezoelectric Sensors for Vibrotactile Feedback. *Front. Robot. AI*, 2(January):1–11, 2016.
- [27] Chansu Suh, Jordi Condal Margarit, Yun Seong Song, and Jamie Paik. Soft Pneumatic Actuator skin with embedded sensors. In *IEEE Int. Conf. Intell. Robot. Syst.*, pages 2783–2788, 2014.

REFERENCES

- [28] Ellen T. Roche, Robert Wohlfarth, Johannes T B Overvelde, Nikolay V. Vasiliyev, Frank A. Pigula, David J. Mooney, Katia Bertoldi, and Conor J. Walsh. A bioinspired soft actuated material. *Adv. Mater.*, 26(8):1200–1206, 2014.
- [29] M Hamed, P Salimi, A Aliabadi, and M Vismeh. Toward intelligent ankle foot orthosis for foot-drop, a review of technologies and possibilities. In *Biomed. Eng. (ICoBE), 2015 2nd Int. Conf.*, pages 1–6, 2015.
- [30] Yong Lae Park, Bor Rong Chen, Carmel Majidi, Robert J. Wood, Radhika Nagpal, and Eugene Goldfield. Active modular elastomer sleeve for soft wearable assistance robots. In *IEEE Int. Conf. Intell. Robot. Syst.*, pages 1595–1602, 2012.
- [31] Yong-Lae Park, Jobim Santos, Kevin G. Galloway, Eugene C. Goldfield, and Robert J. Wood. A soft wearable robotic device for active knee motions using flat pneumatic artificial muscles. In *2014 IEEE Int. Conf. Robot. Autom.*, pages 4805–4810, 2014.
- [32] Fan-Zhe Low, Hong Han Tan, Jeong Hoon Lim, and Chen-Hua Yeow. Development of a Soft Pneumatic Sock for Robot-Assisted Ankle Exercise. *J. Med. Device.*, 10(1):014503, 2016.
- [33] Saivimal Sridar, Corey J. Majeika, Phillip Schaffer, Matthew Bowers, Seiichiro Ueda, Andrew J. Barth, Jon L. Sorrells, Jon T. Wu, Thane R. Hunt, and Marko Popovic. Hydro Muscle -a novel soft fluidic actuator. *2016 IEEE Int. Conf. Robot. Autom.*, pages 4014–4021, 2016.
- [34] Elliot W Hawkes, David L Christensen, and Allison M Okamura. Design and implementation of a 300% strain soft artificial muscle. In *2016 IEEE International Conference on Robotics and Automation (ICRA)*, pages 4022–4029. IEEE, 2016.
- [35] Alan T Asbeck, Robert J Dyer, Arnar F Larusson, and Conor J Walsh. Biologically-inspired soft exosuit. In *2013 IEEE 13th International Conference on Rehabilitation Robotics (ICORR)*, pages 1–8. IEEE, 2013.
- [36] Volker Bartenbach, Kai Schmidt, Matthias Naef, Dario Wyss, and Robert Riener. Concept of a Soft Exosuit for the Support of Leg Function in Rehabilitation. In *IEEE Int. Conf. Rehabil. Robot.*, pages 125–130, 2015.

- [37] Ye Ding, Ignacio Galiana, Alan Asbeck, Brendan Quinlivan, Stefano Marco, and Maria De Rossi. Multi-joint Actuation Platform for Lower Extremity Soft Exosuits. In *IEEE Int. Conf. Robot. Autom.*, pages 1327–1334, 2014.
- [38] Ye Ding, Ignacio Galiana, Alan Asbeck, Stefano De Rossi, Jaehyun Bae, Thiago Santos, Vanessa Araujo, Sangjun Lee, Kenneth Holt, and Conor Walsh. Biomechanical and Physiological Evaluation of Multi-joint Assistance with Soft Exosuits. In *IEEE Trans. Neural Syst. Rehabil. Eng.*, volume 0, pages 1–1, 2016.
- [39] Inc Images Scientific Instrument. Nitinol / Flexinol® Actuator Wire, 2016.
URL <http://www.imagesco.com/articles/nitinol/04.html>.
- [40] Vishalini Bundhoo. *Design and evaluation of a shape memory alloy-based tendon-driven actuation system for biomimetic artificial fingers*. PhD thesis, University of Victoria, 2009.
- [41] Vishalini Bundhoo, Edmund Haslam, Benjamin Birch, and Edward J. Park. A shape memory alloy-based tendon-driven actuation system for biomimetic artificial fingers, part I: design and evaluation. *Robotica*, 27(01):131, 2009.
- [42] Ehsan Tarkesh, Mohammad H Elahinia, and Mohamed Samir Hefzy. Developing an active ankle foot orthosis based on shape memory alloy actuators. In *ASME 2007 Summer Bioengineering Conference*, pages 769–770. American Society of Mechanical Engineers Digital Collection, 2007.
- [43] Leia Stirling, Chih Han Yu, Jason Miller, Elliot Hawkes, Robert Wood, Eugene Goldfield, and Radhika Nagpal. Applicability of shape memory alloy wire for an active, soft orthotic. *J. Mater. Eng. Perform.*, 20(4-5):658–662, 2011.
- [44] S. Pittaccio, S. Viscuso, M. Rossini, L. Magoni, S. Pirovano, E. Villa, S. Besseghini, and F. Molteni. SHADE: A shape-memory-activated device promoting ankle dorsiflexion. *J. Mater. Eng. Perform.*, 18(5-6):824–830, 2009.
- [45] Thomas P Chenal, Jennifer C Case, Jamie Paik, and Rebecca K Kramer. Variable Stiffness Fabrics with Embedded Shape Memory Materials for Wearable Applications. In *2013 IEEE/RSJ Int. Conf. Intell. Robot. Syst.*, pages 2827–2831, 2014.

REFERENCES

- [46] Simone Pittaccio and Stefano Viscuso. Shape memory actuators for medical rehabilitation and neuroscience. *Smart Actuation and Sensing Systems-Recent Advances and Future Challenges*, 4:83–120, 2012.
- [47] William Coral, Claudio Rossi, Julian Colorado, Daniel Lemus, and Antonio Barrientos. Sma-based muscle-like actuation in biologically inspired robots: a state of the art review. *Smart Actuation and Sensing Systems-Recent Advances and Future Challenges*, pages 53–82, 2012.
- [48] Jianjun Zhang, Yuehong Yin, and Jianying Zhu. Sigmoid-based hysteresis modeling and high-speed tracking control of SMA-artificial muscle. *Sensors Actuators, A Phys.*, 201:264–273, 2013.
- [49] A. Villoslada, A. Flores, D. Copaci, D. Blanco, and L. Moreno. High-displacement flexible Shape Memory Alloy actuator for soft wearable robots. *Rob. Auton. Syst.*, 73:91–101, 2015.
- [50] Kazuto Takashima, Jonathan Rossiter, and Toshiharu Mukai. McKibben artificial muscle using shape-memory polymer. *Sensors Actuators, A Phys.*, 164 (1-2):116–124, 2010.
- [51] Yiğit Mengüç, Yong-Lae Park, Ernesto Martinez-Villalpando, Patrick Aubin, Miriam Zisook, Leia Stirling, Robert J Wood, and Conor J Walsh. Soft wearable motion sensing suit for lower limb biomechanics measurements. In *2013 IEEE International Conference on Robotics and Automation*, pages 5309–5316. IEEE, 2013.
- [52] Yiğit Mengüç, Yong-Lae Park, Hao Pei, Daniel Vogt, Patrick M Aubin, Ethan Winchell, Lowell Fluke, Leia Stirling, Robert J Wood, and Conor J Walsh. Wearable soft sensing suit for human gait measurement. *The International Journal of Robotics Research*, 33(14):1748–1764, 2014.
- [53] Jean Baptiste Chossat, Yong Lae Park, Robert J. Wood, and Vincent Duchaine. A soft strain sensor based on ionic and metal liquids. *IEEE Sens. J.*, 13 (9):3405–3414, 2013.
- [54] N.C. C. Goulbourne, S. Son, and J.W. W. Fox. Self-sensing McKibben actuators using dielectric elastomer sensors. *Proc. SPIE*, 6524:652414–652414–12, 2007.

- [55] Yong Lae Park and Robert J. Wood. Smart pneumatic artificial muscle actuator with embedded microfluidic sensing. *IEEE SENSORS 2013 - Proc.*, pages 1–4, 2013.
- [56] Wyatt Felt and C David Remy. Smart braid: Air muscles that measure force and displacement. In *2014 IEEE/RSJ International Conference on Intelligent Robots and Systems*, pages 2821–2826. IEEE, 2014.
- [57] Wyatt Felt, Khai Yi Chin, and C. David Remy. Contraction Sensing with Smart Braid McKibben Muscles. In *IEEE/ASME Trans. Mechatronics*, volume 4435, pages 1–1, 2015.
- [58] MingKun Chang. Adaptive Self-Tuning Fuzzy Controller for a Soft Rehabilitation Machine Actuated by Pneumatic Artificial Muscles. *Open J. Appl. Sci.*, 5(5):199–211, 2015.
- [59] Erik H. Skorina, Ming Luo, Selim Ozel, Fuchen Chen, Weijia Tao, and Cagdas D. Onal. Feedforward augmented sliding mode motion control of antagonistic soft pneumatic actuators. *Proc. - IEEE Int. Conf. Robot. Autom.*, 2015-June(June):2544–2549, 2015.
- [60] Joshua Bishop-Moser and Sridhar Kota. Design and Modeling of Generalized Fiber-Reinforced Pneumatic Soft Actuators. In *IEEE Trans. Robot.*, volume 31, pages 536–545, 2015.
- [61] A. Hošovský, J. Pitel, K. Žídek, M. Tóthová, J. Sárosi, and L. Cveticanin. Dynamic characterization and simulation of two-link soft robot arm with pneumatic muscles. *Mech. Mach. Theory*, 103:98–116, 2016.
- [62] PhysicalSolutions. Understanding Planes and Axes. <https://www.physical-solutions.co.uk/wp-content/uploads/2015/05/Understanding-Planes-and-Axes-of-Movement.pdf>, 2016. [Online; accessed 10-Sep-2016].
- [63] Archibald Vivian Hill. The heat of shortening and the dynamic constants of muscle. *Proceedings of the Royal Society of London. Series B-Biological Sciences*, 126(843):136–195, 1938.
- [64] Jianjun Zhang and Yuehong Yin. Sma-based bionic integration design of self-sensor–actuator-structure for artificial skeletal muscle. *Sensors and Actuators A: Physical*, 181:94–102, 2012.

REFERENCES

- [65] Felix E Zajac. Muscle and tendon: properties, models, scaling, and application to biomechanics and motor control. *Critical reviews in biomedical engineering*, 17(4):359–411, 1989.
- [66] David G Lloyd and Thor F Besier. An emg-driven musculoskeletal model to estimate muscle forces and knee joint moments in vivo. *Journal of biomechanics*, 36(6):765–776, 2003.
- [67] Massimo Sartori, David G Lloyd, Monica Reggiani, and Enrico Pagello. A stiff tendon neuromusculoskeletal model of the knee. In *2009 IEEE Workshop on Advanced Robotics and its Social Impacts*, pages 132–138. IEEE, 2009.
- [68] Walter Maurel, Yin Wu, Nadia Magnenat Thalmann, and Daniel Thalmann. *Biomechanical models for soft tissue simulation*. Springer, 1998.
- [69] Margareta Nordin and Victor Hirsch Frankel. *Basic biomechanics of the musculoskeletal system*. Lippincott Williams & Wilkins, 2001.
- [70] L Schatzmann, P Brunner, and HU Stäubli. Effect of cyclic preconditioning on the tensile properties of human quadriceps tendons and patellar ligaments. *Knee Surgery, Sports Traumatology, Arthroscopy*, 6(1):S56–S61, 1998.
- [71] Judson T Bauman. *Fatigue, Stress, and Strain of Rubber Components*. Hanser Publications, 2008.
- [72] Qinwu Xu and Bjorn Engquist. A mathematical and physical model improves accuracy in simulating solid material relaxation modulus and viscoelastic responses. *arXiv preprint arXiv:1412.5225*, 2014.
- [73] Annalisa Tirella, Giorgio Mattei, and ARTI Ahluwalia. Strain rate viscoelastic analysis of soft and highly hydrated biomaterials. *Journal of Biomedical Materials Research Part A*, 102(10):3352–3360, 2014.
- [74] Tongqing Lu, Jikun Wang, Ruisen Yang, and TJ Wang. A constitutive model for soft materials incorporating viscoelasticity and mullins effect. *Journal of Applied Mechanics*, 84(2):021010, 2017.
- [75] Ana Paula Delowski Ciniello, Carlos Alberto Bavastri, and Jucélio Tomás Pereira. Identifying mechanical properties of viscoelastic materials in time domain using the fractional zener model. *Latin American Journal of Solids and Structures*, 14(1):131–152, 2017.

- [76] R Sanjeevi. A viscoelastic model for the mechanical properties of biological materials. *Journal of biomechanics*, 15(2):107–109, 1982.
- [77] David Roylance. Engineering viscoelasticity. *Department of Materials Science and Engineering–Massachusetts Institute of Technology, Cambridge MA*, 2139:1–37, 2001.
- [78] Gill A Pratt and Matthew M Williamson. Series elastic actuators. In *Proceedings 1995 IEEE/RSJ International Conference on Intelligent Robots and Systems. Human Robot Interaction and Cooperative Robots*, volume 1, pages 399–406. IEEE, 1995.
- [79] Jerry E Pratt and Benjamin T Krupp. Series elastic actuators for legged robots. In *Unmanned Ground Vehicle Technology Vi*, volume 5422, pages 135–144. International Society for Optics and Photonics, 2004.
- [80] Samuel K Au and Hugh M Herr. Powered ankle-foot prosthesis. *IEEE Robotics & Automation Magazine*, 15(3):52–59, 2008.
- [81] Stefan S Groothuis, G Rusticelli, A Zucchelli, Stefano Stramigioli, and Raf-faella Carloni. The vsaut-ii: A novel rotational variable stiffness actuator. In *2012 IEEE International Conference on Robotics and Automation*, pages 3355–3360. IEEE, 2012.
- [82] Shane A Migliore, Edgar A Brown, and Stephen P DeWeerth. Novel nonlinear elastic actuators for passively controlling robotic joint compliance. *Journal of Mechanical Design*, 129(4):406–412, 2007.
- [83] David Rollinson, Steven Ford, Ben Brown, and Howie Choset. Design and modeling of a series elastic element for snake robots. In *ASME 2013 Dynamic Systems and Control Conference*. American Society of Mechanical Engineers, 2013.
- [84] Federico Parietti, Gabriel Baud-Bovy, Elia Gatti, Robert Riener, Lino Guzzella, and Heike Vallery. Series viscoelastic actuators can match human force perception. *IEEE/ASME Transactions on Mechatronics*, 16(5):853–860, 2011.
- [85] Alexander Schepelmann, Kathryn A Geberth, and Hartmut Geyer. Compact nonlinear springs with user defined torque-deflection profiles for series elastic

REFERENCES

- actuators. In *2014 IEEE International Conference on Robotics and Automation (ICRA)*, pages 3411–3416. IEEE, 2014.
- [86] Jessica Austin, Alexander Schepelmann, and Hartmut Geyer. Control and evaluation of series elastic actuators with nonlinear rubber springs. In *2015 IEEE/RSJ International Conference on Intelligent Robots and Systems (IROS)*, pages 6563–6568. IEEE, 2015.
- [87] Sai-Kit Wu, Garrett Waycaster, and Xiangrong Shen. Electromyography-based control of active above-knee prostheses. *Control Engineering Practice*, 19(8):875–882, 2011.
- [88] Fausto A Panizzolo, Ignacio Galiana, Alan T Asbeck, Christopher Siviy, Kai Schmidt, Kenneth G Holt, and Conor J Walsh. A biologically-inspired multi-joint soft exosuit that can reduce the energy cost of loaded walking. *Journal of neuroengineering and rehabilitation*, 13(1):43, 2016.
- [89] Song Joo Lee and Joseph Hidler. Biomechanics of overground vs. treadmill walking in healthy individuals. *Journal of applied physiology*, 104(3):747–755, 2008.
- [90] Gabriele Bovi, Marco Rabuffetti, Paolo Mazzoleni, and Maurizio Ferrarin. A multiple-task gait analysis approach: kinematic, kinetic and emg reference data for healthy young and adult subjects. *Gait & posture*, 33(1):6–13, 2011.
- [91] YaLi Han and XingSong Wang. The biomechanical study of lower limb during human walking. *Science China Technological Sciences*, 54(4):983–991, 2011.
- [92] Han Yali and Wang Xingsong. Biomechanics study of human lower limb walking: Implication for design of power-assisted robot. In *2010 IEEE/RSJ International Conference on Intelligent Robots and Systems*, pages 3398–3403. IEEE, 2010.
- [93] Jason K Moore, Sandra K Hnat, and Antonie J van den Bogert. An elaborate data set on human gait and the effect of mechanical perturbations. *PeerJ*, 3: e918, 2015.
- [94] Anastasia Protopapadaki, Wendy I Drechsler, Mary C Cramp, Fiona J Coutts, and Oona M Scott. Hip, knee, ankle kinematics and kinetics during stair ascent

- and descent in healthy young individuals. *Clinical biomechanics*, 22(2):203–210, 2007.
- [95] Robert Riener, Marco Rabuffetti, and Carlo Frigo. Stair ascent and descent at different inclinations. *Gait & posture*, 15(1):32–44, 2002.
- [96] Andrew Stuart McIntosh, Karen T Beatty, Leanne N Dwan, and Deborah R Vickers. Gait dynamics on an inclined walkway. *Journal of biomechanics*, 39(13):2491–2502, 2006.
- [97] ME Roebroeck, CAM Doorenbosch, J Harlaar, R Jacobs, and GJ Lankhorst. Biomechanics and muscular activity during sit-to-stand transfer. *Clinical Biomechanics*, 9(4):235–244, 1994.
- [98] Margaret KY Mak, Oron Levin, Joseph Mizrahi, and Christina WY Hui-Chan. Joint torques during sit-to-stand in healthy subjects and people with parkinson’s disease. *Clinical Biomechanics*, 18(3):197–206, 2003.
- [99] Samantha M Reid, Scott K Lynn, Reilly P Musselman, and Patrick A Costigan. Knee biomechanics of alternate stair ambulation patterns. *Medicine and science in sports and exercise*, 39(11):2005, 2007.
- [100] PJ Rowe, CM Myles, C Walker, and R Nutton. Knee joint kinematics in gait and other functional activities measured using flexible electrogoniometry: how much knee motion is sufficient for normal daily life? *Gait & posture*, 12(2):143–155, 2000.
- [101] Shalimar Abdullah. Usage of synthetic tendons in tendon reconstruction. In *BMC proceedings*, volume 9, page A68. BioMed Central, 2015.
- [102] Sarah E Duenwald, Ray Vanderby, and Roderic S Lakes. Viscoelastic relaxation and recovery of tendon. *Annals of biomedical engineering*, 37(6):1131–1140, 2009.
- [103] David Roylance. Mechanical properties of materials. *Massachusetts Institute of Technology*, pages 51–78, 2008.
- [104] Robert O Ebewele. *Polymer science and technology*, chapter Mechanical Properties of Polymers I. CRC press, 2000.

REFERENCES

- [105] Oberg E., Jones F., Horton H., Ryffel H., and McCauley C. *Machinery's Handbook (30th Edition)*, chapter Properties of Plastics. Industrial Press, 2016.
- [106] ASTM D412-06ae2. Standard Test Methods for Vulcanized Rubber and Thermoplastic Elastomers - Tension. Technical report, ASTM International, West Conshohocken, PA, 2006.
- [107] ASTM D638-14. Standard Test Method for Tensile Properties of Plastics. Technical report, ASTM International, West Conshohocken, PA, 2014.
- [108] Mohammad Sadeghi and Fereidoon Behnia. Optimum window length of savitzky-golay filters with arbitrary order. *arXiv preprint arXiv:1808.10489*, 2018.
- [109] Instron. Yield strength. <https://www.instron.co.uk/en-gb/our-company/library/glossary/y/yield-strength>, 2019. [Online; accessed 28-Aug-2019].
- [110] Jennifer C Case, Edward L White, and Rebecca K Kramer. Soft material characterization for robotic applications. *Soft Robotics*, 2(2):80–87, 2015.
- [111] Mats Delin, Rodney W Rychwalski, Michael J Kubát, and Josef Kubát. Volume changes during stress relaxation in polyethylene. *Rheologica acta*, 34(2):182–195, 1995.
- [112] Chiwon Lee, Myungjoon Kim, Yoon Jae Kim, Nhayoung Hong, Seungwan Ryu, H Jin Kim, and Sungwan Kim. Soft robot review. *International Journal of Control, Automation and Systems*, 15(1):3–15, 2017.
- [113] Priyanshu Agarwal and Ashish D Deshpande. Series elastic actuators for small-scale robotic applications. *Journal of Mechanisms and Robotics*, 9(3):031016, 2017.
- [114] Leandro Tomé Martins, Christopher A Arend Tatsch, Eduardo Henrique Ma-cieli, Reinhard Gerndt, and Rodrigo da Silva Guerra. A polyurethane-based compliant element for upgrading conventional servos into series elastic actuators. *IFAC-PapersOnLine*, 48(19):112–117, 2015.
- [115] Nevio Luigi Tagliamonte, Dino Accoto, and Eugenio Guglielmelli. Rendering viscoelasticity with series elastic actuators using cascade control. In *2014*

- IEEE International Conference on Robotics and Automation (ICRA)*, pages 2424–2429. IEEE, 2014.
- [116] C Machiraju, A-V Phan, AW Pearsall, and S Madanagopal. Viscoelastic studies of human subscapularis tendon: Relaxation test and a wiechert model. *Computer methods and programs in biomedicine*, 83(1):29–33, 2006.
- [117] Jorgen S Bergstrom. *Mechanics of solid polymers: theory and computational modeling*, chapter 9, pages 437–446. William Andrew, 2015.
- [118] Z Zhang and K Friedrich. Artificial neural networks applied to polymer composites: a review. *Composites Science and technology*, 63(14):2029–2044, 2003.
- [119] Mira Trebar, Zoran Susteric, and Uros Lotric. Predicting mechanical properties of elastomers with neural networks. *Polymer*, 48(18):5340–5347, 2007.
- [120] Alejandro E Rodríguez-Sánchez, Elías Ledesma-Orozco, Sergio Ledesma, and Agustín Vidal-Lesso. Application of artificial neural networks to map the mechanical response of a thermoplastic elastomer. *Materials Research Express*, 2019.
- [121] Shahzad Maqsood Khan, Samander Ali Malik, Nafisa Gull, Sidra Saleemi, Atif Islam, and Muhammad Taqi Zahid Butt. Fabrication and modelling of the macro-mechanical properties of cross-ply laminated fibre-reinforced polymer composites using artificial neural network. *Advanced Composite Materials*, pages 1–15, 2019.
- [122] Z Zhang, P Klein, and K Friedrich. Dynamic mechanical properties of ptfe based short carbon fibre reinforced composites: experiment and artificial neural network prediction. *Composites Science and Technology*, 62(7-8):1001–1009, 2002.
- [123] Z Zhang, K Friedrich, and K Velten. Prediction on tribological properties of short fibre composites using artificial neural networks. *Wear*, 252(7-8):668–675, 2002.
- [124] MS Al-Haik, MY Hussaini, and H Garmestani. Prediction of nonlinear viscoelastic behavior of polymeric composites using an artificial neural network. *International journal of plasticity*, 22(7):1367–1392, 2006.

REFERENCES

- [125] Mohammad Hossien Saeidirad, Abbas Rohani, and Saeed Zarifneshat. Predictions of viscoelastic behavior of pomegranate using artificial neural network and maxwell model. *Computers and Electronics in Agriculture*, 98:1–7, 2013.
- [126] Yubin Gao, Haibin Li, Guangmei Wei, and Yun He. Viscoelastic analysis of a sleeve based on the bp neural network. *Journal of Mechanical Science and Technology*, 29(11):4621–4629, 2015.
- [127] Necat Altinkok and Rasit Koker. Use of artificial neural network for prediction of physical properties and tensile strengths in particle reinforced alüminum matrix composites. *Journal of materials science*, 40(7):1767–1770, 2005.
- [128] Srinivasu Gangi Setti and RN Rao. Artificial neural network approach for prediction of stress–strain curve of near β titanium alloy. *Rare Metals*, 33(3):249–257, 2014.
- [129] Ivan Jenik, Petr Kubík, Frantisek Sebek, Jiri Hulka, and Jindrich Petruska. Sequential simulation and neural network in the stress–strain curve identification over the large strains using tensile test. *Archive of Applied Mechanics*, 87(6):1077–1093, 2017.
- [130] Basem F Yousef, Abdel-Hamid I Mourad, and Ali Hilal-Alnaqbi. Prediction of the mechanical properties of pe/pp blends using artificial neural networks. *Procedia Engineering*, 10:2713–2718, 2011.
- [131] Ivan Kopal, Marta Harničárová, Jan Valíček, and Milena Kušnerová. Modeling the temperature dependence of dynamic mechanical properties and viscoelastic behavior of thermoplastic polyurethane using artificial neural network. *Polymers*, 9(10):519, 2017.
- [132] Ivan Kopal, Ivan Labaj, Marta Harničárová, Jan Valíček, and Dušan Hrubý. Prediction of the tensile response of carbon black filled rubber blends by artificial neural network. *Polymers*, 10(6):644, 2018.
- [133] Mukta Paliwal and Usha A Kumar. Neural networks and statistical techniques: A review of applications. *Expert systems with applications*, 36(1):2–17, 2009.
- [134] G Gary Wang and S Shan. Review of metamodeling techniques in support of engineering design optimization. *Journal of Mechanical Design*, 129(4):370–380, 2007.

- [135] Timo Koskela et al. *Neural network methods in analysing and modelling time varying processes*. Helsinki University of Technology, 2003.
- [136] MathWorks®. Improve Shallow Neural Network Generalization and Avoid Overfitting. <https://uk.mathworks.com/help/deeplearning/ug/improve-neural-network-generalization-and-avoid-overfitting.html>, 2019. [Online; accessed 28-Aug-2019].
- [137] Greg A Johnson, Dawn M Tramaglini, Rebecca E Levine, Kazunori Ohno, Nam-Yong Choi, and Savio L-Y. Woo. Tensile and viscoelastic properties of human patellar tendon. *Journal of orthopaedic research*, 12(6):796–803, 1994.
- [138] Hans U Stäubli, Lukas Schatzmann, Peter Brunner, Liliana Rincón, and Lutz-P Nolte. Mechanical tensile properties of the quadriceps tendon and patellar ligament in young adults. *The American journal of sports medicine*, 27(1):27–34, 1999.
- [139] Wilian M dos Santos and Adriano AG Siqueira. Impedance control of a rotary series elastic actuator for knee rehabilitation. *IFAC Proceedings Volumes*, 47(3):4801–4806, 2014.
- [140] Xianbo Xu and Nikhil Gupta. Artificial neural network approach to predict the elastic modulus from dynamic mechanical analysis results. *Advanced Theory and Simulations*, 2(4):1800131, 2019.
- [141] David Rollinson, Yigit Bilgen, Ben Brown, Florian Enner, Steven Ford, Curtis Layton, Justine Rembisz, Mike Schwerin, Andrew Willig, Pras Velagapudi, et al. Design and architecture of a series elastic snake robot. In *2014 IEEE/RSJ International Conference on Intelligent Robots and Systems*, pages 4630–4636. IEEE, 2014.
- [142] HEBI Robotics. <https://www.hebirobotics.com/>, 2019. [Online; accessed 28-Aug-2019].
- [143] Edgar Bolivar, David Allen, Gregory Ellson, Jorge Cossio, Walter Voit, and Robert Gregg. Towards a series elastic actuator with electrically modulated stiffness for powered ankle-foot orthoses. In *2016 IEEE International Conference on Automation Science and Engineering (CASE)*, pages 1086–1093. IEEE, 2016.

REFERENCES

- [144] Glenn Mathijssen, Dirk Lefeber, and Bram Vanderborght. Variable recruitment of parallel elastic elements: Series–parallel elastic actuators (spea) with dephased mutilated gears. *IEEE/ASME Transactions on Mechatronics*, 20(2):594–602, 2014.
- [145] David A Winter. *Biomechanics and motor control of human movement*. John Wiley & Sons, 2009.
- [146] Maxon. Maxon RE motor. https://www.maxongroup.com/medias/sys_master/root/8833415839774/19-EN-130.pdf, 2019. [Online; accessed 28-Aug-2019].
- [147] Maxon. Maxon Planetary Gearhead. https://www.maxongroup.com/medias/sys_master/8831071158302.pdf, 2019. [Online; accessed 28-Aug-2019].